ABSTRACT

Title of Dissertation: HARNESSING DEGRADABLE MATERIALS TO STUDY AND ENGINEER LYMPH NODE FUNCTION

James I. Andorko, Doctor of Philosophy, 2017

Dissertation directed by: Christopher M. Jewell
Assistant Professor
Fischell Department of Bioengineering

Vaccines have benefited global health by controlling or eradicating multiple previously fatal diseases. While many early vaccines were efficacious, sophisticated new vaccines and immunotherapies need to address current challenges in the field, including diseases that avoid immune detection or lack strong molecular targets for the immune system. Overcoming these hurdles requires strategies to specifically control the magnitude and type of immune response generated. Biomaterials offer attractive features to achieve this goal, including protection of encapsulated signals, controlled release of cargos, and tunable features for cell targeting. Intriguingly, recent research reveals many common biomaterials activate the immune system, even without other signals. This intrinsic activation results, at least in part, from biomaterial physicochemical features that mimic pathogens and other foreign materials. Surprisingly, although degradable materials are being intensely studied as

vaccines carriers, little research has investigated how the intrinsic immunogenicity of these materials changes as polymers degrade. The work in this dissertation reveals parameters impacting material intrinsic immunogenicity and exploits this new understanding to test the influence of biomaterial-based vaccines on the function of lymph nodes (LNs), key tissues that coordinate immunity. In the first aim, the immunostimulatory properties of a library of degradable polymers, poly(beta-amino esters) (PBAEs), were investigated in cell and animal models. PBAEs in soluble forms did not activate innate immune cells (e.g., dendritic cells, DCs). When PBAEs were formulated into particles to mimic a common vaccine strategy, DC activation increased in a molecular weight-specific manner. Using intra-lymph node (*i.LN.*) injection, a novel technique to control the dose, kinetics, and combination of signals in LNs, PBAE intrinsic immunogenicity was confirmed in mice. In the second aim, microparticles encapsulating immune signals were introduced into mice via *i.LN.* injection and immune responses were quantified in treated LNs, untreated LNs, and in blood. These results elucidated the interplay between local LN rearrangement and systemic antigen-specific responses which ultimately led to prolonged survival in cancer models. By understanding how the properties and administration of biomaterial-based vaccines impact immunity, this dissertation provides information that can help create new design rules for future vaccines that actively direct the immune system toward a desired response.

HARNESSING DEGRADABLE MATERIALS TO STUDY AND ENGINEER LYMPH NODE FUNCTION

by

James Imre Andorko

Dissertation submitted to the Faculty of the Graduate School of the
University of Maryland, College Park, in partial fulfillment
of the requirements for the degree of
Doctor of Philosophy
2017

Advisory Committee:
Professor Christopher Jewell, Chair
Professor Jonathan Bromberg
Professor Steven Jay
Professor Peter Kofinas
Professor David Mosser, Dean's Representative

Dedication

To my wife,

Who has been there by my side through it all,

Motivating and inspiring me beyond what words can describe.

You and me together, we can do anything.

Acknowledgements

First, thank you Chris for all of your guidance and support. You have provided me with countless opportunities through the years which I am extremely grateful for. Thank you to the current and past members of the Jewell Lab for all the advice, support, and time you have given to me. A special thanks to Kevin for all the time assisting me with my projects, Lisa for enduring this journey with me from the start, and Krystina for the countless conversations, lunches, and breaks from lab that have kept me grounded these past years. To the Bromberg and Martin labs, I have appreciated all of the time, expertise, and discussions you have shared with me during our time collaborating. A big thanks to Niki, my parents, and siblings for all of their love, encouragement, and for sometimes answering the phone when I call in traffic.

Table of Contents

List of Tables

List of Figures

List of Commonly Used Abbreviations

Antigen Presenting Cells	APCs
Cytotoxic T Lymphocytes	CTLs
Danger-Associated Molecular Patterns	DAMPs
Dendritic Cells	DCs
Extracellular Matrix	ECM
Germinal Center	GC
High Endothelial Venules	HEVs
Lipopolysaccharide	LPS
Lymph Nodes	LNs
Major Histocompatibility Complex	MHC
Microparticles	MPs
Molecular Weight	MW
Nanoparticles	NPs
Ovalbumin	OVA
Pathogen-Associated Molecular Patterns	PAMPs
Pattern Recognition Receptors	PRRs
Poly(beta-amino esters)	PBAEs
Poly(lactic-co-glycolic acid)	PLGA
Poly(inosinic:cytidylic acid)	PolyIC
Secondary Lymphoid Organs	SLOs
Toll-Like Receptors	TLRs
Toll-Like Receptors Agonist	TLRa

Chapter 1: Introduction

The ability to reprogram the immune system via vaccination has proven to be a powerful tool in combating disease worldwide.[1] The immune system provides the first line of defense against pathogens and disease, by creating a barrier and rapid recognition system for identifying foreign materials. Through the use of a variety of cells and molecules, the immune system can then eliminate these harmful materials. Vaccines include three main parts: i) the antigen, a fragment of the specific pathogen or molecule that determines the selectively of the immune response, ii) an adjuvant, which activates or amplifies the immune response to an antigen, and iii) a vehicle or carrier to stabilize the immune cargos. The introduction of economical, global vaccination has allowed people around the world to receive vaccines, leading to communicable diseases to be reduced or eradicated.[1] However, there are still barriers limiting the progress in vaccine development. First, vaccines are not available for many important diseases impacting human health (e.g., infections, cancer) which require identification of new antigens for efficacy. Also, because of the use of live or attenuated pathogens within some vaccines, a safety risk is involved since mutation can occur, as well as the possibility of acute toxicity at the injection site. Further, even with clinically approved adjuvants such as aluminum salts (alum), the mechanism of action is poorly defined, making it difficult to improve upon or mimic the response to these materials in a rational way.[2] Because of these limitations and the empirical, inefficient nature of vaccine development, clinical approval of vaccines has slowed and a number of recent late-stage clinical trials have failed, leading to

enormous losses in scientific and financial resources.[3-8] These issues have motivated researchers to design tunable systems that can provide fundamental knowledge to enable rational design approaches to build vaccines that are more effective and can be created more quickly to save resources.

Biomaterials provide a unique platform to serve as these modular systems for vaccines and immunotherapies. Biomaterials are either naturally-derived building blocks (e.g., lipids, proteins, peptides, polysaccharides, nucleic acids) or synthetically derived (e.g., polymers, metals, ceramics). They can be used as vehicles to deliver immune signals and offer tunable properties that can control the loading and release of encapsulated antigen and adjuvant. These features create platforms for tunable release of signals that can provide increased exposure to antigen to drive robust immune response that are specific and provide long-lasting protection (i.e., immune memory). While initially biomaterials were thought to be bioinert and thus not influence immune response, surprisingly, the past decade has revealed a growing number of studies indicating materials can be recognized by and alter immune function. In some cases, this influence results in the administered vaccine being cleared from the body rapidly and as a consequence, reduces potency. In other examples, researchers have found many common biomaterials promote inflammatory responses and immune activation.[9] Based on these revelations, there is a pressing need to further evaluate how the properties of materials are driving this intrinsic immunogenicity so that vaccines can be designed to actively direct the immune system towards a desired response.

One particular tissue type of interest for vaccines and immunotherapy are the lymph nodes (LNs). These tissues coordinate the immune response by providing a location for the cells of the innate immune system, which rapidly respond to pathogens, to interact with cells responsible for adaptive immunity, which create specific, long-lasting responses.[10] Interestingly, recent research has shown that structural components of LNs can rearrange following treatment, altering the local microenvironment to promote interactions between these cells.[11, 12] Changes to the local LN environment ultimately control the resulting systemic response. With this new understanding of how local changes can bring about systemic responses, we developed a method for directly injecting LNs of mice.[13, 14] Since biomaterials are used as vaccine carriers, this platform provides a tool to directly deposit these materials into LNs, controlling the dose, kinetics, and combinations of signals that reach these tissues, and allowing for investigation into how their properties impact local and systemic responses.

The work in this dissertation combines material science and engineering techniques with biological and immunological assays in both cell and animal models to study the impact that biomaterials have on the immune response. The material science techniques used were polymer synthesis and characterization via nuclear magnetic resonance and gel permeation chromatography, micro and nanoparticle fabrication, and characterization of material physicochemical properties. These were coupled with cell culture, primary cell isolation, animal handling and manipulation, flow

cytometry, and histological analyses to provide a unique setting to investigate two main objectives listed below:

1. Evaluate how the intrinsic immunogenicity of biomaterials is altered during degradation of polymeric carriers
    a. Study how the form of polymer influences innate cell activation
    b. Determine if intrinsic immune function is attributed to the molecular weight of materials
    c. Link changes in innate cell activation driven by specific polymer properties to adaptive cell responses

2. Employ *i.LN.* injection as a tool to investigate changes in local, treated tissues and assess the link to systemic immunity
    a. Determine if *in vitro* intrinsic activation of degradable polymers translates to animal models
    b. Investigate impact of vaccine deposition on local LN resident innate and adaptive immune cells
    c. Enumerate the antigen-specific systemic response following treatment to determine the efficacy in a cancer model

The objectives outlined above advance the understanding of intrinsic immunogenicity by elucidating how modulation of the immune system is altered over time as a material degrades. While many pre-clinical vaccines and immunotherapies use

biomaterials carriers, researchers have yet to fully characterize how materials properties impact immunogenicity and have not investigated how this may change with carrier stability. Additionally, this work provides new knowledge of how the localization of biomaterials and immune signals in LNs influences these tissues and how these local changes alter the resulting, antigen-specific systemic response. These outcomes provide a basis for the design of future vaccines and immunotherapies that are fabricated from materials specifically selected to push the immune response toward a desired response. This new insight could be applied to a number of disease models, either to promote a pro-inflammatory immune response needed for many cancer therapies or, conversely, to encourage an anti-inflammatory environment that is beneficial for control of autoimmune diseases.

The next chapter begins with a detailed overview of the immune system and reviews some of the recent work involving biomaterials and how they are used to modulate the immune system toward immunogenic responses that are pro-inflammatory with applications for cancer, or tolerogenic responses which restrain the immune system and could be beneficial for autoimmune diseases. **Chapter 3** investigates how the intrinsic properties of a model degradable polymer impact innate and adaptive immune cells *in vitro*. **Chapter 4** expands on this work to generalize these findings across a small library of polymers and correlates immunogenicity to a characteristic molecular weight range. **Chapter 5** introduces intra-lymph node (*i.LN.*) injection and reveals that the intrinsic immunogenicity of the polymers from **Chapters 3 and 4** also translates to animal models. **Chapter 6** uses *i.LN.* injection to deposit

biomaterial-based vaccines into LNs and investigate the local and systemic responses to treatment in a cancer model. **Chapter 7** introduces a new technology created to immobilize cancer cells while maintaining their free-floating dynamics, which allows for drug screening of therapeutics and potential identification of new tumor antigens. In **Chapter 8**, the knowledge about biomaterial immunogenicity gained from this work and other recent studies involving vaccines and immunotherapies is discussed in the context of tissue engineering, a field that relies on biomaterials but has yet to capitalize on the potential of the immunogenic features of materials. **Chapter 9** details ongoing and future research directions that must be taken to further understand how the properties of materials and localization to immune tissues ultimately impact immunity. **Chapter 10** lists the contributions to science that have resulted from this work. This dissertation ends with an appendix cataloging the publications that I am a contributing author on, an appendix of my patent and intellectual property filings, and a list of references.

Chapter 2: Harnessing Biomaterials to Engineer the Lymph Node Microenvironment for Immunity or Tolerance[1]

2.1 Introduction

Vaccination has produced one of the greatest impacts on human health in history [1]. No other break-through has virtually eradicated fatal diseases like polio or small pox with just a few doses. However, many diseases impacting public health create complex challenges for existing vaccine and immunotherapy strategies. For example, HIV evades clearance by mutation and concealment in the mucosa, tumors actively suppress tumor-destructive immune cells, and many treatments for autoimmune disease lack specificity. To address challenges such as these, new vaccines and immunotherapies will need to generate potent responses against specific molecules – termed antigens – while also tuning the characteristics of these responses to combat a target disease. Lymph nodes (LNs) and the spleen are some of the key structures that coordinate the type and specificity of these responses.

In the last several years, the impact of nanoparticles (NPs), microparticles (MPs), and other biomaterial vaccine and immunotherapy carriers on LNs has been an intriguing area of focus. These studies reveal the potential of biomaterials to program the local LN microenvironment to control systemic immune response. The broad potential of

[1]Adapted from J.I. Andorko, K.L. Hess, and C.M. Jewell "Harnessing biomaterials to engineer the lymph node microenvironment for immunity or tolerance." *AAPS Journal*. 2015, 17, 323-328.

biomaterials for vaccination and immunotherapy has recently been reviewed [15-17]. This paper focuses more specifically on the interactions of biomaterials with LNs and other immune tissues (*e.g.*, spleen) during the generation of stimulatory or regulatory immune responses. The discussion begins with background describing how adaptive immune responses are generated, with an emphasis on the active role that LN tissues and resident cells play in these processes. Key recent examples are then discussed to demonstrate how biomaterials enhance the generation of immunity, for example against a foreign pathogen, or of tolerance, such as to combat autoimmune disease. The review concludes by identifying unanswered questions and highlighting some of the ways in which answers to these questions could inform new approaches to exploit the interactions between biomaterials and LNs for vaccination, immunotherapy, and tissue engineering.

2.2 Adaptive immunity requires structured interactions between immune cells

2.2.1 Antigens in peripheral tissue must reach LNs to initiate adaptive immune response

The innate immune system is comprised of first-response defense mechanisms including i) skin that creates a physical barrier against pathogens, ii) immune cells that home to and engulf pathogens or other immunogenic structures, and iii) receptors that detect broad classes of molecular patterns absent in mammals but present in viruses and bacteria. In contrast, adaptive immunity involves the generation of immune responses specific for a particular molecule, termed an antigen. Generation and control of these antigen-specific responses require complex interactions between

immune cells, antigens, and soluble factors in secondary lymphoid organs (SLOs) [18, 19]. These tissues include the spleen, LNs, and Peyer's patches. The spleen samples circulating antigens present in blood, while specialized nodules termed Peyer's patches sample antigens in mucosal tissues such as the small intestine.

LNs are found throughout the body, concentrating antigens from a network of lymphatic vessels that continually sample tissue for antigens or other immune signals [20, 21]. Soluble antigens with molecular weights of ~70kDa or with particle size between 20-50nm passively drain along the lymphatics, while larger antigens or pathogens are phagocytosed and carried to these LNs by specialized antigen presenting cells (APCs) such as dendritic cells (DCs) (**Figure 2.1A**) [15, 22]. APCs continually survey tissue and blood for inflammatory signals and antigens, which upon detection, stimulate phagocytosis and a change in the expression of homing receptors that allows antigen-experienced APCs to travel to nearby "draining" LNs [20]. In LNs, processed antigens are presented by APCs to activate resident T and B lymphocytes. Activated lymphocytes and molecules secreted by these cells (*e.g.*, antibodies) exit LNs and search the periphery to immobilize or destroy the pathogens against which they are armed in LNs. Thus LNs are key structures that vaccines and immunotherapies must reach to generate antigen-specific responses that can combat pathogens and diseased tissue located in other regions of the body.

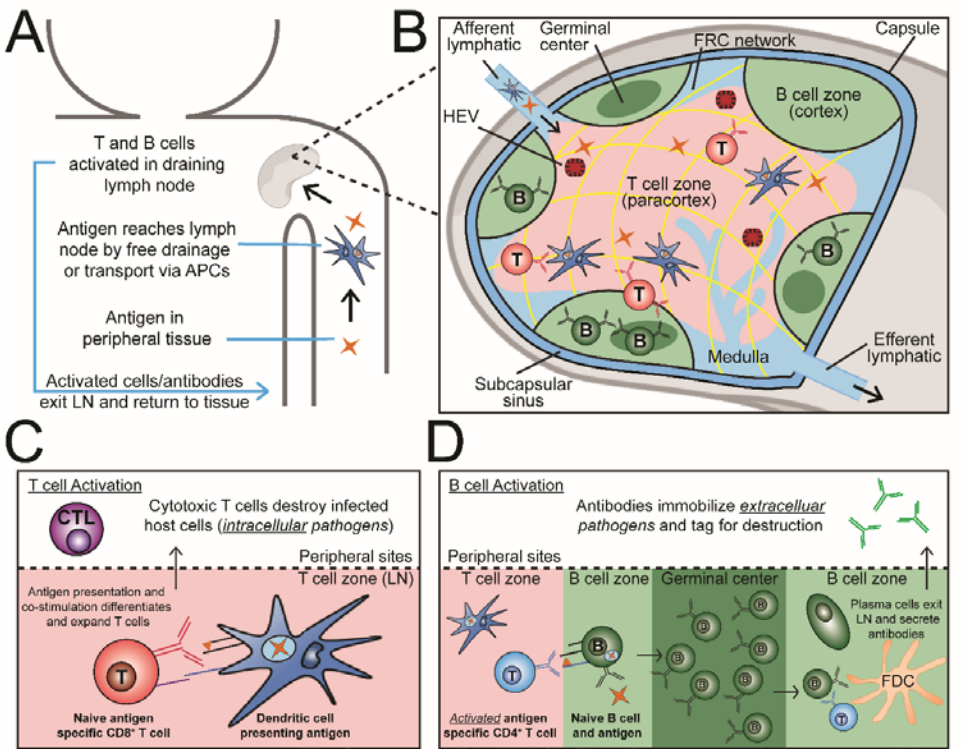

Figure 2.1: Schematic overview of cell-mediated and antibody-mediated relating to the LN.
(A) Graphical depiction of antigen drainage through lymphatics and APC-aided transport to LNs. (B) Illustration of the LN microenvironment containing key cells and stromal structures. (C) Activation of cytotoxic T cell is induced by DCs which process and present antigens with co-stimulatory molecules to naïve CD8+ T cells within the T cell zones of LNs. (D) B cell activation occurs after an activated CD4+ helper T cell bind to B cells presenting the same antigen at the periphery of the LN follicle. Activated B cells then migrate to GCs where proliferation, somatic mutation, and, with the help of follicular DCs and follicular helper T cells, affinity maturation occur. These processes result in plasma cells that exit the LN and secrete high affinity antibodies.

2.2.2 LNs contain supportive stromal components, B cell zones, and regions rich in APCs and T cells

LNs are bean-shaped structures surrounded by a collagen-rich fibrous capsule (**Figure 2.1B**). Antigens – in soluble form or phagocytosed within APCs – enter LNs via the afferent lymphatic that drains lymph fluid flowing from upstream lymphatic vessels [20, 21]. This fluid travels around the periphery via the subcapsular sinus (SCS), a region rich in macrophages able to take up and process incoming antigen or particles, and is dispersed throughout the LN by supportive stromal tissues that

include fibroblastic reticular cells (FRC) and extracellular matrix (ECM) components secreted by FRCs [18]. This network of conduits and cells ensures small, soluble antigens can efficiently penetrate deep into LNs.

DCs and T cells comprise an interior region of LNs called the paracortex ("T cell zone"), while B cells and specialized follicular dendritic cells (FDCs) make up a surrounding cortex called the "B cell zone" (**Figure 2.1B**) [23, 24]. The degree of intermingling between these two regions is controlled by soluble chemotactic factors called chemokines. The chemokines CCL19 and CCL21 attract T cells expressing CCR7 to the paracortex, while CXCL13 attracts B cells expressing CXCR5 to the follicles of the cortex [23, 24]. During generation of adaptive immunity, this balance changes: B cells upregulate CCR7 receptors for CCL19/CCL21, while T cells upregulate CXCR5 receptors for CXCL13, promoting interactions between APCs, T cells, and B cells at the interface of the T and B cell zones. The purpose of these interactions is to generate effector cells and secreted antibody molecules specific for a particular antigen encountered in organs, blood, or peripheral tissue. Upon activation and expansion, T cells and B cells are collected and exit the LN through the medulla and efferent lymphatic. Structures called high endothelial venules (HEVs) also connect LNs with circulatory vasculature, serving primarily as a conduit for lymphocytes to travel between blood and LNs. A summary of the key cells and structures of the LN can be found in **Table I**.

Table 2.1: Key Cells and Structures Comprising Lymph Nodes

Cell or tissue	Acronym	Key Function
Professional antigen presenting cell	APC	Cells exhibiting a primary function of processing and presenting antigen. Key populations include DCs, B cells, and macrophages.
Dendritic cell	DC	APCs surveying peripheral tissue for antigen. DCs take up antigen, migrate to LNs, then present antigen to T and B cells to generate antigen-specific immunity.
T lymphocyte	T cell	Cells involved in direct cell killing of infected host cells ($CD8^+$ cytotoxic T cell population) and helper functions that support antibody production ($CD4^+$ helper T cells).
B lymphocyte	B cell	Cells that differentiate to plasma cells that are able to secrete antibody molecules that bind antigens. Binding leads to neutralization or destruction of these targets.
Fibroblastic reticular cells	FRC	Stromal cells that support trafficking of soluble signals and antigen throughout LNs. These cells also organize LN structure by secreting extracellular matrix components.
Follicular dendritic cell	FDC	Specialized dendritic cell able to capture and present antigen to B cells in GCs to promote high-affinity antibodies.
Capsule		Dense layer of connective tissue that surrounds the internal structure of LNs.
Afferent lymphatics		Entry of antigen and immune cells from lymphatics.
Efferent lymphatics		Exit of immune cells from lymph node to lymphatics.
Subcapsular sinus	SCS	Drains and distributes lymph throughout LNs.
Medulla		Drains activated lymphocytes in LNs to efferent lymphatics for return to tissue and blood.
High endothelial venule	HEV	Portal allowing exchange of lymphocytes with blood.
T lymphocyte zone (paracortex)		Interior domain rich in T cells and DCs.
B lymphocyte zone (cortex)		Follicular region located at the peripheries of the paracortex that is rich in B cells and FDCs.
Germinal center	GC	Structures that form to co-mingle specialized DCs, helper T cells, and B cells during induction of high affinity antibodies.

2.2.3 Adaptive immunity requires specific interactions between APCs, T cells, and B cells in LNs

The major classes of adaptive responses include *cell-mediated immunity*, through which cytotoxic T lymphocytes directly destroy infected host cells; and *antibody-mediated immunity*, which involves binding, neutralization, and clearance of antigens by circulating antibodies specific for these pathogens. In the simplest sense, cell-mediated immunity removes intracellular pathogens such as viruses, while antibodies are able to address extracellular toxins and pathogens (*e.g.*, bacteria). Cell-mediated and antibody-mediated responses develop following the activation of naïve, antigen-specific T cells and B cells, respectively [25, 26]. These processes involve interactions with APCs in LNs or other SLOs. Naïve $CD8^+$ T cells are activated by DCs that have encountered, processed, and are presenting the antigen these T cells are specific for (i.e., a "cognate" antigen) (**Figure 2.1C**). Importantly, this activation requires that the cognate antigen be presented by the APCs in a protein complex called major histocompatibility complex I (MHC-I). Activation also requires co-stimulatory surface molecules that are expressed when DCs encounter inflammatory signals – often adjuvants in the case of vaccines. These agents enable DCs to co-present co-stimulatory signals to $CD8^+$ T cells during antigen presentation. This set of interactions causes $CD8^+$ T cells to expand and differentiate to cytotoxic T lymphocytes (CTLs) that migrate from LNs to destroy host cells expressing the target antigen (*e.g.*, due to a viral infection). A similar process occurs in DCs presenting antigen in MHC-II to $CD4^+$ helper T cells that play an important role in the activation of B cells to produce antibodies.

B cell activation is initiated when B cells in the cortex encounter their cognate antigen, altering the balance of chemokine receptors on these cells and causing migration toward the T cell zone (**Figure 2.1D**). Simultaneously, helper $CD4^+$ T cells with the same antigen-specificity migrate toward the B cell zone following activation by DCs. B cells are activated at the edge of the cortex by these helper $CD4^+$ T cells, then move back into the cortex and proliferate to form a germinal center (GC). In GCs, the affinity of the proliferating B cell for the cognate antigen is increased through interaction with resident FDCs that deliver survival signals to B cells that strongly bind antigens presented by FDCs. These processes involve somatic mutation and affinity maturation and are detailed in recent reviews [27, 28]. The result of these events is the differentiation of B cells to plasma cells that migrate to the periphery and bone marrow to secrete high affinity, antigen-specific antibodies that enter blood and peripheral tissue.

2.2.4 The LN microenvironment actively impacts the development of immunity or tolerance

One of the fascinating developments over the past decade has been the realization that stromal components of LNs and other SLOs not only serve a structural function, but also actively promote immunity or tolerance. For example, in the absence of antigen and activating signals, T and B cell zones are maintained in a segregated arrangement (**Figure 2.2A)** [29]. In contrast, during generation of adaptive immunity, the LN rearranges to promote specific types and durations of interactions between APCs, T

cells, and B cells (**Figure 2.2B**) [29]. The FRC network and other stromal components support interactions such as these through production of ECM components, transport of antigens and signaling molecules (*e.g.*, chemokines and cytokines), and establishment of conduits through which lymphocytes travel. Recent studies also illustrate that lymphocytes migrate toward discrete microdomains of LNs during inflammation and immunity compared with migration during tolerance. These effects also correlate with up regulation and down regulation of specific stromal components such as laminins [12]. Thus, the combinations of antigens and immune signals present in LNs, along with the specific organization of these tissues, help determine the types of immune responses that develop systemically. Below we discuss how biomaterials offer new ways to control these parameters to promote stimulatory immune responses (i.e., immunity), as well as to regulate or redirect response toward immune tolerance.

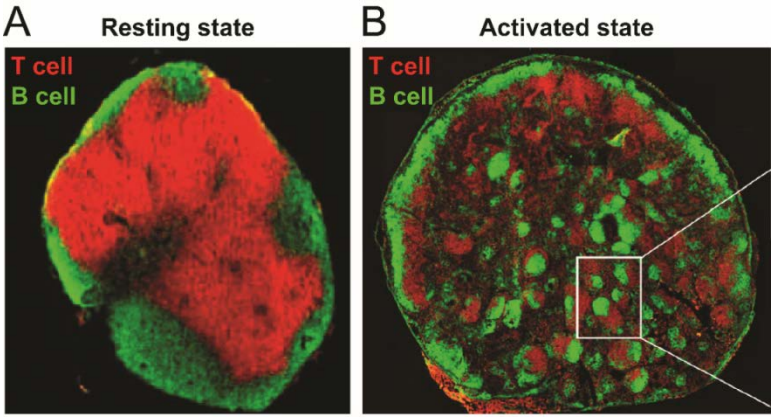

Figure 2.2: LN reorganization during generation of adaptive immune response.
(A) A LN in a resting state with distinct B cell and T cell zones. (B) After activation with antigen and a strong adjuvant (Complete Freund's Adjuvant), the LN microenvironment rearranges to promote intermingling of B cell and T cell zones and formation of GCs. Adapted with permission [29].

2.3 Biomaterials exhibit material properties that activate immune pathways

The physicochemical properties of biomaterials can act as intrinsic immune signals that help shape immunity. Some of the properties which have been studied along these lines – reviewed in [15-17] – include molecular weight, surface chemistry, and particle shape and size. This body of work has demonstrated that biomaterial properties alter lymphatic transport, DC uptake and activation, activation of inflammatory pathways (*e.g.*, toll-like receptors, TLRs; inflammasomes), and secretion of signaling proteins called cytokines [22, 30-43]. For example, carriers such as poly(lactic acid-co-glycolic acid) (PLGA) and polystyrene have been shown to activate the immune system through inflammasome signaling even in the absence of other immune signals or adjuvants – agents added to vaccines to enhance immune response [44-46]. Since synthetic biomaterials such as PLGA or naturally occurring biomaterials like chitosan are becoming ubiquitous in the design of vaccine and immunotherapy carriers, understanding the link between material properties and immune response could allow more rational design of materials that serve not only as carriers, but also as agents that actively "tune" immune responses to combat infectious diseases, cancer, or autoimmunity. Thus this review focuses on the impact of biomaterials on LN organization and function to promote immunity or to regulate immune response (tolerance). Emphasis is also placed on highlighting new approaches reported in the last several years. **Table II** summarizes the examples presented below that investigate NPs and other biomaterial-based vaccines to help control the structure and function of LNs and other SLOs.

Table 2.2: Examples Demonstrating the Impact of Biomaterials on LN Function

Setting	Biomaterial	Functional impact on lymph node	Ref.
Immunity	Poly (lactic acid-co-glycolic acid)/polystyrene	Inflammasome activation and increase in IL-1β secretion	[44, 45]
Immunity	Chitosan/Heparin	Increase in GC formation compared to soluble TNF	[47]
Immunity	Pluronic-stabilized poly(propylene sulfide)	Targeting of tumor-draining LN; delivery of vaccines overcame immunosuppressive tumor environment by activating DCs and increasing the $CD8^+$ T cells to T_{REG} ratio	[48, 49]
Immunity	Lipid vesicles and micelles	Effective drainage to LN sinuses and increased uptake by APCs leading to increased antigen-specificity and cytokine secretion	[40]
Immunity	ICMVs	Trafficking to LN-resident macrophages and DCs in SCS; Induces GC formation resulting in long lasting, high avidity antibodies	[50-52]
Immunity	PLGA with Adjuvants/OVA	Adjuvant-loaded NPs synergistically increase antibody-mediated immunity through creation of GCs and high avidity antibodies	[53]
Immunity	Lipid stabilized PLGA	Increased antigen specific CTLs and antibody production caused by local depot effect in LNs	[54, 55]
Tolerance	Poly(lactic-co-glycolic acid)	Trafficking to LNs; preferential uptake by macrophages and DCs; increases DC activation and $CD4^+$ helper T cell proliferation; upregulation of PD-L1; induction of antigen-specific $FoxP3^+$ T-cells	[17, 56-60]
Tolerance	Liposomes	Uptake by LN-resident APCs leading to expansion of T_{REGS} specific for self-antigens included in liposomes	[61]
Tolerance	Iron oxide	Expansion of low avidity T_{REGS} in and around LNs that suppress antigen presentation by APCs and directly kill APCs	[62]
Tolerance	Polystyrene beads	Support antigen presentation to DCs leading to inactivation of antigen-specific $CD4^+$ T-cells; reduction of $CD4^+$ and $CD45^+$ cell infiltration into CNS; reduction in antigen-specific inflammatory T-cell proliferation	[63]

Table 2.2: Examples Demonstrating the Impact of Biomaterials on LN Function *(cont.)*

Setting	Biomaterial	Functional impact on lymph node	Ref.
Tolerance	Poly(ethyleneimine)	Trafficking to follicular and marginal zones of LNs; promotes interactions between DCs and T cells with regulatory characteristics	[64]
Tolerance	Poly(ethylene glycol) and poly(lactide)	DCs and T-cells modified by particles drain to LNs, reducing the number and proliferative capacity of effector T cells; increase T_{REGS} in LNs; decrease IFN-γ-producing cells	[60, 65, 66]

2.4 The interactions of biomaterials in LNs can be exploited to enhance immunity

Biomaterials provide a unique platform for vaccination and immunotherapy. Interestingly, these materials can mimic some features of clinically-approved adjuvants (*e.g.*, alum), for example, by condensing or encapsulating antigen or other immune signals into particulate structures with sizes ranging from tens of nanometers to several microns. This size range allows efficient uptake by APCs. Biomaterials can also be used to passively or actively target immune tissues such as LNs. Lastly, these materials allow co-delivery of multiple cargos (*e.g.*, antigen, adjuvant, drug) and controlled release of vaccine and immunotherapy components. This last feature of co-delivery is becoming increasingly important in modulating the types of responses that are generated for a specific vaccine or therapy. The sections below will provide specific examples of how these properties are being harnessed to enhance "traditional" immune responses aimed at arming the body to destroy infectious pathogens or cancer.

2.4.1 Particle size helps determine the trafficking and retention of biomaterials in LNs

Both traditional (i.e. soluble) and biomaterials-based vaccine components must reach LNs to generate adaptive immune responses. Several groups have carefully controlled the size of NPs and other vaccine carriers to passively target LNs and the DCs residing in these tissues. For example, by altering particle size, the effectiveness of drainage through the lymphatics and the retention time within LNs can be changed. In studies conducted by Reddy *et al.*, poly(propylene sulfide) NPs with defined sizes were injected intradermally into the tail of mice and the particle drainage through the lymphatics to LNs was monitored [22, 67]. 20nm and 45nm particles drained effectively through lymphatic vessels to the LNs, while 100nm particles largely remained at the injection site. Additionally, 20nm particles were preferentially taken up by LN-resident macrophages and DCs. These particles were also retained in LNs for more than 4 days [67]. A related study demonstrated that the surface chemistry of NPs increased DC activation and antigen-specific T cell responses in LNs, underscoring that both physical and chemical properties of materials play a role in skewing immune function [22].

The route of injection also helps define if and how NPs of a given size will reach LNs. For example, injection of 90nm virus-like particles via multiple different injection routes (*e.g.*, subcutaneous, intraperitoneal, intramuscular, intradermal) resulted in unique particle drainage patterns to the inguinal, lumbar, popliteal, and sciatic LNs [68]. Notably, intradermal injections resulted in NPs localized in the SCS

of the sciatic and popliteal LNs, supporting the hypothesis that these relatively small diameter NPs were transported via lymphatic vessels to the LNs. As opposed to larger particles trafficked to LNs by APCs, these smaller particles drain freely to the LNs through the afferent lymphatics and can then be scavenged by SCS-resident APCs (*e.g.*, macrophages). Thus, by controlling the injection route and size of NPs or MPs, the domains that these materials reach in LNs can be controlled. This strategy provides a route to design vaccines that specifically target APCs within LNs for phagocytosis, or that are small enough to penetrate deeper into other domains (*e.g.*, T cell zone).

Though there are only a handful of approved – or nearly approved – adjuvants in the United States and European Union developed over the last century, in a sense, these agents are the original biomaterial-based vaccine components. One of the most widely used is aluminum salts (alum), and others include emulsions (MF59 and AS03), liposomes (AS01), and synthetic DNA and RNA sequences (PolyIC and CpG). Though there is still some debate as to the mechanism by which alum or other adjuvants enhance vaccination, these materials often persist at the injection site to serve as a depot (i.e., "controlled" antigen release) and increase antigen phagocytosis and presentation that enhances DC activation [2]. In a direct comparison of alum with poly(lactic acid) (PLA) MPs, intramuscular immunization with either PLA or alum promoted antigen-specific antibodies. Interestingly, PLA MPs increased expression of MHC-I and MHC-II molecules on DCs, while alum only increased MHC-II expression [46]. This finding suggests particle-based vaccines may generally enhance

antigen cross-presentation – a process by which DCs can present phagocytized antigens in MHC-I molecules to enhance $CD8^+$ T cell-mediated adaptive response instead of MHC-II molecules which is the traditional route for phagocytized antigens. In addition to particle size, recent studies have investigated the role that the geometry of vaccine carriers plays in immunogenicity. These studies demonstrate that the shape and aspect ratio of synthetic carriers play an important role in modulating T cell activation [41]. Thus, future vaccines could combine the rational selection of properties such as size or shape with targeting or controlled release of multiple antigens, adjuvants, or immune signals.

2.4.2 Molecular markers can be used to effectively target LN-resident cells

In addition to passive targeting by size, LNs and LN-resident cells are being actively targeted by conjugating NPs and MPs with specific ligands or receptors. One of the molecules that has been targeted is DEC-205 (CD205), a transmembrane protein found primarily on DCs. Monoclonal antibodies specific to DEC-205 have been used to decorate acid-degradable polymer and liposome vaccines loaded with model antigens (*e.g.*, SIINFEKL from ovalbumin) and B16-melanoma antigens [69, 70]. Treatment of mice with anti-DEC-205 particles increased the amount of vaccine present in DCs residing in the inguinal LN following subcutaneous immunization, and in the popliteal LN following a footpad injection. When administered with LPS or IFN-γ to activate DCs, this increase in vaccine accumulation in the LNs correlated to increases in splenic cytotoxic T lymphocytes. Following an intravenous melanoma challenge, the number of tumors in the lungs decreased in mice treated with anti-

DEC-205 particles compared to control particles conjugated to an irrelevant targeting peptide. This approach demonstrates the promise of actively-targeting biomaterials to specific LN-resident populations to enhance systemic adaptive immune responses.

Liu *et al.* recently used albumin as a shuttle to direct lipid-based vaccines to LNs [40]. Albumin is a serum protein that serves to transport fatty acids from the blood into lymphatics and to LNs. To exploit this pathway, lipids containing an albumin binding domain made from a diacyl tail were conjugated to peptide antigens and CpG - a TLR9 agonist that activates TLR pathways triggered by non-mammalian DNA (*e.g.*, from bacteria) (**Figure 2.3A**). These materials are able to self-assemble into micelles when placed in aqueous solution due to the hydrophobic diacyl lipid tail. Following subcutaneous injections in mice, albumin-targeted micelles efficiently drained to axillary and inguinal LNs, while formulations with low albumin binding domains were not effectively trafficked to LNs. Interestingly, by altering the length of a polyethylene glycol (PEG) spacer or increasing the number of carbons in the lipid backbone, vaccine accumulation in the draining LNs could be controlled (**Figure 2.3B**) [40]. Mechanistic studies revealed that micelle stability played a crucial role in how these materials were trafficked to LNs. Micelles were stabilized with guanine repeat units. Stabilization with four or more guanine repeats (Lipo-G4-CpG) did not support trafficking of micelles to LNs, whereas reversible (i.e., non-stabilized) micelles assembled with zero or two guanine repeats (Lipo-CpG and Lipo-G2-CpG, respectively) reached LNs and were co-localized with macrophages and DCs (**Figure 2.3C**). The dependence of LN trafficking on structure suggests that in the micelle

form, albumin is unable to access the binding domain (diacyl lipid tail), preventing albumin-mediated trafficking to LNs. Building on these findings of increased accumulation and retention time of the albumin-binding micelle vaccines in LNs, peptides specific to HPV-derived cervical cancer or melanoma were added to these structures and used to immunize mice after tumor inoculation. In both of these disease settings, a striking increase in antigen-specific $CD8^+$ T cells and functional inflammatory cytokines (IFN-γ and TNF-α) was observed, resulting in tumor regression and prolonged survival in immunized mice. These highly promising outcomes are fundamentally a result of the higher concentrations (targeting) and retention (exposure time) in LNs, important characteristics that motivate the discussion below on the role that duration and concentration of antigen and immune signals in LNs play in driving immunity.

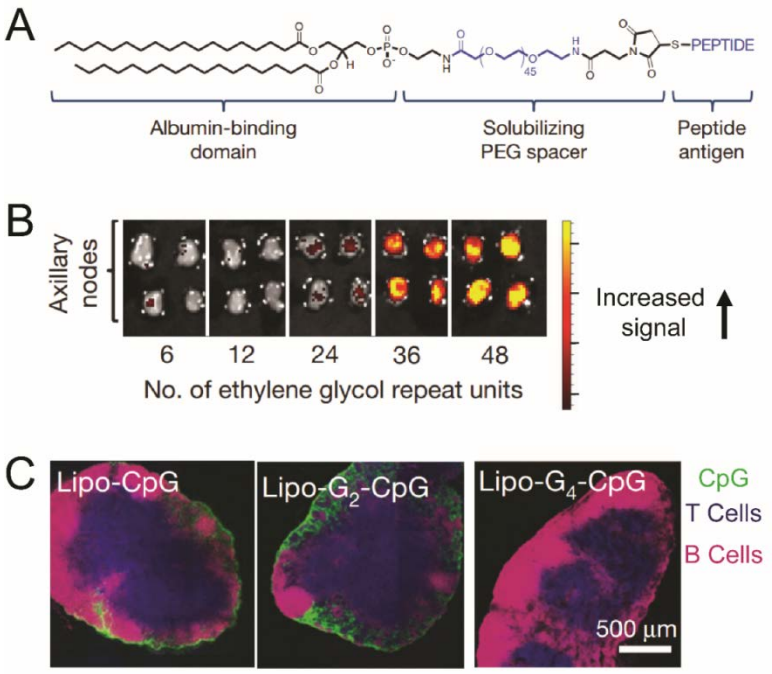

Figure 2.3: Trafficking of lipid-based vaccines depends on material properties.
(A) Schematic of amphiphile structure containing an albumin-binding domain, PEG spacer, and peptide antigen. (B) Excised LNs of mice imaged by IVIS 24h after treatment with fluorescent amphiphiles with increasing PEG spacer length. (C) Immunohistochemical staining of inguinal LNs following treatment with micelles with varying amounts of guanine repeats. CpG (green), T cells (CD3, blue), B Cells (B220, pink). Adapted with permission [40].

2.4.3 The kinetics and concentration of antigen delivery in LNs can be exploited to enhance immunity

An intriguing study by Johansen *et al.* demonstrated that concentration and duration by which antigens, adjuvants, and immune signals reach LNs are just as important as how efficiently these signals reach LNs. In these studies, mice were immunized subcutaneously with soluble antigen and adjuvant using well-defined doses and injection regimens: i) one bolus dose, ii) regularly-spaced, equivalent doses, iii) regular injections with exponentially-decreasing doses, or iv) regular injections with exponentially-increasing doses (**Figure 2.4a**). Across all of these regimens, only mice receiving exponentially increasing doses exhibited significantly increased IFN-γ

secretion by $CD8^+$ T cells (**Figure 2.4b**). Functionally, this effect significantly enhanced antiviral response upon a viral challenge with lymphocytic choriomeningitis virus [58]. These results suggest that the persistence and accumulation of antigen and inflammatory signals is important in inducing effective adaptive immune responses. For this reason, the controlled release properties of biomaterials are, and have been, of great interest for vaccine and immunotherapy applications. As illustrated by several of the examples highlighted in the following sections, these approaches hold great potential to direct response, while also reducing the burden on patients through decreasing the number or frequency of injections and treatments.

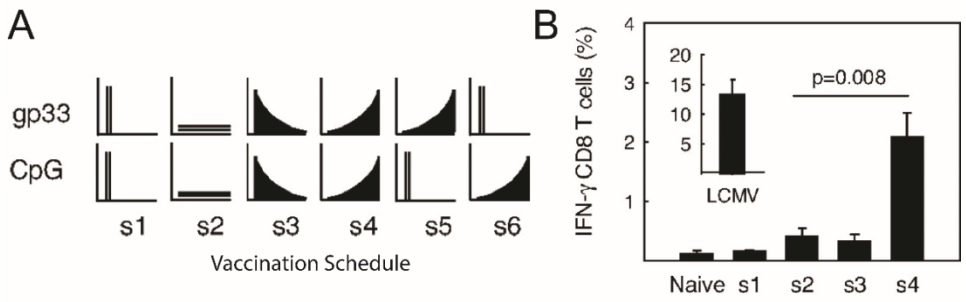

Figure 2.4: Immune signal timing and presence in LNs promotes immunity.
(A) Subcutaneous dosing schedule of mice with antigen (gp33) and adjuvant (CpG). (B) IFN-γ production of $CD8^+$ T cells 8 days after vaccination with the schedule seen in (A) and restimulation of blood lymphocytes with gp33. Adapted with permission [58].

2.4.4 Biomaterials carry immune signals to LNs to promote changes in LN structure and function

As alluded to above, NPs, MPs, and other biomaterials offer a unique opportunity to alter local LN structure, and subsequently, systemic immunity by delivering combinations of antigens and adjuvants. This approach has recently been exploited to

enhance antibody-mediated immunity by promoting GC creation. These microdomains are required for activation and differentiation of B cells into plasma cells that secrete high-affinity antibodies targeting a specific pathogen. One promising example of this strategy is the synthesis of NPs from interbilayer-crosslinked multilamellar vesicles (ICMVs) [50-52]. ICMVs are synthesized by fusing liposomes using divalent cations to form multilamellar vesicles, then crosslinking and PEGylating these structures into 100-300nm particles. ICMVs have been loaded with a range of vaccine cargos including models antigens (ovalbumin,OVA), helper T cell peptides, and antigens for malaria and simian immunodeficiency virus (SIV) gag. Following subcutaneous immunization in mice, ICMVs are retained in the draining LN for over 2 weeks and co-localized with macrophages and DCs of the SCS, suggesting that both drainage via lymphatics and transport after APC phagocytosis contributed to ICMVs trafficking to LNs [50]. Importantly, immunization with ICMVs increases the number of GCs in the draining LNs compared to soluble vaccine formulations (**Figure 2.5A**) [50]. These structures dramatically enhance cell- and antibody-mediated immunity by increasing antigen-specific $CD8^+$ T cells and antigen-specific serum antibody levels, respectively. Mice immunized and boosted subcutaneously with ICMV formulations loaded with malaria antigens (VMP-ICMV) generated high levels of malaria-targeted antibodies compared to vaccination with alum as an adjuvant. Strikingly, this effect persisted for more than 400 days after inoculation [50]. Since GCs formation is integral for high affinity antibody production and strong humoral immune responses, continued development of materials that promote these structures may be particularly

advantageous for parasitic diseases (*e.g.*, malaria) which involve extracellular pathogens that could be bound or neutralized by antibodies. Thus, understanding the link between biomaterial features that are trafficked to particular domains (*e.g.*, SCS, B cell follicles) or support specific interactions or microdomain formation (*e.g.*, GCs) is an important avenue for future research.

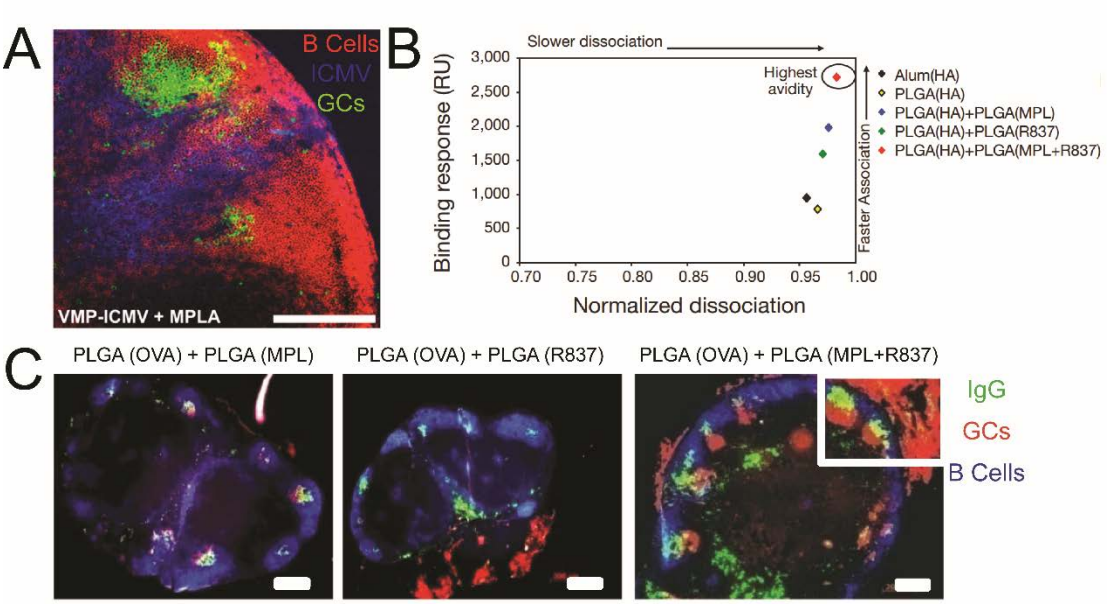

Figure 2.5: Biomaterial vaccines can enhance GC formation and antibody avidity.
(A) Confocal micrograph showing GC formation in draining LN 2 weeks after subcutaneous injection of ICMVs. B cells (red, B220), ICMV (blue), GC (green, GL-7). (B) HA-binding affinity of serum-derived antibodies from mice immunized with biomaterial vaccine formulations 28 days prior. (C) 28 days after immunization, draining LNs were excised and stained for GC formation. GC (red, GL-7), B cells (blue, B220), IgG (green). Panel (A) adapted with permission [50]. Panels (B) and (C) adapted with permission [53].

Several other approaches using conventional or biomaterials-based vaccines have sought to induce GCs by delivery of multiple adjuvants or TLR agonists. The Pulendran lab has studied the effect of NPs loaded with multiple TLR agonists in individual particles compared with co-loading these signals in the same particle [53]. In these studies, GC formation was strongly dependent on the particle loading scheme used to deliver the TLR agonists. Compared with alum, PLGA NPs loaded with OVA

and TLR4 agonist (MPL) or loaded with OVA and TLR7 agonist (R837) increased GC formation in the LNs of mice following subcutaneous injection. Strikingly, mice treated with particles loaded with OVA, along with both TLR4 and TLR7 agonists exhibited a synergistic increase in GCs that also increased the avidity of antibodies (**Figure 2.5B, C**) [53]. TLR4 and TLR7 pathways detect bacterial polysaccharides and viral RNA, respectively. Thus, triggering both of these pathways may enhance B cell (TLR4) and T cell (TLR7) activation, as well as generally increase DC functions such as antigen presentation and co-stimulation. The effects of this more robust activation of immune pathways may help inform the design of future materials that contain multiple immune cues.

Recently, vaccines composed of chitosan and heparin have been used to mimic specialized molecules called granules [47]. Granules are stable particles secreted by specialized immune cells (mast cells) in response to a range of stimuli that can include pathogen recognition. These particles contain pro-inflammatory cytokines such as TNF-α that promote local inflammation. Following footpad immunization with antigen-loaded NPs designed to mimic granules, NPs localized to the SCS in LNs of mice and increased the number of GCs. The resulting enhancement to antibody-mediated immunity increased the survival of mice during a lethal flu challenge. Interestingly, empty particles without cytokines also caused a modest increase in GCs [47]. This effect emphasizes the theme that biomaterials can enhance immunity through both the properties they provide (*e.g.* targeting, co-delivery,

controlled release), as well as stimulatory pathways activated by the structural features of these materials.

2.4.5 NP vaccines can break tumor tolerance through local changes in tumor-draining LNs

The examples highlighted thus far share the aim of generating effective immune responses against foreign pathogens. However, another prominent goal of biomaterials-based vaccines and immunotherapies is centered on treating cancer. Cancer cells and the tumor microenvironment exhibit a number of characteristics that hinder the ability of the immune system to fight cancer [71]. Notably, effective treatments must generate robust responses against antigens overexpressed on tumors, allow efficient homing of immune cells to tumors, maintain the function of tumor-primed immune cells in the immunosuppressive tumor environment, and generate tumor-specific memory cells that quickly destroy nascent tumor cells to prevent relapse. This a daunting set of challenges, but combination therapies leveraging biomaterials and the immune system offer many features that could help address these hurdles. Kwong *et al.* have created liposomes containing both a PEG/CpG lipid that was conjugated via lipid insertion and anti-CD40 antibodies that were added via maleimide chemistry. When these materials are injected into solid tumors, the liposomes drain to nearby LNs and remain in LN sinuses [72]. This persistence causes a local adjuvant effect in LNs for at least 48 hours that allowed for a majority of LN-resident APCs (DCs and macrophages) to uptake the particles containing CpG, resulting in prolonged survival of mice during tumor challenge compared to PBS

controls. Additionally, while soluble treatments caused a bimodal effect of further increasing survival in some mice compared to the liposomes and causing earlier death in others, liposomal delivery reduced systemic toxicity by decreasing adverse side effects such as weight loss and inflammatory cytokines (IL-6) in blood [72].

Stephan *et al.* approached cancer immunotherapy with biomaterials by modifying the surface of T cells with liposomes or polymeric NPs loaded with cytokines or adjuvants. This approach employed biocompatible thiol chemistry to conjugate these materials to cells without altering key T cell functions (*e.g.*, proliferation, antigen recognition) [73]. Importantly, tumor specific $CD8^+$ T cells modified with NPs then injected into mice maintained the ability to home to tumor cells, carrying particles and cargo to these sites. This unique approach allowed efficient delivery of cytokine-loaded NPs to melanoma tumors and resulted in rapid proliferation of tumor-specific $CD8^+$ T cells in LNs. Mechanistically, T cells conjugated with NPs polarized $CD8^+$ T cells toward a central memory phenotype which is more effective at breaking tumor immunosuppression. Thus, mice treated with these tumor-specific T cells modified with NPs eradicated tumors, while untreated mice and mice treated with soluble drugs and T cells all succumbed.

Jeanbart *et al.* recently exploited preferential drainage of 30nm poly(propylene sulfide) (PPS) NPs in tumor-draining LNs and distal LNs (i.e., non-draining) for cancer therapy [48]. This work revealed that tumor-draining LNs were enlarged compared to distal LNs. DCs and $CD8^+$ T cells in tumor-draining LNs also expressed

high levels of PD-L1 and PD-1, respectively. Binding of PD-1 on $CD8^+$ T cells to the cognate ligand (PD-L1 on APCs), negatively regulates T cell proliferation and pro-inflammatory cytokine secretion, leading to suppression of T cell function. This suppression supports tumor growth during cancer. In these studies, it was shown that while the tumor-draining LN was immunosuppressed, these tissues also contained more antigen specific T-cells, likely due to the proximity to the tumor [48]. Building on this observation, PPS NPs were conjugated with CpG and mixed with antigen-loaded NPs, then injected intradermally into the footpads of mice. NPs containing CpG and tumor antigen (TRP2) or a model antigen (OVA) were injected in the footpad on the same side as tumor induction. This approach resulted in targeting of NPs to the tumor draining LN. Mice treated in this manner with NPs containing CpG and TRP2 or OVA reduced tumor growth in a melanoma model and in an OVA-expressing lymphoma model. These improvements also correlated with an increase in $CD8^+$ T cells specific for the corresponding antigens. Targeting the tumor-draining LN also led to a decrease in the number of immunosuppressive cells (*e.g.*, T_{REGS}) compared with mice injected on another limb to target the non-tumor draining LN [48]. A related study employed similar NPs co-loaded with CpG and Paclitaxel – a powerful chemotherapeutic – to create a multi-functional cancer therapy [49]. Together, these studies highlight the impact of local delivery on efficacy, with particles reaching tumor-draining LNs providing a significantly improved outcome compared with particles targeted to non-draining LNs. As discussed earlier, once NPs reach LNs, there are also opportunities to direct immunity by delivering multiple

signals or by controlling the release of antigens, adjuvants, and other signals. Below, new direct approaches to achieve LN delivery are discussed.

2.4.6 Intra-lymph node injection allows direct targeting and local engineering of the LN environment

Building on the idea that the kinetics and combinations of immune signals delivered to LNs play an integral role in the development of cell-mediated and antibody-mediated immunity, an intriguing area of fundamental and clinical research has focused on direct injection of vaccines to LNs. In humans, intra-LN (*i.LN.*) injection generally involves injection of soluble vaccine components to LNs using ultrasound guidance, whereas preclinical studies in mice utilize tracer dyes or surgical procedures to access the LN for injection [54, 55, 74, 75]. Several important papers from the Kündig lab describe clinical trials demonstrating that *i.LN* injection can safely promote tolerance to allergens while dramatically reducing both the cumulative treatment dose and the treatment time [75, 76]. These fundamental discoveries support the use of *i.LN.* delivery as a route for generating potent immune response with staggeringly small doses. This approach is particularly attractive for therapeutic applications, and has nucleated a number of additional recent and ongoing clinical trials for chronic conditions, cancer, and allergies [58, 74, 75, 77-85]. For example, patients immunized *i.LN.* with a vaccine against grass pollen became tolerized after 3 injections over 8 weeks compared to the 54 injections over 3 years when treated with subcutaneous immunization [75]. Strikingly, the overall dose needed to evoke this tolerance was more than 1000x lower using *i.LN.* injections compared with

conventional vaccination routes. In a similar study, tolerance to a cat dander allergen was achieved after 3 *i.LN.* injections and this tolerance persisted for more than 300 days [76]. While *i.LN.* injection may be less suited for wide-spread prophylactic vaccination due to the need for ultrasound guidance and a trained administrator, this is an intriguing idea for therapeutic vaccines and immunotherapies that rely on delivery of several vaccine components to LNs. However, many of these approaches employ multiple injections, or multiple cycles of injections to increase the frequency or duration of exposure to antigen. Thus, coupling *i.LN.* injection with biomaterials could further enhance the performance of new therapeutic vaccines and immunotherapies while reducing the dose, number, or frequency of injections.

Along these lines, Mohanan *et al.* tested the delivery of common particle formulations (*e.g.*, liposomes, NPs) along intradermal, intramuscular, subcutaneous, and *i.LN.* routes. The response to particles laden with OVA antigen or OVA and adjuvants was then assessed by antibody titers and cytokine secretion across injection routes. Formulations injected *i.LN.* resulted in the highest antigen-specific IgG2a antibody titers regardless of whether or not a TLR agonist (CpG, TLR9) was present in particles. This approach also increased the secretion of INF-γ from splenocytes in the presence and absence of adjuvants [86].

Jewell *et al.* developed a non-surgical route for enhancing cell-mediated and antibody-mediated immunity by *i.LN.* injection with lipid-stabilized polymer particles loaded with adjuvant [54, 55]. In this study, lipid-coated NPs or MPs loaded with the

TLR3 agonist poly(inosinic:cytidylic acid) (PolyIC) were injected with OVA antigen into the muscle or into the inguinal LNs of mice (**Figure 2.6A**). MP formulations were retained in the LN as 'depots' for at least 4 days, while soluble vaccine formulations were quickly cleared. The increased retention of MPs also controlled release and drove accumulation of PolyIC within the LN and in LN-resident APCs, resulting in more enduring activation of DCs (**Figure 2.6B**) [54]. These effects potently expanded antigen-specific $CD8^+$ T cells circulating in blood one week after receiving a single *i.LN.* injection, an effect that was not observed with soluble vaccine formulations (**Figure 2.6C**). Mice immunized with MPs also developed strong antibody responses (**Figure 2.6D**), demonstrating promotion of both cell-mediated and antibody-mediated immune responses. $CD8^+$ T cells from MP-immunized mice also exhibited larger, more robust cytokine secretion, and all of these trends persisted for at least 6 weeks without boosting. Interestingly, NPs also increased the number of antigen-specific $CD8^+$ T cells and the level of cytokines secreted from these cells compared with soluble vaccines, but at levels lower than those observed in mice vaccinated with MPs [54]. This effect was a function of vaccine retention in LNs, with NPs exhibiting a retention time intermediate between the quick-draining soluble formulations and the well-retained MP vaccine depots. Thus, delivery of controlled release depots in LNs mimics the accumulating dosing schemes discussed earlier (**Fig. 2.3A**) for soluble vaccines and with *i.LN.* clinical trials, but with fewer or less frequent injections [58]. Such approaches could also help ensure that each component of multifunction vaccines reaches LNs with the correct combinations, doses, or release kinetics.

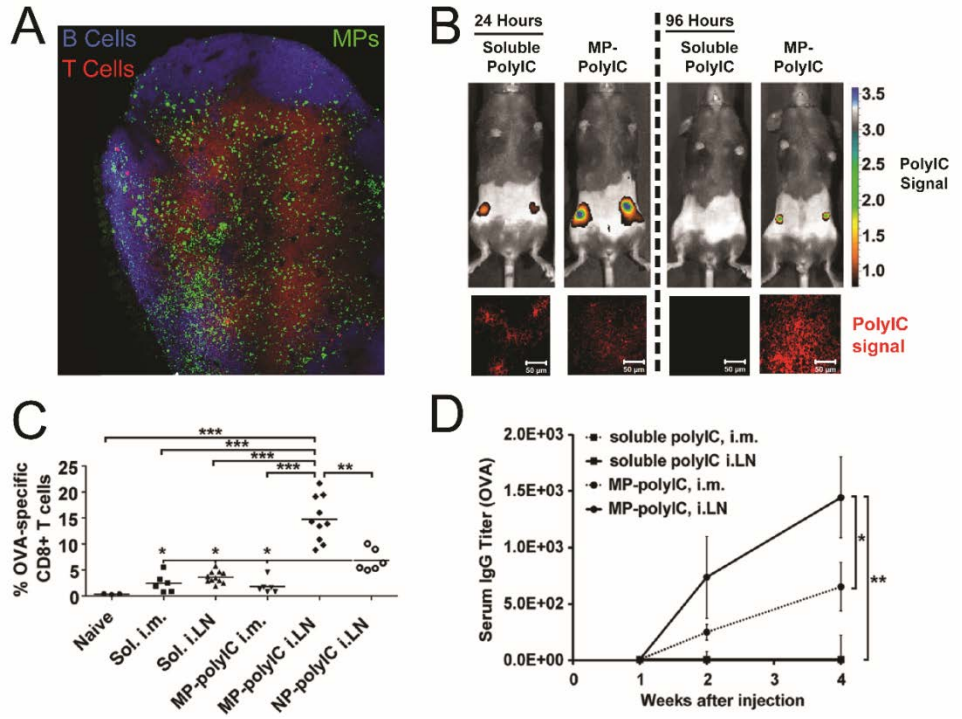

Figure 2.6: MP depots promote cell-mediated and antibody-mediated immunity after *i.LN.* injection.
(A) Representative image of inguinal LN following *i.LN.* injection of fluorescent MPs. B cells (blue, B220), T cells (red, CD3), MPs (green). (B) PolyIC signal measured *in vivo* (top) and histological sections of excised LNs (bottom) showing PolyIC signal 24 hours and 96 hours after *i.LN.* injection. (C) OVA-tetramer staining showing percent of blood $CD8^+$ cells specific to OVA 7 days after intramuscular or *i.LN.* injections. (D) OVA-specific IgG serum titers after intramuscular and *i.LN.* immunization with soluble or MP formulations. Adapted with permission [54].

2.5 Biomaterials can alter LN function to promote immune tolerance

The examples discussed thus far have used biomaterials to promote stimulatory or inflammatory immune responses for vaccination against pathogens or cancer. However, in the past few years, enormous progress has been made in harnessing biomaterials to regulate dysfunctional or unwanted immune reactions. Many of these detrimental reactions occur in autoimmune diseases such as multiple sclerosis, diabetes, rheumatoid arthritis, and lupus, as well as in the rejection of tissue grafts

and organ transplants. In multiple sclerosis for example, myelin – the protein that insulates neurons in the central nervous system (CNS) – is incorrectly recognized as foreign by lymphocytes and antibodies [87-89]. This recognition leads to infiltration of these cells and molecules into the CNS, resulting in inflammation and destruction of myelin, and ultimately, neurologic decline. As with the generation of immunity against foreign antigens in healthy individuals, T cells and antibody-producing B cells recognizing self-antigens are also expanded in LNs by APCs presenting these self-molecules. Thus, biomaterials have recently been applied to autoimmunity to stop these reactions by destroying (deletion) or inactivating (anergy) pathogenic cells, or by expanding specialized regulatory T cells (T_{REGS}) which are able to suppress lymphocytes reactive against self-molecules such as myelin. Broadly speaking, these regulatory mechanisms all contribute to immune "tolerance", a state in which the immune system does not attack, or no longer attacks, a particular peptide, protein, or cell type. One of the greatest challenges facing new therapies for autoimmunity is the induction of self-antigen specific tolerance that prevents harmful self-reactions without impairing the rest of the immune system. This side effect is a persistent problem with many of the drugs currently used to treat patients with autoimmune disorders: lifelong treatment regimens with broad immunosuppressants are vital to manage disease, but cause patients to be immunocompromised. In this section, we will highlight some of the ways in which the interactions between biomaterials and LNs or LN-resident cells are being harnessed to promote tolerance. While the discussion below is focused on the connection between biomaterials and LNs to promote tolerance, several recent reviews provide additional perspective on

opportunities to apply biomaterials to autoimmune diseases and tolerance [15, 17, 90].

2.5.1 Particles can carry regulatory signals to LNs to alter the interactions of APCs and lymphocytes

One of the most fundamental ways in which biomaterials can be harnessed to promote tolerance is as a carrier of drugs or other immune signals to LNs or other immunological sites [57, 61, 62, 91-97]. In LNs, these cargos can influence the interactions and functions of LN-resident cells, in similar ways to those exploited to promote stimulatory responses or immunity. PLGA NPs for example have been loaded with mycophenolic acid (MPA), an immunosuppressant used in transplants [57]. Systemic injection of these particles resulted in drainage to the spleen and LNs, where particles were preferentially taken up my macrophages and DCs. During transplant studies, APCs in the LNs of mice treated with particles exhibited elevated levels of PD-L1 (inhibitory ligand) that limited the ability of APCs to prime T cells reactive against antigens expressed on the tissue grafts. Thus, MPA-loaded particles draining to LNs delivered signals that impaired the ability of APCs to expand graft/self-reactive T cells, resulting in tolerance that improved graft survival [57].

The ability of biomaterials to co-deliver multiple cargos has also been exploited to regulate the function of APCs in LNs. In these studies, liposomes were loaded with a self-antigen that is recognized as foreign in mouse models of arthritis, along with a small molecule inhibitor of NF-κβ, a protein complex that controls inflammation and

that is over-expressed in many chronic inflammatory diseases (i.e., arthritis) [61]. Uptake of liposomes by LN-resident APCs reduced NF-κβ levels and the proliferation of self-reactive T cells, leading to reduced severity of arthritis. These effects were achieved in part through the expansion of T_{REGS} in mice treated with the liposomes [61]. Importantly, the T_{REGS} generated in this study were specific for the self-antigens included in the liposomes, emphasizing the goal stated earlier: inducing tolerance against specific self-antigens, without broad suppression of normal immune functions.

One intriguing approach being developed to promote antigen-specific tolerance is based on design of NPs decorated with complexes of self-antigen loaded in MHC molecules [62]. As discussed earlier, MHCs are the complexes APCs load antigens into for presentation to lymphocytes, along with costimulatory signals. Presentation of antigen in MHCs without co-stimulation can cause T cells to become inactive or promote regulatory functions. In this study, iron oxide NPs were functionalized with complexes of MHC and self-antigens associated with disease in type 1 diabetes (T1D), without co-stimulatory signals [62]. Treatment of prediabetic or diabetic mice with NPs resulted in expansion of a pool of low avidity (i.e., weakly binding) regulatory T cells in and around LNs near the pancreas – the organ destroyed by self-reactive immune cells in diabetes. These cells suppressed antigen presentation by APCs in these LNs, as well as exhibited direct APC killing in the pancreatic LNs (PLN) compared with LNs remote from the pancreas (MLN) (**Figure 2.7A**) [62]. The decrease in APC numbers and activation levels prevented expansion of self-reactive T

cells that otherwise could have migrated to and attacked the pancreas. The effects of this treatment were striking, maintaining and restoring control of blood glucose in mouse models of T1D when mice were treated with MHC/NP complexes loaded with T1D antigens, but not when mice were treated with MHC/NP complexes loaded with irrelevant antigens or following injection of soluble T1D antigens (**Figure 2.7B**) [62]. Thus, the examples in this section underscore the potential of NPs to deliver drugs and immune signals to alter the interactions of APCs and lymphocytes in LNs during inflammation and autoimmunity.

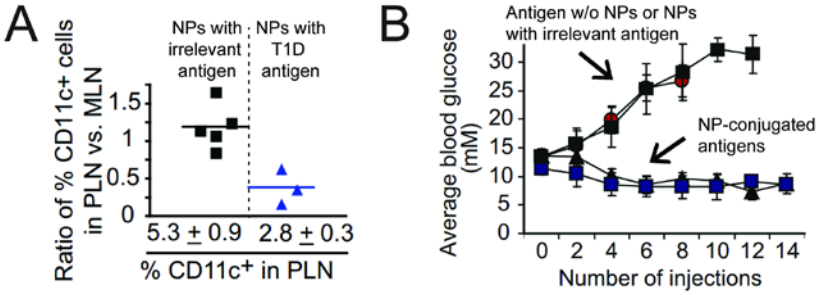

Figure 2.7: NPs decorated with self-antigen loaded MHC induce DC death and regulate diabetes. (A) NPs decorated with MHC molecules specific to T1D are able to reduce the ratio of $CD11c^+$ DCs in the pancreatic LN (PLN) to distal LNs such as the mesenteric LN (MLN) compared to peptide MHC NPs loaded with an irrelevant antigen control. (B) Mice with T1D treated with NPs conjugated with MHC/diabetes antigen complexes maintain normal blood glucose levels compared to treatments with soluble peptide or peptide MHC complexes loaded with irrelevant antigens. Adapted with permission [62].

2.5.2 Association of cargo with biomaterials can alter antigen trafficking to promote tolerance

Another set of approaches recently harnessed to generate tolerance with biomaterials exploits the differences in the mechanisms by which soluble and particulate antigens are trafficked in LNs and spleens. Whereas relatively low molecular weight soluble antigens are dispersed throughout SLOs (i.e., LNs, spleen) by the stromal conduits,

macrophages and other APCs in the SCS engulf and process larger particles to support presentation of antigenic fragments from these materials. These differences have been exploited to promote antigen-specific tolerance by conjugating 500nm polystyrene beads (PSB) or PLGA particles with a myelin peptide (MYE) – the self-antigen attacked by the immune system in MS [63, 98]. Following *i.v.* injection, antigen-conjugated particles drained to the spleen and were localized to macrophages expressing the scavenger receptor MARCO, whereas free antigen was not (**Figure 2.8A, B**) [63]. The MARCO receptor plays an important role in clearing apoptotic cell debris – processes that normally occur without inflammation. Thus PSB-MYE may support presentation of MYE peptide to APCs in a manner that promotes tolerance (*e.g.*, without co-stimulation). This idea was supported by studies demonstrating that antigen-specific cells in LNs of treated mice exhibited reduced proliferation when challenged with antigen. Treatment with PSB-MYE formulations also effectively treated progressive and recurring models of MS in mice, while treatment with PSBs decorated with irrelevant antigen (PSB-OVA) did not (**Figure 2.8C**). These findings illustrate the antigen-specific nature of tolerance in this system. Mechanistically, this efficacy resulted from increased T_{REG} function, along with reductions in activity of inflammatory T cells (*e.g.*, through anergy/inactivation) [63]. These suppressive effects resulted in reduced lymphocyte infiltration to the CNS and decreased inflammatory cytokines [98].

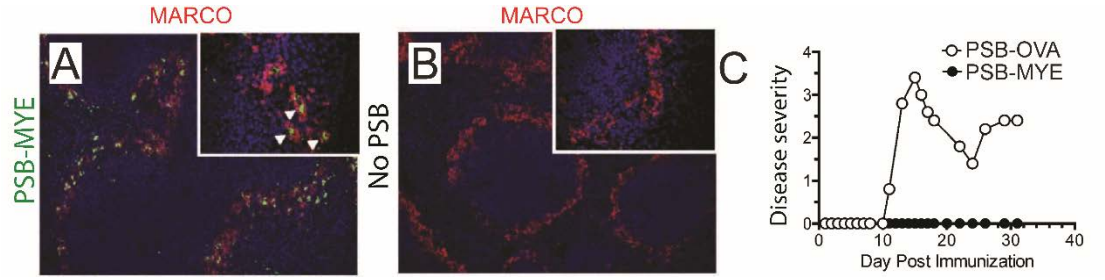

Figure 2.8: Particles targeting the MARCO receptor induce tolerance against a mouse model of multiple sclerosis.
(A) Immunohistochemical staining of spleens following intravenous injection of polystyrene particles conjugated with a myelin peptide (PSB-MYE, green) showing co-localization of particles with MARCO (red) (B) Immunohistochemical staining as in (A) of spleen after treatment without polystyrene particles (No PSB). (C) Disease severity following immunization with PSB-MYE or polystyrene particles conjugated with an irrelevant peptide (PSB-OVA) showing that antigen-specificity is necessary for treatment. Adapted with permission [63].

Approaches related to the PSB strategies have also been applied to other targets including transplantation and inflammatory diseases including colitis, peritonitis, and myocardial infarction [99, 100]. Of note are studies with inflammatory models using particles exhibiting controlled surface charges but lacking specific antigens. These studies have revealed that inflammatory monocytes engulf negatively-charged particles and migrate to the spleen instead of inflammation sites, resulting in apoptosis of these cells and reduced inflammation. Interestingly, neutral particles did not support these therapeutic effects [99]. Thus, this strategy could provide a general, non-antigen specific route for reducing inflammation, and further underscores the role of physicochemical properties in determining the types of immune responses biomaterials elicit. Along these same lines, Broere and colleagues have shown that the response to antigen encapsulated in polymers with different carrier structures alters how LN-resident APCs present and interact with helper T cells in LNs [56, 59]. In particular, PLGA NPs and TMC-TPP (N-trimethyl chitosan-tri-polyphosphate) NPs both increased DC activation and $CD4^+$ helper T cell proliferation in LNs, but

PLGA promoted regulatory function and reduced hypersensitivity reactions while TMC-TPP stimulated antibody responses. Although the mechanisms of these differences are under investigation, potential contributing factors may include size (which could alter how antigen is trafficked in LNs) or the duration over which these particles release antigen [56].

In addition to solid polymer particles encapsulating or displaying antigen, electrostatically-driven condensation of immune signals such as bacterial DNA affects how these components are trafficked within LNs. An approach based on this idea recently revealed that particles formed from bacterial DNA and poly(ethyleneimine) (PEI), a cationic polymer, were rapidly trafficked to the follicular and marginal zones of LNs and the spleen. These complexes stimulated enzyme pathways that promoted DCs and T cells with regulatory characteristics, effects not observed when either PEI or bacterial DNA was administered alone [64]. Together the examples highlighted in this subsection illustrate the potential of designing specific structures or chemistries into biomaterials that can help actively direct how NPs and cargos are trafficked in LNs, as well as to alter the interactions between LN-resident APCs and lymphocytes.

2.5.3 Biomaterials can be used to directly modify cells to exploit regulatory immune pathways

In addition to using particles to transport drugs to LNs, or change how antigens are processed, several recent approaches have directly modified APCs, lymphocytes, or

red blood cells with NPs to promote tolerance or regulate immune response. One group used nanoprecipitation to prepare particles from PEG and poly(lactide) (PLA) conjugated with an immunosuppressant (cyclosporine A, CsA) [65, 66]. CsA-loaded particles were phagocytized by DCs incubated with these carriers *in vitro*, and subsequent injection of these DCs into mice resulted in drainage of the particle-loaded DCs to LNs. These cells locally reduced the number and proliferative capacity of effector T cells in LNs. Other approaches have focused on modification of T cells with, for example, NPs decorated with antibodies specific for the $CD4^+$ molecules expressed on helper T cells [60]. These particles were loaded with leukemia inhibitory factor (LIF) – a cytokine that can promote the development of T_{REGS} – then incubated with donor-reactive cells from the spleens of mice. CD4-targeted LIF-NPs bound $CD4^+$ T cells *in vitro* and transfusion of these cells significantly increased the percentage of T_{REGS} in LNs over 5 days. Thus, modifying T cells with regulatory immune signals can serve as a route to deliver cues to LNs that alter how T cells develop during antigen presentation. This goal of controlling T cell differentiation shares similarities with the work of Stephan, *et al.*, though their approach aimed to generate immunostimulatory responses for cancer therapy by modifying T cells, as discussed earlier [73].

Significant fractions of erythrocytes (i.e., red blood cells) are rapidly produced and destroyed on a daily basis in healthy individuals. In these cases, cell destruction occurs through a non-pathogenic mechanism of cell death, apoptosis [101]. This mechanism does not induce pro-inflammatory immune responses against these cells

owing to natural regulatory mechanisms that clear self-antigens without co-stimulation, or due to activation of suppressive pathways triggered by apoptotic cell debris. This natural tolerance pathway has recently been exploited to generate antigen-specific tolerance against model antigens in disease models of T1D [102]. To conduct these studies, a target antigen (OVA) was conjugated to a peptide (ERY1) that binds glycophorin-A molecules (GYPA) expressed on the surface of erythrocytes (**Figure 2.9A**). *Ex vivo* incubation of ERY1-OVA with mouse erythrocytes resulted in efficient labeling of these cells with the target antigen (**Figure 2.9B, bottom**), whereas incubation of un-modified OVA with red blood cells did not result in cell labeling (**Figure 2.9B, top**). Intravenous injection of cargo-modified ERY1 (*e.g.*, OVA, fluorescent dye) quickly labeled circulating erythrocytes and led to increased trafficking to the spleen and uptake by resident APCs. Mice treated with ERY1-OVA after injection of OVA-responsive transgenic T cells exhibited reduced proliferation of these cells in LNs and in the secretion of inflammatory cytokines (*e.g.*, IFNγ) (**Figure 2.9C**). This idea was also exploited to protect mice from T1D by stimulating proliferation and rapid deletion of self-reactive $CD4^+$ T cells in LNs when mice were treated with ERY1 conjugated to T1D antigens, but not when soluble T1D antigens were administered. Together, these approaches demonstrate that a diverse set of cell modification approaches can alter how APCs and T cells function, as well as harness natural apoptotic clearance and tolerance mechanisms to regulate or redirect inflammatory immune reactions.

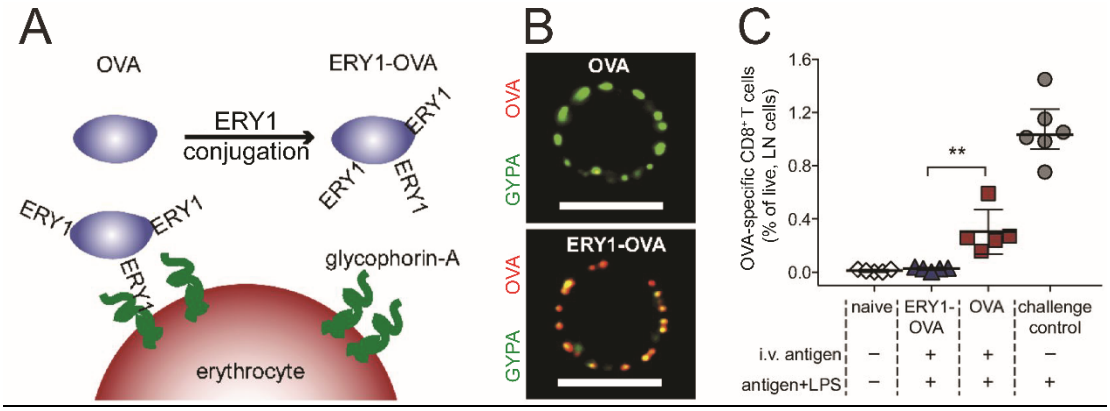

Figure 2.9: Erythrocyte decorating with NPs leads to immune tolerance.
(A) Graphic depicting the conjugation of OVA-NPs to the surface of erythrocytes via ERY1 binding of glycophorin-A. (B) Confocal images showing an erythrocyte treated with soluble OVA (top) and with OVA-NP (bottom). OVA (red) is colocalized with glycophorin-A (GYPA, green). (C) Percentage of antigen-specific $CD8^+$ T cells within the draining LN 4 days after immunization with erythrocytes labeled with OVA-NPs (ERY1-OVA) or soluble OVA. Adapted with permission [102].

2.6 Conclusions and looking forward

Biomaterials have already demonstrated great potential in the field of immunology. In coming years, continuing to improve our understanding of how material properties impact molecular signaling will remain an important issue, as this knowledge will lead to more rational design of vaccines. Employing biomaterials as tools to study new fundamental questions will also provide new opportunities to inform vaccine and immunotherapy design. An exciting avenue of research centers on engineering biomaterials with specific properties that allow for precise interactions with LNs and LN-resident cell populations that effectively modify the structure of these tissues. Some of these questions may also focus on understanding how the kinetics and combinations of immune signals in LNs impact stromal function (*e.g.*, FRC network, laminins), and if these changes can be induced or exploited to direct immunity. Another interesting approach on the horizon is the design of artificial LNs or SLOs

that could locally recapitulate the functions of these tissues, perhaps eliminating the targeting challenges facing many vaccines and treatments. Biomaterials offer unique opportunities to address each of these areas, and the answers to these questions will continue to push the forefront of what may become possible in modulating immune function.

In **Chapter 3**, a common, biodegradable polymer system is used to investigate intrinsic immunogenicity. The form of the polymer (soluble or particulate) as well as other physicochemical properties are explored to determine which features of biomaterials most influence their intrinsic ability to activate the immune system. In particular, these studies focus on how immunogenicity evolves over time, as materials degrade and the physicochemical properties change.

Chapter 3: Intrinsic immunogenicity of rapidly-degradable polymers evolves during degradation[2]

3.1 Introduction

Biomaterials have become important components in many emerging vaccine and immunotherapy strategies. These materials provide cargo protection, controlled release of antigens or immune signals, and targeting of immune cells and secondary lymphoid organs such as lymph nodes (LNs) – key tissues that help coordinate immune function [103-105]. Intriguingly, as mentioned in **Chapter 2**, several recent studies demonstrate that poly(lactic-co-glycolic acid) (PLGA), polystyrene, chitosan, and other polymers ubiquitous in the biomedical field exhibit intrinsic immunostimulatory properties, even in the absence of antigens, adjuvants, or other immune signals [9, 45, 103, 106-109]. Pattern recognition receptors (PRRs) of the innate immune system have the ability to recognize pathogen-associated and danger-associated patterns through Toll-like receptor (TLR) and inflammasome pathways (e.g., nucleotide-binding oligomerization domain-like receptors, Rig-like helicases) [110]. These pathways drive pro-inflammatory caspases and cytokines that many polymers such as PLGA or polystyrene are able to activate. For example, when dendritic cells (DCs) are treated with PLGA or non-degradable polystyrene particles and a TLR agonist (TLRa), these particles cause an increase in expression of surface

[2]Adapted from J.I. Andorko, K.L. Hess, K.G. Pineault, and C.M. Jewell. "Intrinsic immunogenicity of rapidly-degradable polymers evolves during degradation." *Acta Biomater.* 2016, 32, 24-34.

activation markers (e.g., CD40, CD80, CD86) [9, 45, 109]. Many of these important polymers also increase inflammatory cytokines such as IL-1β, a key mediator of the inflammasome that supports early immune responses [9, 45, 110]. Several studies have investigated the link between these types of inflammatory/immunostimulatory processes and physicochemical polymer properties such as molecular weight (MW),[107, 111-114] particle size,[108, 115-117] charge,[118, 119] hydrophobicity,[120] shape,[41, 121, 122] and chemical functionality [123-128]. These studies confirm polymer properties can modulate immune function. Developing a better understanding of these phenomena and how immunogenicity evolves during degradation could support rational design of polymers that serve not only as carriers but also as agents that help direct or tune immune response.

The mechanistic studies above have focused on non-degradable or slowly-degrading polymers such as polystyrene and PLGA, respectively. However, vaccines which allow for tunable, rapid delivery of antigens, adjuvants, or other small molecules offer new potential for modulating the development of specific immune characteristics, for example, by rapidly releasing immune-polarizing drugs during DC activation or T cell expansion. Poly(beta-amino esters) (PBAEs) are cationic, pH-sensitive polymers that degrade over hours to days depending on polymer structure [129, 130]. PBAEs have been used in drug delivery, for DNA and RNA delivery, and as vaccine carriers [131-141]. In the latter case, PBAEs are have been used for DNA vaccination through condensation of nucleic acids encoding plasmid antigens to promote T cell mediated anti-tumor responses, to drive antibody response, or for siRNA immunotherapy to

preferentially target glioblastoma, [142-148]. Although PBAEs are becoming increasingly useful in vaccination and immunotherapy, little is known about if and how these materials elicit intrinsic immunostimulatory or inflammatory effects, and how the rapid degradation of PBAEs or other materials changes the intrinsic immunogenic properties in cells or tissues.

We hypothesized that PBAEs would exhibit intrinsic immunostimulatory effects that change as a function of polymer form (i.e., free, particles) and the extent of polymer degradation (MW). To test this idea, a prototypical PBAE, Poly 1, was synthesized from a four-carbon diacrylate monomer. The ability of this material to activate DCs and T cells in co-culture was then assessed (**Figure 3.1**). Free Poly1 did not activate DCs or drive synergistic responses during co-treatment with a TLRa. Since the immune system has evolved to detect particulate materials and pathogens, we tested if the properties of PBAE particles change during degradation and if these effects impact intrinsic immunostimulatory function. In contrast to free polymer, particles formed from intact Poly1 using electrostatic condensation to mimic a common vaccine formulation method exhibited significant intrinsic immunostimulatory function that decreased with the extent of polymer degradation. These changes corresponded to changing physicochemical properties including increasingly negative particle charges, increased particle diameter, and decreased particle concentration. Mechanistic studies using particles assembled from Poly1 fragments with distinct MWs confirmed this trend, revealing that Poly1 differentially activates immune cells in culture in a manner that is dependent on both the form of the polymer and the MW

(i.e., degree of degradation). These studies confirm the intrinsic immunogenicity of PBAEs and provide insight into how the evolving properties of degradable polymers drive immunogenicity in ways that could support design of new vaccine carriers able to adjuvant or modulate immune function.

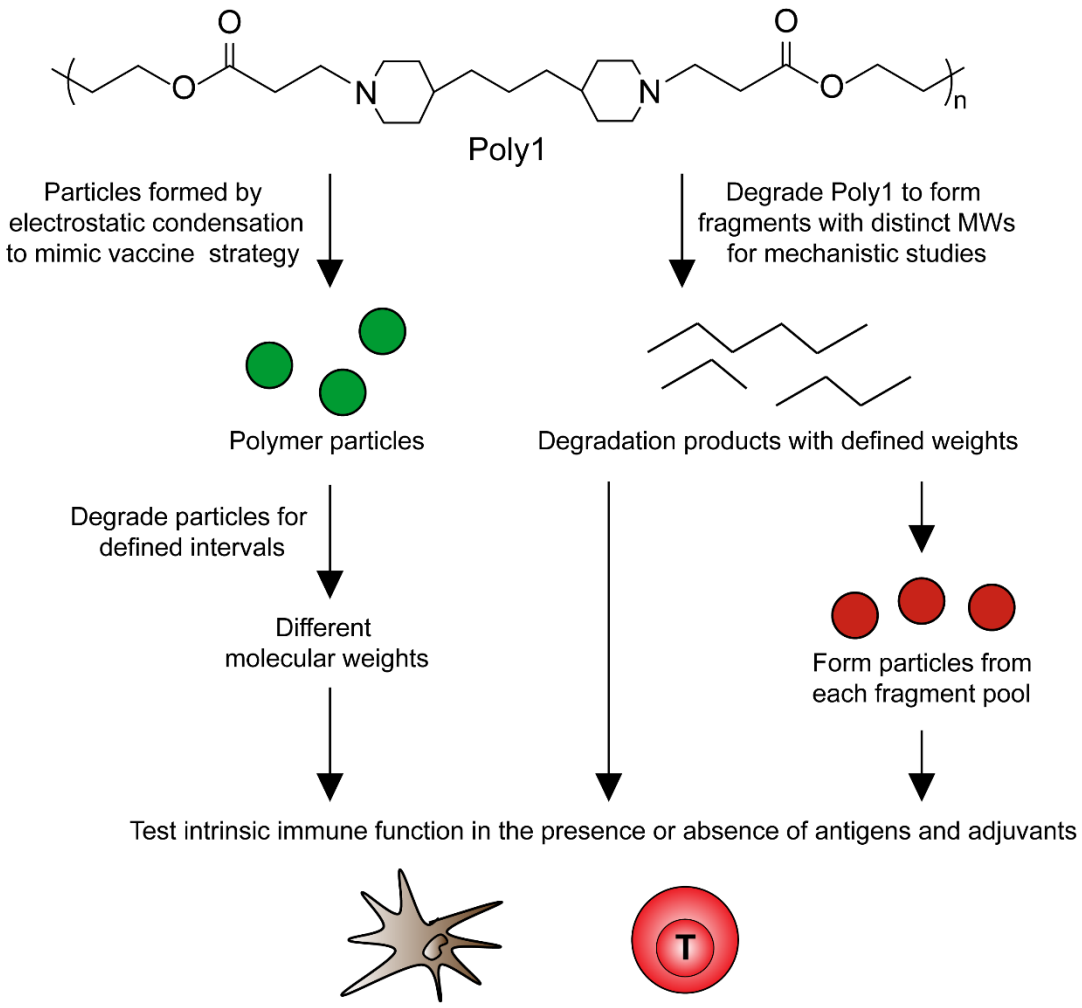

Figure 3.1: Schematic depicting the approach to investigate the intrinsic immunogenicity of Poly1, a degradable, cationic PBAE.
DCs and T cells are treated with free Poly1 or one of two Poly1 particle formulations: i) particles formed from intact Poly1 then degraded to mimic a common vaccine formulation strategy, or ii) Pools of Poly1 degradation fragments with distinct MWs formed into particles to mechanistically study the link between PBAE properties (e.g., MW, physical form) and DC activation, antigen presentation, and T cell function.

3.2 Materials and Methods

3.2.1 Materials

Monomers for polymer synthesis (1,4-butanediol diacrylate and 4,4′-trimethylenedipiperidine) were purchased from Alfa Aesar and Sigma-Aldrich, respectively. Tetrahydrofuran (THF), diethyl ether, sodium acetate (SA) buffer, poly(sodium 4-styrenesulfonate) (SPS), and lipopolysaccharide from Escherichia coli 0111:B4 (LPS) were also purchased from Sigma-Aldrich. THF used in GPC studies was purchased from Macron Fine Chemicals. Agilent LS EASICAL PS-1 polystyrene GPC standards were from Fisher Scientific. Deuterated-chloroform ($CDCl_3$) was bought from Cambridge Isotope Laboratories. RPMI-1640 media was purchased from Lonza. Fetal bovine serum (FBS) was supplied by Corning. Low MW polyinosinic-polycytidylic acid (PolyIC) was purchased from Invivogen. CD11c microbeads were purchased from Miltenyi Biotec. Spleen Dissociation Medium and CD4 negative selection kits were from STEMCELL Technologies. Carboxylate-functionalized and amine-functionalized polystyrene particles were purchased from Polysciences and Spherotech, Inc.. Brefeldin A and fluorescent antibody conjugates were purchased from BD or eBioscience. 5(6)-Carboxyfluorescein diacetate N-succinimidyl ester (CFSE) was purchased from Sigma-Aldrich. 40 μm cell strainers were from VWR.

3.2.2 Cells and Animals

Female C57BL6 mice (4-8 weeks, stock #000664) and male C57BL/6-Tg(Tcra2D2,Tcrb2D2)1Kuch/J (2D2) mice (10-12 weeks, stock #006912) were from Jackson Laboratories. The 2D2 strain displays $CD4^+$ T cell receptors transgenic for

myelin oligodendrocyte glycoprotein, residues 35-55 (MOG_{35-55}). All animals were cared for in compliance with Federal, State, and local guidelines, and using protocols reviewed and approved by the University of Maryland's Institutional Animal Care and Use Committee (IACUC).

3.2.3 Poly1 synthesis, degradation, and characterization

Poly1 was synthesized via a Michael-type addition reaction as described previously [129, 130, 132]. Briefly, 9 mmol of 4,4′-trimethylenedipiperidine was dissolved in anhydrous THF to form a 500 mg mL^{-1} solution. This solution was added to 9 mmol of 1,4-butanediol diacrylate and the reaction was heated to 50°C and stirred for 16 hours. The reaction was cooled to room temperature and the resulting polymer was precipitated in vigorously stirred ice cold diethyl ether. After collecting the polymer and washing with additional diethyl ether, the polymer was lyophilized. A 16 mg mL^{-1} solution of Poly1 was prepared in $CDCl_3$ and ^1H NMR was used to confirm the structure. Poly1 was dissolved in THF at 2.5 mg mL^{-1} and a THF-based gel permeation chromatography (GPC) system (Waters) was used to determine polymer MW compared to polystyrene standards. For degradation studies, Poly1 was placed in either pH 7 buffer (1x PBS) or pH 5 buffer (100 mM SA) and incubated at 37°C for increasing intervals to form polymer fragments. Following incubation, the degraded samples were lyophilized and MW (weight average) was determined by GPC.

3.2.4 Poly1 particle formation and characterization

Poly1 particles were assembled from either intact polymer then degraded, or assembled from polymer fragments with distinct MWs formed by degradation prior to particle assembly. For the former studies, intact Poly1 was used to prepare particles via electrostatic condensation by mixing 5 mM Poly1 and 20 mM SPS at a SPS:Poly1 w/w ratio of 1:1.6. These particles were then incubated at 37°C for specific intervals to determine how degradation of particles influences the intrinsic immune activity. For mechanistic studies involving pre-degraded polymer, Poly1 was degraded in pH 5 buffer for specific intervals to form fractions with distinct MW fragments of Poly1, then mixed with SPS as above to prepare particles. For each particle preparation, 400 µg of 5 mM Poly1 was used to form particles with SPS in pH 5 water while maintaining a fixed overall volume. Thus the amount of polymer (Poly1, SPS) was constant in either case, irrespective of whether particles were formed from intact Poly1 then degraded, or assembled from Poly1 fragments. GPC, as above, was used to quantify the extent of degradation for Poly1 particles formed then degraded. Laser diffraction (Horiba LA950) was used to determine the diameter of the particles. Zeta potential was determined using a Malvern Zetasizer Nano ZS90.

3.2.5 DC activation, antigen presentation, and flow cytometry

Primary $CD11c^+$ DCs were isolated from spleens of C57BL6 mice via positive selection using the recommended protocols for Spleen Dissociation Medium (STEMCELL) and CD11c Microbeads (Miltenyi). Isolated DCs were plated at 100,000 cells per well in a 96 well plate and cultured at 37°C, 5% CO_2. DCs were cultured in RPMI 1640 medium supplemented with 10% FBS, 2 mM L-glutamine, 1x

non-essential amino acids, 10 mM HEPES buffer, 1x penicillin and streptomycin, and 55 μM β-mercaptoethanol. For DC activation studies, DCs were treated with either buffer ("vehicle"), 10 μg mL^{-1} of TLR3a (PolyIC), 1 μg mL^{-1} of TLR4a (LPS), 400 ng of Poly1 in free form or in one of two particle formulations: i) particles assembled from intact Poly1 incubated to form degraded fractions from each time point, or ii) particles assembled from each molecule weight fraction of degraded polymer. A subset of these formulations was also studied in combination with the TLRa treatments, as indicated. For all DC studies, 48 hours after treatment, cells were stained for viability (DAPI) and for surface activation markers (i.e., CD40, CD80, CD86, and Major Histocompatibility Complex II (MHCII)) using fluorescent antibodies conjugates. Cells were examined by flow cytometry (BD CantoII) and data were analyzed using FlowJo v. 10 (TreeStar). For antigen presentation assays, DCs were co-incubated with 1 μg of a model antigen (SIINFEKL) in soluble form and each of the polymer formulations indicated and hypothesized to exhibit an adjuvant effect. After 48 hours, cells were stained with an antibody specific to SIINFEKL presented via MHCI (H-$2K^b$) then analyzed by flow cytometry to determine the percentage of DCs processing and presenting SIINFEKL in MHCI.

3.2.6 DC/T cell co-culture and T cell proliferation

For studies involving DC and T cell co-cultures, primary DCs ($CD11c^+$) were isolated from C57BL6 mice as above, and then treated with Poly1 in free or particle form. A sub-optimal dose (0.05 μg in 10 μL) of a model antigen (MOG_{35-55}) in soluble form was added to all wells to serve as the cognate antigen for transgenic 2D2 T cells.

After 48 hours in culture, $CD4^+$ T cells were isolated from the spleens of 2D2 mice using the manufacturer's recommended protocol (STEMCELL). Following isolation, T cells were labeled with CFSE by adding 50 µM of CFSE (in media) per mL of cells, incubated for 5 minutes at room temperature, and then washed twice with 10 volumes of media. 300,000 CFSE-labeled $CD4^+$ 2D2 T cells were added to each well containing DCs, then incubated for 72 hours with 50% media replacement every 24 hours. After incubation, cells were collected, and stained with DAPI and antibodies specific to the T cell surface markers (i.e., CD3e, CD4). Flow cytometry was used to determine the extent of T cell proliferation via CFSE dilution, with cells gated beyond the second generation selected as a criterion for proliferated cells.

3.2.7 Statistical Analysis

One way ANOVA with a Tukey post-test was performed using Graphpad Prism (version 6.02) for statistical testing. A p-value less than 0.05 was considered significant.

3.3 Results

3.3.1 Poly1 degrades to form low MW fragments

Poly1 was synthesized and the reaction product was confirmed via NMR after 16 hrs of synthesis (**Figure 3.2A**). Poly1, with a MW of 3.8kDa (**Figure 3.2B**), was then dissolved in pH 5 buffer. The MW of Poly1 decreased to 39.9% (~1.5kDA) of the starting MW over 24 hours and to 8.4% (0.3kDa) of the starting MW over one week

(**Figure 3.2B,C**). This degradation rate corresponded to a half-life of ~17.7 hours and as previously reported [129], degrades to form byproducts of 1,4 butanediol and bis(β-amino acid). The intrinsic immunogenicity as polymers degrade to fragments was then studied in culture and in mice using Poly1 in different forms (i.e., free, particles) and at different extents of degradation (i.e., MWs).

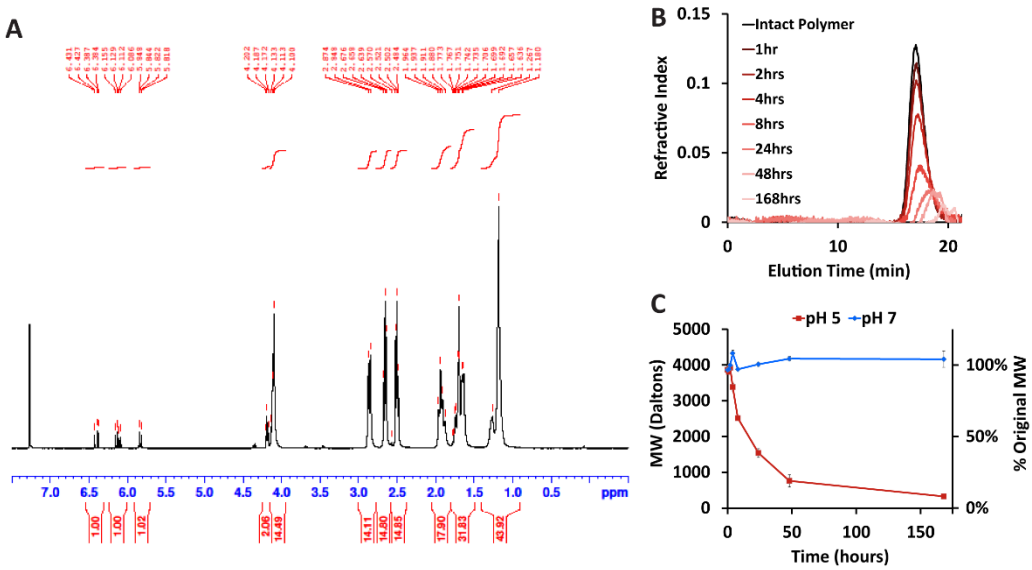

Figure 3.2: Poly1 synthesis, characterization, and degradation to low MW polymer chains over one week in buffer.
(A) ^{1}H NMR shifts of Poly1 integrated with respect to deuterated chloroform including chemical shift definitions. (B) GPC chromatograph depicting the change in MW of Poly1 after degradation in pH 5 buffer (100mM SA). Increased elution time correlates to lower MW fragments. (C) Poly1 MW changes after incubation in pH 5 and pH 7 (1x PBS) buffers. Data are relative to polystyrene standards and pooled from three independent experiments for each incubation time. Error bars represent SEM.

3.3.2 Poly1 in free form does not activate DCs

DCs were incubated with Poly1 degradation fragments that were 100%, 88%, 40%, 20%, or 8% of the starting MW. These fragments were used to treat primary DCs in the absence of antigen or adjuvants. Following treatment, common DC activation markers were investigated including MHCII, a peptide responsible for presenting

antigen to T cells, CD80 (B7-1) and CD86 (B7-2) which are costimulatory markers that need to be co-expressed with MHC complexes in order for proper T cell activation, and CD40, a membrane protein also expressed on DCs when activated that has links to both humoral and cell-mediated lymphocyte activation [149-152]. Compared with control cells treated with buffer (**Figure 3.3, "vehicle"**), free Poly1 (**Figure 3.3, blue**) did not increase characteristic DC activation markers including CD40 (**Figure 3.3A**), CD80 (**Figure 3.3B**), CD86 (**Figure 3.3C**), and MHCII (**Figure 3.3D**). To test if free Poly1 mediated a synergistic effect on DC activation in the presence of other adjuvants, DCs were co-cultured with Poly1 fragments and a TLR3a (PolyIC, **Figure 3.3, red**) or a TLR4a (LPS, **Figure 3.3, green**). DCs treated with PolyIC or LPS were strongly activated, but DCs treated with both Poly1 and either TLRa did not exhibit any further increases in activation. These data indicate that Poly1 in free form does not exhibit strong intrinsic immunogenicity or cause synergistic effects in the presence of other adjuvants (i.e., TLR3a, TLR4a).

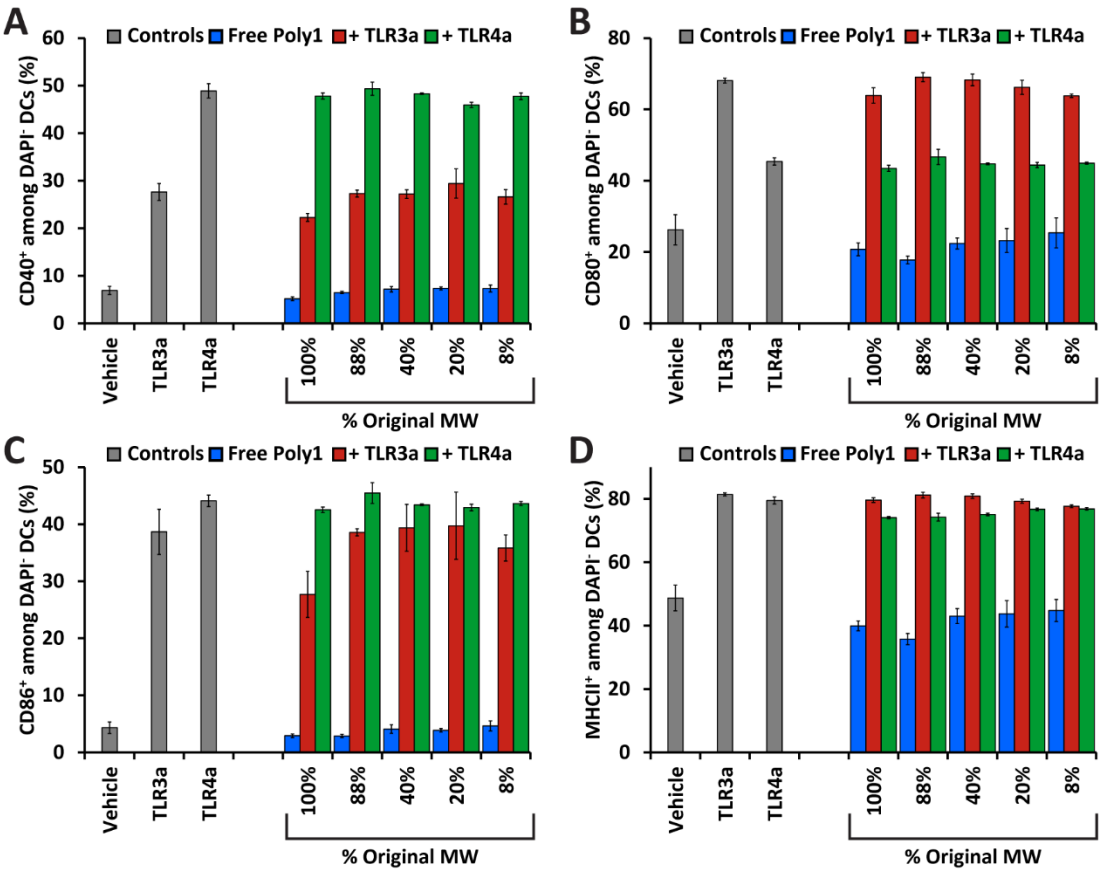

Figure 3.3: Free Poly1 does not activate DCs.
Expression levels of (A) CD40, (B) CD80, (C) CD86, or (D) MHCII on primary CD11c$^+$ DCs treated with free Poly1 degradation fragments of varying MW. Cells were incubated for 48 hours with the indicated Poly1 fragments in the absence (blue) or presence of a TLR3a (PolyIC, red) or TLR4a (LPS, green), respectively. Expression levels are indicated among DAPI$^-$ cells and are representative of three similar experiments with samples conducted in triplicate with error bars depicting SEM.

3.3.3 Particles assembled from intact Poly1 exhibit the greatest levels of intrinsic immunogenicity at early stages of degradation

We hypothesized that the form of polymer in solution may impact the intrinsic immune characteristics of Poly1 by altering the ability of APCs to detect, internalize, and process Poly1. To test this idea in a well-controlled manner, particles were formed by electrostatic condensation of Poly1 with a stable polyanion (SPS). This approach mimics a common particle synthesis strategy used in DNA vaccination

whereby antigen-encoding plasmid is condensed by PBAEs or other cationic polymers or lipids. These particles were then incubated in buffer at 37°C. GPC results confirmed that over time, Poly1 in the particles continued to degrade, leading to a reduction in MW and a lower particle concentration that resulted in increased optical transmittance (**Figure 3.4**). During this process, particle size increased, while zeta potential – which was initially positive (~15 mV) – decreased (**Figure 3.5A,B**). Further, the number of particles decreased to undetectable levels as degradation progressed (**Figure 3.4C, 3.5A**). Particle size measurements (volume basis, **Figure 3.6**A) and image analysis (**Figure 3.6C**) at each stage of degradation revealed that the decreased particle concentration was due not only to degradation, but also from aggregation of individual particles into larger, but fewer, agglomerates. After confirming SPS had no effect on cell viability (**Figure 3.7**), we screened the immunogenicity of the Poly1 particles by treating DCs with particles at each stage of degradation. While SPS at the concentration used was non-immunogenic, Poly1 particles at early stages of degradation strongly activated DCs (**Figure 3.5C-F)**. This activation then waned as a function of increasing particle degradation time and decreasing MW (**Figure 3.5C-F**). These effects were most evident in CD86 and CD80 expression – markers associated with co-stimulation. Thus, particles formed from Poly1 exhibit intrinsic immunogenicity, and these effects vary as a function of polymer degradation which alters the physicochemical properties of these particles. Building on this discovery, we designed a series of experiments to examine how the extent of polymer degradation influences particle properties and immune function in cells and mice.

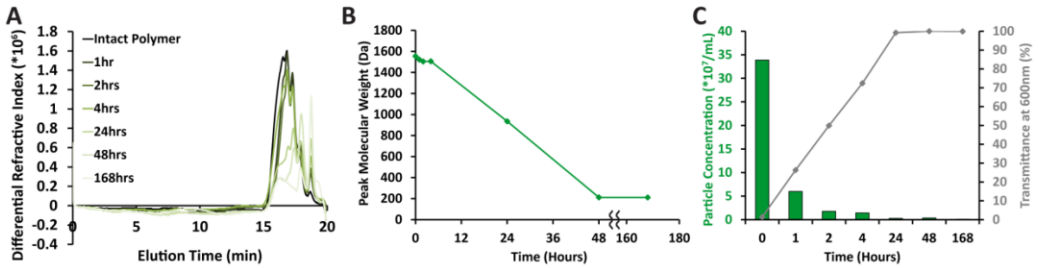

Figure 3.4: Poly 1 particles degraded for specific intervals following formation exhibit a rapid drop in MW that decreased particle concentration.
(A) GPC chromatograph depicting the change in MW of Poly1 particles after degradation in pH 5 buffer (100mM SA). Increased elution time correlates to lower MW fragments. (B) The peak corresponding to the MW distribution of Poly1 changes as particles degrade in pH 5 buffer. (C) Particle concentration and transmittance of Poly1 particles formed by condensing intact Poly1 prior to degradation alters over the extent of degradation.

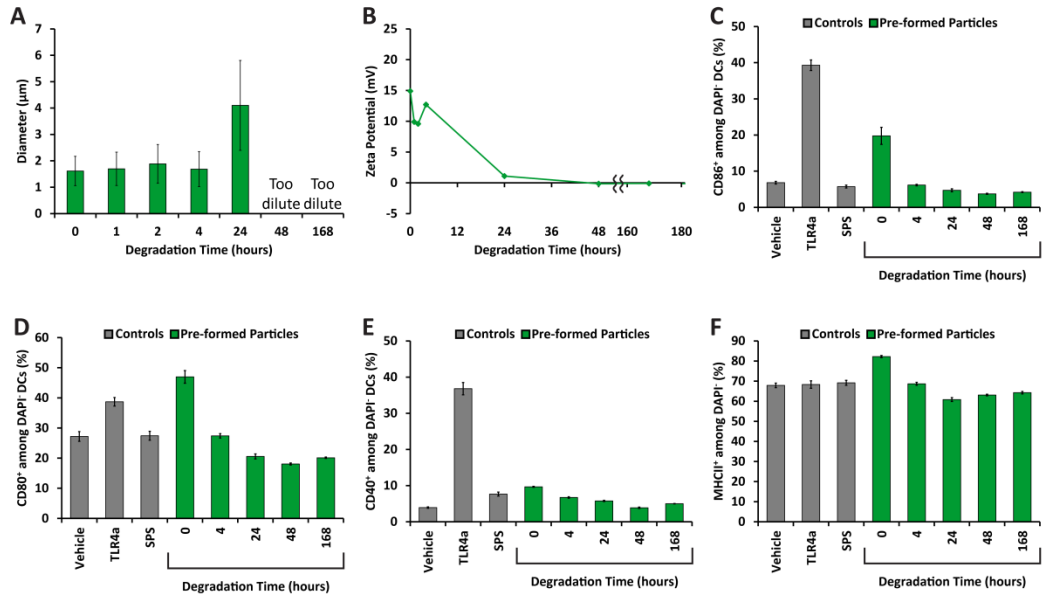

Figure 3.5: Pre-formed particles exhibit intrinsic characteristics that activate DCs during early stages of particle degradation.
(A) Particle size and (B) zeta potential shift as a function of degradation time. "Too dilute" designates formulations for which size measurements could not be reliably obtained due to insufficient particle concentration at long degradation times. Expression of (C) CD86, (D) CD80, (E) CD40, or (F) MHCII after treatment of $CD11c^+$ DCs with 400 ng of Poly1 particles at varying extents of degradation. Data correspond to samples prepared in triplicate with error bars representing SEM. For panel B, error bars are smaller than the data markers.

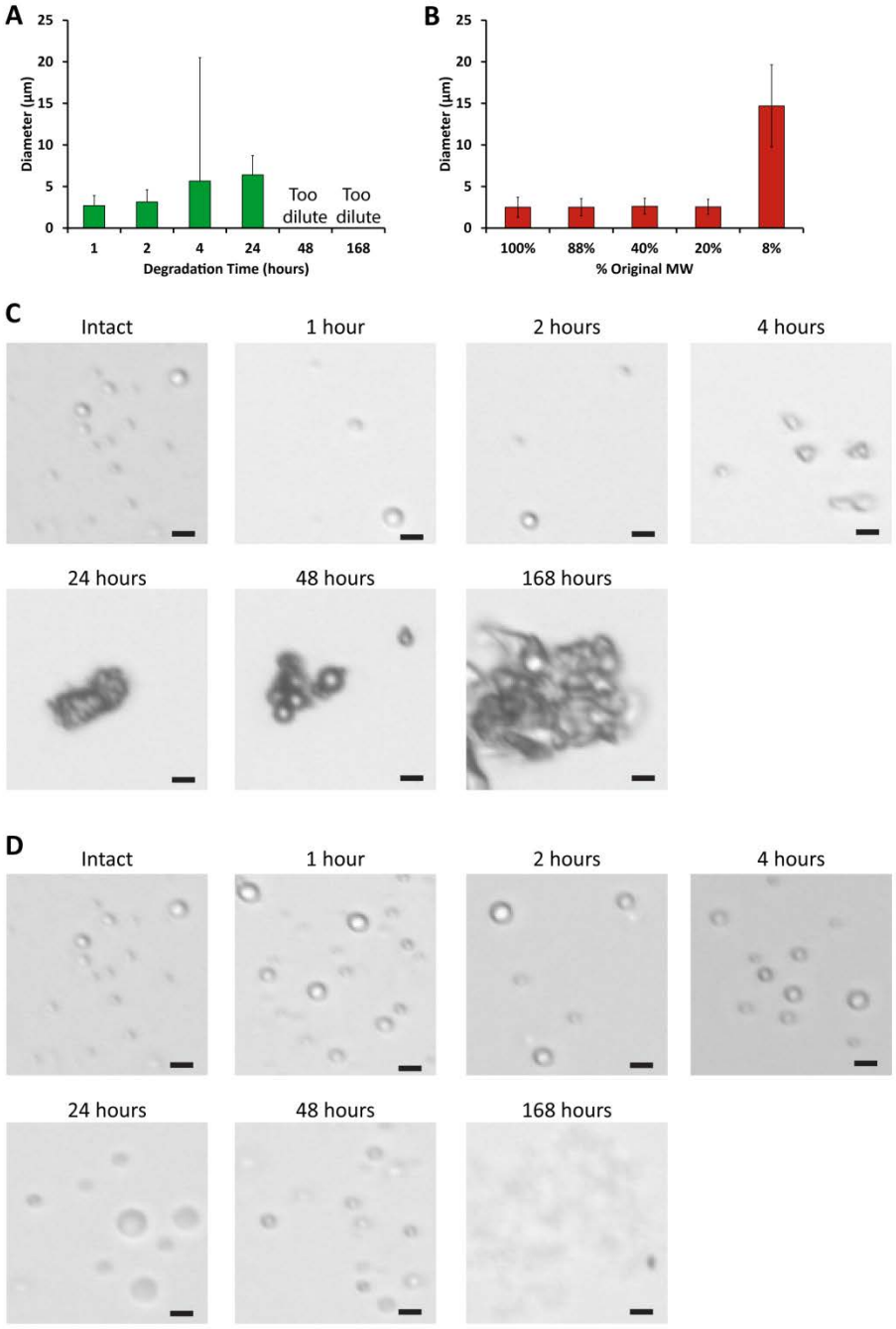

Figure 3.6: Degrading Poly1 particles result in large particle size due to aggregation.
Average particle diameter by volume of Poly1 particles formed then degraded (A) or formed using pre-degraded Poly1 (B) increases with extent of degradation. 'Too dilute' designates particle formulations that when measuring size did not result in a reliable reading due to insufficient particle concentration. Microscope images of Poly1 particles formed then degraded (C) or formed using pre-degraded Poly1 (D) confirm the presence of particle aggregates.

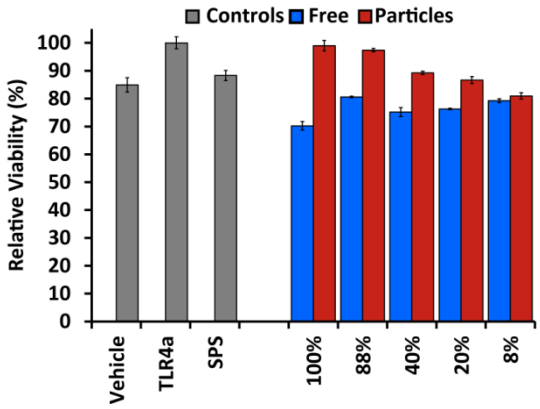

Figure 3.7: Poly1 does not influence DC viability.
SPS or Poly1 in free and particle form did not influence DC viability 48 hours after treatment. Data are representative of three similar experiments with samples prepared in triplicate. Error bars represent SEM.

3.3.4 Immunogenicity of particles assembled from Poly1 fragments depends on the extent of degradation

To more directly isolate the role of MW in defining the intrinsic immunogenicity of PBAEs, we used Poly1 fragments with distinct MWs as in **Figure 3.2** to form particles through condensation with SPS. As observed with particles degraded after formation (**Figure 3.4C**), the concentration of Poly1 particles formed from distinct MW fragments generally decreased with degradation time while transmittance increased. Interestingly, a slight increase in particle concentration was observed at 4 hrs (**Figure 3.8A**), and also observed by microscopy (**Figure 3.6D**). Depending on the degree of degradation, particles formed using each pool of Poly1 fragments exhibited sizes of 1.62 μm for intact polymer, increasing to 9.96 μm when particles were formed from fragments collected after a one week degradation period (**Figure 3.8B**). The zeta potential of particles, which was positive (~15 mV) at early stages, became highly negative as particles were formed with Poly1 fragments at greater

extends of degradation; particles formed with Poly1 fragments degraded for one week exhibit values of -9 mV (**Figure 3.8C**). In general, as the degree of degradation increased, particles exhibited more negative surface charges, and by the end of the study, a greatly increased diameter. Compared to the aggregation observed in particles formed prior to degradation (**Figure 3.6A,C**), particles formed from pre-degraded Poly1 remained largely free of aggregation until mostly degraded by 168 hours. These results were indicated by particle size analysis (**Figure 3.6B**) and inspection of microscopy images (**Figure 3.6D**). We next tested the ability of these particles to activate DCs. Poly1 particles exhibited significant levels of DCs activation when prepared from intact poly1 or Poly1 fragments from short degradation times (i.e., high MW) (**Figure 3.8D-G**). These effects then decreased as a function of polymer degradation time, with near-baseline activation levels by the end of the study. Interestingly, CD80 and CD86 levels were elevated with Poly1 fragments degraded to 40% of the original MW, an observation that correlated with a transiently-elevated particle concentration at this point.

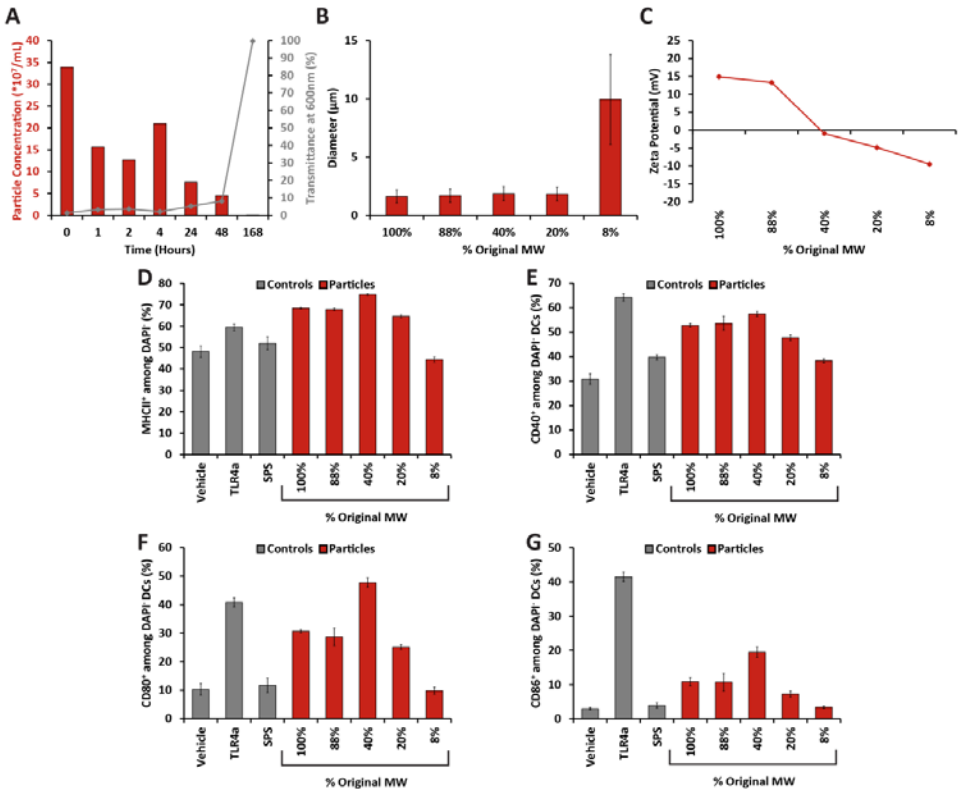

Figure 3.8: Poly1 particles formed with pre-degraded Poly1 fragments induce MW-dependent activation of DCs.
(A) Particle concentration and transmittance of particles formed by condensing Poly1 fragments generated by degradation in buffer prior to condensation. (B) Particle size and (C) zeta potential of Poly1 particles alters the extent of degradation. Expression levels of (D) MHCII, (E) CD40, (F) CD80, or (G) CD86 following treatment of primary $CD11c^+$ DCs with 400 ng of Poly1 particles at different extents of degradation. Vehicle and TLR4a indicate cells treated with buffer or LPS, respectively. Analysis was conducted 48 hours after treatment. Expression levels are indicated among $DAPI^-$ cells (i.e., live cells). Data are representative of three similar experiments with samples prepared in triplicate. Error bars represent SEM. For panel C, error bars are smaller than the data markers.

3.3.5 Poly1 particles increase antigen presentation through MHCI and MHCII, and drive T cell expansion

To test if Poly1-induced DC activation impacts antigen presentation, DCs were treated with a model antigen (SIINFEKL) and either free Poly1 or particles formed from each MW pool of poly1 fragments. SIINFEKL presented by these cells in MHCI ($H\text{-}2K^b$) was then quantified by flow cytometry. While free Poly1 (**Figure 3.9A, blue**) did not cause a significant increase in antigen presentation compared to

controls (**Figure 3.9A, gray**), DCs treated with Poly1 particles (**Figure 3.9A, red**) caused a dramatic increase in SIINFEKL presentation. In agreement with DC activation data (**Figure 3.8D-G**), presentation levels depended on the extent of degradation, with the highest levels associated with Poly1 degraded for short times (i.e., higher MWs) (**Figure 3.9A**). These results indicate that Poly1 particles stimulate DCs in a manner that enhances the ability of DCs to effectively present antigen via the MHCI pathway – an arm of adaptive immunity important in response to viral infection.

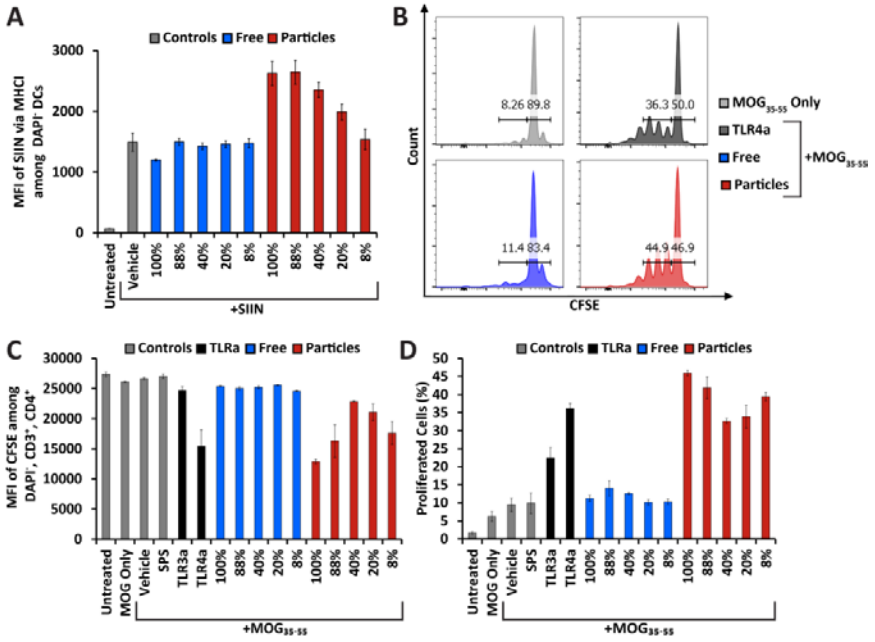

Figure 3.9: Poly1 particles increase MHCI-mediated antigen presentation and antigen-specific T cell proliferation.
(A) MFI of signal pertaining to SIINFEKL presented in MHCI following treatment of DCs with no SIINFEKL ("Untreated", gray), buffer with SIINFEKL ("SIIN Only", gray), free Poly1 with SIINFEKL (blue), or Poly1 particles with SIINFEKL (red) and gated under $DAPI^-$ cells. 48 hours after treatment of primary DCs as in (A) but with 0.25ug mL^{-1} of a different model antigen, MOG_{35-55},$CD4^+$ cells isolated from 2D2 mice with T cell receptors specific to MOG_{35-55} were added to the wells and incubated for 72 hours. (B) Representative flow cytometry traces showing CFSE dilutions after treatment with MOG_{35-55} and either buffer ("MOG Only", gray), TLR4a LPS ("TLR4", black), free Poly1 ("Free", blue), and Poly1 particles formed ("Particles", red). (C) MFI of CFSE signal among $DAPI^-/CD3^+/CD4^+$ cells following treatments as in (B). (D) Percentage of $DAPI^-/CD3^+/CD4^+$ cells proliferated beyond the 2nd generation following treatment as in (B) as determined by CFSE dilution. The Poly1 MW used for treatment is displayed under each bar as a percent of original MW. Samples were prepared in triplicated and errors bars represent SEM.

To determine if DC activation and antigen presentation induced by Poly1 particles drives T cell expansion, $CD11c^+$ DCs from C57BL6 mice were co-cultured with $CD4^+$ transgenic T cells from 2D2 mice. T cells from 2D2 mice display T cell receptors specific for a well-defined cognate antigen (MOG_{35-55}). In these studies, DCs were cultured for 48 hours with MOG_{35-55} and either free Poly1, Poly1 particles formed with pre-degraded Poly1, LPS, or buffer. Freshly isolated $CD4^+$ 2D2 T cells labeled with CFSE were then added to the culture for 72 hours. **Figure 3.9B** depicts representative flow cytometry traces of CFSE dilutions (among $DAPI^-/CD3^+/CD4^+$ cells) for each treatment group. Samples treated with vehicle and MOG_{35-55} or positive controls (i.e., LPS with MOG_{35-55}), caused 8.26% (**Figure 3.9B, light gray**) and 36.3% (**Figure 3.9B, dark gray**) of T cells to proliferate beyond the second generation (**Figure 3.9B, left gates**), respectively. Consistent with DC activation and antigen presentation studies (**Figure 3.8 and Figure 3.9A**), cultures treated with free Poly1 (**Figure 3.9B, blue**) did not exhibit differences in T cell proliferation compared to the vehicle control (**Figure 3.9B, gray**). Intriguingly, cells treated with Poly1 particles (**Figure 3.9B, red**) induced strong T cell proliferation, resulting in three distinct generations beyond the second generation. This expansion was comparable to that observed in co-cultures treated with a strong TLR3a or TLR4a (i.e., PolyIC, LPS, respectively) and much greater than the negligible expansion observed in vehicle-treated cultures (**Figure 3.9B,C,D**). Compared with free Poly1, Poly1 particles caused significantly more proliferation as reflected in both MFI analysis (**Figure 3.9C**) and as a percentage of proliferated cells for each formulation (**Figure 3.9D**). The effect of Poly1 particles on proliferation was also weakly influenced by the

extent of degradation (i.e., MW), with proliferation generally decreasing at lower MWs (**Figure 3.9C,D**). However, the statistical power of these trends were weak. Thus, Poly1 particles induce DC activation and antigen presentation that drives antigen-specific T cell expansion in a manner that is at least partially dependent on the extent of polymer degradation.

3.4 Discussion

In vaccination and immunotherapy, biomaterials offer the ability to control the delivery kinetics of immune signals; however, how the intrinsic immunogenicity of synthetic carriers change as these materials degrade is an area that is not well studied. Several recent studies demonstrate the intrinsic effects of polymer chemistry and physicochemical properties. For example, the Rotello group investigated the effect of specific chemical groups on inflammatory cytokine production using well- controlled chemistry to display these moieties on stable, gold nanoparticles.[120] Here, we have carried out mechanistic studies to test if the changing properties of polymer particles during degradation alters dendritic cell activation, processing and presentation of antigen through MHC-I and MHC-II pathways, and expansion of antigen-specific T cells. To explore these possibilities, we used PBAEs as a rapidly-degradable carrier platform. Since PBAEs are commonly used to condense nucleic acids for gene therapy or DNA vaccination, we formed particles by electrostatic condensation to mimic this polymer-enable vaccination strategy [142-148]. This approach also eliminated stabilizers, surfactants, or other complex compositions required for nanoparticle and microparticle vaccines synthesized by methods such as

emulsion/phase inversion. These additional components could hinder isolation of the immunogenic effects of PBAEs and the change in these characteristics during degradation.

Our primary findings in this study are i) that PBAEs exhibit intrinsic immunogenicity, and ii) that the extent of this activity depends both on the form and extent of degradation of Poly1. Past studies with low MW fragments of polymers such as hyaluronic acid indicate that these materials - which were 4-14 oligosaccharides in size (1500-5300 Da) - induce DC activation, cytokine secretion, and T cell proliferation, while high MW hyaluronic acid (80,000-1,000,000 Da) does not [111, 112]. In contrast, our studies with free PBAEs reveal that free Poly1 does not activate DCs (**Figure 3.3**). This observation may result from the inability of DCs to efficiently internalize the soluble/relatively low MWs that both intact and degrading Poly1 exhibit. Although DCs use pinocytosis to internalize smaller antigens, DCs are able to sample larger, particulate antigens more efficiently through phagocytosis [153].

Unlike free Poly1, particles formed from intact Poly1 were immunogenic, exhibiting the greatest activity at early stages of degradation, with diminishing intrinsic function at longer times. Poly1 MW became significantly lower at these longer intervals, while the charge became negative, particle size became much larger, and particle concentration decreased (**Figure 3.4, 3.5A-B**). Thus, a likely explanation for the decreasing immunogenicity in **Figure 3.5C-F** observed with increased degradation

time is i) the reduced number of particles to interact with immune cells, ii) the negative surface charge that could hinder association with negatively charged cell membranes [154], and iii) large particle sizes that limits the efficiency of endocytosis.

Our findings that Poly1 particles formed from intact Poly1 exhibit changing immunogenicity as Poly1 degrades motivated mechanistic studies to investigate more directly how Poly1 fragments alter the properties – and resulting immunogenicity – of particles. Thus we prepared particles from pools of Poly1 fragments with distinct MW ranges. As with our studies involving particles degraded after formation from intact Poly1 (**Figure 3.5**), we discovered that particle size increased inversely with the MW of the Poly1 fragments used for assembly, and zeta potential became increasingly more negative with increased degradation time (**Figure 3.8**). In general, the trends in DC activation were also similar (**Figure 3.8D-G**), with greater activation at lower extents of degradation where particle size was low (~2μm) and zeta potential was less negative. When Poly1 particles were formed from smaller MW fragments to mimic longer degradation times, particles became larger (**Figure 3.8B**) and surface charge shifted from positive to neutral or slightly negative (**Figure 3.8C**). However, we also observed a transient elevation in activation with particles formed from fragments 40% of the starting MW, though the statistical power of this trend was weak. Our observation of this effect underscores an important role for particle concentration, as the properties of particles formed with these fragments resulted in an increased concentration of particles (**Figure 3.7D, Figure 3.8A**) for the same polymer mass used for the other fragment pools. Together, these data suggest several

conclusions. First, activation is high when particles are at an easily-internalized size (e.g., one to several microns), but before exhibiting a strong negative surface charge that could hinder electrostatic association with negatively charged cell membranes. As degradation continues to greater extents (e.g., 8% of starting MW), particle diameters reach sizes that may be too large to internalize and exhibit negative surfaces. Second, since the Poly1 dose was fixed, particle concentration changes both because polymer is degrading and due to aggregation that results in larger, but fewer, particles. These effects result in particle concentration generally decreasing with time. The transient increase in concentration – and corresponding increase in DC activation – observed with the 40% fragments could result from dispersion of small aggregates (e.g., dimers or trimers) that may form during initial condensation, but that are separated as the particles begin to degrade. However, additional studies are needed to confirm this possibility. In support of the types of interactions discussed in this section, Bishop *et al.* similarly observed that directly synthesizing PBAEs with different MWs impacts the size and zeta potential of electrostatically-condensed PBAE particles, though this study did not investigate the immunogenicity of the particles [155]. Together, the two approaches we used to characterize the impact of MW on the changing immunogenicity of Poly1 reveal that these changes are a function, at least in part, of changes in particle charge, size, and concentration that result during degradation.

Another interesting result was observed in studying the impact of Poly1 particle treatment on the presentation of antigen through MHCI and MHCII. The MHCI

pathway is important in promoting cell-mediated (i.e., $CD8^+$ T cells) responses to destroy cells infected with intracellular pathogens (i.e., viruses) and in new therapeutics such as cancer vaccination and immunotherapy. Our studies reveal an increase in SIINFEKL antigen presentation at low extents of degradation (**Figure 3.9A**). Using T cells from transgenic mice, we also discovered that, in general, Poly1 particles cause an adjuvant effect to promote antigen-specific proliferation through the MHCII pathway at levels that are comparable to those observed in mice treated with LPS and the cognate antigen (**Figure 3.9B-D**). Further, proliferation was not observed when only the antigen was present. Proliferation was only a weak function of MW, though this may be expected due to the exponential nature of T cell expansion and the complexity of the signals playing a role in engaging the T cell receptor (e.g., DC signals, cytokines/soluble factors, cell-cell contacts). These co-cultures studies demonstrate that Poly1 particles serve as adjuvants by activating DCs to present antigen through both the MHCI and MHCII pathways, as well as enhancing the co-stimulatory molecules needed to expand antigen-specific T cells. These data also highlight the ability of Poly1 – even in the absence of any other immune cues – to drive functional responses in a manner that is dependent on the form and degradation state of the polymer.

The “danger model” describes the evolution of immune pathways that function by detecting pathogens through broad structural features that are uncommon in animals and humans [156]. Some of these characteristics include materials in a particulate form (e.g., virion particles, bacterial cells), short hydrophobic fragments, and

polymers or other repetitive structures such as the polysaccharides that commonly comprise bacterial membranes. In our studies, when Poly1 particles were at an optimal size for internalization and positive or neutral, activation was greatest. These effects correlated to other functions such as antigen presentation and proliferation. However at low molecular weights, activation diminished. Thus, in line with the danger model, our results suggest that broad physicochemical features (e.g., size, charge), as well as direct effects from changing MW and number of repeat units – account for the evolving immunostimulatory properties of Poly1.

3.5 Conclusion

Previous studies have confirmed the intrinsic immunogenicity of several biomaterials important in the delivery of drugs, vaccines, and immunotherapies. However, these studies have not focused on how this activity may evolve as materials degrade, and have not been carried out using rapidly-degradable polymer classes such as PBAEs. Here, we have demonstrated that PBAEs, an important polymer class in recent drug delivery and vaccine studies, exhibit strong intrinsic immune effects in a particle form, but not in a free form. Our results also indicate that these effects depend on the extent of polymer degradation, and at least in part, occur because the degrading polymer impacts particle properties such as size, charge, and concentration. Future studies involving treatment of mice with Poly1 at differing extents or rates of degradation will reveal how these materials impact LN structure and function with respect to polymer properties. Additionally, more mechanistic studies could investigate how treatment with PBAEs influences various DC subsets as well as the

entry and processing of antigen in these cells. This approach could also provide new knowledge of how the intrinsic immunogenicity observed here or with other polymers translates to polarization of functional immune outcomes when antigens or other adjuvants are present. Ultimately, this knowledge could contribute to the design of polymers that allow better control over the types, durations, and magnitudes of responses generated with new vaccines or immunotherapies.

Building on the studies performed in this chapter, in **Chapter 4**, a small library of PBAEs was synthesized to form polymers with similar structures but different starting MWs. Using these polymers, we generalize the findings that PBAEs are intrinsically immunogenic by identifying particular physicochemical properties that promote this activation and are maintained across the polymers.

Chapter 4: Impact of Molecular Weight on the Intrinsic Immunogenic Activity of Poly(Beta Amino Esters)[3]

4.1 Introduction

New vaccine and immunotherapies that employ biomaterial carriers have the ability to protect encapsulated immune cargos, control the release kinetics of these components, and target specific immune cells or organs such as lymph nodes (LNs) - tissues that coordinate adaptive immunity.[103-105] Despite these advantages, many recent studies outline above also show that many biomaterials, including poly(lactic-co-glycolic acid) (PLGA), polystyrene, and chitosan exhibit intrinsic immunostimulatory properties that can activate immune cells, even in the absence of adjuvants or inflammatory cues.[9, 45, 103, 106-109, 157] This immune stimulation can occur through activation of pattern recognition receptors (PRRs), the inflammasome, and toll-like receptor (TLR) signaling. These receptors are found on and within many immune cells, including dendritic cells (DCs) – antigen presenting cells (APCs) that link innate and adaptive immunity.[110] When immature DCs are plated on a thin-film of PLGA, for example, the DCs become activated, increasing co-stimulatory markers (CD80, CD86, and CD83) and antigen presentation complexes.[109, 157] These effects drive increased pro-inflammatory cytokine secretion and T-cell proliferation *in vitro*,[109, 157] features in line with seminal *in*

[3]Adapted from J.I. Andorko, K.G. Pineault, and C.M. Jewell. "Impact of molecular weight on the intrinsic immunogenic activity of poly(beta amino esters)." *J Biomed Mater Res A.* 2017, 105, 1219-1229.

vivo studies illustrating the intrinsic immune effects of PLGA and polystyrene.[9, 45] One recent strategy seeks to simplify vaccines and immunotherapies by eliminating carriers completely using self-assembly of immune signals in a manner that mimics attractive features of biomaterials.[158-162] Alternatively, understanding the interactions between biomaterials with defined properties and the immune system could enable design of new carriers that deliver vaccine and immunotherapy cargos with direct control over the particular immune functions or phenotypes that arise from these treatments.

Building on this discovery of intrinsic immunogenicity and as mentioned in **Chapter 3**, many studies have set out to understand the link between immunogenicity and physicochemical properties such as molecular weight (MW),[107, 111-114] particle size,[108, 115-117] charge,[118, 119] hydrophobicity,[120] shape,[41, 121, 122] and chemical functionality.[123-128] For instance, silica micro-rods functionalized with poly(ethylene glycol) (PEG), PEG-RGD, or PEG-RDG to facilitate cellular uptake and incubated with bone marrow derived DCs cause increased activation and cytokine secretion, a phenomena that also occurs when these materials are implanted subcutaneously in mice.[128] Research by the Anderson lab recently explored how size and shape impact innate immunity in response to implanted biomaterials. These studies revealed that larger particles reduced the foreign body response in mice and non-human primates.[116] As one illustration, comparing macrophage responses to low and high MW hyaluronic acid, low MW hyaluronic acid promoted a classically activated-like state of increased pro-inflammatory genes and cytokines, while high

MW hyaluronic acid induced alternative macrophage activation, highlighting MW as a key polymer property in these activation studies.[114]

While many biomaterials carriers use polymer degradation to achieve controlled release of immune cargos, the link between the extent of degradation and the evolution of intrinsic immunogenicity is not well understood. This information is important because during degradation, as material properties change, immune cells and tissues interact with the initial and the altered forms of biomaterials, making it difficult to discern the impact of the signal and the carrier at a particular time (corresponding to a particular degradation state). Toward addressing this gap, in **Chapter 3**, a rapidly-degradable poly(beta-amino ester) (PBAE) was used to show that these polymers exhibit intrinsic immunogenic activity, and importantly, that the extent of the effects are dependent on the degree of polymer degradation.[163] PBAEs are cationic, pH-sensitive polymers used in drug and DNA delivery owing to their ability to efficiently condense nucleic acids and promote endosomal escape via the proton sponge effect.[129, 130, 132, 134, 135, 137, 138, 141, 164, 165] PBAEs have been employed in DNA vaccination by condensing plasmid DNA encoding antigens relevant for both cellular- and antibody-mediate immunity.[142-148] In the previous research outlined in **Chapter 3**, a prototypical PBAE, denoted as Poly1, did not activate primary DCs in a free (soluble) form but was able to activate DCs when formulated into particles via electrostatic condensation, a technique mimicking a common DNA vaccine modality.[163] Importantly, the PBAE particles caused

differential activation of DCs and T cells depending on the extent of polymer degradation.

Expanding on the results from **Chapter 3**, in this work, the intrinsic immunogenicity of a small library of PBAEs with similar structures but different starting MWs was investigated. PBAEs were synthesized from diacrylate monomers with an increasing number of carbons in the backbone, then degraded in a controlled fashion to form fragments. Using electrostatic condensation mimicking commonly used DNA vaccine formulation strategies, we formed particles using these sets of materials. MW was determined before and during degradation, and the immunogenicity was then investigated during culture with primary DCs (**Figure 4.1**). We show that the properties (e.g., size, charge, concentration) of fragments and particles are a function of the extent of degradation, and these changes alter the intrinsic immunogenicity. Further, irrespective of starting MW, the intrinsic immunogenicity reaches a maximum as polymers degrade to a range of ~1500-3000 Da. This knowledge could provide insight into the design of future vaccine carriers with properties that actively modulate the immune response towards a particular phenotype, allowing for more rational design of carriers used in vaccines and immunotherapies for infectious disease, cancer, or autoimmunity.

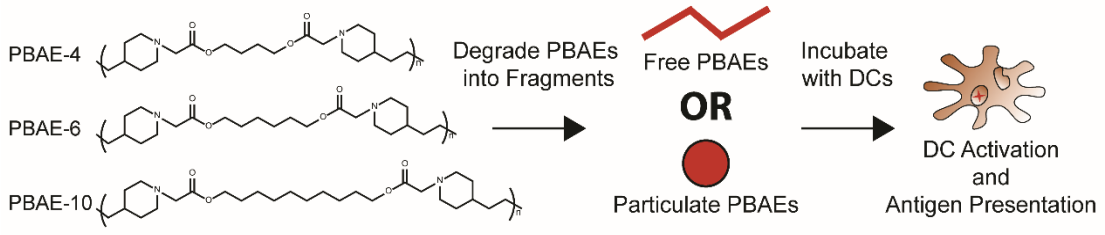

Figure 4.1: Schematic representation of PBAE preparation and treatment.
PBAEs were fabricated to have similar structures but increasing carbons in the polymer backbone are degraded into fragments, formed into particles, and cultured with DCs to determine how the properties of PBAEs impact DC activation and antigen presentation.

4.2 Materials and Methods

4.2.1 Materials

Diacrylate monomers used in polymer synthesis (1,4-butanediol diacrylate, 1,6-hexanediol diacrylate, and 1,10-decanediol diacrylate) were purchased from Alfa Aesar and 4,4′-trimethylenedipiperidine was purchased from and Sigma–Aldrich. Tetrahydrofuran (THF), diethyl ether, sodium acetate (SA) buffer, poly(sodium 4-styrenesulfonate) (SPS), and lipopolysaccharide from Escherichia coli 0111:B4 (LPS) were also purchased from Sigma–Aldrich. THF used in GPC studies was purchased from Macron Fine Chemicals. Agilent LS EASICAL PS-1 polystyrene GPC standards were from Fisher Scientific. Deuterated-chloroform ($CDCl_3$) was bought from Cambridge Isotope Laboratories. RPMI-1640 media was purchased from Lonza (Allendale, NJ). Fetal bovine serum (FBS) was supplied by Corning (Tewksbury, MA). Low MW polyinosinic-polycytidylic acid (PolyIC), a TLR3 agonist (TLRa), was purchased from Invivogen. CD11c microbeads were purchased from Miltenyi Biotec. Spleen Dissociation Medium was from STEMCELL Technologies. 4',6-diamidino-2-phenylindole, dihydrochloride (DAPI) was purchased from Thermo

Scientific and fluorescent antibody conjugates were purchased from BD or eBioscience.

4.2.2 Cells and animals

C57BL/6J Mice Stock #000664 (Individual, Female, 4-8 weeks old) were from Jackson Laboratories and used as a source of primary DCs. All animals were cared for in compliance with Federal, State, and local guidelines and using protocols approved by the University of Maryland's Institutional Animal Care and Use Committee (IACUC).

4.2.3 PBAE synthesis, characterization, and degradation

PBAEs were synthesized with a Michael-type addition reaction similar to the reaction previously described in **Chapter 3**.[163] Briefly, 4,4′-trimethylenedipiperidine was dissolved in anhydrous THF to form a 500 mg mL^{-1} solution. This solution was added to one of three diacrylates, 1,4-butanediol diacrylate, 1,6-hexanediol diacrylate, or 1,10-decanediol diacrylate, in equal molar ratios (9 mmol) to form either PBAE-4, PBAE-6, or PBAE-10, respectively. The reaction was heated to 50°C and stirred for 16 h, then cooled to room temperature. The resulting polymers were precipitated in ice cold hexanes or diethyl ether. After collection and additional washing in the solvent used for precipitation, each polymer was lyophilized. After drying, each PBAE was prepared at 16 mg mL^{-1} solution in $CDCl_3$, and ^1H nuclear magnetic resonance (NMR) spectroscopy was performed to confirm polymer structure. A THF-based gel permeation chromatography (GPC) system was utilized to determine the

starting MW of each PBAE and the MW at distinct degradation times relative to polystyrene standards. For degradation studies, each PBAE was dissolved in pH 5 SA buffer at 1mM and incubated at 37°C for increasing time intervals (e.g., 0-168 h) to form free polymer fragments. Following incubation, degraded samples were lyophilized and the resulting MW (weight average) was determined by GPC as described above. Degradation constants (λ) were calculated for each PBAE using the exponential decay equation:

$$y=MW_i e^{-\lambda x} \quad (1)$$

where MW_i was the intact (starting) MW of each PBAE.

4.2.4 PBAE particle formation and characterization

Each formulation of PBAEs was assembled into particles through electrostatic condensation by mixing 1mM of intact (full MW) or degraded PBAE fragments with distinct MWs with 20mM of anionic polymer (SPS) at a 1:2 SPS:PBAE w/w ratio. 400 μg of PBAEs were used for each particle formulation, while maintaining a fixed overall volume. Zeta potential of PBAE particles was determined using a Malvern Zetasizer Nano ZS90 and particle diameter was determined using laser diffraction (Horiba LA950). Particle concentration was calculated by mixing a known volume of PBAE particles with Trypan Blue at a 1:1 v/v ratio and counting using a hemocytometer. Transmittance was determined at 600nm using an Evolution 60 UV-visible spectrophotometer. Particles were imaged using an Olympus IX83 microscope.

4.2.5 Flow cytometry, DC activation, and antigen presentation

PBAE intrinsic immunostimulatory ability was tested using primary $CD11c^+$ DCs isolated from spleens of C57BL6 mice using recommended protocols for Spleen Dissociation Medium and CD11c Microbeads. Isolated DCs were plated at 100,000 cells per well in 96 well plates and cultured at 37°C, 5% CO_2 in RPMI 1640 supplemented with 10% FBS, 2 mM L-glutamine, 1x non-essential amino acids, 10 mM HEPES buffer, 1x penicillin and streptomycin, and 55 μM β-mercaptoethanol. For activation studies, DCs were treated with either 10 μg/mL of TLR3 agonist (PolyIC), 1 μg/mL of TLR4 agonist (LPS), a vehicle control of buffer, or 400 ng of each PBAE in free or particle formulations, fabricated from low MW PBAE fragments. For antigen presentation experiments, primary DCs were isolated and treated as above with the addition of 1 μg of soluble model antigen SIINFEKL (SIIN) to samples. After 48 hours in culture, cells were stained using fluorescently-tagged antibodies (BD) for viability (DAPI) and either of the classic DC activation markers (e.g., CD80, CD86, CD40, and I-A/I-E (mouse MHCII)) or an antibody specific to SIIN presenting within MHCI $H\text{-}2K^b$ (eBioscience). Flow cytometry was used to quantify relative viability (% cells $DAPI^-$ relative to a positive control) and the extent of surface marker presentation (activation) and SIIN presentation via median fluorescent intensity (MFI) and the percentage of cells highly expressing each marker. Correlations between particle properties (MW, concentration, diameter, and zeta potential) and DC activation (expression of CD40, CD80, CD86, and I-A/I-E) were determined by plotting properties versus activation and determining if any trend was present.

4.2.6 Statistical Analysis

For *in vitro* studies, two way ANOVA with a Tukey post-test was performed using Graphpad Prism (version 6.02) for statistical testing. A *p*-value less than 0.05 was considered significant.

4.3 Results

4.3.1 PBAE synthesis and characterization

A small library of PBAEs with similar chemical structures but with different numbers of carbons in the diacrylate monomer backbone was synthesized via a Michael-type addition reaction. The chemical structures of PBAE-4 (which has the same structure as Poly1 used in experiments throughout **Chapter 3**) (**Figure 4.2A, top**), PBAE-6 (**Figure 4.2A, middle**), and PBAE-10 (**Figure 4.2A, bottom**), were confirmed using ^{1}H NMR. As expected, increasing the numbers of carbons in the diacrylate backbone during synthesis resulted in increased area under the curve in the alkane region (1.0-1.5ppm), with PBAE-10 exhibiting the greatest level of alkane bonds (**Figure 4.2A, dotted boxes**). Using THF-based GPC, chromatographs were obtained for each PBAE prior to degradation to determine the starting MW (**Figure 4.2B**). PBAE-4 had the lowest MW of 2319 ± 81 Da, while PBAE-6 had a larger MW of 3178 ± 192 Da, and PBAE-10 had the highest starting MW of 5045 ± 99 Da (**Figure 4.2C**). After degrading each PBAE for up to 168h (1 week) in SA buffer at 37°C, the change in MW for each PBAE was determined and degradation constants (λ) were calculated. Interestingly, each of the PBAEs exhibited similar degradation rates, with PBAE-4

and PBAE-6 resulting in a value of λ = -0.9, and PBAE-10 degraded at a slightly faster rate (λ = -1.1) (**Figure 4.2D**).

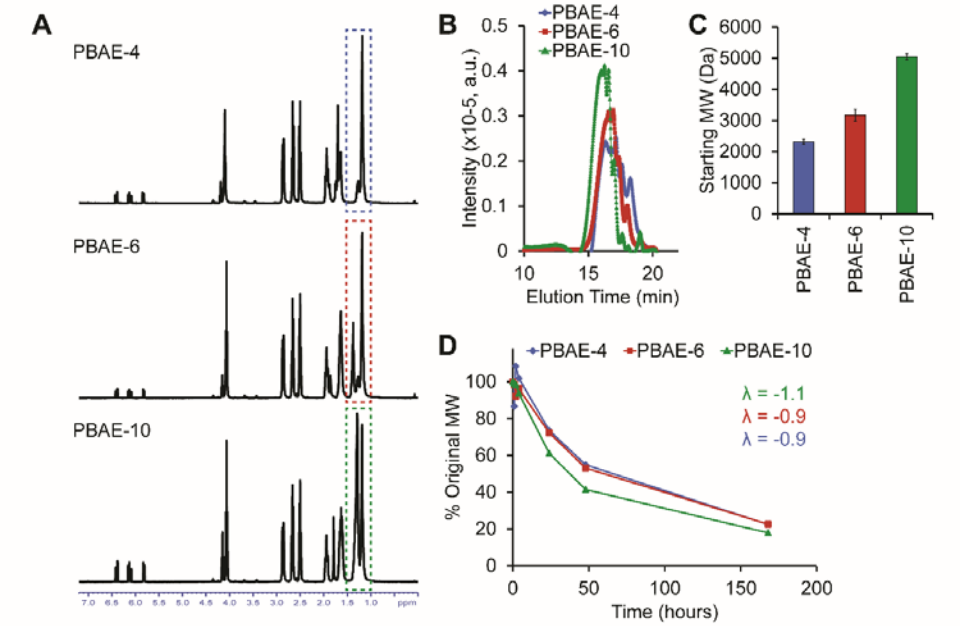

Figure 4.2: PBAEs are synthesized with similar structures but varied starting MW.
(A) NMR spectrographs of PBAE-4, PBAE-6, and PBAE-10 showing chemical structures only differ in the alkane region (1.0-1.5ppm, boxed region). (B) GPC chromatographs of intact PBAE-4 (blue), PBAE-6 (red), and PBAE-10 (green) depicting differential starting MW (C). (D) Degradation profiles and constants (λ) for PBAE-4 (blue), PBAE-6 (red), and PBAE-10 (green) after being incubated in pH 5 buffer for 7 days at 37°C. Samples were prepared in triplicated and errors bars represent SEM.

4.3.2 Fabrication and characterization of PBAE particles

After confirming the structure of each PBAE after synthesis, we investigated how the MW of PBAE fragments generated across similar degradation rates influenced the formation and properties of particles. Intact and degraded forms of PBAE-4, PBAE-6, and PBAE-10 were fabricated into particles through electrostatic condensation with SPS, a technique we previously used to mechanistically investigate intrinsic activation and which eliminates confounding factors such stabilizers commonly used in emulsion/phase inversion formulations.[142-148, 163] With respect to particle

diameter, particles formed from intact PBAE-4 (i.e., prior to degradation) were micron sized, with an average diameter of 1.61 ± 0.52 μm (**Figure 4.3A; blue**). These particles also exhibited a positive zeta potential of 6.34 ±1.08 mV (**Figure 4.3B; blue**). Upon degradation, PBAE-4 particles exhibited similar sizes around 1.60 μm – regardless of the extent of degradation – until particles were prepared from PBAE-4 degraded for 168h (22.5% of starting MW). At this point, particle size increased and particle concentration decreased, as indicated by an increase in transmittance (**Figure 4.3A, C, D; blue**). The zeta potential of PBAE-4 particles, while initially positive, became increasingly negative when fabricated with PBAE-4 that was degraded for increased time (i.e., lower MW). In a similar fashion, particles synthesized from PBAE-6 showed initial diameters of 1.59 ±0.52 μm but with a zeta potential of 9.09 ± 0.79 mV (**Figure 4.3A, B; red**), slightly higher than the zeta potential of particles formed with intact PBAE-4. These PBAE-6 particles also showed increasingly negative zeta potential when formed with degraded PBAE-6 fragments and maintained their diameter, concentration, and transmittance until formed with PBAE-6 that was degraded for 168h (22.6% of starting MW) (**Figure 4.3; red**). Surprisingly, PBAE-10 had an initial particle size on the nanometer scale, with particles formed from intact PBAE-10 exhibiting a diameter of 191.09 ± 75.06 nm (**Figure 4.3A; green**) and a strongly positive zeta potential of 19.57 ± 2.19 mV (**Figure 4.3B; red**). While PBAE-10 particle zeta potential decreased slightly when formed with degraded PBAE-10 fragments, it remained positive throughout, with a zeta potential of 4.22 ± 1.64 mV when formed with PBAE-10 degraded for 168h (17.9% of starting MW). Interestingly, PBAE-10 particle size increased rapidly, with

particles formed with PBAE-10 degraded for 48h exhibiting particle sizes greater than 5 µm (**Figure 4.3A; green**). Over this same interval, particle concentration quickly dropped (**Figure 4.3C, D; green**). Light microscopy revealed the morphology and relative concentration of particles in each of the formulations over time. PBAE-4 and PBAE-6 formed uniform, monodispersed spherical particles at each degradation time point until 168h, where particle concentration (i.e., the number of individual particles) dramatically decreased as the presence of large agglomerates and aggregated particles increased (**Figure 4.4; left and center**). Particles formed with PBAE-10, while much smaller, also aggregated more at earlier times, with large agglomerations at the longer degradation times (**Figure 4.4; right**).

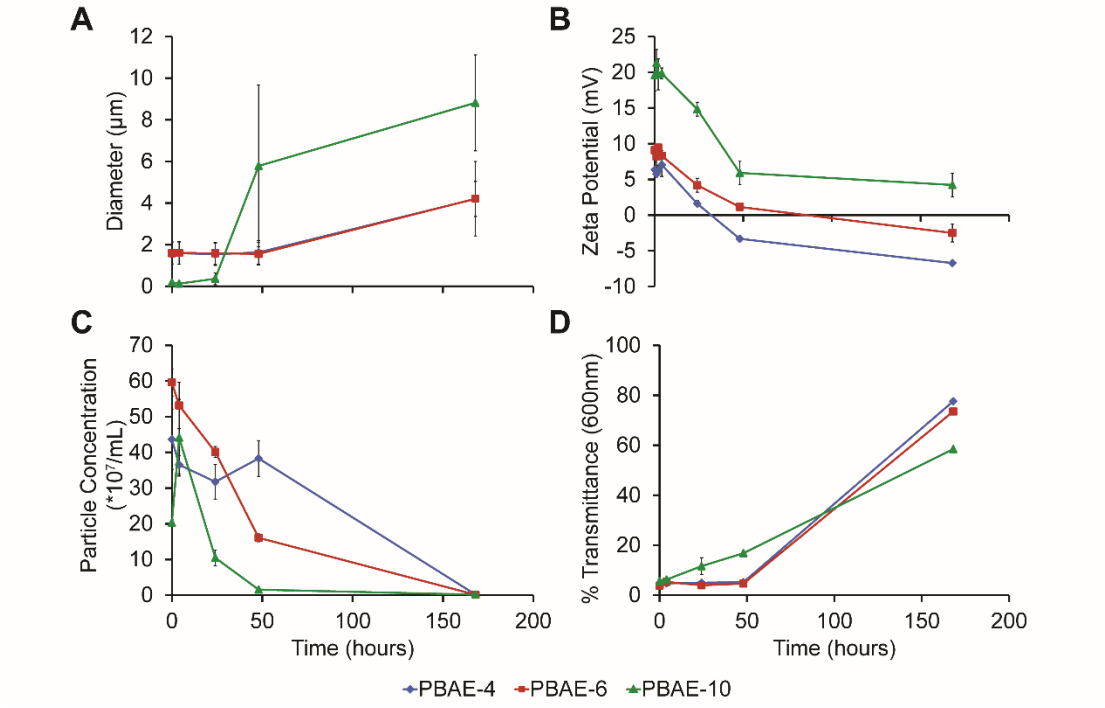

Figure 4.3: Physicochemical properties of particles formed from degraded PBAEs alters as a function of degradation time and MW.
(A) Particle size, (B) zeta potential, (C) conentration, and (D) percent transmittance for particles formed from intact and degraded forms of PBAE-4 (blue), PBAE-6 (red), and PBAE-10 (green). Samples were prepared in triplicated and errors bars represent SEM.

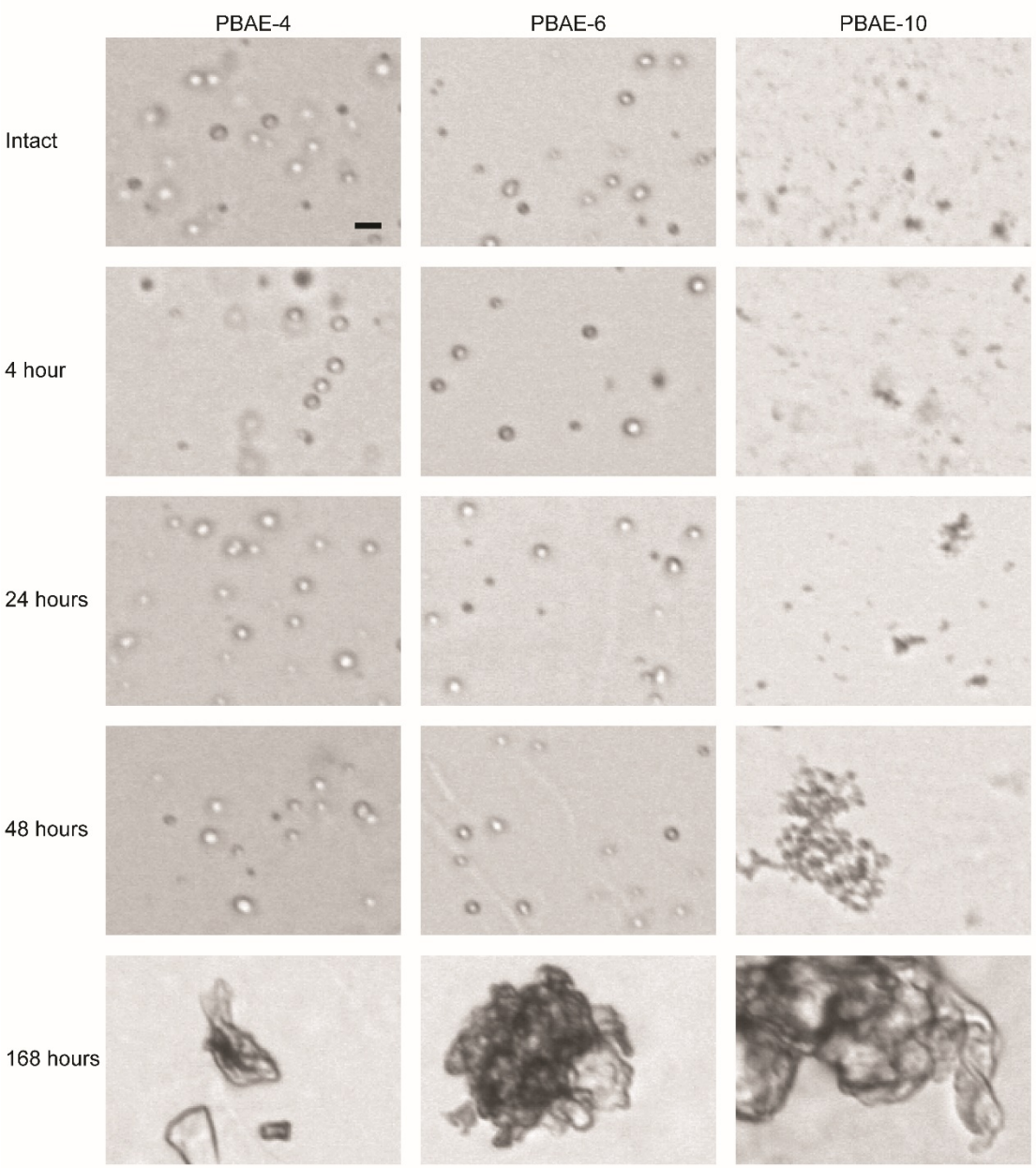

Figure 4.4: Increased degradation time leads to particle aggregation.
Bright field micrographs of particles formed from PBAE-4, PBAE-6, and PBAE-10 that were degraded for 0, 4, 24, 48, or 168 hours. Increased degradation time led to aggregation of particles, most apparent in PBAE-10 particles starting at early times and in PBAE-4 and PBAE-6 by 168 hours. Scale bar= 5μm for all images.

4.3.3 PBAE particles are non-toxic, activate DCs, and promote antigen presentation

Using sets of particles analogous to those above, primary DCs were cultured with each PBAE formulation to assess the intrinsic immunogenic properties of the polymers as a function of the extent of degradation for each structure. Cytotoxicity was first investigated to ensure that the dose of PBAEs used in these experiments did not detrimentally affect DCs. As expected with unstimulated primary immune cells, viability was low in untreated and vehicle controls, and high in cells treated with strong activating signals: positive controls of either LPS or PolyIC, TLR4a and TLR3a, respectively. None of the PBAE formulations caused toxicity relative to untreated, media controls (**Figure 4.5A**). In some cases, treatment with PBAE-4 and PBAE-6 particles led to significant increases in viability – analogous to results observed in control wells stimulated with the positive control adjuvant treatments (**Figure 4.5A**). In a free form, PBAEs did not induce any increase in viability relative to untreated controls (**Figure 4.5A**).

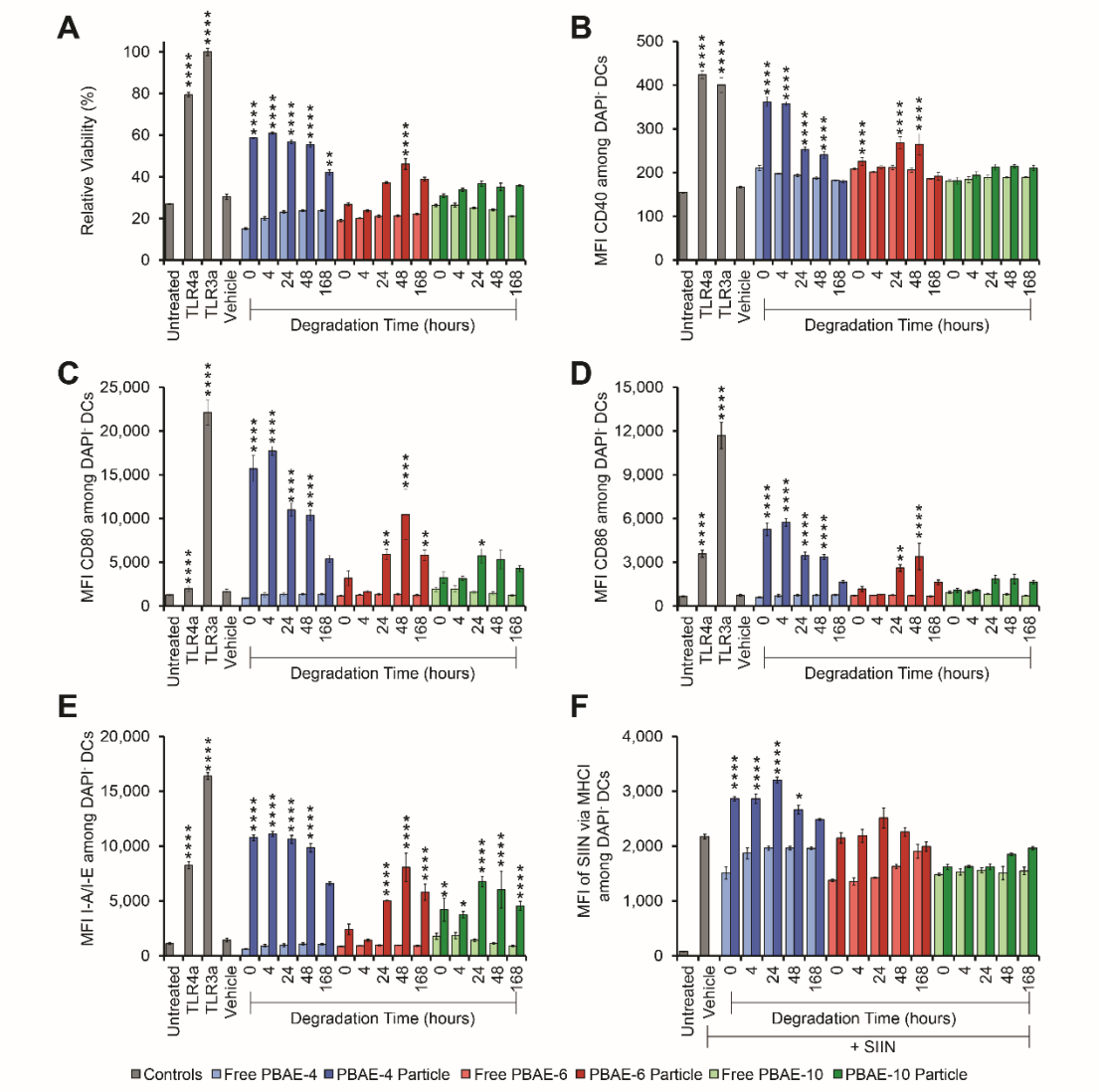

Figure 4.5: PBAE particles exhibit intrinsic immunogenicity as a function of degradation and MW.

(A) Relative viability of DCs after 48 hours in culture treated with LPS ("TLR4a", gray), PolyIC ("TLR3a", gray), buffer only ("Vehicle", gray), soluble PBAE-4 (light blue), PBAE-6 (light red), and PBAE-10 (light green) or PBAE-4 (dark blue), PBAE-6 (dark red), and PBAE-10 (dark green) particles or left untreated ("Untreated", gray). Expression levels of classic DC activation markers (B) CD40, (C) CD80, (D) CD86, and (E) I-A/I-E following treatment as above, gated under $DAPI^-$ cells. (F) MFI of signal pertaining to SIINFEKL presented in mouse MHCI following treatment of DCs with no SIINFEKL ("Untreated", gray), buffer with SIINFEKL ("Vehicle", gray), or SIINFEKL treatment with soluble PBAE-4 (light blue), PBAE-6 (light red), and PBAE-10 (light green) or PBAE-4 (dark blue), PBAE-6 (dark red), and PBAE-10 (dark green) particles, gated under $DAPI^-$ cells. Samples were prepared in triplicated and errors bars represent SEM. (* $p<0.05$; ** $p<0.01$; *** $p<0.001$, ****$p<0.0001$).

We next assessed DC activation by measuring expression of the surface markers CD40, CD80, CD86, or I-A/I-E (mouse MHCII). None of the free forms of the PBAEs activated DCs (**Figure 4.5B, C, D, E, lighter shades**). PBAE-4 particles caused potent activation at time points corresponding to early stages of degradation and then returned to basal levels at longer degradation times (**Figure 4.5B, C, D, E, dark blue**). PBAE-6, which exhibited a higher starting MW but a similar degradation profile to PBAE-4, also activated DCs. However, PBAE-6 particles, which caused little activation at early degradation times, activated DCs to the greatest extent at intermediate levels of degradation (i.e., 24h, 48h) (**Figure 4.5B, C, D, E, dark red**). For PBAE-4 and PBAE-6, the most significant effects were measured for markers of co-stimulation (CD80 and CD86) and antigen-presenting (I-A/I-E). In some cases, these increases were comparable to or exceeded the levels of activation observed when DCs were treated with LPS or PolyIC. PBAE-10, which had the highest starting MW, had minimal effects on activation compared to PBAE-4 and PBAE-6; activation only occurred with the longest extents of degradation and was primarily limited to increases in I-A/I-E expression (**Figure 4.5B, C, D, E, dark green**). Similar trends to those above were evident in analyzing DC activation as a percentage of total cells expressing each activation marker (**Figure 4.6**).

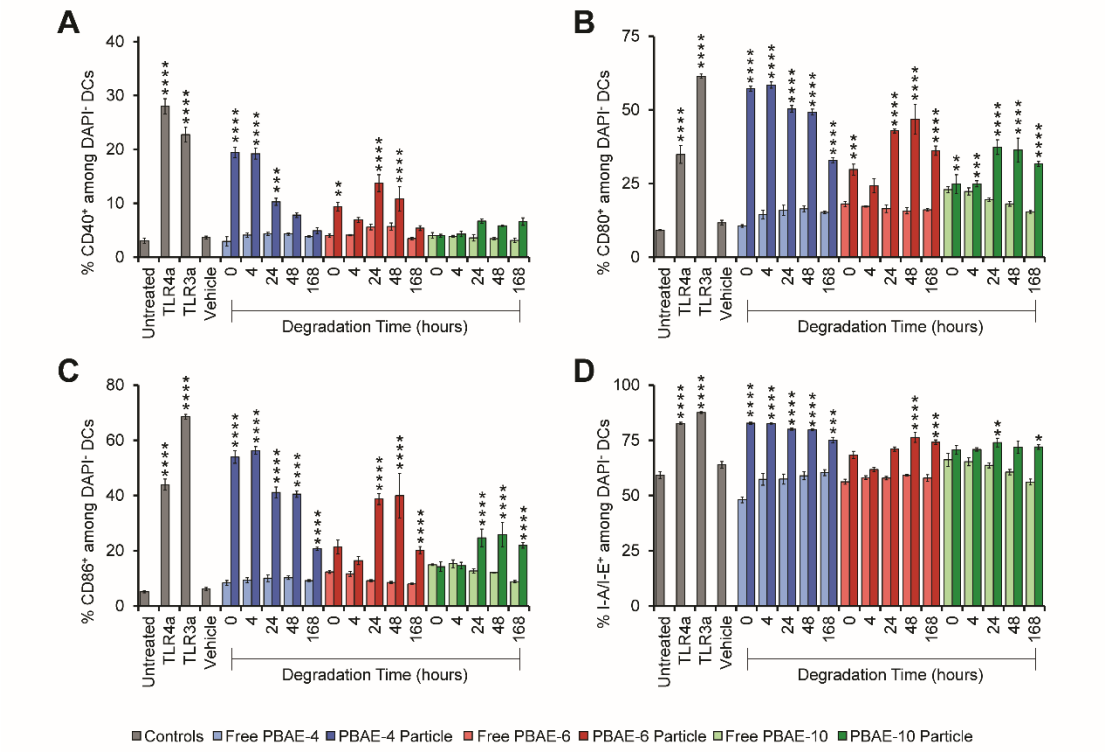

Figure 4.6: PBAE particles induce higher frequencies of DC activation markers.
Frequency of cells expressing high levels of (A) CD40, (B) CD80, (C) CD86, and (D) I-A/I-E after 48 hours in culture treated with LPS ("TLR4a", gray), PolyIC ("TLR3a", gray), buffer only ("Vehicle", gray), soluble PBAE-4 (light blue), PBAE-6 (light red), and PBAE-10 (light green) or PBAE-4 (dark blue), PBAE-6 (dark red), and PBAE-10 (dark green) particles or left untreated ("Untreated", gray), gated under $DAPI^-$ cells. Samples were prepared in triplicated and errors bars represent SEM. (* $p<0.05$; ** $p<0.01$; *** $p<0.001$, ****$p<0.0001$).

Building on the clear levels of DCs activation observed for each PBAE, we explored if these changes drove antigen presentation, the next step in generating functional T cell and B cell responses. To study this, primary DCs were treated with each PBAE in a free form or the various particle forms, along with a model antigen, SIINFEKL peptide. This peptide was selected to support direct measurement of peptide presentation by using an antibody that binds SIINFEKL when presented in the mouse MHCI complex. In agreement with low levels of activation observed with free forms of PBAEs (**Figure 4.5**), free forms of PBAEs along with SIINFEKL did not increase antigen presentation compared to a vehicle control containing only SIINFEKL and no

PBAEs (**Figure 4.5F**). Treatment with PBAE-4 particles resulted in statistically significant increases in antigen presentation at early extents of degradation; these increases then diminished at longer degradation time (**Figure 4.5F, dark blue**). Interestingly, while not statistically significant, the antigen presentation profiles for PBAE-6 and PBAE-10 mimicked the DC activation profiles; PBAE-6 had exhibited a transient increase at intermediate MWs (**Figure 4.5F, dark red**) and PBAE-10 caused small increases at the late stages of degradation (**Figure 4.5F, dark green**).

To determine if generalizable trends occurred between PBAE properties and DC responses, we analyzed the responses as a function of the physical properties of the particles formed from each set of PBAEs. **Figure 4.7** plots the MW of each PBAE against the level of each DC activation marker, indicated by MFI. In each of these analyses, the dotted line represents the value for the DCs treated with buffer alone (vehicle controls). While no global relation was apparent, when analyzing the CD40 marker, a trend developed in which fragments with MW in the range of ~1500-3000 Da were immunogenic (**Figure 4.7A**). For the costimulatory markers CD80 and CD86, activation was seen at all low MWs until reaching a maximum around a MW of ~2000- 2500 Da. Trends for I-A/I-E were even less apparent, but generally, activation was higher at lower MWs. Similar analyses were performed to compare particle size, zeta potential, and concentration to DC activation (**Figure 4.8**). While particle concentration did not seem to have a large impact on activation (**Figure 4.8A**), in general, particle sizes between 1-4μm (**Figure 4.8B**) and neutral to slightly positive zeta potentials (**Figure 4.8C**) induced the most potent activation.

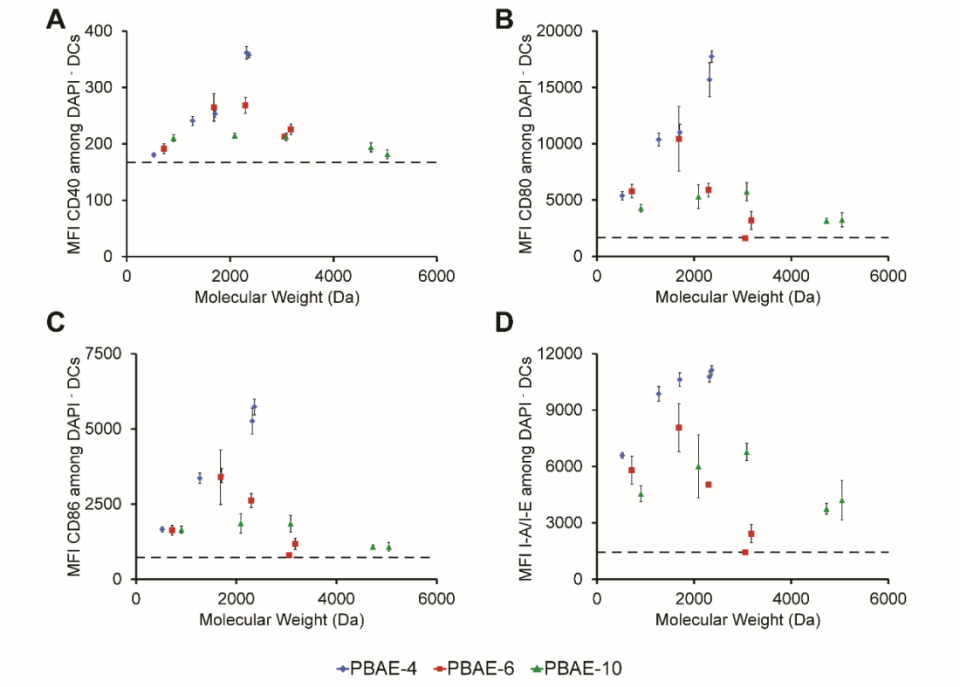

Figure 4.7: Correlation between PBAE MW and DC activation.
Expression levels of DC activation markers (A) CD40, (B) CD80, (C) CD86, and (D) I-A/I-E correlated to the MW of PBAE-4 (blue), PBAE-6 (red), and PBAE-10 (green) used to form the particles. Dotted lines represent the mean value for DCs treat with buffer alone (vehicle control). Samples were prepared in triplicated and errors bars represent SEM.

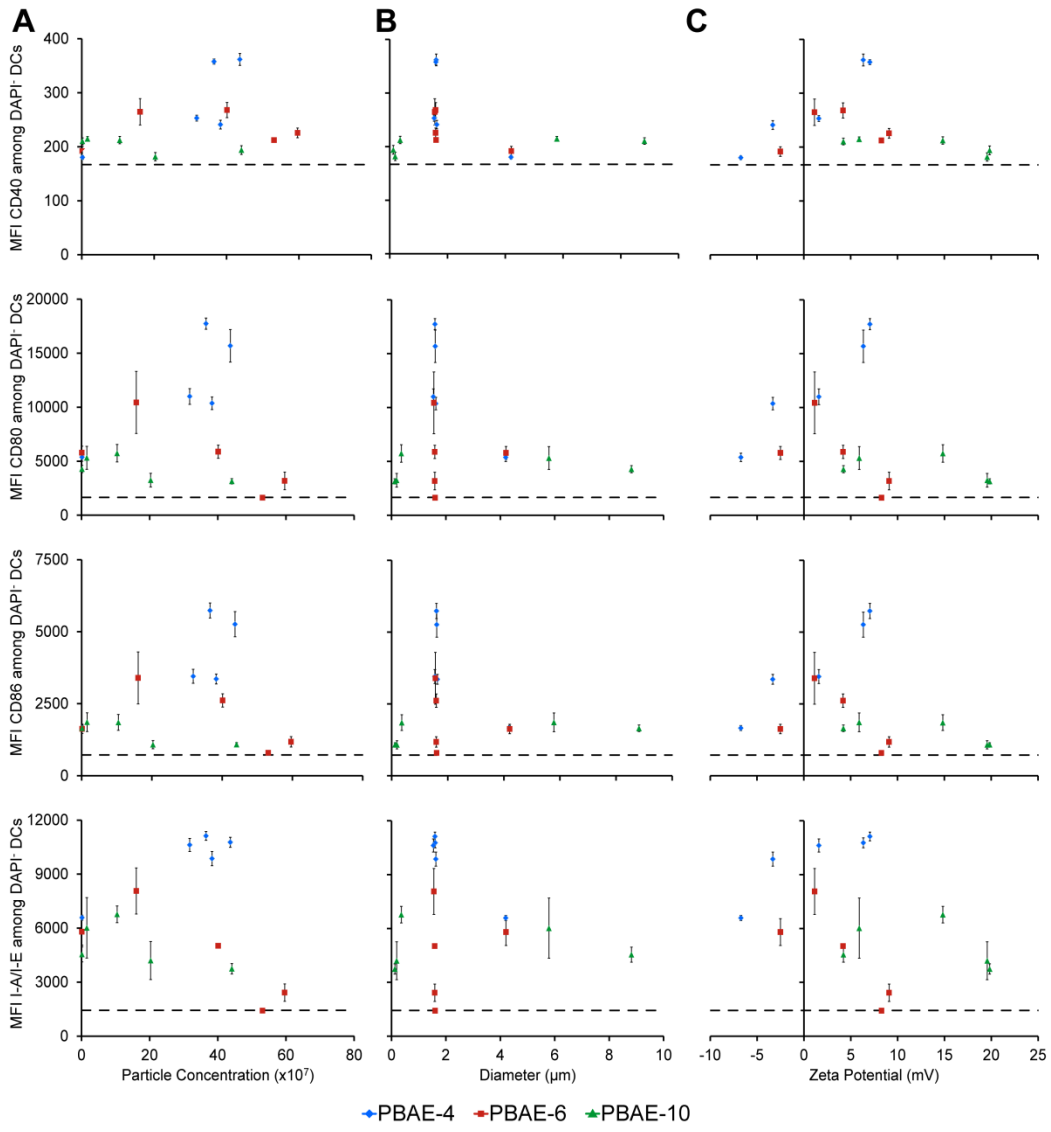

Figure 4.8: Correlation between DC activation and PBAE particle concentration, diameter, and zeta potential.
Expression levels of DC activation markers CD40, CD80, CD86, and correlated to the (A) PBAE particle concentration, (B) diameter, and (C) zeta potential of PBAE-4 (blue), PBAE-6 (red), and PBAE-10 (green) used to form the particles. Dotted lines represent the mean value for DCs treat with buffer alone (vehicle control). Samples were prepared in triplicated and errors bars represent SEM.

4.4 Discussion

Countless studies aim to exploit the ability of biomaterials to encapsulate, transport, and control the release of drugs or vaccine cargos by physically and chemically

tuning materials. Physicochemical properties of materials that evolve during degradation can impact interactions with immune cells, particularly DCs; these cells play an integral role in linking innate and adaptive immunity. However, this evolution of intrinsic immunogenicity is poorly understood and there is a need to understand what properties cause these responses, as well as how significant the effects are. In our previous research, we used a PBAE as a prototypical, rapidly-degrading polymer to test if this class of polymer also exhibits intrinsic immunogenic properties.[163] Here we expanded on our previous findings to a small library of PBAEs, synthesized to have similar polymer structures but with different starting MWs.

One of our most interesting results was that irrespective of starting MW, the immunogenicity of each degrading polymer peaked when the MW decreased to a range of ~1500-3000 Da; these effects were irrespective of the degradation time to reach this range. The immune system has evolved to detect foreign pathogens that have structures not commonly found in humans and animals. Interestingly, many of the characteristics that activate inflammasomes, TLRs, and other danger-sensing pathways include particulate form, hydrophobic fragments, and short repetitive motives—for example, that might resemble bacterial polysaccharides.[156] The degraded particles we studied share some of these features. Further, although the immunogenicity of PLGA as a function of degradation state has not been studied, more general reports on PLGA and other common materials indicate that intrinsic immunogenicity is driven at least in part by inflammasome and TLR signaling.[9, 45] Thus the effects we observed with PBAEs might also trigger these pathways, doing so

in a manner that is optimal during the low MWs mentioned above. This is an intriguing idea as polymers might be designed to degrade or evolve in ways that activate target pro-immune pathways. *in vitro* studies investigating the link between PBAE degradation and the mechanism of uptake by antigen presenting cells could provide insight into which immune-stimulatory pathways are activated, for example, by first systematically inhibiting specific internalization mechanisms. During these studies, the activity level of surface, cytosolic, or endosomal pattern recognition receptors (e.g., TLRs, inflammasome) could then be used to link uptake, processing, and pro-immune signaling. Similarly, *in vivo* studies in TLR and inflammasome knock-out mice could provide insight in a more translational setting. This exciting avenue of research could shed new insight into how the properties and stability of carriers impact processing and immune cell activation.

When evaluating each property's influence on activation, MW seemed to play the clearest role (**Figure 4.7**), as just discussed, while size, zeta potential, and concentration were less distinct (**Figure 4.8**). The optimal particle diameter for DC uptake is in the range of ~1-6μm, though in our studies, not all particles of this size caused DC activation (**Figure 4.8B**). Additionally, while the most potent activation occurred with slightly negatively or positively charged particles, there was little correlation between zeta potential or concentration with activation. Based on these observations, it is likely that a combination of particle properties are impacting DC activation and the intrinsic immunogenicity of PBAEs cannot be attributed to a single physicochemical property. This is of course a complex system, and in other biological

contexts studying similar ideas, analogous trends are arising. For example, one recent study demonstrates that platelet-like particles require an optimal set of properties (i.e., size, shape, functionality) to reduce bleeding time in contrast to optimizing a single property.[166]

The evolution of particle concentration also exhibited some interesting dynamics which could impact immunogenicity or inform design rules. PBAEs at early extents of degradation initially remained stable, with PBAE-4 and PBAE-6 forming micron-sized particles and PBAE-10 forming nanoparticles (**Figure 4.3A**). However, when formed with PBAEs that were degraded for longer times (e.g., lower MW), the resulting PBAE particles aggregated, leading to a larger average size. Due to aggregation of many smaller particles into one larger particle, with increased average size, there was a corresponding decrease in particle concentration. This effect could decrease particle uptake by DCs because of the larger particle sizes, and also because of the decreasing number of particles (i.e., there are fewer, but larger particles).[167] Future studies might also yield new insight by focusing on the most immunogenic fragments and investigating how changing a particular particle property alters immune function. For example, using the most immunogenic forms of the degraded PBAEs to form particles with a range of sizes, then testing how these changes impact DC activation. Such experiments might allow isolation of the relative importance of polymer properties (e.g., MW, structure) compared with more general features such as particle size.

In general, the zeta potential for each PBAE became more negative when formed with PBAEs that were degraded for a longer time (**Figure 4.3B**). Interestingly, while PBAE-4 and 6 both became negatively charged, PBAE-10 particles maintained a positive charge, regardless of the MW of the PBAE used to form the particles (**Figure 4.3B**). With increasingly negative zeta potential, particles could be less likely to associate with the negatively charged cell membrane of DCs, again leading to diminished activation. In gene and drug delivery, cationic materials are often desired for condensing nucleic acids, and also for aiding in association with negatively charged cell membranes. However, recent studies also indicate that surface charge modulates immunogenicity. For example, one recent study demonstrated that negatively charged polymer particles can be used to promote immunological tolerance.[99] Thus the role of charge in intrinsic immunogenicity remains amorphous, and is likely one of several important parameters impacting immune signaling and interactions with antigen presenting cells.

In addition to assessing the role of MW, we successively increased the number of carbons in the backbone of each PBAEs. We hypothesized this change might increase polymer hydrophobicity, decreasing the degradation rate while maintaining the same chemical functionality on each polymer. However, between the different polymers, the degradation constants were similar (λ=-0.9 to λ=-1.1), preventing study of the role of degradation rate. This line of investigation might be facilitated in future studies by increasing the difference in the number of carbons in the backbone.

Lastly, we also observed that PBAEs caused some characteristic effects on viability relative to what one might find with strong inflammatory or danger signals. Each PBAE, regardless of formulation or MW, was nontoxic to the primary splenic DCs over a 48 hour culture. In some cases, PBAE particles had a statistically higher viability compared to the untreated control, suggesting the particle-induced stimulation activates some of the same cell survival and maintenance signals triggered by strong adjuvants such as LPS.[168] Additionally, only PBAE particles were immunogenic, not free forms, further emphasizing the role of form in which the materials are encountered. The activation profile for each of the PBAEs, while similar for each individual polymer across the markers, varied across the different polymers. These results are in agreement with previous studies by Babensee group which reveals DCs plated on a variety of natural and synthetic biomaterial films differentially activate DCs.[109, 157]

4.5 Conclusion

Our results demonstrate PBAEs exhibit intrinsic immunogenicity that changes with degradation state, but irrespective of starting properties, immunogenicity reaches a peak as polymer MW decreases to low values. Other properties (e.g., size, charge, concentration) also changed as a function of degradation state; these changes occurred with changes in DC function, but not in a way that could be correlated. Thus, elucidating the role of each property requires greater understanding of how properties changing in combination impact the interactions and signaling in DCs. However, the current studies support the conclusion that the immunogenicity of

several different polymers evolves during degradation, and that these materials are most immunogenic as particles reach MWs in a characteristic range. Ultimately, through continued investigation of the mechanism of action of degradable polymers, new knowledge could allow for better design of polymer carriers that accounts for how these materials might interact differently with the immune system over the course of degradation.

In the coming chapters, biomaterials including PBAEs are introduced into LNs of mice to probe if these intrinsic immunogenic properties are conserved in animals. **Chapter 5** introduces the methods for intra-lymph node (*i.LN.*) injection, a non-surgical technique to directly deposit materials into LNs of mice. Using this tool, the dose, kinetics, and combinations of signals that reach these important immune tissues can be controlled, allowing investigation into the impact that each of these immune cues has on the resulting immune response.

Chapter 5: Intra-lymph Node Injection of Biodegradable Polymer Particles[4]

5.1 Introduction

The lymph nodes (LNs) are the tissues of the immune system that coordinate the adaptive immune response. At this immunological site, antigen presenting cells (APCs) prime naïve lymphocytes against specific foreign antigens to activate cell-mediated and antibody-mediated immune responses. LNs have thus become an attractive target for delivery of vaccines and immunotherapies. Unfortunately, most vaccine strategies result in inefficient, transient delivery of antigen and adjuvants to the lymphoid tissue.[17] Approaches that improve the targeting and retention of vaccine components in LNs could therefore have a significant impact on the potency and efficiency of new vaccines.

One strategy for circumventing the challenge of LN targeting that has demonstrated great interest in new clinical trials is direct, intra-LN (*i.LN.*) injection.[83, 84, 169] These trials employed ultrasound guidance to deliver vaccines to LNs as a simple outpatient procedure. Compared to traditional peripheral injection routes, this approach resulted in significant dose-sparing and improved efficacy in therapeutic

[4]Adapted from a) J.I. Andorko*, L.H. Tostanoski*, E. Solano, M. Mukhamedova, and C.M. Jewell. "Intra-lymph node injection of biodegradable polymer particles." *J Vis Exp.* 2014, 83 and b) J.I. Andorko, K.L. Hess, K.G. Pineault, and C.M. Jewell. "Intrinsic immunogenicity of rapidly-degradable polymers evolves during degradation." *Acta Biomater.* 2016, 32, 24-34.

contexts including allergies and cancer.[83, 84, 169] These studies employed *i.LN.* injection of soluble vaccines (i.e., biomaterial-free) which were rapidly cleared by lymphatic drainage. Therefore, multiple injections – or cycles of multiple injections – were administered to achieve these impressive therapeutic effects. Improved retention in the LN could enhance the interaction between antigen and/or adjuvant and immune cells, further improving the potency of immune cell priming. This potential is supported by recent studies that show kinetics of antigen and adjuvant delivery play a critical role in determining the specific immune response generated.[54, 170, 171] Further, localizing and minimizing drug and vaccine doses could reduce or eliminate systemic effects, such as chronic inflammation.

Biomaterials have been studied extensively to enhance the potency and efficiency of vaccines.[17, 172, 173] Encapsulation in or adsorption on biomaterial carriers can physically shield cargo from degradation and overcome solubility limitations. Another notable feature of biomaterial carriers, such as polymeric micro- or nano-particles, is the ability to co-load several classes of cargo and, subsequently, release these cargos over controlled intervals. However, a significant limitation that continues to hinder biomaterial vaccines and immunotherapies *in vivo* is inefficient targeting of immune cells and limited trafficking to lymph nodes. For example, peripheral injection of biomaterial vaccines through conventional routes (e.g., intradermal, intramuscular) typically exhibit poor LN targeting, with up to 99% of the injected material remaining at the site of injection.[169, 174] More recently, the size of biomaterial vaccine carriers has been tuned to improve preferential trafficking or

drainage of these vaccines to LNs through interstitial flow.[172, 174] These advances have led to enhanced cellular and humoral immune responses, underscoring the importance of targeting and engineering the LN environment for new vaccines.

Building on recent studies employing surgical techniques for *i.LN.* injection in mice,[170, 171, 175, 176] we developed a quick, non-surgical strategy for injecting biomaterial vaccines, comprised of combines lipid-stabilized polymer particles, to LNs of mice to generate controlled release vaccine depots.[54, 177] The early studies combining *i.LN.* delivery with biomaterial vaccine carriers potently enhanced CD8 T cell response within 7 days after a single injection of controlled release vaccine depots.[54] A strong humoral response (i.e., antibody titers) was also generated; and both enhancements were linked to increased retention of vaccine components in LNs that was mediated by controlled release from the biomaterial carriers. Interestingly, the size of vaccine particles altered the fate of these materials once in the LNs: nanoscale particles showed heightened direct uptake by cells, while larger microparticles remained in the extracellular LN environment and released cargo (e.g., adjuvant) that was taken up by LN-resident antigen presenting cells.[54]

The work below describes the *i.LN.* technique used to control the dose, kinetics, and combination of immune signals that reach LNs. First, as a proof of concept, biodegradable lipid-stabilized polymer particles were synthesized using a modified double emulsion strategy and the particle properties were characterized by laser diffraction and microscopy.[54, 177] These particles were then injected directly into

the inguinal LNs identified non-surgically using a common, non-toxic tracer dye.[178] Post-injection analysis of LNs by histology or flow cytometry verified the distribution of particles within the LN environment and monitored cellular uptake and retention of particles over time. When *i.LN.* injection was used to explore the intrinsic immunogenicity of PBAEs that were previously found to be immunostimulatory in cell studies (see **Chapters 3 and 4**), PBAE particles caused increased to the number and activation states of LN-resident cells.

5.2 Materials and Methods

5.2.1 Synthesis of Lipid-stabilized PLGA Micro- and Nanoparticles

In a 7 mL glass vial, lipids (DOPC, DSPE-PEG, and DOTAP, Avanti Polar Lipids) were mixed at a 60:20:20 molar ratio and dried nitrogen gas for 10 minutes. In a separate, 20 mL glass vial, 80 mg of PLGA (Sigma-Aldrich) was dissolved in 5 mL of dichloromethane to generate a polymer stock solution. 5 mL of the PLGA polymer solution was added to the vial containing the dried lipids, capped, and vortexed for 30 seconds.

For microparticles synthesis, the organic phase containing the polymer and lipid were sonicated on ice at 12 W. A water-in-oil (w/o) emulsion was created by adding 500 µL of distilled H_2O and the solution was sonicated for 30 seconds at 12 W on ice. During sonication, the vial was gently rocked up and down and side to side around the sonicator tip to ensure complete emulsification. The water-in-oil-in-water (w/o/w)

emulsion was formed by pouring the first w/o emulsion into 40 mL of H_2O in a 150 mL beaker which was then homogenized for 3 minutes at 16,000 rpm. For nanoparticle synthesis the first sonication was at 14 W for 30 seconds. The second emulsion was formed by pouring the w/o emulsion into 40 mL of H_2O in a 150 mL beaker and sonicating for 3-5 minutes at 14 W on ice. To remove the excess solvent, microparticle or nanoparticle w/o/w emulsions were stirred overnight. For particles containing a fluorescent dye, 10 µL of DiD (Invitrogen) was added to the organic phase with the polymer and lipids prior to sonication. For particles containing peptide, 1mg of fluorescein-labeled myelin oligodendrocyte glycoprotein, residues 35-55, was suspended in the 500 µL of distilled H_2O used to form the first emulsion.

The following morning, after allowing ~16 hours for the organic phase to evaporate, particles were washed and collected. To do this, the emulsion was poured through a 40 µm nylon mesh cell strainer into a 50 mL conical tube. Microparticles were then centrifuged for 5 minutes at 5,000x g. Nanoparticles were collected by centrifuging for 5 minutes at 24,000x g. The supernatant was then decanted, particles were washed by re-suspending in 1 mL of H_2O, and then transferred to 1.5 mL microcentrifuge tubes. Particles were then collected by centrifuging for 5 minutes at 5,000x g (for microparticles) or 24,000x g (for nanoparticles). Particles were washed twice more by removing supernatant, re-suspending in 1 mL H_2O, and centrifuging as above. After washing, particles were suspended in 1 mL H_2O for immediate use, or lyophilized for extended storage.

5.2.2 PLGA Particle Characterization

Particle size was determined using a Horiba LA-950 via the manufacturer's protocol. Briefly, 10mL of distilled H_2O was added to the clean glass fraction cell with a magnetic micro stir bar. After aligning the lasers, a baseline reading was recorded with the fraction cell containing only distilled H_2O. Then, 10 μL of particle suspension (typically approximately 0.5 mg) was added into the fraction cell, ensuring enough particles were added to generate signal strength in the appropriate range as indicated on the instrument software interface. Particle size was measured using a refractive index of 1.60 by both a number and volume basis.

To visualize particles, particle suspensions were diluted to 1 mg/mL in deionized water. Then, a microscope slide was prepared by adding 3 μL of the diluted particle suspension and mounted using a coverslip at a 45° angle to avoid bubble formation. Particle images were captured using bright field and the appropriate filter sets for any fluorescent cargo.

5.2.3 PBAE synthesis, degradation, and characterization and particle fabrication

PBAEs were synthesized via a Michael-type addition reaction as described previously in **Chapters 3 and 4** [129, 130, 132, 163, 179]. Briefly, 9 mmol of 4,4′-trimethylenedipiperidine was dissolved in anhydrous THF to form a 500 mg mL^{-1} solution. This solution was added to 9 mmol of 1,4-butanediol diacrylate and the reaction was heated to 50°C and stirred for 16 hours. The reaction was cooled to room temperature and the resulting polymer was precipitated in vigorously stirred ice

cold diethyl ether. After collecting the polymer (Poly1) and washing with additional diethyl ether, the polymer was lyophilized. A 16 mg mL^{-1} solution of Poly1 was prepared in $CDCl_3$ and ^1H NMR was used to confirm the structure. Poly1 was dissolved in THF at 2.5 mg mL^{-1} and a THF-based gel permeation chromatography (GPC) system (Waters) was used to determine polymer MW compared to polystyrene standards. To form particles, Poly1 was first degraded by incubating in pH 5 buffer (100 mM SA) at 37°C for 24 hours to form polymer fragments. Poly1 particles were then assembled via electrostatic condensation by mixing 5 mM degraded Poly1 and 20 mM SPS at a SPS:Poly1 w/w ratio of 1:1.6.

5.2.4 Preparation of Mice for i.LN. Injection

A 0.1% (w/v) solution of tracer dye (Evan's Blue, VWR) was formed by dissolving 10 mg of dye powder with 10 mL of distilled H_2O and sterilized using a 0.2 μm syringe filter. One day prior to injection, 4-6 week old C57BL6 mice (Jackson Laboratories) were anesthetized using isoflurane. All studies conducted were done in accordance with approval from the University of Maryland IACUC. To evaluate depth of anesthesia, a toe pinch reflex test was performed and breathing rate was monitored throughout to ensure a respiratory rate of approximately 100-140 BPM. Next, the hair at base of tail and hindquarter of the mouse was shaved using clippers. Hair was removed from the ventral side of the animal and laterally around to the dorsal side just above the joint of the hind leg (hip).

To administer tracer dye, 10 μL of dye solution was transferred into a microcentrifuge tube and aspirated into a 21 gauge needle attached to a 1 mL syringe.

Dye solution was injected subcutaneously on each side of the tail base where the hair was clipped. To remove the remaining hair on the mouse, a mild depilatory cream was applied via cotton swabs and allowed to incubate on the skin for ~3 minutes. After incubation, using a wet gloved hand, depilatory cream was gently rubbed into skin and then removed by wetting a gloved hand with warm H_2O and rubbing tail base and hindquarter repeatedly. Any residual depilatory was removed from the mouse by wetting a paper towel with warm H_2O and in a single motion, wiping the lower portion of mouse. Mice were then allowed to recover under a heat lamp and once fully recovered, returned to holding.

5.2.5 i.LN. injection of PLGA or PBAE particles into inguinal LNs of mice

A day after prepping the mice for injection, mice that were shaved and injected with tracer dye were anesthetized using isoflurane. Drainage of the tracer dye was then visually confirmed in each inguinal LN (the LN appears as a dark spot near the hind thigh and abdomen). Particles were then prepared in distilled H_2O at desired injection concentrations, 10 µL of the particle solution was transferred into a microcentrifuge tube, and aspirated into a 31 gauge insulin needle attached to a 1 mL syringe. For studies with Poly1, 6.5 µg of free Poly1, Poly1 particles, or a sham consisting of buffer were prepared for injection into each inguinal LN. After visualizing the LNs, the skin around the LN was tightened using the thumb, index finger, and middle finger to pull skin taunt and allow for controlled placement of the injection volume. Then, LNs were injected by approaching the LN with the needle at a 90° angle to the skin and penetrating the skin over the dyed LN to a depth of ~1 mm before slowly

injecting. After injection, mice recovered under a heat lamp and returned to holding or conduct additional testing.

5.2.6 In vivo DC activation, LN cell phenotyping, and lymphadenopathy

24 hours after injection of PBAEs in particle or soluble form, mice were euthanized and the inguinal LNs were removed and placed in PBS. A single cell suspension was prepared by passing each LN through a 40 μm strainer with PBS and the total cell number was enumerated using an automated cell counter (NanoEnTek). A portion of the cells were then stained for surface markers using fluorescent antibodies (BD Biosciences, eBioscience, Abcam) and analyzed by flow cytometry for viability ($DAPI^-$), phenotype (DC, $CD11c^+$; B cell, $B220^+$; T cell, $CD3^+$), and DC activation markers (i.e., CD40, CD80, CD86, MHCII).

5.3 Results

5.3.1 Lipid-stabilized particles fabricated with varied sizes can encapsulate immune signals

Figure 5.1 depicts the synthesis and characterization of biodegradable polymer particles, stabilized by amphiphilic lipids. The PLGA particles resulting from the double emulsion, solvent evaporation synthesis protocol (**Figure 5.1A**) were first qualitatively assessed by visual inspection of the final emulsions generated. Particle batches were homogenous, stable emulsions with an opaque appearance. Quantitative assessment of particle synthesis was performed using laser diffraction to analyze size

distribution (**Figure 5.1B**). As expected, the resulting PLGA particles had a tight, monomodal distribution for both microparticles and nanoparticles, indicating a uniform population. The synthesis parameters described in this chapter generated number-averaged distributions centered at approximately 100 nm or 3 µm for nanoparticles and microparticles, respectively. Further qualitative assessment of particle synthesis was achieved through the incorporation of multiple classes of fluorescent cargo. In **Figure 5.1C**, microscopy images of microparticles loaded with a fluorescent peptide ('Peptide', green), a lipophilic dye ('Partile', red), and an overlay image (yellow) confirmed creation of particles within the desired size range and encapsulation of peptide within the volume of the particle.

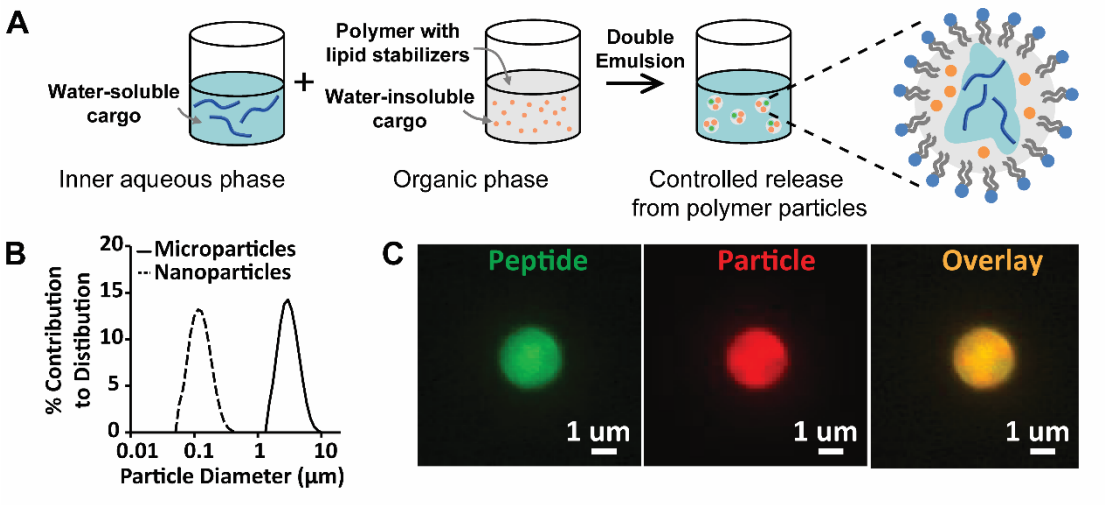

Figure 5.1: Synthesis and characterization of lipid stabilized particles.
(A) Schematic diagram describing the synthesis of lipid-stabilized particles prepared by emulsion/solvent evaporation. (B) Size distributions of microparticles (solid line, diameter = 2.8 µm) and nanoparticles (dashed line, diameter = 113 nm). (C) Fluorescent microscopy images of particles loaded with fluorescently-labeled peptide and a fluorescent particle dye. Labels: peptide (green), particle (red), and the overlay (yellow).

5.3.2 PLGA particles can be successfully deposited into LNs

Following the successful fabrication of particles, *i.LN.* injection was used to introduce these materials into LNs. The first two panels of **Figure 5.2** illustrate the preparation of animals for the *i.LN.* injection strategy described above. Inguinal LNs were first marked by peripheral injection of a non-toxic tracer to identify the location for subsequent *i.LN.* injection of particles (**Figure 5.2A**).[54] Drainage of the tracer dye following subcutaneous injection at the tail base enabled the visualization of the inguinal LNs (**Figure 5.2B**).[54]

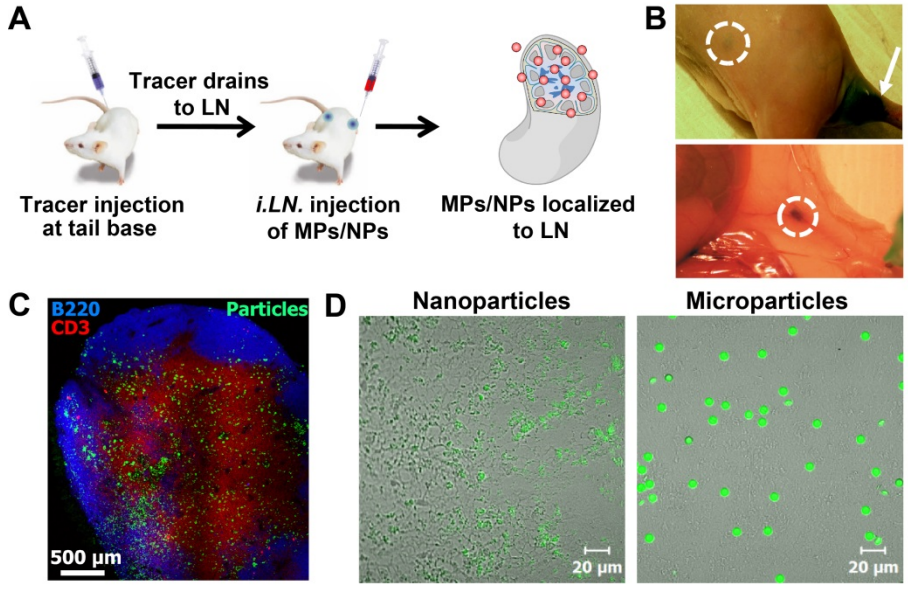

Figure 5.2: *i.LN.* Injection and distribution of biodegradable particles within LNs.
(A) Methodology for *i.LN.* injection. (B) Visualization of LNs in a mouse through skin (upper image) and following necropsy (lower image).[54] (C) Histological staining of a LN confirming deposition and distribution of fluorescently-labeled polymer microparticles (particles, green; T-cells, red; B-cells, blue). (D) Fluorescently-labeled nanoparticles (50 nm, left image) and microparticles (6 µM, right image) in LNs 24 hours after injection.

Confirmation of local delivery to the inguinal LN can be evaluated through observation or histology. In these studies, LN volume was monitored visually during injection as an indicator of successful injection. In general, LNs will swell after

successful injection, allowing for efficient cargo distribution throughout the LN structure, without significant leakage to adjacent tissues or cells. Also, after injection, the injected fluid displaced and diluted the tracer dye within the LN, causing the concentration and coloring of the dye to become less intense following treatment. Histological processing of excised LNs was used to definitively confirm delivery of cargo to the lymphoid tissue, as shown in **Figure 5.2C** and **Figure 5.2D**.

5.3.3 Poly1 particles activate DCs and expand immune cells in mice

After using PLGA particles as a model system to confirm that biomaterials could be directly deposited into LNs using *i.LN.* injection, the effect of Poly1 on secondary lymphoid organs and local immune function was determined using this technique.[13, 14]. Poly1 was successfully synthesized, degraded into low molecular weight fragments, and formulated into particles after degradation (See **Figures 3.2, 3.6, 3.8**). To study the effect of Poly1 *in vivo*, vehicle (i.e., buffer), free Poly1, or Poly1 particles were introduced to the inguinal LNs of mice. After 24 hours, mice were euthanized and LNs were collected. Following treatment, the percentage of $CD11c^+$ DCs found in the LNs treated with vehicle, free Poly1, or Poly1 particles (**Figure 5.3A**) did not significantly change, regardless of treatment. Next, we assessed the impact of Poly1 treatment on the activation of LN-resident cells by measuring expression of CD40 (**Figure 5.3B**), CD80 (**Figure 5.3C**), CD86 (**Figure 5.3D**), and MHCII (**Figure 5.3E**). Treatment with free Poly1 (**Figure 5.3, blue**) did not alter activation compared with the vehicle injection control (**Figure 5.3, gray**). In contrast, Poly1 particles (**Figure 5.3, red**) caused a significant increase in the percentage of

cells expressing each marker compared to vehicle or to free Poly1 treatments. In line with the results of the DC activation studies, treatment with Poly1 particles (**Figure 5.3F, red**) also increased the total number of cells compared to treatments with vehicle (**Figure 5.3F, gray**) or free Poly1 (**Figure 5.3F, blue**). No significant differences were observed in the relative levels of B and T lymphocytes (**Figure 5.3G, H**) between each group, although treatment with Poly1 particles appeared to cause a modest increase in T cells and a corresponding decrease in B cells. These results indicate that Poly1 exhibits intrinsic immunogenicity both in primary immune cells and in animals.

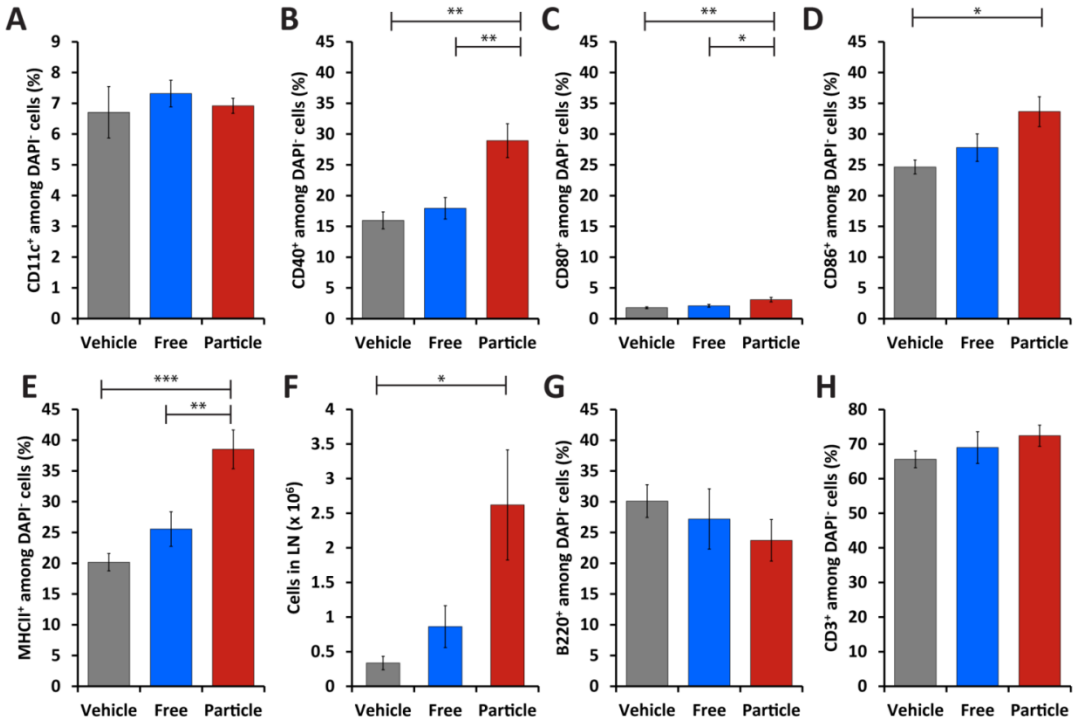

Figure 5.3: Poly1 particles induce DC activation and lymphadenopathy while maintaining cell phenotype balance following *i.LN* injection into inguinal LNs of mice.
(A) Percentage of $CD11c^+$ DCs in LN and expression levels of DC activation markers (B) CD40, (C) CD80, (D) CD86, and (E) MHCII following treatment of C57BL6 mice treated with buffer alone ("Vehicle", gray) or 24 hour degraded (40% original of MW) free Poly1 ("Free", blue) or Poly1 particles ("Particle", red). (F) Lymphadenopathy as determined by total cell number and percentage of B cells (G) and T cells (H) in the LN following treatment as in (A-E). Data are representative of measurements of at least four LNs with error bars representing SEM. (* $p<0.05$; ** $p<0.01$; *** $p<0.001$).

5.4 Discussion

The *i.LN.* injection technique described in this Chapter allows for controlled delivery of vaccines to LNs and to LN-resident antigen presenting cells. Biomaterials encapsulating various immune cargos can be localized within the LN, enabling manipulation of the doses of one or more types of cargo delivered to the LN microenvironment. The localization and controlled release from polymer particles has been shown to generate a potent cellular and humoral immune response at significantly lower doses than conventional approaches. Further, through the manipulation of biomaterial carrier size, the primary mode of cellular processing can be modulated between direct uptake of nanoparticles or extracellular cargo release from larger microparticles.[54] These results establish the feasibility of *i.LN.* biomaterial delivery as a platform for therapeutic vaccine delivery.

PLGA particles were chosen as a model biomaterial system to test *i.LN.* injection because the synthesis of PLGA particles by emulsion/solvent evaporation has been widely employed in drug delivery applications.[180, 181] Thus potential challenges associated with this technique relate mostly to successful identification and deposition of vaccines in the LN target site. To facilitate visualization of target inguinal LNs, tracer dye that specifically drains to LNs was used and hair was removed by shaving and the application of a depilatory. To further identify a successful injection, injected mice can be necropsied and the size of LNs from treated animals can be compared with an uninjected control LN. One limitation of this technique is the physical limit of the injection volume that can be loaded into the LN structure. In our studies, an

injection volume of 10 µL is used for introduction into mice, though other studies have reported larger injection volumes at least as high as 20 µL.[176] However, direct delivery of vaccines via *i.LN.* injection permits dramatic dose-sparing so the function of these vaccines should generally not be limited by volume constraints.

As noted, changing the physical properties of particles (i.e., size) is an effective mechanism to alter the pathway or outcomes induced by biomaterials and encapsulated cargos in LN tissue. The double emulsion, solvent evaporation synthesis allowed for simple, procedural modifications to alter size and can be used in the future to incorporate a variety of cargos or polymers that can alter other physical or chemical properties such as surface charge or functionality, and the rate of biodegradation/cargo release.[181, 182] For example, the release kinetics can be tuned through alternative polymer compositions, and surface function can be altered using modified lipid compositions or poly(vinyl alcohol). The cargo loaded in particles can be easily manipulated to contain different antigens or adjuvants for target pathogens. The advantage of this approach is achieved through the combination of *i.LN.* delivery with local, controlled release of cargo from biomaterials. This synergy establishes a platform that can be exploited to efficiently generate adaptive immune responses using minute doses and with reduced non-specific/systemic side effects.

To begin to investigate how polymer carriers may be causing some of these non-specific side effects, *i.LN.* injection was use to explore if the intrinsic immunogenicity

of PBAEs revealed in **Chapters 3 and 4** translated to mice. When Poly1 was introduced into mice, we discovered that Poly1 alters the composition and function of LNs. Local injection in these studies allowed careful control over the composition and dose of the materials in LNs, revealing that, in agreement results from cell studies (see **Chapters 3.3 and 4.3**), Poly1 (i.e., PBAE-4) is immunogenic *in vivo* and that the level of this activity depends on the material properties (**Figure 5.3**). Treatment with Poly1 particles led to an increase in the number of cells in LNs and activated DCs, while the effects of free Poly1 on LN-resident cells were more modest. Together, these observations suggest that the intrinsic immunogenicity of Poly1 promotes a general (innate) stimulatory effect, with only a weak polarization of the T or B cell compartment. However, these analyses were carried out after 24 hours; at later time points and in future studies when antigen and adjuvant are present, antigen-specific effects may be observed. Supporting this possibility, a small biasing toward the T cell compartment was observed in LNs after treatment with Poly1 particles, slightly increasing the frequency of T cells (**Figure 5.3H**) and slightly decreasing the frequency of B cells (**Figure 5.3G**).

5.5 Conclusion

The continued exposure of LNs to vaccine cargos has shown to result in a robust systemic immune response. The new, *i.LN.* injection technique outlined in this chapter provides a platform to directly control the amount of immune signals that reach LNs without relying on inefficient, passive drainage. Through the use of this

tool, precise control over the timing and combination of signals to these important immune tissues allows for the study of the local response to these tissues.

In this chapter, the intrinsic immunogenicity of a degradable PBAE was investigated and confirmed in an animal model. In **Chapter 6**, *i.LN.* injection is used to introduce biomaterial carriers encapsulating vaccine components into LNs of mice. These studies provide new knowledge of how these cues impact the local LN microenvironment and the resulting, antigen-specific, systemic immune response.

Chapter 6: Targeted programming of the lymph node environment causes evolution of local and systemic immunity[5]

6.1 Introduction

Historically vaccine design has focused on generating potent, specific immune responses. However, equally important for vaccines aimed at persistent and emerging diseases, is the need to better control the nature of the immune responses that are generated. For example, in the context of cancer vaccination, tumor-specific $CD8^+$ T cells that exhibit memory-like characteristics and proliferate at very high rates might help overcome the immunosuppressive tumor microenvironment[183, 184]. Even vaccines aimed at well controlled pathogens – such as flu – could benefit from formulations that offer better immunomodulatory capabilities, in this example, by conferring increased production of mucosal antibodies[185]. Another area of intense research along these lines is in the exploitation of new adjuvants – such as toll like receptor agonists (TLRas) that stimulate pathogen-detecting inflammatory pathways. These molecules can be delivered alone, or in combination to create polarizing or synergistic effects[186-190]. Better understanding of the effects of specific vaccine components, adjuvants, and carriers, along with knowledge of how these agents work together, would help support the design of more effective vaccines.

[5]Adapted from J.I. Andorko*, J.M. Gammon*, L.H. Tostanoski, Q. Zeng, and C.M. Jewell. "Engineering local lymph node function with degradable polymer depots to generate systemic antigen-specific immunity." *Cel. Mol. Bioeng.* 2016, 9, 418-432.

Lymph nodes (LNs) are tissues that initiate, maintain, and regulate adaptive immune response, and are thus critical targets for vaccines and immunotherapies. At these sites, antigen presenting cells (APCs) display antigens to T and B cells with the same specificity to mount antigen-specific effector function[20]. Thus the local signals integrated in LNs help define the specificity, magnitude, and nature of the resulting systemic responses. A key hurdle facing new vaccines and immunotherapies is efficiently targeting these sites[191]. For example, to effectively prime lymphocytes against a specific antigen, both the antigen and an adjuvant or other stimulatory immune signal need to be localized to the same tissue, while the combinations and relative concentrations of vaccine components dramatically impact the characteristics of this response. Unsurprisingly, significant interested has developed in strategies that allow more efficient delivery to LNs and more precise control over the local environment in these tissues.

To address the challenges above, many reports in the past several decades have investigated biomaterial carriers (e.g., polymer particles[49, 192], liposomes[193-196]) that encapsulate or adsorb combinations of antigens and adjuvants.[103] The tunable sizes, particulate nature, and ability to co-deliver cargos make these vehicles attractive as vaccine formulations that can be injected and drain to LNs or can be carried there by APCs[15]. Particle size plays a major role in the efficiency and route by which these vaccines reach LNs[197], an area that has been heavily investigated[15, 103]. While many exciting approaches have been reported, even those that generate robust immune responses are limited in the control they provide

over the routes or doses by which particles reach LNs after injection. Instead, vaccines generally rely on passive draining through lymphatic vessels, uptake by APCs and subsequent trafficking to LNs, or more recently, active targeting using receptor/ligand interactions[15, 103]. Thus, a relatively small faction of the total injected dose actually reaches LNs[105, 197], increasing the required dose in some cases, or preventing efficacious response in others. These effects are also important since some vaccine or immunotherapy components have toxic or inflammatory effects that limit the dose or frequency of administration.

A consideration specific to biomaterial carriers is the growing list of polymers, such as poly(lactic-co-glycolic acid) (PLGA), polystyrene, and others[103, 198-200], that exhibit intrinsic inflammatory effects even in the absence of other immune signals[103]. PLGA, for example, is used in countless vaccine and immunotherapy studies, but can activate the inflammasome and increases stimulatory response to TLRas[200]. While these are characteristics that can be harnessed, they can also complicate vaccine research because of the increased complexity resulting from "carrier-effects" that alters how the immune system responds to antigens or other vaccine components. A better understanding of how immune signals – and their biomaterial carriers – interact with the local LN microenvironment, and how these interactions direct systemic immunity would help improve vaccine performance, while also contributing to more rational vaccine design strategies.

We recently developed a strategy to deposit biomaterial vaccine depots directly in LNs of mice using intra-lymph node (*i.LN.*) injection (see **Chapter 5**) [13, 14, 198]. This platform allows direct control over delivery of vaccine components to LNs, and sustained release of encapsulated cargo within these tissues. In previous work using *i.LN.* delivery, microparticles (MPs) encapsulating adjuvant generate more potent responses than nanoparticles or soluble adjuvant because these large particles are better retained in LNs[13]. Therefore, in this work, *i.LN.* injection of adjuvant-loaded MPs was used as a tool to study the evolution of these local and systemic responses over time in mice. The data demonstrates that *i.LN.* deposition of vaccine depots consisting of PLGA MPs loaded with a TLR3a and suspended in soluble ovalbumin (OVA) antigen increases the number of APCs and lymphocytes in LNs over the course of 7 days. Treatment does not alter the relative composition of these compartments, but does increase the activation of resident APCs. A single treatment with these vaccine depots expands antigen-specific $CD8^+$ T cells locally in treated LNs and systemically in peripheral blood, evolving from a potent effector response at day 7 to a memory response by day 28. It is next revealed that this approach is generalizable: *i.LN.* injection of vaccine depots loaded with either PolyIC or CpG – potent TLRas being explored in human trials – and then mixed with conserved human melanoma antigens potently expand tumor-specific $CD8^+$ T cells. These effects correlate with slowed tumor progression during an aggressive challenge with metastatic melanoma. Together this work demonstrates that local programming of distinct LNs with adjuvant depots can be used to drive local alterations that promote immunity that is systemic and antigen-specific.

6.2 Materials and Methods

6.2.1 Particle Synthesis

Degradable MPs synthesized via a double-emulsion, solvent evaporation technique[13, 14]. For lipid stabilized particles, 1,2-dioleoyl-sn-glycero-3-phosphocholine, 1,2-distearoyl-sn-glycero-3-phosphoethanolamine-N-[amino(polyethylene glycol)-2000], and 1,2-dioleoyl-3-trimethylammoniumpropane (Avanti Polar Lipids) were prepared at a 60:20:20 mol ratio and dried under nitrogen. 80mg of PLGA (Sigma) was dissolved with the 5.15μmol of lipids in 5mL of dichloromethane. An inner aqueous phase containing 500μL of water or 5mg of polyinosinic-polycytidylic acid (PolyIC) (Invivogen) in 500μL of water was added to this organic phase containing polymer and lipid and sonicated for 30 seconds at 12W to form the first emulsion. This emulsion was then added to 40mL of water, homogenized for 3min at 16,000rpm, and then allowed to evaporate overnight while stirring to remove any excess organic solvent. Particles stabilized with poly(vinyl alcohol) (PVA, Sigma) were formed as above by removing lipids and replacing the second water phase with a 2% w/v solution of PVA. For particles containing CpG (sequence: 5' T-C-C-A-T-G-A-C-G-T-T-C-C-T-G-A-C-G-T-T 3', IDT), 3mg of CpG in 500μL of water was used for the first aqueous phase. After overnight stirring, all particle formulations were passed through a 40μm cell strainer to remove any large aggregates and collected via centrifugation (5000*g*, 5min, 4°C). Supernatants were removed and particles were washed three times with 1mL of water then suspended in water or PBS for animal studies, or lyophilized and stored at 4°C prior to use. For

preparation of fluorescently-labeled particles, 5μL of DiI (Invitrogen) was added to the organic phase.

6.2.2 Particle Characterization

Particle diameter was determined using an LA-950 laser diffraction analyzer (Horiba). Zeta potential was measured using a Malvern Zetasizer Nano ZS90. PolyIC and CpG loading levels were determined via UV/Vis spectrophotometry after hydrolyzing a known mass of lyophilized particles overnight in 0.2N NaOH. Absorbance values were compared to standard curves of known masses of PolyIC or CpG to determine a mass of cargo per mass of polymer.

6.2.3 i.LN. Injection

For each animal study, were prepared as outlined in **Chapter 5.** Briefly, a small region of fur was removed from the lateral hind quarter of 4-6 week old C57BL6 mice (The Jackson Laboratory) by shaving the area and applying a mild depilatory. Tracer dye (Evan's Blue) was then injected subcutaneously (*s.c.*) on each side of the tail base as previously reported[13, 14, 198]. After allowing 16hrs for the tracer dye to drain to the inguinal LNs for visualization, a 31G insulin needle was used to inject 10μL containing the indicated treatment into each inguinal LN. For visualization of particles in LNs, 1mg of DiI labeled MPs were injected. For model antigen studies, vaccinations consisted of 1mg of particles encapsulating ~8.5μg PolyIC/mg MPs suspended in PBS with 25μg soluble ovalbumin (OVA, Worthington) ('PolyIC MP/OVA'), an injection of 1mg of PLGA MPs with no cargo ('Empty'), or an injection of buffer alone ('sham'), as indicated. In experiments comparing PolyIC and

CpG depots, equivalent doses of adjuvant encapsulated in MPs were administered *i.LN*, after being suspended in PBS with 25 μg of soluble OVA or soluble Trp2 (SVYDFFVWL, Genscript) antigens. After priming, mice were boosted with soluble vaccine treatments *s.c.* at each side of tail base at day 21, with each injection consisting of 25 μg antigen + 25 μg adjuvant. For studies comparing melanoma antigens (Trp2, hgp100), treatments included 1mg of particles containing ~3.5μg CpG/mg MPs suspended in PBS with 25μg of soluble Trp2 ('CpG MP/Trp2') or soluble hgp100 (KVPRNQDWL, Genscript; 'CpG MP/hgp100') antigens, or strong pre-clinical vaccine consisting of 50μg of CpG and 50μg peptide formulated with montanide ISA 51 (Seppic; 'Montanide/CpG/Trp2' or 'Montanide/CpG/hgp100'). After vaccinating *i.LN.* at day 0, subsequent boosts for MP groups were given at days 15 and 36 post prime and were identical to the prime but administered *s.c.* at the tail base. For the montanide groups, all injections were *s.c.*, but the second boost consisted of soluble Trp2 or soluble hgp100 mixed with CpG (see caption). All animal studies were approved by the University of Maryland IACUC and conducted in accordance with local, state, and federal guidelines.

6.2.4 Tissue Collection, Processing, and Flow Cytometry

At the indicated times after treatment, LNs were collected from mice, placed in PBS, and processed into single cell suspensions by mechanical dissociation through a 40μm strainer. Cells were split into three portions. One portion of cells was centrifuged (800*g*, 5min, 4°C) and suspended in FACS buffer (1x PBS with 1% w/v bovine serum albumin, Sigma) containing 1% DAPI (Invitrogen) and Liquid

Counting Beads (BD) to quantify cell viability and enumerate total cell numbers using a FACS Canto II (BD), respectively. The other two portions of cells were washed once with 1mL of FACS buffer then blocked with Fc Block (anti-CD16/CD32, BD) for 10 minutes at room temperature to inhibit any non-specific binding. After blocking, one portion of cells was stained for innate cell type and activation with indicated antibodies against cell surface markers including CD11c, F480, CD40, CD80, CD86, and I-A/I-E (mouse MHCII). Cells were then washed twice, suspended in FACS buffer, and quantified via flow cytometry. The final portion of cells was stained for lymphocyte populations and antigen-specific tetramer levels. First, 25μL of anti-SIINFEKL tetramer was added and incubated for 30min at room temperature. Then, 25μL of antibodies against surface markers including B220, CD3, CD4, and CD8 were added and incubated for 20min at room temperature. Cells were then washed and evaluated, as above. The frequency of each cell population (percent of parent population) and number of counted cells per identical acquisition volume (80μL) was evaluated. The B220 antibody was purchased from eBiosciences and all other antibodies were purchased from BD.

6.2.5 MHC Tetramer Staining of Peripheral Blood

Every 7 days, 100μL of blood was collected from mice treated as above via submandibular bleeding. Red blood cells were removed by adding 1mL of ACK lysis buffer to the blood, incubating for 3min, collecting cells via centrifugation (800*g*, 5min, 4°C), and repeating with 1mL of fresh ACK lysis buffer. After the second round of ACK lysis buffer, cells were suspended in FACS buffer, blocked with Fc

Block, and stained with a tetramer specific for either SIINFEKL (CD8-epitope of OVA), Trp2, or hgp100 for 30min at room temperature. All tetramers were purchased from MBL International. Following incubation, cells were stained against surface markers CD3, CD8, CD44, and CD62L for 20min at room temperature. After washing twice with FACS buffer, cells were suspended in FACS buffer containing DAPI and the percentage of antigen-specific cytotoxic T cells ($DAPI^-$, $CD8^+$, $tetramer^+$) was quantified via flow cytometry. To determine generation of central memory T cell phenotypes, $tetramer^+$ $CD8^+$ cells were gated for $CD44^{high}/CD62L^{high}$ populations and compared to the percentage of effector memory T cells ($CD44^{high}/CD62L^{low}$).

6.2.6 Tumor Challenge Studies

In some studies, after treating mice with the indicated vaccines, mice were administered 300,000 B16-F10 cells (ATCC) in 100μL of 1x PBS *s.c.* at the hind flank. Each day following inoculation, body weight was monitored and tumor burden were calculated as a product of two orthogonal diameters. Mice were euthanized according to IACUC-approved humane endpoints when the aggregate tumor burden reached $150mm^2$.

6.2.7 Immunohistochemical Analysis

At indicated time points, inguinal LNs were removed and frozen in OCT compound (Tissue-Tek). Using a Microm HM 550 cryostat (Thermo Fisher Scientific Inc.), 6μm sections of LNs were cut, transferred to slides, and allowed to dry overnight. LN

tissue was then fixed for 5min in ice-cold acetone then washed in 1x PBS. Samples were then blocked for non-specific binding of secondary antibody using 5% goat and 5% donkey serum in 1x PBS for 30min. After washing in PBS, tissues were stained for cell surface markers including B220 (eBioscience), CD3 (Abcam), and CD11c (BD) for 1hr at room temperature. After washing twice with PBS, fluorescent secondary antibodies (Jackson Immunoresearch) were added for 45min then washed three more times. After staining, sections were fixed with 4% paraformaldehyde, washed with PBS, quenched with 1% glycerol in PBS, and washed again before mounting in Prolong Diamond Antifade Mountant (LifeSciences) and imaging using an Olympus IX83 fluorescent microscope. Processing of images was conducted versus an antibody iso-type control and levels were adjusted equally for all similar channels.

6.2.8 Statistical Analysis

Student's *t* tests were used in comparison of two groups. One-way ANOVA with a Tukey post-test was used to compare three or more groups, or two-way ANOVA for comparisons over time. In all cases, analyses were carried out with Graphpad Prism (version 6.02). Error bars in all panels represent the mean ± SEM and p-values < 0.05 were considered significant. Levels of significance were defined as *$p<0.05$; **$p<0.01$; ***$p<0.001$; ****$p<0.0001$.

6.3 Results

6.3.1 PLGA MPs are dispersed in LNs following i.LN. injection

PLGA MPs were synthesized via a double-emulsion/solvent evaporation technique allowing for the inclusion of negatively charged nucleic acid TLRa adjuvants PolyIC or CpG with loading levels of 8.5μg/mg MP or 3.5μg/mg MP, respectively (**Table 6.1**). Addition of PolyIC led to an increase in particle diameter from 2.2μm to 4.3μm and a shift in zeta potential from 24.9mV to -23.7mV; replacement of PolyIC with CpG led to similar shifts (**Table 6.1**). To first confirm retention of injected MPs into LNs, we injected DiI-labeled MPs into inguinal LNs of mice using the approach we previously described (**Figure 6.1A**)[13, 14, 198]. 28 days after injection, LNs were removed and then stained for B cell (**Figure 6.1B, cyan**) and T cell zones (**Figure 6.1B, white**). Fluorescent microscopy confirmed retention of MPs in the LNs at this time point (**Figure 6.1B, green**).

Table 6.1: Characteristics of adjuvant loaded PLGA-MPs used in *i.LN.* injection studies.

	Diameter (μm)	Loading (μg cargo/mg MP)	Zeta Potential (mV)
Empty	2.19 ± 0.14	n/a	24.93 ± 0.91
PolyIC	4.26 ± 0.09	8.53 ± 0.46	-23.70 ± 0.71
CpG	4.02 ± 0.14	3.45 ± 0.37	-23.23 ± 2.54

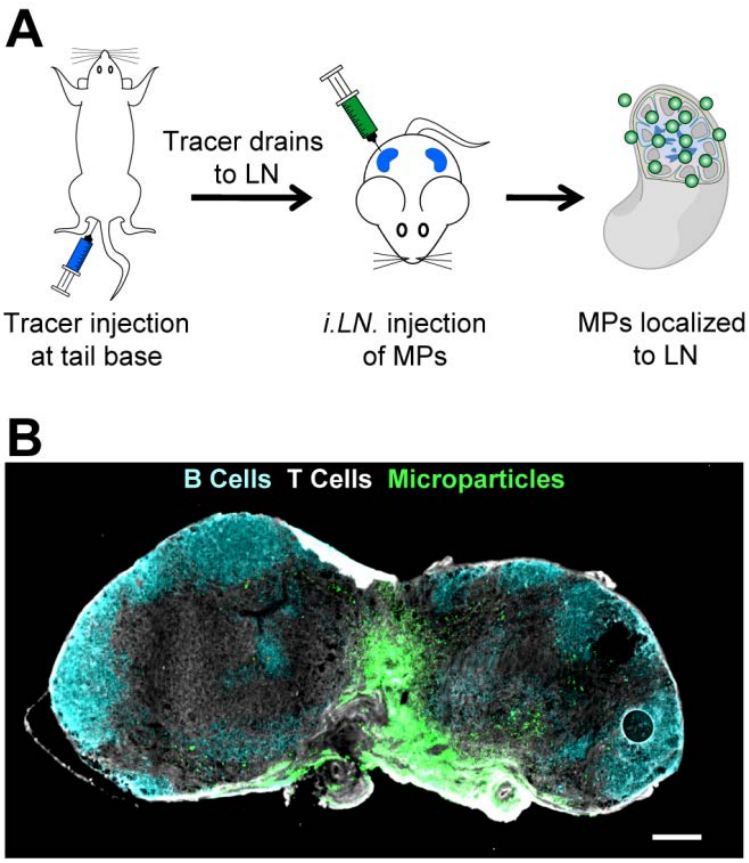

Figure 6.1: Vaccine depots can be locally deposited in LNs via *i.LN.* injection.
(A) Schematic depicting *i.LN.* injection of vaccine depots. A tracer dye is injected *s.c.* at the tail base, which then drains to the inguinal LNs allowing visualization of the LN through the skin. Vaccine depots can then be injected into the LN. (B) Histological section of LN 28 days after *i.LN.* injection of fluorescent depots. B cells ($B220^+$, cyan), T cells ($CD3^+$, white), PLGA MPs (DiI, green). Scale bar= 200μm.

6.3.2 i.LN. injections of PolyIC MP/OVA increases the number of APCs and lymphocytes in LNs

After confirming MPs are retained in LNs of mice over 4 weeks, we used *i.LN.* injection to administer a vaccine of PolyIC MPs mixed with soluble OVA (PolyIC MP/OVA), or to administer a buffer injection (sham). Cell viability and the frequency and number of DCs, macrophages, T cells, and B cells in the treated nodes were then monitored over 1 week using identically-treated sets of groups. Following treatment,

PolyIC MP/OVA, while slightly diminishing initial cell viability relative to sham, did not impact viability after 1 week (**Figure 6.2A**). Particles did cause an increase in the overall number of cells (**Figure 6.2B**), as well as the volume of each LN (discussed below), with nodes treated with PolyIC MP/OVA exhibiting significantly more cells per LN than the sham at day 1 ($p<0.01$); a similar trend was observed over one week. In investigating how PolyIC MP/OVA treatment influenced innate immune cell populations, we discovered the frequency of DCs ($CD11c^+$) did not significantly change over 1 week, while a slight elevation in macrophage ($F4/80^+$) frequency was observed (**Figure 6.2C**). However, the number of each of these cell types (normalized to equivalent tissue cell suspensions) increased over time, with significantly more DCs ($p<0.001$) and macrophages ($p<0.01$) accumulating in the LNs over 7 days following PolyIC MP/OVA injection (**Figure 6.2D**). Similarly, we observed modest changes in the frequency of lymphocytes in the B cell ($B220^+$) and T cell ($CD3^+$; $CD3^+/CD4^+$; $CD3^+/CD8^+$) compartments relative to sham injections (**Figure 6.3A**). However, enumeration of the number of lymphocytes again revealed PolyIC MP/OVA increased the number of cells in each population, with the maximum difference between groups occurring 7 days after the immunization. Immunohistochemical staining of the LNs at 1 day (**Figure 6.4A**) and 7 days (**Figure 6.4B**) after injection confirmed the increased total number of cells, indicated by the increased area evident in each section; all sections are presented at the same scale. These studies also qualitatively confirmed the increased DC levels we measured in response to PolyIC MP/OVA treatment relative to sham, and the increase in DC number as a function of time. These trends are illustrated in the insets of **Figure 6.4B**

at day 7 (i.e., sham vs. PolyIC MP/OVA) and the insets of **Figure 6.4A** and **Figure 6.4B** for PolyIC MP/OVA (i.e., day 1 v. day 7), respectively.

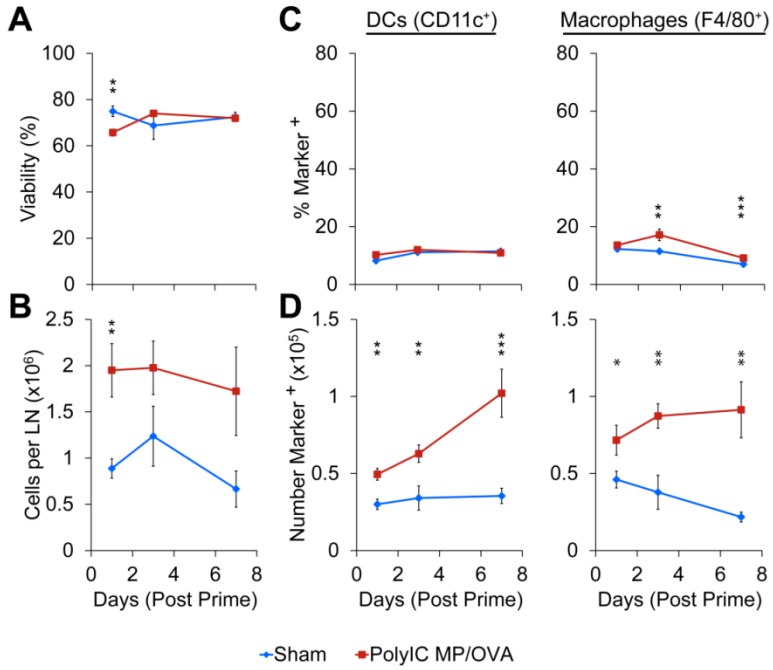

Figure 6.2: *i.LN.* injection of PolyIC MP/OVA depots increases innate cell numbers in the LNs without affecting cell viability.
(A) Viability and (B) total number of LN cells after *i.LN.* injection of PolyIC MP/OVA depots or a sham injection of PBS at days 1, 3, and 7. (C) Percentage of total LN cells which are DCs ($CD11c^+$) and macrophages ($F480^+$) and (D) number of DCs and macrophages in LNs counted in an identical acquisition volume (80µL). n=9-10 LNs per group with bars depicting mean ± SEM. (*p<0.05; **p<0.01; ***p<0.001).

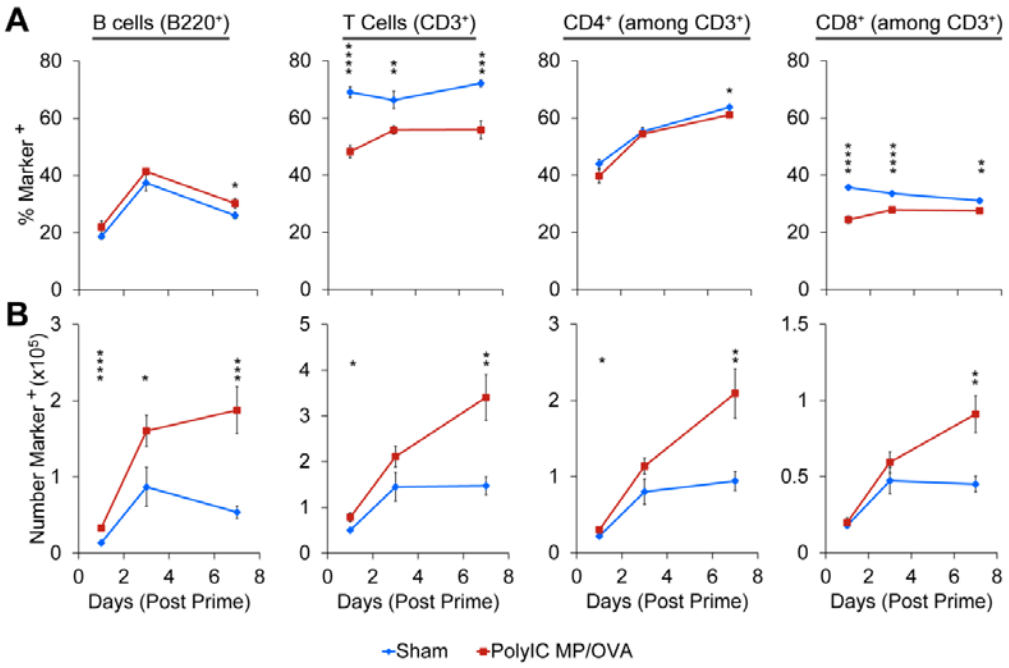

Figure 6.3: *i.LN.* injection of PolyIC MP/OVA depots increases total number of T and B lymphocytes within LNs.

(A) Percentages and (B) total numbers of B cells ($B220^+$), T cells ($CD3^+$) as well as $CD4^+$ T cells ($CD3^+$/ $CD4^+$) and $CD8^+$ T cells ($CD3^+$/ $CD8^+$) in LNs after *i.LN.* injection of PolyIC MP/OVA depots or a sham injection of PBS at days 1, 3, and 7. Numbers are counted in an identical acquisition volume (80µL). n=9-10 LNs per group with bars depicting mean ± SEM. (*p<0.05; **p<0.01; ***p<0.001; ****p<0.0001).

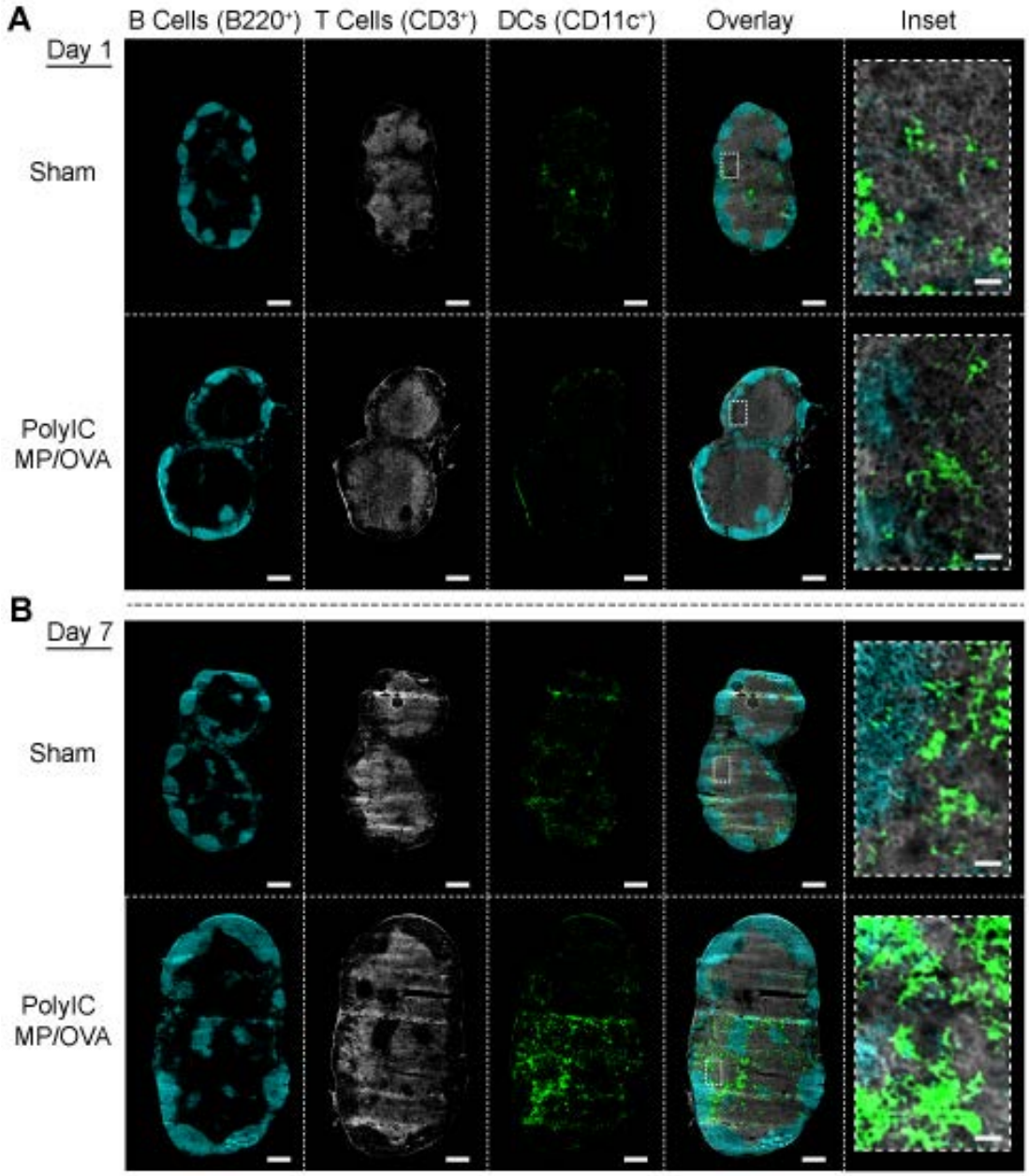

Figure 6.4: Increased LN size and DC numbers in LNs occurs by day 7 after *i.LN.* injection of PolyIC MP/OVA depots.
Histological staining of LNs for B cells ($B220^+$, cyan), T cells ($CD3^+$, white), and DCs ($CD11c^+$, green) in LNs 1 day **(A)** and 7 days **(B)** after *i.LN.* injection of PolyIC MP/OVA depots or a sham injection of PBS. Scale bar= 400μm; 20μm in inset.

6.3.3 PolyIC MP/OVA treatment activates LN-resident APCs

After determining that *i.LN.* treatment with PolyIC MP/OVA increases the number of APCs, we tested if these populations exhibited an increased activation state by staining for surface activation markers associated with co-stimulation and antigen presentation (i.e., CD40, CD80, CD86, I-A/I-E). In all cases, PolyIC MP/OVA caused a significant increase in the number of cells positive for each marker compared to the sham injected control (**Figure 6.5A**). Interestingly, the number of activated DCs increased over time with the highest levels of each marker occurring 7 days after treatment (**Figure 6.5A, red**). The macrophage population exhibited similar activation effects (**Figure 6.5B**). However, compared to DCs, which showed increases in the number of cells expressing each marker over time, only CD40 and I-A/I-E increased as a function of time. Macrophage expression levels of CD80 and CD86 – while higher than levels in sham-injected nodes – remained at a near-constant, elevated level over one week.

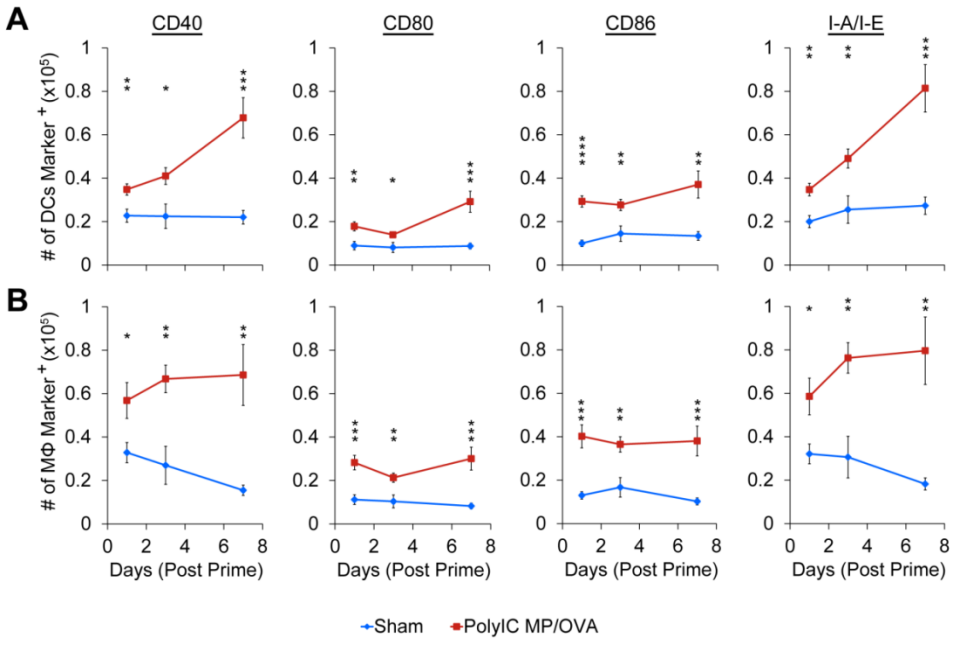

Figure 6.5: PolyIC MP/OVA depots injected *i.LN.* drive prolonged increase in surface activation marker expression in DCs and macrophages.
Number of DCs (A) and macrophages (B) in LNs expressing activation markers CD40, CD80 CD86 and I-A/I-E at 1, 3, and 7 days after *i.LN.* injection of depots. Numbers are counted in an identical acquisition volume (80µL). n=9-10 LNs per group with bars depicting mean ± SEM. (*p<0.05; **p<0.01; ***p<0.001; ****p<0.0001)

6.3.4 Local changes in APC function drive local and systemic antigen-specific CD8+ T cell response

We next used MHC-I tetramer staining to investigate if the local activation we observed drove generation of antigen-specific T cells, both in treated nodes and systemically. Analysis of LNs after treatment revealed that vaccinating with PolyIC MP/OVA increased both the frequency and number of antigen-specific $CD8^+$ T cells within the LN (**Figure 6.6A, B**). While the sham injection (**Figure 6.6A, B, blue**) remained at a constant, low level, the PolyIC MP/OVA treated mice exhibited a significant ($p<0.01$) increase in SIINFEKL-specific T cells 7 days after priming. To investigate how these local changes to the LN microenvironment impacted systemic

changes in antigen-specific responses, mice were treated with either PolyIC MP/OVA, empty MPs, a sham injection, or left untreated. After vaccination on Day 0, blood was collected weekly and SIINFEKL tetramer staining was used to determine the percentage of antigen-specific $CD8^+$ T cells circulating in peripheral blood. **Figure 6.6C-F** depicts representative flow cytometry plots showing the gating scheme applied to samples from naïve (**Figure 6.6C, gray**), sham (**Figure 6.6D, blue**), empty MP (**Figure 6.6E, green**), or PolyIC MP/OVA (**Figure 6.6F, red**) treated mice 7 days after immunization. The average SIINFEKL tetramer levels revealed that treatment with PolyIC MP/OVA significantly increased ($p<0.0001$) systemic levels of SIINFEKL-specific $CD8^+$ T cells 7 days after treatment, followed by a prototypical contraction period through day 28 (**Figure 6.6G**). The elevated level of SIINFEKL-specific $CD8^+$ T cells at day 28 suggested development of immune memory, which we assessed using common markers for effector T cells and memory T cells among $CD8^+$/$Tetramer^+$ cells. These studies revealed a nearly 2-fold increase in the percentage of central memory T cells ($CD62L^{high}$/$CD44^{high}$ among SIINFEKL-specific $CD8^+$) and a subsequent decrease in effector memory phenotypes ($CD62L^{low}$/$CD44^{high}$) over this same time (**Figure 6.6H**).

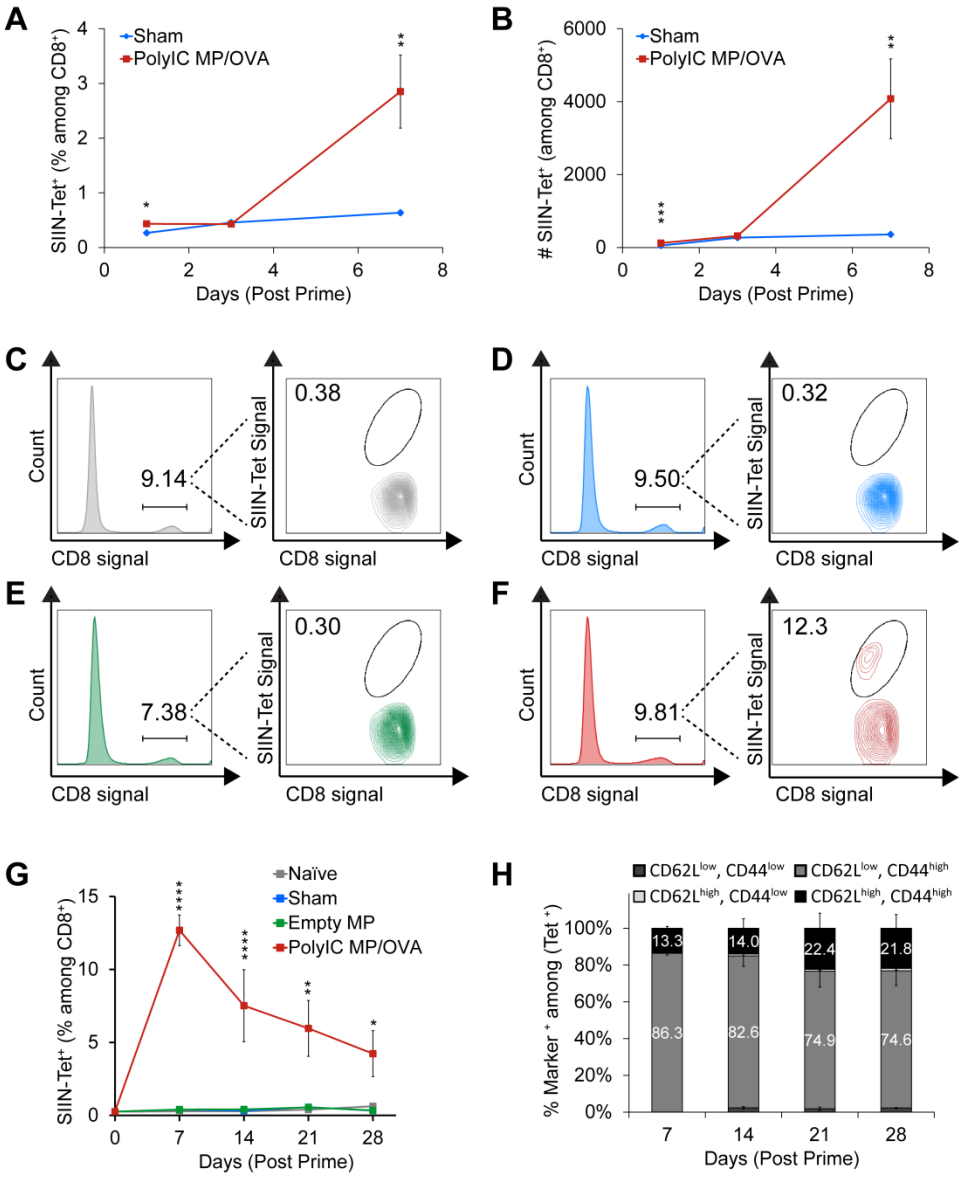

Figure 6.6: *i.LN.* injection of depots drives antigen-specific T cell responses locally in LNs and systemically in the periphery.
(A) Percentage and (B) numbers of SIINFEKL-tetramer^{+} CD8^{+} T cells in LNs at 1, 3 and 7 days after *i.LN* injection of PolyIC MP/OVA depots or a PBS sham injection. Numbers are counted in an identical acquisition volume (80µL). n=9-10 LNs per group with bars depicting mean ± SEM. (**p<0.01; ***p<0.001) Mice were immunized *i.LN.* with PolyIC MP/OVA depots, Empty MPs, a sham injection of PBS or left untreated (naïve), and leukocytes from peripheral blood were stained for SIINFEKL-tetramer^{+} CD8^{+} T cells weekly starting 7 days after immunization. Representative flow cytometry plots illustrating the gating scheme for SIINFEKL tetramer staining of untreated mice (C), mice immunized *i.LN.* with a sham injection of PBS (D), Empty MPs (E), or PolyIC MP/OVA depots (F) 7 days after treatment. (G) Mean percentage of SIINFEKL-tetramer positive T cells and (H) percentage of SIINFEKL positive T cells with effector (CD62L^{low}/CD44^{high}) or memory phenotypes (CD62L^{high}/CD44^{high}) in mice from treatment groups detailed in C-F. n=8 mice for Day 0, n=10 mice per group at Day 7, and n=4-5 mice per group for Days 14-28. (**p<0.01; ***p<0.001; ****p<0.0001 between CpG MP groups and naïve; $^{\#\#}$p<0.01; $^{\#\#\#}$p<0.001; $^{\#\#\#\#}$p<0.0001 between CpG MP groups and montanide).

To test the robustness and modularity of this platform, we next tested if *i.LN.* injection expands antigen-specific T cells with vaccines containing different TLRas or other antigens, in particular, Trp2 peptide – a clinically-relevant tumor associated antigen conserved in murine and human melanoma[201]. Depots were formulated with either PolyIC or CpG – a potent adjuvant being studied to induce anti-tumor immunity[49, 202] – and mixed with soluble OVA or Trp2. Mice were immunized *i.LN* at day 0 with vaccine depots encapsulating identical doses of adjuvant, and then boosted at day 21 with soluble vaccine components *s.c.* at the tail base. At days 7 and 28 (7 days after the prime and boost injections), peripheral blood was drawn and MHC-I tetramer staining was used to quantify the percentage of antigen specific $CD8^+$ T cells (Trp2 tetramer for Trp2 immunized mice, SIINFEKL tetramer for OVA immunized mice). For mice immunized with OVA vaccine depots both treatments induced very potent antigen-specific responses, but no significant differences were measured between responses induced by CpG MPs and PolyIC MPs at either day (**Figure 6.7, left**). However, in mice treated with Trp2 vaccine depots, a significantly higher level of Trp2 specific $CD8^+$ T cells was observed in mice immunized with CpG depots compared to PolyIC depots at both time points (**Figure 6.7, right**).

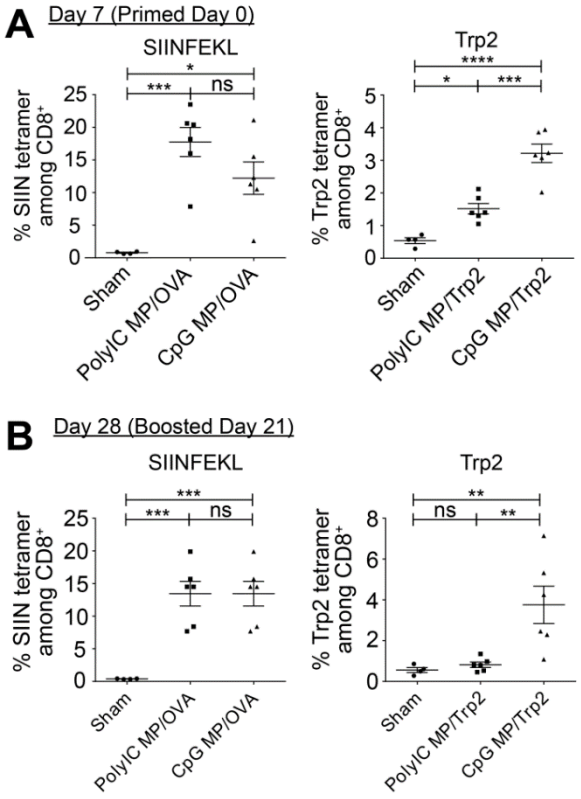

Figure 6.7: CpG MPs induce superior tumor-specific CTL responses compared to PolyIC MPs. Mice were primed at day 0 *i.LN.* will either PolyIC MPs or CpG MPs, and either a model antigen (OVA) or a melanoma associated antigen (Trp2) in a soluble form. Mice were boosted at day 21, and antigen-specific MHC-I tetramer was used to measure antigen specific $CD8^+$ T cell responses compared to a sham injection. **(A)** 7 days after priming, PolyIC and CpG MPs both induced potent levels of SIINFEKL-specific $CD8^+$, but no differences were observed as a function of TLRa. In the Trp2 model, both PolyIC and CpG MPs increased the levels of Trp2-specific CD8+ T-cells, with CpG exhibiting a statistically significant increase compared to both the sham and PolyIC MP injections. **(B)** At day 28, 7 days after the boost, a similar response was seen with a robust response in the OVA model for both PolyIC and CpG MPs, but without dependence on the specific TLRa included in the particles. In the Trp2 studies, only CpG MPs induced a significant, potent recall response. (* $p<0.05$; ** $p<0.01$; *** $p<0.001$; **** $p<0.0001$).

6.3.5 Local administration of CpG particles promotes anti-tumor immunity

We next used an aggressive melanoma model – B16-F10 – to test the functionality of anti-tumor immunity induced by vaccine depots administered by the *i.LN.* route. Since vaccine depots formulated with CpG promoted superior expansion of Trp2-specific cytotoxic T lymphocytes (CTLs) compared with PolyIC (**Figure 6.7**), we

immunized mice with CpG depots containing 3.5μg of CpG and suspended in either Trp2, or another conserved melanoma antigen, hgp100[203, 204]. In these studies, mice were primed on day 0 with either CpG MP/tumor antigen, or as a potent benchmark, 50μg CpG and tumor antigen emulsified in montanide, one of the strongest adjuvants currently under study[205, 206]. Animals were then boosted on day 15 with identical doses and formulations, but all injections were administered *s.c.* as a heterologous prime-boost regimen. MHC-I tetramer staining for either Trp2- or hgp100-specific $CD8^+$ T cells revealed formulations containing CpG MPs exhibited significant increases in these populations relative to other groups after both priming and booster injections (**Figure 6.8A, B**). After a second boost on day 36, mice were challenged with B16-F10 metastatic melanoma by implantation of 3×10^5 cells *s.c.* at the hind flank. Compared to the untreated group (**Figure 6.8C, H**), the mice primed *s.c.* with montanide/CpG/hgp100 (Fig. 8D, H) or *i.LN.* with CpG MPs/hgp100 (**Figure 6.8F, H**) did not exhibit any therapeutic gains. In contrast, *i.LN* immunization with CpG MP/Trp2 slowed tumor growth, resulting in 40% survival at day 20 (**Figure 6.8G, H**), while all untreated mice succumbed by this day (**Figure 6.8C, H**). Interestingly, while Montanide/CpG/Trp2 prolonged survival of mice to 29 days after tumor challenge (**Figure 6.8E, H**) the effect appeared less potent than those generated by CpG MP/Trp2 vaccine regimens, which survived for up to 35 days. The mean survival was 23.0±4.5 days for the CpG MP/Trp2 treated group, compared to 20.0±2.4 days for the Montanide/CpG/Trp2 treated group, and 16.3±1.7 days for the untreated group, further demonstrating the ability of local LN treatment to promote functional, systemic immunity.

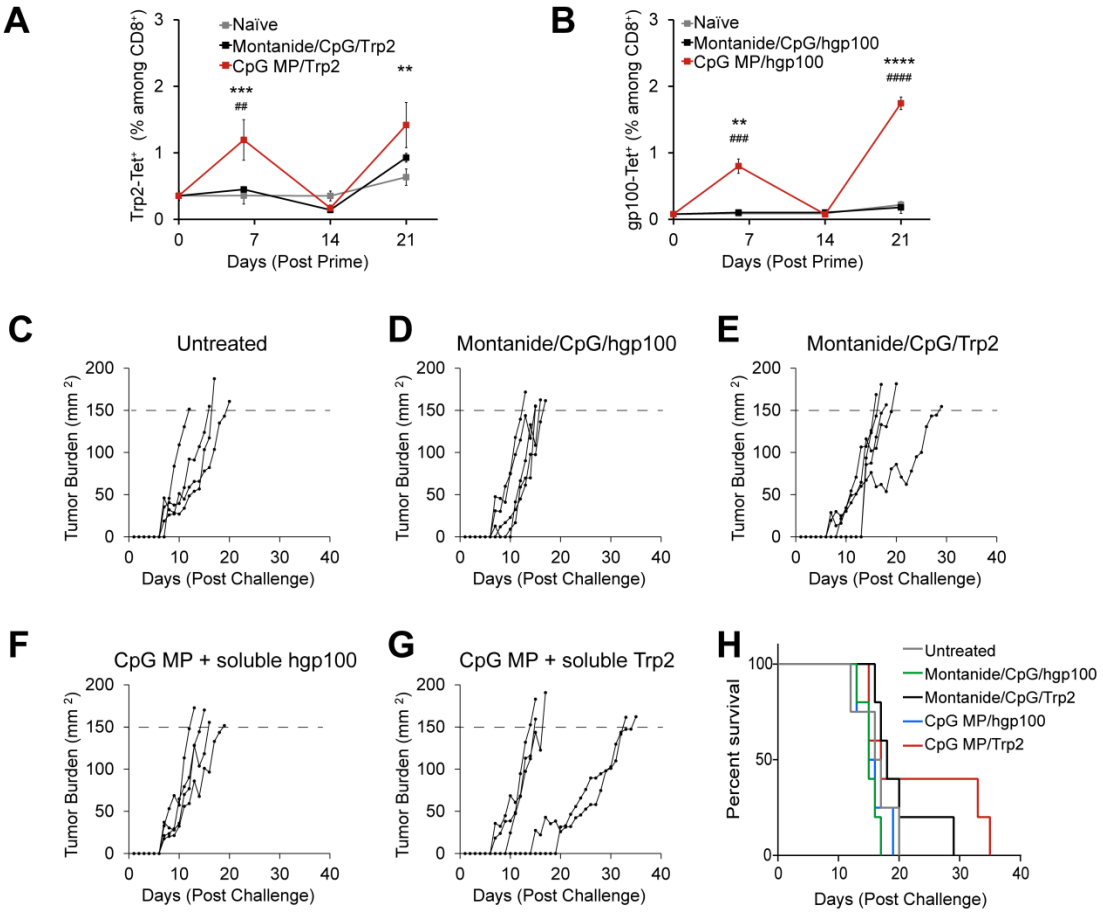

Figure 6.8: *i.LN.* injection of CpG MP/Trp2 depots promote functional anti-tumor immunity. (A) Mice were left untreated, immunized *s.c.* with Montanide/CpG/Trp2, or immunized *i.LN.* with CpG MP/Trp2, followed by *s.c.* boosts consisting of identical treatments at Day 15. Trp2-tetramer specific T cells were quantified in peripheral blood at 6, 14 and 21 days after immunization. (B) A study conducted using identical treatment regimens as in (A), but including an additional tumor antigen, hgp100. hgp100-specific CD8+ T cell responses in peripheral blood were quantified using hgp100 MHC-I tetramer in peripheral blood at 6, 14 and 21 days after immunization. Values indicate mean ± SEM. (**p<0.01; ***p<0.001; ****p<0.0001 between CpG MP groups and naïve; $^{\#\#}$p<0.01; $^{\#\#\#}$p<0.001; $^{\#\#\#\#}$p<0.0001 between CpG MP groups and montanide). (C-H) Mice were left untreated, immunized with Montanide/CpG/hgp100, Montanide/CpG/Trp2, CpG MP/hgp100 (*i.LN.*), or CpG MP/Trp2 (*i.LN.*) followed by *s.c.* boosts at Day 15 and Day 36 as described in the methods. 43 days after the priming injection, mice were challenged with B16-F10 melanoma. Individual tumor traces of untreated mice (C), mice immunized with Montanide/CpG/hgp100 (D), Montanide/CpG/Trp2 (E), CpG MP/hgp100 (F) and CpG MP/Trp2 (G). (H) Percent survival of mice in the groups shown in C-G.

6.4 Discussion

Biomaterials offer a robust platform to co-deliver immune signals, target vaccines to specific tissues, and control delivery kinetics. However, most vaccines have complex

formulations with multiple components, and understanding how each component influences the immune response alone or together has been challenging thus far. Previous research has shown that altering material properties can influence and improve the targeting of vaccines to LNs through lymphatic drainage or trafficking within specific APCs after internalization[48, 49, 67, 191, 207]. *i.LN.* delivery, however, offers a unique opportunity to directly study how the form and combination of signals that ultimately reach LNs impact immune response without the complexities that occur after vaccines are administered by traditional routes. For example, even efficacious vaccines only result in a small fraction of the injected dose reaching the LN and spleen – as little as 0.1%, whereas pre-clinical and clinical trials studying *i.LN.* delivery of soluble vaccines have demonstrated dose-sparing factors as high as 10^6 relative to common peripheral injection routes[77, 78, 80]. With respect to nanoparticles, past studies have revealed that particles administered along common peripheral routes drain to LNs most efficiently when the diameters are in the range of 20-30nm, whereas even 100nm particles drain an order of magnitude less efficiently[197]. Microparticle drainage relies heavily on APC trafficking[103]. Past findings from our lab demonstrate that improved retention of adjuvant in LNs achieved by encapsulation in MPs too large to freely drain from LNs after *i.LN.* injection drives very strong T cell responses compared to equivalent doses of soluble adjuvant administered *i.LN.*, or adjuvant MPs administered peripherally (e.g., in muscle)[13]. In contrast, nanoparticles or soluble adjuvant are retained in LNs at intermediate and low levels, respectively, driving correspondingly lower responses relative to MPs[13]. Thus, *i.LN.* injection of MPs was used to add new understanding

of how these local treatments alter LN function over time, and how this local evolution impacts systemic immunity.

With respect to local changes in LNs, several of the findings together suggest an adjuvant mechanism underpinned by increased activation of LN-resident APCs. First, generally a large difference was observed in the number of immune cells in treated nodes relative to sham injections, with more modest differences in the relative cell compositions. These frequencies – for both innate and adaptive immune cells – were similar to those previously reported in LNs of C57BL6 mice[208]. Second, persistence of fluorescent MPs was observed for at least 4 weeks 9 (**Figure 6.1B**), and increased activation of LN-resident APCs (e.g., macrophages, DCs) as soon as 1 day after injection. Thus, one important role for the depots appears to be enhanced local APC function that could help increase lymphocyte proliferation and infiltration. The resulting antigen-specific responses showed enhancements consistent with strong T cell response. For example, OVA-specific T cells developed locally in LN over 7 days, by which time a dramatic increase was measured in peripheral blood. This evolution is consistent with primed lymphocytes migrating out of the LNs as they expand against SIINFEKL presented in these sites[209]. Similarly, a shift towards a central memory phenotype and away from effector response was also observed over time, a goal for effective vaccines[210]. Interestingly, it was observed that both depots and sham injections caused modest – sometimes, transient – increases in the frequency of B cells and $CD4^+$ T cells. Thus, an additional enhancing mechanism could be mild inflammation caused by injection that, for example, could upregulate

adhesion molecules (e.g., P-, E-selectin) to better retain circulating T and B cells. The absence of toxicity, and the intact follicular structure of LNs after either sham or adjuvant MP treatment, further supports the compatibility of this strategy for fundamental or applied uses.

The link between the kinetics of vaccine dosing and induction of immune response is well established, with elegant studies demonstrating that increasing dosing regimens drive synergistic immune responses more effectively than equivalent doses administered in a bolus or at evenly spaced equal doses.[211] This discovery supports the basic premise for delivery of controlled release depots to LNs, as the local dose of vaccine components locally increases in LNs as cargo is released from degrading polymer particles[13]. Further, while there is significant potential made possible by determining whether vaccine particles loaded with antigen, adjuvant, or both might be most potent for a particular vaccine[187], design of adjuvant-loaded particles offer the appeal of “plug-n-play” vaccination whereby the particle is simply mixed with a soluble adjuvant of interest.

It was found that *i.LN.* injection of adjuvant MPs drove antigen-specific T cell responses against both model antigen (i.e., OVA) and tumor-associated antigens (i.e., Trp2, gp100) mixed with the depots. Interestingly, for OVA, both PolyIC-loaded and CpG-loaded depots performed equivalently, while CpG was more effective in generating responses against tumor-associated antigens. CpG has stimulated great interested in pre-clinical cancer studies owing to effective priming of CTL

response[49, 196, 202, 212, 213]. Thus, *i.LN.* delivery of CpG MPs mixed with common conserved melanoma antigens was benchmarked against these same antigens emulsified with CpG and montanide, one of the strongest vaccine formulations under study[205, 206]. With respect to both tumor-specific T cell expansion and anti-tumor immunity, *i.LN.* depots were superior to montanide, but interestingly, the dose of CpG in MP formulations (3.5 μg/LN) was 14-fold lower than the 50 μg dose of CpG emulsified in the montanide vaccines. Thus, although the efficacy achieved with *i.LN.* depots in this study was modest (~40% of mice exhibited significantly increased survival), the enhanced performance compared with montanide and this dose-sparing supports the potential of future MP-based vaccines administered to LNs.

There are some considerations that might account for the limited efficacy observed in tumor challenge studies. First, the chosen melanoma model is highly aggressive. Second, general features of the tumor microenvironment likely limit immunogenicity, including suppression and antigen editing that prevents tumor-specific CTLs from maintaining function or recognizing antigens in tumors[184, 214]. Third, in these experiments, much higher frequencies of SIINFEKL-specific T cell responses were observed after a single *i.LN* immunization with OVA depots relative to either melanoma antigen, even after the latter were administered in several booster injections. OVA is a foreign antigen, whereas Trp2 and hgp100 are self-antigens and typically much less immunogenic. Since cross-presentation of minimal epitope peptides – such as Trp2 and hgp100 – can enhance immunogenicity[15, 193, 215,

216], encapsulation of antigen in MPs alone, or in conjunction with adjuvant might offer one route to further improve potency. However, since significant populations of antigen-specific $CD8^+$ T cells were generated against either tumor antigen, more robust responses might improve effectiveness. Along these lines, recent pre-clinical and clinical studies reveal simultaneously activating multiple TLR pathways during cancer therapy can enhance therapeutic efficacy[217-220], suggesting another strategy based on loading of MPs with multiple TLRas.

i.LN. delivery of MPs also provides some unique opportunities to impact the tumor microenvironment through appropriate selection of the LN for injection. In these studies, the inguinal LN was selected for ease of injection based on previous work (see **Chapter 5**), and what has been used in recent human trials involving *i.LN.* delivery of soluble tumor antigens to inguinal LNs[221]. However, this technique could also be used to target tumor draining lymph nodes (TDLN), sites which have recently been shown to be effective for passive targeting of cancer vaccines[48, 49, 183, 222]. Remarkably, several landmark studies also demonstrate that both anti-tumor T cells and regulatory T cells (T_{REGs}) – cells that suppress anti-tumor response in tumors – are primed in the same LN[223, 224]. Thus, direct LN targeting of TDLNs might allow local polarization toward effector cells while also reducing suppressive T_{REGs} that play an important role in maintaining the suppressive tumor microenvironment. This may further provide an opportunity to effectively combat tumors without affecting natural regulatory activity in other distant LNs. It is also possible that targeting TDLNs is not necessary if optimized particles expand tumor-

specific cells that are able to migrate to tumors, but further studies will be needed to investigate this possibility. Finally, creating opportunities to overcome the suppressive characteristics of tumors by directly targeting the TDLN, or pairing with exciting new immunotherapies such as checkpoint blockades could also have offer significant potential for cancer vaccination[225, 226].

6.5 Conclusion

i.LN. injection allows direct control over the dose and combinations of materials administered to LNs, supporting a new approach for studying the impact of vaccines on the LN microenvironment. Here, it is demonstrated that a single *i.LN.* injection into both inguinal LNs of mice can lead to dramatic local changes in these tissues, increasing the number and function of both APCs and lymphocytes. The local changes result in systemic, but antigen-specific pro-immune function that provides functional anti-tumor immunity in a melanoma model. Thus, this approach might hold clinical utility for vaccines based on intra-LN controlled release of antigens and adjuvants, while also providing a strategy to evaluate the immunogenicity of biomaterial carriers themselves, or to design carriers loaded with defined combinations of antigens and adjuvants.

This chapter studies cancer vaccines using *i.LN.* injection as a well-defined model, but an important clinical issue for cancer therapy is identifying new therapeutic targets. This requires new tools to study cancer cells in a meaningful microenvironment. **Chapter 7** discusses a collaborative project with the University of

Maryland Medical School in which I created a system to immobilize cells while maintaining their free-floating dynamics. This platform allowed for real time imaging of metastatic cell phenomena and drug screening of potential therapeutics.

Chapter 7: Lipid tethering of breast tumor cells enables real-time imaging of free-floating cell dynamics and drug response[6]

7.1 Introduction

Cancer metastasis occurs when epithelial tumor cells travel through non-adherent microenvironments, like the bloodstream or lymphatics, to a distant organ. The presence of tumor cells in the non-adherent microenvironment of the bloodstream, known as circulating tumor cells (CTCs), has been detected in numerous epithelial cancers including breast, prostate, colon, and lung [227]. CTCs are an early indicator of clinical spread of disease and their levels correlate with decreased patient survival [228, 229]. Based on the increasing clinical relevance of CTCs, understanding their molecular profile is emerging as a new opportunity to gain insight on disease progression and patient prognosis beyond enumeration alone. Though progress has been made on technologies to enhance the identification and enumeration of CTCs [227, 230, 231], major limitations remain in performing downstream functional studies due to challenges with accurate detection and the low number of CTCs that can be retrieved from patient blood (frequency of approximately 1 in 100 million cells in the bloodstream) [227]. Some of the techniques currently being employed to analyze CTCs include fluorescence in situ hybridization, sequencing,

---

[6]Adapted from K. Chakrabarti*, J.I. Andorko*, R.A. Whipple, P. Zhang, E.L. Sooklal, S.S. Martin, and C. M. Jewell. "Lipid tethering of breast tumor cells enables real-time imaging of free-floating cell dynamics and drug response." *Oncotarget.* 2016, 7, 10486-10497.
* denotes equal contributors

immunostaining, xenograft transplantation, and RNA or protein-based analysis [227, 230, 232, 233]. However, these methods do not allow for real-time analysis of CTCs in an environment that preserves their free-floating nature.

Microscopy analysis of CTCs has focused almost exclusively on cells adhered to surfaces (glass, plastic, extracellular matrix (ECM) owing to the ease of imaging and characterization of cells in these static positions. However, the functional and molecular characteristics of adherent and non-adherent tumor cells are dramatically different [234-237]. Thus a critical knowledge gap exists in the understanding of epithelial tumor cells in non-adherent microenvironments, such as those found in blood vessels. Non-adherent breast carcinoma cells, for example, produce unique tubulin-based microtentacles (McTNs) that promote tumor cell aggregation [238, 239], reattachment to endothelial layers [240, 241], and retention of CTCs in the lungs of mice [242, 243]. New enabling technologies to image tumor cells, McTNs, and other features in the absence of ECM attachment could vastly improve the understanding of dynamic cell behaviors that occur in the non-adherent microenvironments encountered by CTCs during metastasis. These tools could also support opportunities for selective targeting of drugs to McTNs or other structures presented preferentially by CTCs during metastatic spread, as well as help address rising concerns that chemotherapies meant to reduce tumor growth may actually increase metastatic risk [244]. Here, we exploited the discovery that McTNs form only when protein-based adhesions are absent to create an innovative platform for real-time imaging of the dynamic features of live, non-adherent tumor cells. This

approach allows new types of information to be collected (e.g., McTN behavior on live cells over time) while reducing variables such as changes in cell function that occur during adhesion or the complexities of imaging cells in suspension that drift or are washed away during microfluidic flow.

Biomaterials offer many attractive features – stability, biocompatibility, versatile chemistries – for controlling cell adhesion. Common approaches include chemically functionalizing surfaces, incorporating cell adhesion peptides, and micropatterning using polymer-based soft lithography or electrospinning techniques. Of particular note, several recent studies have exploited biomaterials to identify CTCs [245-247] or used microfluidic devices to isolate and immobilize CTCs by acoustic separation, topography, controlled flow rates, and antibody traps [248-251]. Polyelectrolyte multilayers (PEMs) are nanoscale, polymeric materials assembled by electrostatic or hydrogen bonding interactions during a layer-by-layer (LbL) deposition process. PEMs can be coated on topographically-complex surfaces (e.g., colloidal, microfluidic) and offer programmable surface functionalities depending on the polymers used to assemble films. PEMs have recently been employed to capture CTCs through incorporation of cytophilic polymers or cell-adhesive proteins that promote CTCs adhesion [252-254]. However, new strategies are needed to study the dynamics of McTNs and other unique metastatic features that form only when CTCs are in non-adherent environments.

To enable this new ability, we identified three design features that would allow prolonged, real-time imaging and drug screening of McTNs on live tumor cells in a free-floating state: 1) optically-clear coatings to support imaging, 2) ability to control microfluidic flow over cells and 3) simple, low-energy manufacturing process. Past studies have demonstrated the utility of PEMs for tuning cell adhesion by varying polymer composition or through addition of lipids, RGD sequences, or other binding moieties [255-260]. Thus we leveraged PEMs to design a platform to immobilize live, detached tumor cells on microfluidic devices. We show that assembling cytophobic PEM films with cytophilic lipid tethers maintains the free-floating properties of tumor cells while providing spatial immobilization of cells. When tethered, McTNs on live cells can be visualized in real time and the dynamics of these structures can be assessed during microfluidic flow of drugs that enhance or destabilize McTNs. This technology could generate fundamental insight into a critical stage of metastasis that has been largely understudied due to technical challenges and support new approaches to exploit McTNs as biomarkers for the metastatic efficiency of tumor cells in diagnosis, prognosis, and targeted drug design.

7.2 Materials and Methods

7.2.1 Cell Lines & Materials

MDA-MB-436 and MCF-7 cell lines were purchased from ATCC and cultured with Dulbecco's Modified Eagle Medium supplemented with 10% fetal bovine serum and 1% penicillin-streptomycin solution. Poly(methacrylic acid) (MW 100,000) and

polyacrylamide (PAAm) (MW 5,000,000-6,000,000) were purchased from Polysciences. Poly(allylamine hydrochloride) (PAH) (MW ~200,000) was purchased from Alfa Aesar. 1,2-dioleoyl-3-trimethylammonium-propane (chloride salt) (DOTAP) and 1,2-dioleoyl-*sn*-glycero-3-phosphocholine (DOPC) were purchased from Avanti Polar Lipids. Colchicine was purchased from Sigma and paclitaxel was purchased from Enzo Life Sciences.

7.2.2 PEM Film Deposition and Characterization on Planar Substrates

For multilayer film deposition, similar to methods previously reported [261], PMA and PAAm were prepared as 0.01M solutions using ultrapure water and adjusted to pH 3. All polymer solutions were filtered with a 0.45 μm cellulose nitrate filter prior to use in multilayer film assembly. For planar substrates, quartz (Chemglass Life Sciences) or silicon (Silicon Inc.) were cut into 5mm x 25mm substrates using a dicing saw (Model 1006, Micro Automation). Cut substrates were cleaned with sequential washing with acetone, ethanol, methanol, and deionized water then charged using an oxygen plasma Jupiter III system (March). These substrates were first immersed in the polycationic solution PAH (0.05M) for 15 mins then rinsed twice using two separate baths of deionized water at pH 3 to remove any excess polymer. This primer layer was followed by immersion of the substrates into polyanionic PMA (0.01M) for 5 mins followed by rinsing as above. The substrates were then immersed in a polycationic solution of PAAm (0.01M) for 5 mins and rinsed. For additional bilayers, the process was repeated without the addition of the primer layer (PAH) until the desired number of bilayers was assembled. Lipid formulations comprised of 1,2-dioleoyl-sn-glycero-3-phosphocholine (DOPC) or 1,2-

dioleoyl-3-trimethylammonium-propane (DOTAP) were obtained from Avanti Polar Lipids. These lipids were prepared as 0.01M solutions with pH 3 deionized water and sonicated for 60 mins in a room temperature water bath. PEMs with a lipid tether were prepared by immersing PEM coated substrates in each lipid solution for 5 mins followed by two rinsing steps. The final, coated substrates were removed from solution, blown dry with compressed, filtered air, and stored at room temperature prior to characterization. Film thickness and optical clarity after deposition onto silicon and quartz substrates were measured using a LSE stokes ellipsometer (Gaertner Scientific Corportation) and by measuring light transmittance at 600nm using an Evolution 60 UV-visible spectrophotometer (Thermo Scientific), respectively.

7.2.3 PEM Film Deposition on Microfluidic Slides and Multi-well Plates

Uncoated microfluidic slides (1µ-Slide VI 0.4) were obtained from Ibidi and tissue culture treated 96-well plates were obtained from Corning. To coat the microfluidic slides, 120µL of each polyelectrolyte solution was added to the microchannels and 75µl of solution was added to each well of the multi-well plate. After incubation, solution was removed via aspiration and rinsed twice for 1 min using 120µL of pH 3 water. Bilayers of PMA and PAAm were assembled and terminated with either DOPC or DOTAP as described above. Following deposition, slides were allowed to air dry for 1 hr at room temperature then stored at room temperature.

7.2.4 Attachment Image Analysis

MDA-MB-436 and MCF-7 breast cancer cells were seeded on PEM coated microfluidic slides (50,000 cells/channel) ranging from 0 to 8 bilayers. An Olympus CKX4 microscope was used for all experiments to capture images at 4x magnification. Three pictures per channel were taken after cell seeding for each condition to quantify initial cell number (t0). At 6 and 24 hrs, media was removed from the channel and the channel was washed once before addition of new media. Three images per channel were taken for each condition. The area of the image occupied with cells (as a percent) was quantified using CellProfiler (Broad institute) and the average from three images was calculated. The average percentage for each condition was then normalized to the area occupied at t0.

7.2.5 Attachment Cell Titer

MDA-MB-436 and MCF-7 breast cancer cells were seeded on PEM coated 96-well plates (20,000 cells/well) ranging from 0 to 8 bilayers. At each time point (1, 3, 6, and 24 hrs), media was removed from the well and the well was washed once before addition of new media. After the 24hr time point an additional wash was done on all wells. Cell number was determined using CellTiter reagent according to manufacturer's instructions. Each time point was normalized to initial cell number from a reading done immediately after cell seeding.

7.2.6 PEM Viability

MDA-MB-436 and MCF-7 breast cancer cells were seeded on PEM coated microfluidic slides with $PMA_4/PAAm_4$ bilayers (50,000 cells/channel). At 0, 6, and 24 hrs Live/Dead (Life Technologies) reagent was added according to manufacturer's instructions. Corresponding phase contrast, live (calcein-AM) green fluorescence, and dead (ethidium homodimer-1) red fluorescence images were taken in triplicate at 4x magnification with an Olympus CKX41 fluorescence microscope. The number of cells in each image was quantified using CellProfiler. The percent of live and dead cells were calculated by quantifying the number of green fluorescence positive and red fluorescence positive cells, respectively, and dividing by total number of cells in the phase contrast image. GFP and Texas Red filters were used to for imaging. MDA-MB-436 and MCF-7 breast cancer cells were plated on 96-well black plates with $PMA_4/PAAm_4$ bilayers (20,000 cells/well). At time 0, 1, 3, 6, and 24 hours Live/Dead reagent was added and read on a plate reader according to manufacturer's instructions. Relative fluorescence units (RFU) were normalized to time 0.

7.2.7 Tethering Washing

MDA-MB-436 and MCF-7 cells were seeded on $PMA_4/PAAm_4$ coated microfluidic slides with DOPC or DOTAP (50,000 cells/channel). Cells were incubated for 1 hr to allow for tethering. To quantify initial cell number, three images per channel were taken for each condition at time 0. After 1 hr, existing media was gently removed from the bottom port of each channel and fresh media was added to the top port. Following a wash, three images were taken per channel for each condition using an

Olympus CKX41 microscope at 4x magnification. This process was repeated for each wash. The area of the image occupied with cells (as a percent) was quantified using CellProfiler and the average from three images was calculated. The average percentage for each condition was then normalized to the area occupied at time 0.

7.2.8 Tethering Viability

MDA-MB-436 and MCF-7 cells were seeded on PMA_4/$PAAm_4$ coated microfluidic slides with DOPC or DOTAP (50,000 cells/channel). Cells were incubated for 1 hr to allow for tethering. After 1 hr, one wash was done where the existing media was gently removed from the bottom port of each channel and fresh media was added to the top port. This wash was to ensure only tethered cells were analyzed. At 0 and 6 hrs after washing, Live/Dead reagent was added according to manufacturer's instructions. Corresponding phase contrast, live (calcein-AM) green fluorescence, and dead (ethidium homodimer-1) red fluorescence images were taken in triplicate. The number of cells in each image was quantified using CellProfiler. The percent of live and dead cells were calculated by quantifying the number of green fluorescence positive and red fluorescence positive cells, respectively, and dividing by total number of cells in the phase contrast image. GFP and Texas Red filters were used to for imaging.

7.2.9 McTN Counting

MDA-MB-436 cells were trypsinized, spun down, and resuspended in phenol red-free and serum-free DMEM. Cells were seeded on $PMA_4/PAAm_4$ coated microfluidic slides, $PMA_4/PAAm_4$ coated microfluidic slides with DOTAP, or a low attach 24-well plate (50,000 cells/channel). Cells were incubated for 1 hr to allow for tethering. After 1 hr, one wash was done where the existing media was gently removed from the bottom port of each channel and fresh media was added to the top port on the DOTAP slides. This wash was to ensure only tethered cells were analyzed. After this wash, CellMask orange (Life Technologies) cell membrane dye was added to each channel to a final concentration of 1:10,000. McTNs were scored blindly in a population of 100 cells/well as previously described [238]. Representative images were taken at 40x magnification with an Olympus CKX41 fluorescence microscope.

7.2.10 Imaging drift and drug treatments

MDA-MB-436 cells were trypsinized, spun down, and resuspended in phenol red-free and serum-free DMEM. Cells were seeded on $PMA_4/PAAm_4$ coated microfluidic slides and $PMA_4/PAAm_4$ coated microfluidic slides with DOTAP (50,000 cells/channel). Cells were incubated for 1 hr to allow for tethering. After 1 hr, one wash was done where the existing media was gently removed from the bottom port of each channel and fresh media was added to top port on the DOTAP slides. This wash was to ensure only tethered cells were analyzed. After this wash, CellMask orange cell membrane dye was added to each channel to a final concentration of 1:10,000.

Cells were treated with 5μM colchicine for 15 mins and 1μg/ml paclitaxel for 120 mins. McTN imaging was done on an Olympus FV100 confocal laser scanning microscope at 60x magnification. Five 1μm slices and 20 frames at a 10 sec frame rate were taken for at least five image sets for each condition. The number of McTNs on each cell was manually counted on five cells per condition using the maximum intensity z-projection at the last frame.

7.2.11 Statistical Analysis

Graphpad Prism (version 6.02) was used to determine all statistic comparisons. Student's t-test and one-way ANOVA tests were performed with a Tukey multiple comparisons post-test as indicated. A p-value of less than 0.05 was considered statistically significant.

7.3 Results

The responses of cancer cells detached from ECM (i.e., in a circulating or free-floating stage) are highly important in survival, apoptosis, metastasis, and even in the expression of stem cell characteristics [262, 263]. However, tumor cells in this state are greatly understudied due to the technical and clinical challenges of continuously imaging cells not adhered to surfaces. Maintaining free-floating cell behavior of breast cancer cells is particularly critical in promoting McTN formation [238]. Thus we used breast tumor cells to first test if programming the compositions of PEM coatings would allow minimal tumor cell adhesion to maintain the free-floating

characteristics (e.g., McTNs) of these cells (**Figure 7.1A**), before adding a lipid tether in subsequent designs.

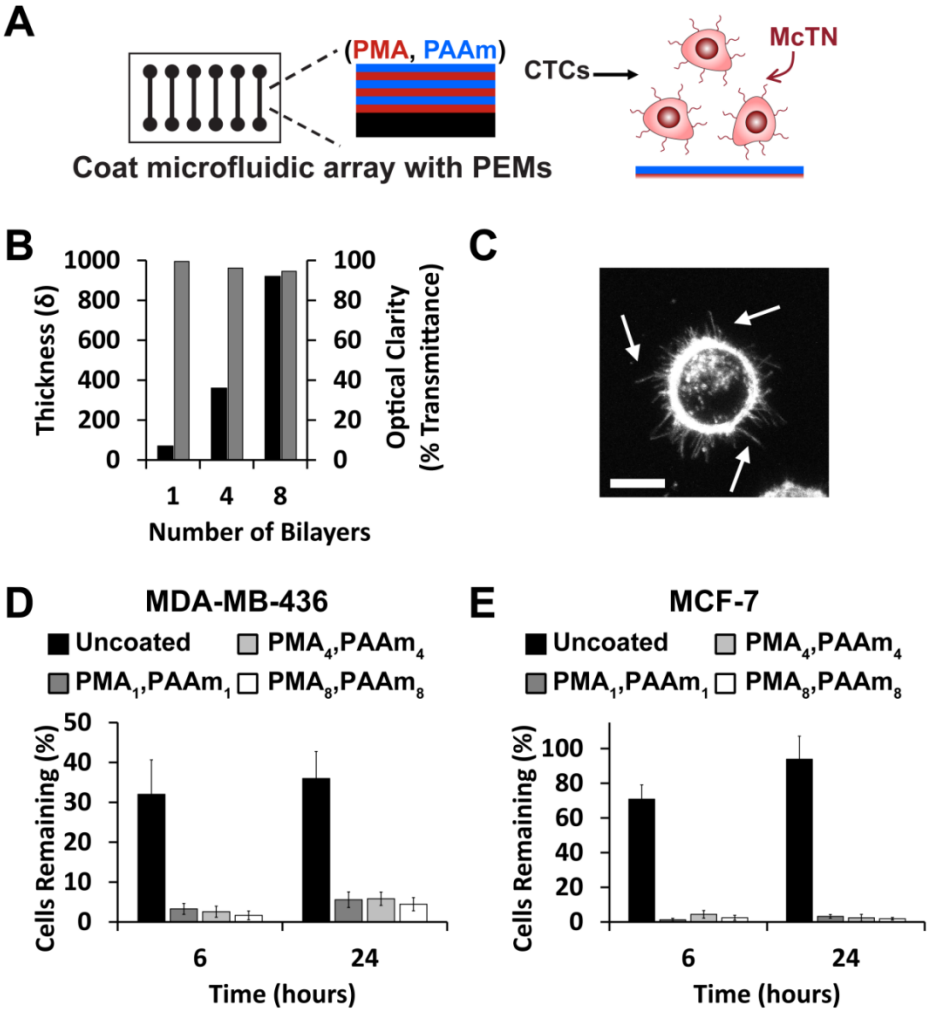

Figure 7.1: PEMs form a cytophobic layer allowing McTN visualization on microfluidic devices. (A) Schematic depicting coating of microfluidic slide with PEMs to maintain free-floating behavior of tumor cells. (B) PEM coatings increase in thickness (left axis, black) with the number of bilayers but maintain optical clarity (right axis, gray). Data (mean ± SEM) correspond to samples in triplicate. (C) Maximum intensity z-projection of MDA-MB-436 cells on $PMA_4/PAAm_4$ surfaces showing McTNs (arrows). Scale bar = 10µm. Percent of (D) MDA-MB-436 and (E) MCF-7 cells (mean ± SEM) remaining on surfaces after washing uncoated slides or slides coated with 1, 4, or 8 PMA/PAAm bilayers. Data represents mean values of three independent experiments.

7.3.1 PEMs inhibit cell attachment allowing for McTN visualization

We formed PEMs from two common polymers, poly(methacrylic acid) and polyacrylamide (PAAm) that have previously been shown to limit cell adhesion of numerous cell types [255, 264]. Substrates coated with PEMs offered precise control over film thickness and did not limit optical transmission, a feature important for pre-clinical and clinical imaging (**Figure 7.1B**). Since human breast tumor cells lines have not yet been tested on PEM-coated substrates, we first confirmed that PMA/PAAm multilayers could prevent cell adhesion in two NCI breast cancer cell lines, MDA-MB-436 and MCF-7. MDA-MB-436 cells seeded on slides coated with cytophobic PEMs maintained McTN display (**Figure 7.1C**), demonstrating for the first time maintenance of free-floating tumor cell behavior by using PEMs. We next coated multi-well culture plates or microfluidic slides with PEMs and allowed cells to attach for 0, 6, and 24 hours. The number of cells remaining after washing at each time point was then quantified by image analysis and cell proliferation (CellTiter). Imaging revealed that PEM-coatings prevented attachment of either cell line (**Figure 7.1D, 7.1E, 7.2A, 7.2B**) for at least 24 hours using 1, 4, and 8 PMA/PAAm bilayers. Cell proliferation data also indicated that deposition of 4 bilayers and 8 PMA/PAAm bilayers showed reduced attachment compared with 1 bilayer for both lines (**Figure 7.3A, 7.3B**). Four bilayer films were prioritized for future experiments since these films formed cytophobic surfaces that most efficiently decreased cell attachment while maintaining McTN activity. Coatings did not impact the viability of either cell line, regardless of substrate (**Figure 7.3C-F, 7.4, 7.5**).

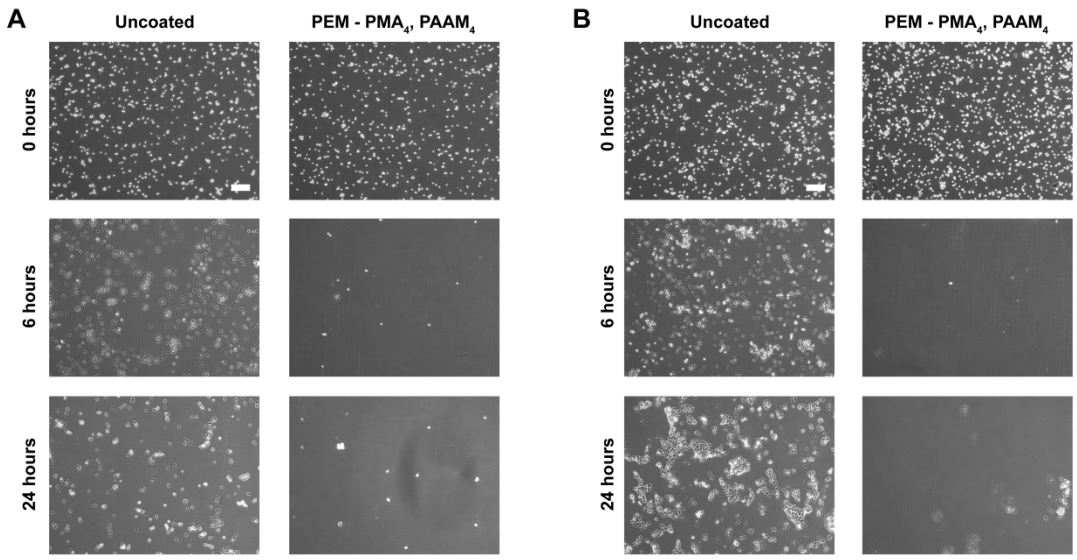

Figure 7.2: PEM prevents attachment of MDA-MB-436 and MCF-7 breast cancer cells.
Representative images of (A) MDA-MB-436 and (B) MCF-7 cells on microfluidic slides with 0 (uncoated) and $PMA_4/PAAm_4$ bilayers after one wash at 0, 6, and 24 hrs at 4x magnification. Scale bar represents 200µm.

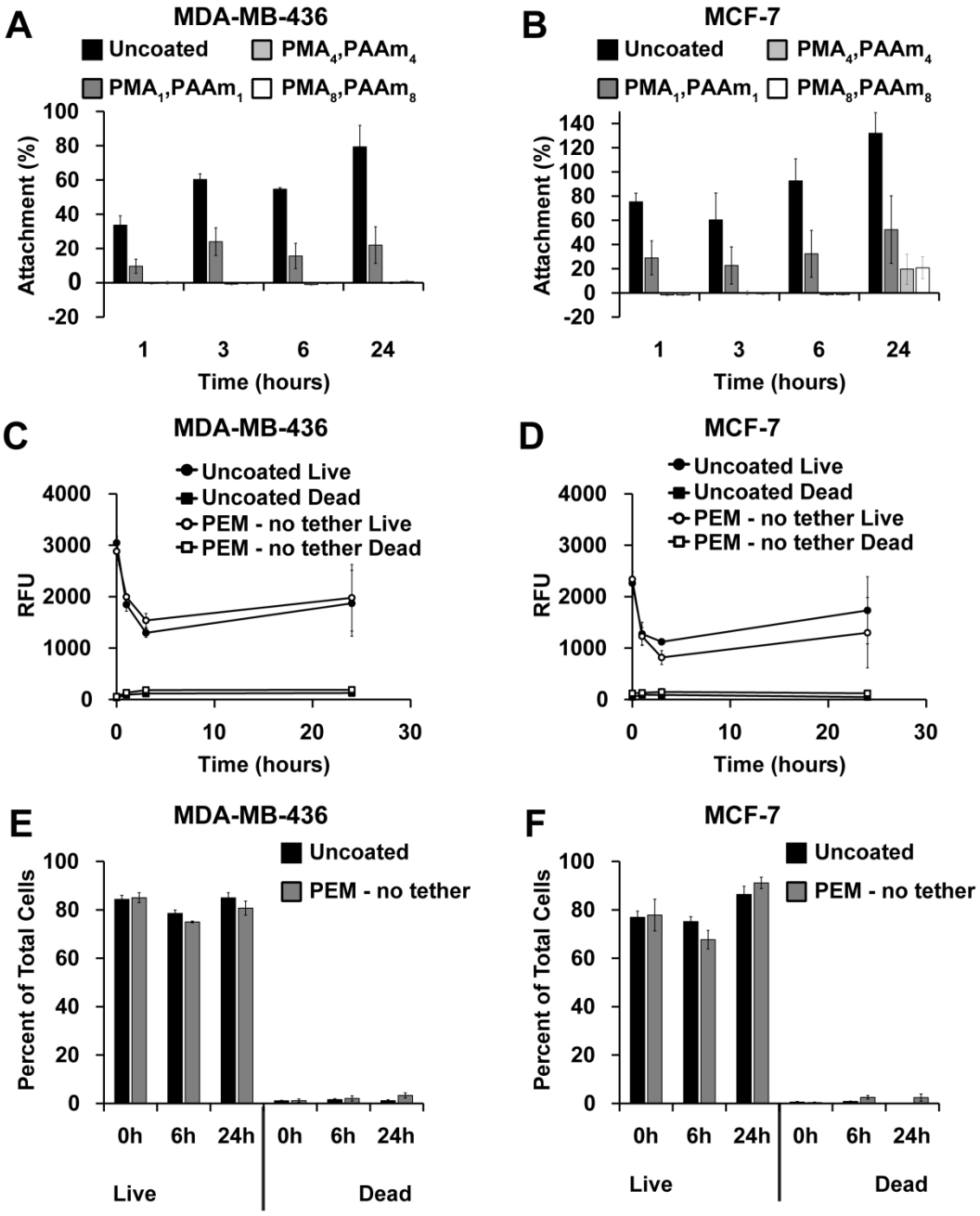

Figure 7.3: PEM prevents cell attachment and does not affect cell viability.
CellTiter analysis of the number of (A) MDA-MB-436 and (B) MCF-7 cells remaining on 96-well plate coated with 0 (uncoat), 1, 4, and 8 PMA/PAAm bilayers after one wash at 1, 3, 6, and 24 hrs normalized to initial cell number. Data represents mean cell attachment from three independent experiments (mean ± SEM). Viability of (C) MDA-MB-436 and (D) MCF-7 cells on a 96-well plate coated with 0 (uncoated), 1, 4, and 8 PMA/PAAm bilayers at 0, 1, 3, 6, and 24 hrs. Data represents mean viability from three independent experiments (mean ± SEM). Viability of (E) MDA-MB-436 and (F) MCF-7 cells plated on microfluidic slides with 0 (uncoated) or $PMA_4/PAAm_4$ bilayers calculated at 0, 6, and 24 hrs. Green fluorescence (live) and red fluorescence (dead) positive cells were quantified for each and divided by total cell number to calculate percent of live and dead cells, respectively using CellProfiler. Data represents mean viability from three independent experiments (mean ± SEM).

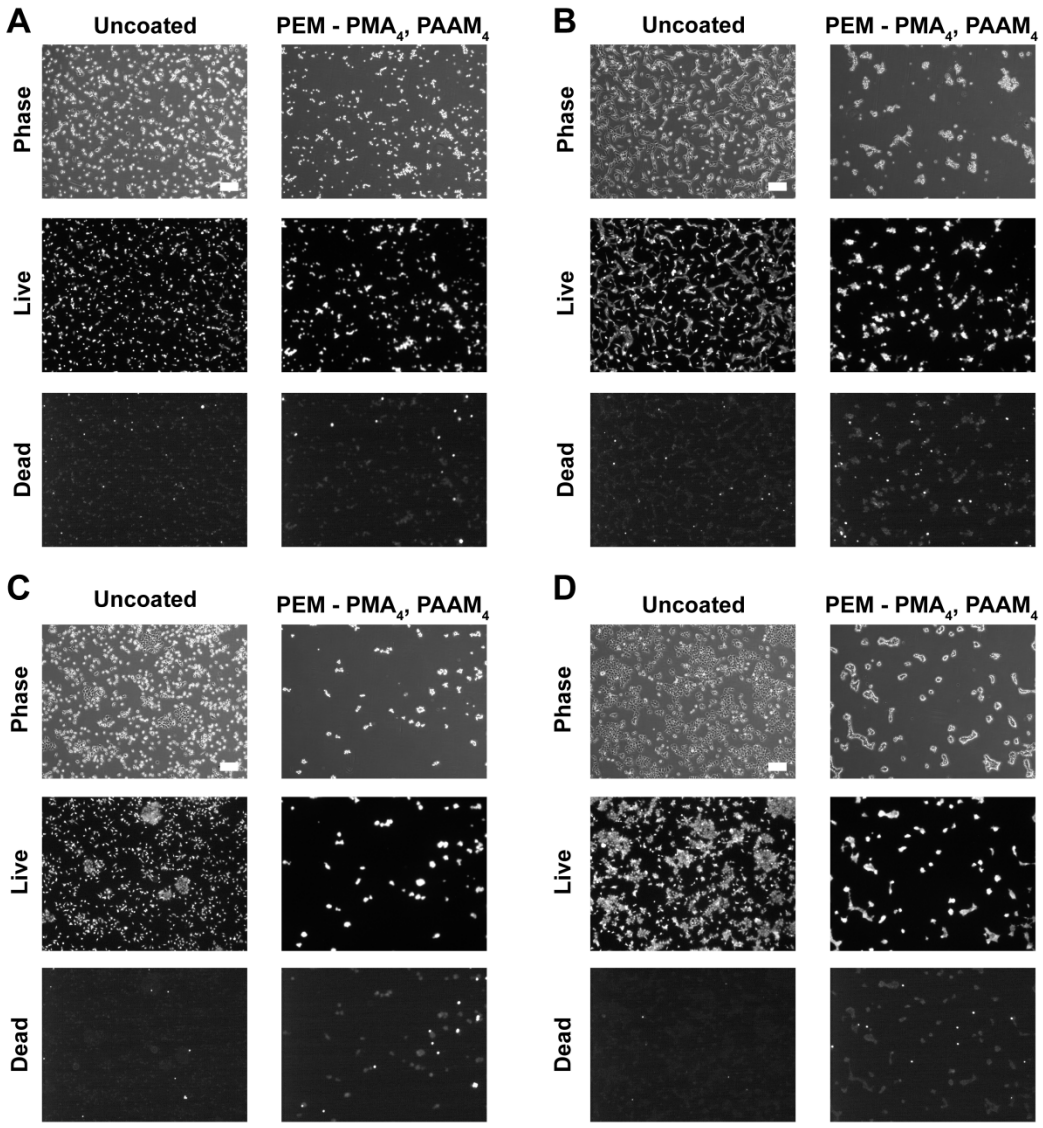

Figure 7.4: PEM does not affect viability of MDA-MB-436 and MCF-7 cells.
Representative images of the viability of MDA-MB-436 plated on microfluidic slides with 0 (uncoated) or $PMA_4/PAAm_4$ bilayers at (A) 6 hrs and (B) 24 hrs. Representative images of the viability of MCF-7 plated on microfluidic slides with 0 (uncoated) or $PMA_4/PAAm_4$ bilayers at (C) 6 hrs and (D) 24 hrs. Phase contrast, live (green fluorescence), and dead (red fluorescence) images taken at 4x magnification. Scare bar represents 200µm.

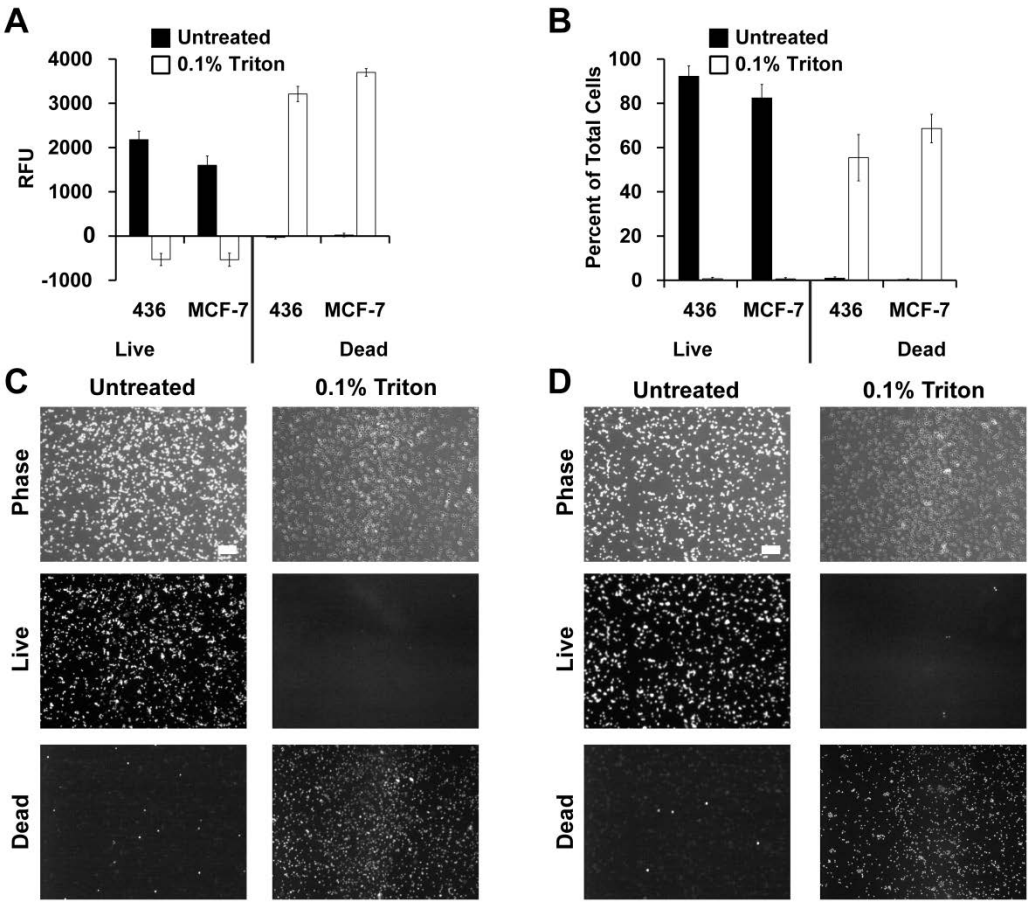

Figure 7.5: Triton-X is a positive control for cell death.
Cell viability of MDA-MB-436 and MCF-7 cells treated with 0.1% Triton-X plated on (A) 96-well plate and (B) microfluidic slides. Green fluorescence (live) and red fluorescence (dead) positive cells were quantified for each and divided by total cell number to calculate percent of live and dead cells, respectively, using CellProfiler. Data represents mean viability from three independent experiments (mean ± SEM). Representative images of (C) MDA-MB-436 and (D) MCF-7 cells treated with 0.1% Triton-X. Phase contrast, live, and dead images taken at 4x magnification. Scale bar represents 200µm.

7.3.2 Modification of PEMs with lipid tethers retains tumor cells after washing

Although PEM-coated surfaces prevented tumor cell attachment and supported free floating behavior, these cells were removed during washing with buffer. Thus we sought to develop a strategy to maintain McTNs while also providing spatial localization during microfluidic flow for real-time imaging and drug screening. We hypothesized that the addition of a terminal lipid layer that interacts with cell

membranes would loosely tether cells to the surface during microfluidic flow. We tested 1,2-dioleoyl-3-trimethylammonium-propane (DOTAP) and 1,2-dioleoyl-*sn*-glycero-3-phosphocholine (DOPC) as cationic and zwitterionic lipids, respectively, owing to the ability of these molecules to interact with the PEMs electrostatically (**Figure 7.6A**). Following addition of DOTAP or DOPC, total film thickness increased, though individual bilayers were still only 20nm and optical clarity remained high (**Figure 7.6B, 7.6C**). We next tested if the addition of lipid supported tethering of breast tumor cells without inhibiting free-floating features such as McTNs. Tumor cells were seeded on microfluidic slides coated with $(PMA/PAAm)_4$ without lipids (PEM-no tether) or with either terminal lipid layer (PEM-DOPC tether, PEM-DOTAP tether). During successive wash steps, DOTAP retained tumor cells more efficiently compared to non-tethered cells seeded on microfluidic slides coated with PEM only (**Figure 7.7A, 7.7B**). MCF-7 cells exhibited significantly higher overall cell retention with PEM-DOTAP compared to PEM only over four washes. MDA-MB-436 cells showed significant retention of cells with PEM-DOTAP for the first wash and continued to tether around 10% of cells for subsequent washes. Tethering was dependent on lipid composition, as after five washes, DOTAP tethered and retained 30% of MCF-7 cells, while DOPC was ineffective at tethering cells during successive washing (**Figure 7.7A, 7.7B** versus **Figure 7.7C, 7.7D**). Representative images of cells from each line tethered on these surfaces are shown in **Figure 7.7E** and **Figure 7.8**. Since DOTAP demonstrated superior tethering for both types of tumor cells, this lipid was prioritized for functional assays.

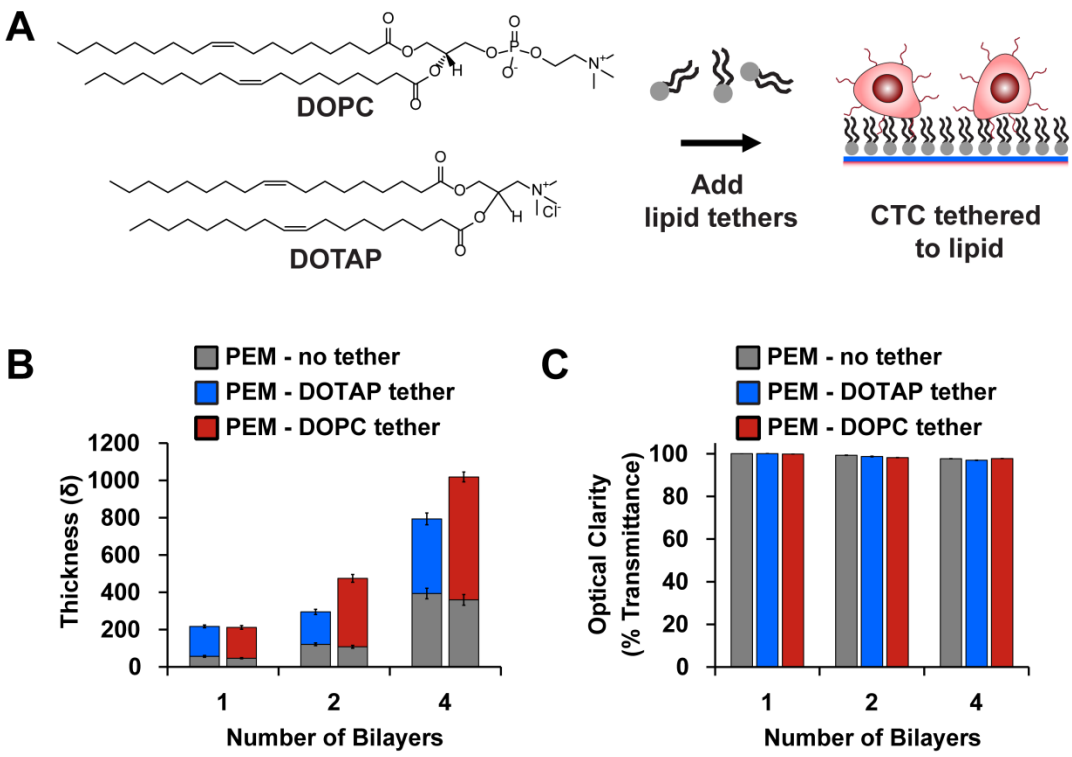

Figure 7.6: Modification of PEMs with lipid tethers.
(A) Schematic depicting how lipid-terminated PEMs promote interaction with tumor cell membranes. (B) Film thickness and (C) optical clarity (mean ± SEM) after addition of DOTAP (blue) and DOPC [249]. Lipids promote growth of film while maintaining an optically-clear substrate for imaging. Data correspond to the mean of samples prepared in triplicate with three measurements per surface.

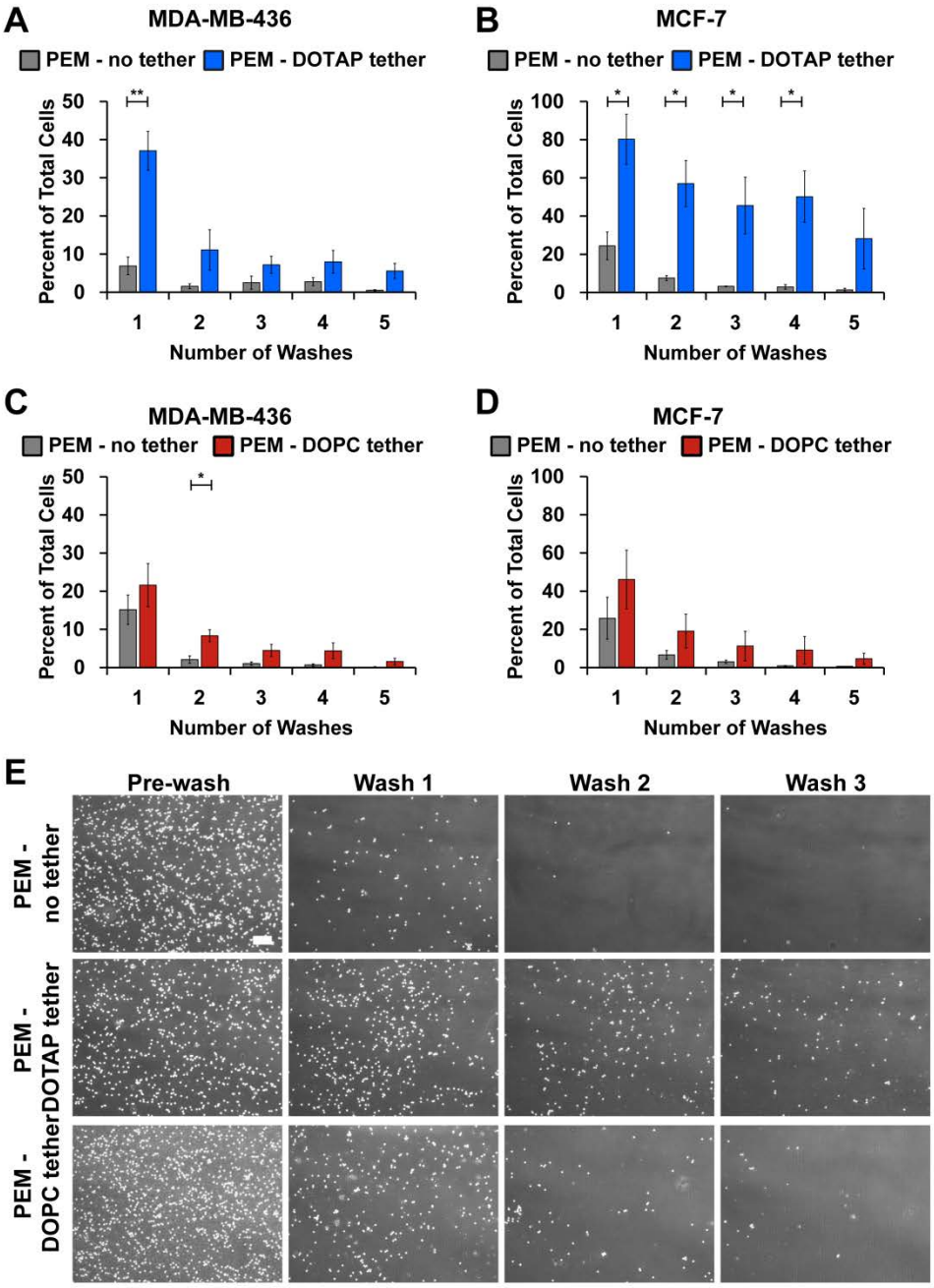

Figure 7.7: DOTAP tethers breast cancer cells.
Percent cell retention of (A) MDA-MB-436 and (B) MCF-7 cells plated on microfluidic slides coated with $PMA_4/PAAm_4$ bilayers alone or with DOTAP. Percent cell retention of (C) MDA-MB-436 and (D) MCF-7 cells plated on microfluidic slides coated with $PMA_4/PAAm_4$ bilayers alone or with DOPC. The remaining cells after each wash was quantified with CellProfiler and normalized to the initial cell number. Data represents mean of triplicate independent experiments (mean ± SEM). (E) Representative images of MDA-MB-436 cells at time 0 and after 3 subsequent washes on $PMA_4/PAAm_4$ bilayers with no tether and with PEM-DOTAP or PEM-DOPC tethers at 4x magnification. Scale bar = 200µm. *$p<0.05$ **$p<0.01$.

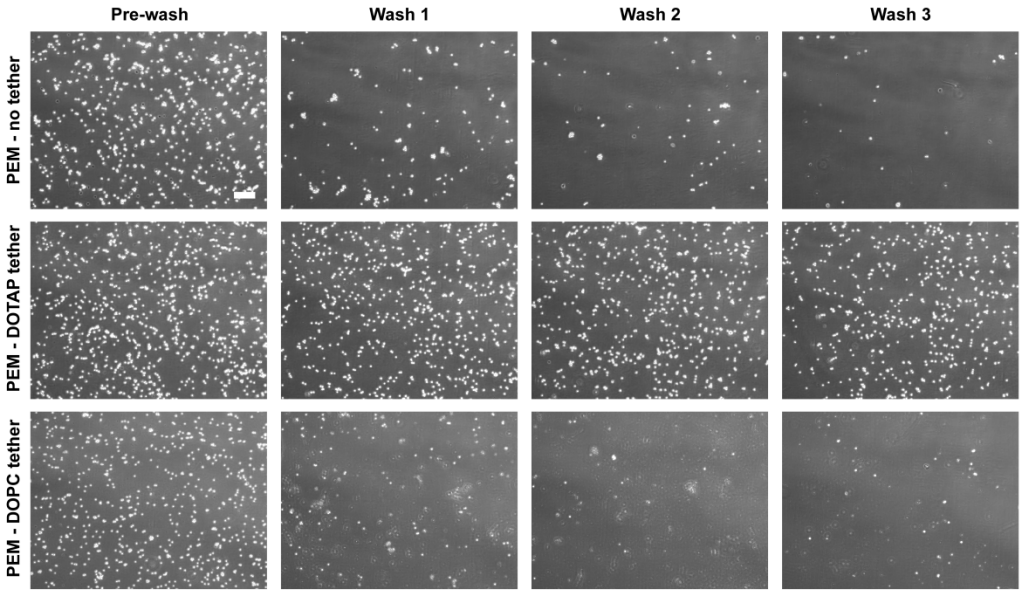

Figure 7.8: DOTAP can tether MCF-7 breast tumor cells.
Representative images of MCF-7 cells seeded on microfluidic slides with PEM-no tether, PEM-DOTAP tether, and PEM-DOPC tether prior to washing and after 3 subsequent washes at 4x magnification. Scale bar represents 200µm.

7.3.3 Lipid tethers preserve McTNs and cell viability

We next determined if lipid tethering with DOTAP maintained free-floating tumor cell characteristics. As a first indicator, McTN frequency was assessed on PEM and PEM-DOTAP surfaces. Blinded McTN counts revealed no differences in McTN frequency on PEM-no tether and PEM-DOTAP surfaces compared to previously published counts on low-attach multi-well plates (**Figure 7.9A**). These results indicate lipid tethering does not impact the ability of MDA-MB-436 cells to assemble McTNs, results confirmed by epifluorescence imaging of McTNs on cells incubated with each type of PEM or substrate (**Figure 7.9B, 7.10A**). MCF-7 cells exhibited similar results (**Figure 7.9A, 7.10B**), though these cells assembled McTN at lower frequencies as previously reported [265]. Further, toxicity studies confirmed tethering

does not impact tumor cell viability (**Figure 7.9C-E, Figure 7.10C-F**). Thus for the first time, our approach allows maintenance of free-floating tumor cell behavior while spatially fixing the location of tumor cells.

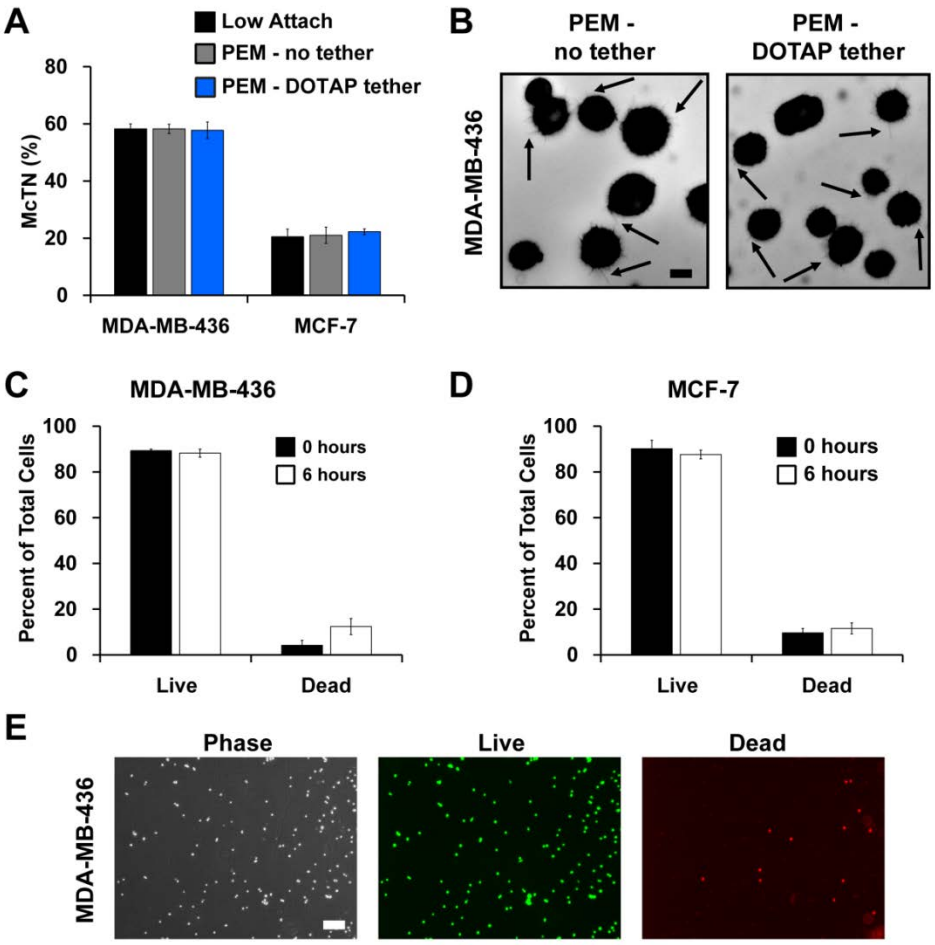

Figure 7.9: Lipid tethering retains free-floating characteristics of breast tumor cells and does not affect cell viability.
(A) McTN quantification of MDA-MB-436 and MCF-7 cells suspended on a low-attach plate, microfluidic slides with PEM-no tether, and microfluidic slides with PEM-DOTAP tether. Data represents blinded quantification of McTN frequency from three independent experiments with 100 cells counted for each (mean ± SEM). (B) Representative images of McTNs (arrows) on MDA-MB-436 cells seeded on PEM-no tether and PEM-DOTAP tether microfluidic slides at 40x magnification. Scale bar = 10µm. Viability of (C) MDA-MB-436 and (D) MCF-7 cells calculated at 0 and 6 hrs after seeding on microfluidic slides with PEM-DOTAP tether. Data represents mean cell viability from three independent experiments (mean ± SEM). (E) Representative images show viability of MDA-MB-436 cells tethered by DOTAP for 6 hrs. Phase contrast, live (green fluorescence), and dead (red fluorescence) images taken at 4x magnification. Scale bar = 200µm.

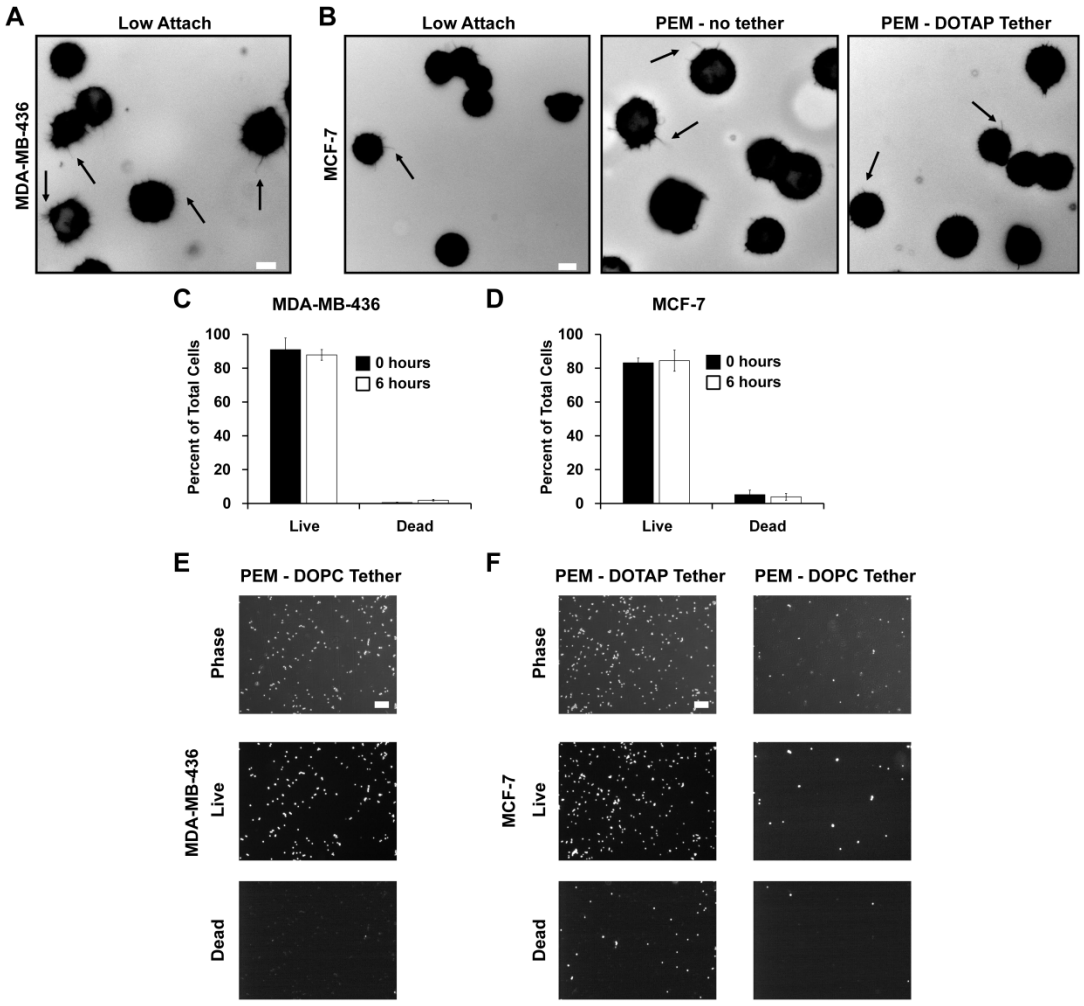

Figure 7.10: Lipid tethering retains microtentacles and does not affect cell viability.
(A) Representative image of McTNs (arrows) on MDA-MB-436 cells on a low-attach plate at 40x magnification. Scale bar represents 10µm. (B) Representative images of McTNs (arrows) on MCF-7 cells on a low-attach plate, microfluidic slide with PEM-no tether, and microfluidic slide with PEM-DOTAP tether at 40x magnification. Scale bar represents 10µM. Viability of (C) MDA-MB-436 and (D) MCF-7 cells calculated at 0 and 6 hrs after seeding on microfluidic slides with PEM-DOPC tether. Green fluorescence (live) and red fluorescence (dead) positive cells were quantified for each and divided by total cell number to calculate percent of live and dead cells, respectively, using CellProfiler. Data represents mean cell viability from three independent experiments (mean ± SEM). (E) Representative images of MCF-7 cells seeded on microfluidic slides with PEM-DOTAP tether for 6 hours. Phase contrast, live, and dead images taken at 4x magnification. Scale bar represents 200µm.

7.3.4 Lipid tethers allow for real-time high resolution McTN imaging in response to drug treatments

One of the greatest challenges in studying free-floating cells is the difficulty in measuring their functional properties or behavior in real time. This is especially apparent when trying to image free-floating cells over time and in three dimensions. Epifluorescence is unable to capture McTNs in high resolution (**Figure 7.9B**). Confocal microscopy of cells labeled with a fluorescent membrane dye improves signal to noise and allows McTNs to be imaged with high contrast (**Figure 7.11Ai, arrows**). However, since McTNs occur on free-floating cells, the time required to generate a 3-dimensional stack of z-slice images for tracing McTN length yields significant blurring as free-floating cells drift over a surface to which they cannot attach. This limitation was encountered when imaging cells exposed to PEM surfaces without lipid tethers (**Figure 7.11Aii, arrows**). The blurring effect of cell drift is even more apparent across a time projection (**Figure 7.11Aiii**). In contrast, tethered breast tumor cells not only maintained McTNs (**Figure 7.11Aiv, arrow**), but also eliminated blurring of McTNs in z-stacks. This strategy also allowed microtentacle length to be traced efficiently across z-stacks (**Figure 7.11Av, arrow**) and limited drift of the cell body during time-lapse imaging (**Figure 7.11Avi**). These phenomena are evident during time-lapse movies of drifting tumor cells seeded on PEM-no tether surfaces, whereas DOTAP tethering caused cells to remain fixed in one location while preserving McTN dynamics. It is interesting to note that debris can be seen moving quickly through the field throughout the movie while the cell remains immobile and centered.

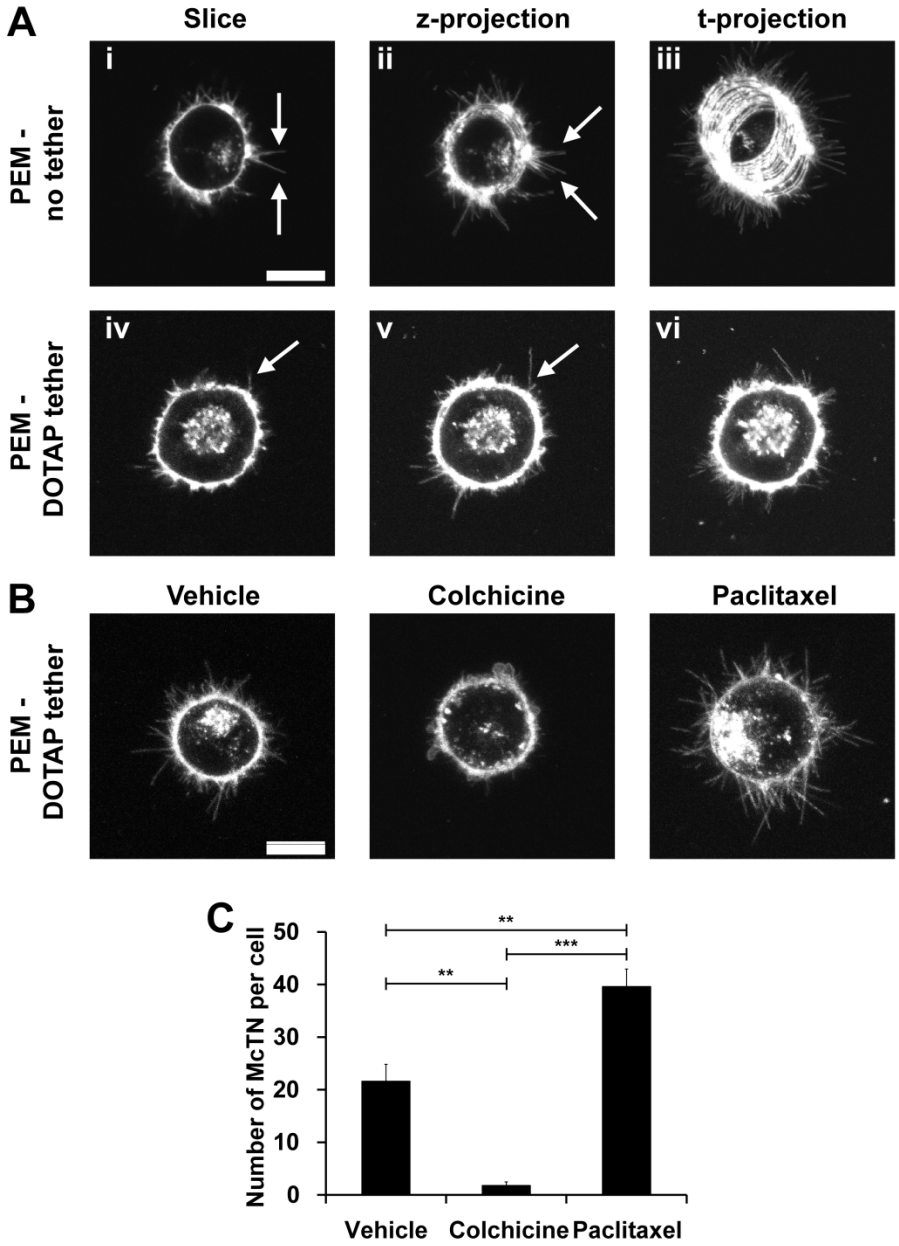

Figure 7.11: Lipid tethering allows for real-time McTN imaging in response to drug treatment and minimizes effects of drift.
(A) McTN (arrows) imaging of MDA-MB-436 cells seeded on microfluidic slides with PEM-no tether (i-iii) and PEM-DOTAP tether (iv-vi). Representative 1µm slice (i and iv), maximum z-projection of 5 slices at one time point (ii and v), and maximum t-projection after 20 frames (iii and vi) are shown at 60x magnification. (B) McTN (arrow) imaging of MDA-MB-436 cells seeded on microfluidic slides with PEM-DOTAP tether after treatment with 5µM colchicine for 15 mins and 1µg/ml paclitaxel for 120 mins. Maximum intensity z-projections of five 1µm slices at one time point are shown at 60x magnification. Complete time-lapse movies are available in Fig. S7. Scale bar = 10µM. (C) Manual quantification of the average number of McTNs per cell (mean ± SEM) in MDA-MB-436 cells treated with colchicine and paclitaxel. **$p<0.01$ ***$p<0.001$.

The major advantage in imaging McTNs over time is being able to study their responses to drugs not only by McTN frequency, but also McTN dynamics. To demonstrate this potential, we recorded three dimensional z-stacks of untreated MDA-MB-436 cells, cells treated with the microtubule destabilizing agent, colchicine, or the microtubule stabilizing agent, paclitaxel. Addition of colchicine decreased McTNs while paclitaxel enhanced McTNs (**Figure 7.11B**). Over time, colchicine shrunk McTNs and increased cell blebbing, whereas paclitaxel hyperstabilized McTNs, dramatically decreasing their dynamics compared to vehicle control. These new trends are clearly observable in high resolution movies that would be otherwise impossible without lipid tethering, since microfluidic flow would wash these cells away or drift would cause blurring. This strategy also creates new opportunities to study free-floating cell properties on a per-cell basis. For example, we measured time-dependent drug response and discovered that treatment with colchicine decreased the mean number of McTN per cell from 21.6 ± 7.2 to 1.8 ± 1.5, while paclitaxel treatment increased the frequency of these structures to 39.6 ± 7.5 McTNs/cell (**Figure 7.11C**).

7.4 Discussion

The majority of cancer-related deaths are due to the spread of tumor cells through the circulation from the primary site to a secondary organ [266]. While in the circulation, tumor cells are in a non-adherent microenvironment that is unlike the conditions in a primary tumor or the metastatic site. In these non-adherent conditions, tumor cells undergo many biochemical and structural changes that affect their sensitivity to

therapies and their overall metastatic efficiency [241, 267]. Classical drug studies and microscopy focus on analyzing tumor cells attached to a substrate due to the practical ease of analyzing cells under static conditions, but these methods do not recapitulate the free-floating environment of CTCs. Therefore, we have developed a microfluidic device that can anchor tumor cells using a lipid moiety while preventing their attachment to a substrate.

In this proof-of-concept study we show that tethering is an effective way to retain the free-floating behavior of cancer cells and provides new opportunities to study their functional properties with high-resolution microscopy through spatial localization. This strategy offers the ability to coat a variety of surfaces, including microfluidics. We show that incorporating a lipid moiety on PEMs can passively immobilize tumor cells in a manner that preserves McTN formation and does not affect cell viability. In this method, no cellular adhesive properties are necessary because the interaction of the cell membrane with the lipid results in cell tethering. Lipids have previously been used to immobilize cells [258, 260]; here we have advanced this idea to create a simple system for studying McTNs on free-floating tumor cells. This approach eliminates the need for solvents, patterning, designed topographies, or antibodies used in other recent studies aimed at promoting adhesion of CTCs. Further, cells can be tethered in complete media and in a short time frame, both enabling real-time study of McTNs on individual CTCs. Therefore, using this technique, tethering of any cell type can be achieved in a simple and rapid manner, making this a robust platform to study free-floating behaviors across various cell types.

In our studies, each PEM lipid formulation tethered cancer cells, but the lipid moiety itself altered cell retention, with DOTAP – a cationic lipid – driving the best tethering. DOPC – a zwitterionic lipid – contains a phosphate group which may cause less favorable interactions with cell membranes compared to DOTAP. While cells were immobilized on the substrate, they remained free-floating owing to the cytophobic nature of the initial PEM coating. There was some loss of tethered cells as a function of the number of washes, but it is likely these interactions can be strengthened by incorporation of cross-linkable lipids [258, 260, 268, 269]. We also observed a difference in the tethering efficiency as a function of cell line, with MCF-7 breast cancer cells exhibiting better tethering compared to MDA-MB-436 cells. These changes may be due to the differences in membrane composition or surface marker expression of each cell line [270].

We demonstrate the utility of tethering for tumor cell analysis by assessing the response of McTNs to microtubule-targeting drugs. Unlike our previous studies, it is now possible to add drugs via microfluidic exchange without displacing cells, allowing time-lapse measurements of colchicine-dependent McTN disruption [238] and paclitaxel-dependent McTN enhancement [244] to be measured with time-lapse imaging for the first time. Our discovery that paclitaxel hyperstabilizes McTNs, for example, is significant since microtubule stability can enhance McTN formation and increase the re-attachment efficiency of tumor cells [244]. Mouse models of metastasis indicate that this increased McTN formation and tubulin stability results in

greater lung trapping of tumor cells [238, 242, 244]. Therefore, analyzing McTN dynamics and their response to drugs has important implications on the metastatic ability of tumor cells. These technological advances should allow many additional quantitative McTN metrics to be accurately measured (length, dynamics, etc.) and also improve on qualitative observations that have until now not been possible on a live, individual cell basis.

High numbers of CTCs correlate with increased metastasis and decreased survival of patients with metastatic cancer [228, 229, 271, 272]. However, CTC enumeration alone may not be a good marker for disease staging and prognosis [271]. Therefore, improved biologic characterization of CTCs is necessary to better understand their clinical value. Numerous new approaches have been designed to improve CTC detection and enumeration, but the ability to study the functional properties of CTCs remains difficult [227]. *Ex vivo* culture of CTCs in non-adherent conditions has provided one method to analyze CTCs from patients [232]. This PEM-lipid tethering technology may be applied to these culturing methods to keep cells from adhering, but offers the unique capabilities of rapid single-cell analysis through staining and imaging in real-time.

Studying the biology of CTCs has suggested important consequences for both metastatic efficiency and the sensitivity of these structures to candidate cancer drugs. Of note, patterns of drug sensitivities have been linked to the genetic mutations present in individual CTC samples from breast cancer and lung cancer patients,

indicating that a change in tumor genotypes during the course of treatment can lead to drug resistance [232, 267, 273]. Our work shows tethering tumor cells allows rapid analysis of specific drug responses in real-time. Markers of epithelial-to-mesenchymal transition (EMT) are also upregulated in CTCs with mesenchymal markers specifically enriched in CTC clusters. These clusters have increased metastatic capabilities compared with single cells alone [233, 274]. Thus our approach can be applied to these existing techniques for fundamental CTC studies at the single-cell level. Assessing the effects of drugs on cell viability, EMT markers, or McTNs could all have implications on their metastatic phenotype. Tethering would also allow these studies to be conducted in a manner that more closely recapitulates the free-floating environment found in circulation. Though our study focuses on the analysis of tumor cells, this simple and rapid tethering technology is translatable to numerous other cell types that are encountered in the blood stream (i.e., red blood cells, platelets, lymphocytes, macrophages) and may function differently in a free-floating environment. With new technologies, CTCs will play an increasing role in informing therapy and disease progression of cancer patients. Toward this goal, tethering CTCs with PEM-lipid films could serve as a new tool to analyze CTC samples to provide better personalized treatment decisions for patients.

7.5 Conclusion

Metastatic cancer cells exhibit dynamic properties when suspended in a free-floating state (e.g., McTNs) that upon evaluation, could inform decisions regarding the diagnosis, prognosis, and drug treatment plan. The technology developed here using

the PEM-lipid tethering system provides a unique platform to immobilize cells while maintaining their free-floating phenotypes. While the above studies just began to investigate the many uses for this technology, it is apparent that the ability to screen cells in real-time could provide useful information rapidly to researchers and clinicians alike.

The previous chapters revealed that properties of materials including their state of degradation can influence the immune system and studied how materials impact immune cells and tissues. These results highlight the opportunities to engineer new materials to specifically control immune function. An exciting field of research where this potential is particularly evident is in tissue engineering and regenerative medicine. Toward realizing this opportunity, **Chapter 8** summarizes the current state of understanding the effect materials have on immunity in vaccine and immunotherapy fields and provides a forward looking perspective on how these properties could be incorporated within tissue engineering constructs to promote a regenerative environment.

Chapter 8: Designing biomaterials with immunomodulatory properties for tissue engineering and regenerative medicine[7]

8.1 Introduction

Biomaterials have enabled advances in fields spanning tissue engineering, drug delivery, vaccination and immunotherapies, and implantable devices. This breadth is due to the ability of these materials to encapsulate and protect cargos (e.g., chemicals, cells, proteins), to provide biocompatible supports (e.g., devices, scaffolds), and to allow facile modification of chemical and physicochemical properties.[275, 276] Not surprisingly, biomaterials range from naturally-occurring biological building blocks to fully synthetic substances. This ever-expanding use of biomaterials is also creating increasing need for deeper understanding of the interactions between materials and the biological environments they encounter. Nowhere is this need more evident than the immune engineering field. Biomaterials are being widely-explored in vaccines and immunotherapies to combat infectious disease, cancer, and autoimmunity, but the early clinical successes of these approaches are few and far between. One of the interesting findings in the field – described in seminal papers published less than a decade ago[9, 45] – is that many biomaterials exhibit intrinsic material properties that can activate immune pathways. This is certainly an opportunity to gain knowledge

[7]Adapted from J.I. Andorko and C.M. Jewell. "Designing biomaterials with immunomodulatory properties for tissue engineering and regenerative medicine." *Bioengineering and Translational Medicine.* 2017. *In press.*

that informs design of materials that could actively bias immune responses toward desired functions. In tissue engineering, many emerging strategies are also employing immune cues and cells in biomaterial-based structures for engineering organs and tissues, and for regenerative medicine. In contrast to vaccine and immunotherapy research, the immunological role that scaffolds or other materials might play – through intrinsic properties, modification of surface chemistry, or other tunable strategies – has yet to take center stage. Since essentially every tissue engineering application either interacts with or specifically seeks to avoid the immune system, understanding these roles could provide a new lever to improve tissue engineering and regenerative medicine.

This review will discuss what has been learned about the role physicochemical properties of biomaterials play in directing immune responses from the vaccine and immunotherapy fields, and analyze how these concepts might be exploited for tissue engineering and regenerative medicine. We begin with a brief introduction to the immune system and the response to injury and implanted materials. Next, we discuss what is known about how immune response is impacted by biomaterial properties such as size, shape, and stability/molecular weight, along with surface features such as chemical functionality, charge, and hydrophobicity (**Figure 8.1**). Then, we describe how the introduction of biomaterial scaffolds, and the specific features of these tissue engineering constructs exhibit intrinsic immunogenic features that can impact immune cell polarization and wound healing. Finally, we highlight new

research directions leveraging the intrinsic properties of materials to control immune function and push the forefront of tissue engineering and regenerative medicine.

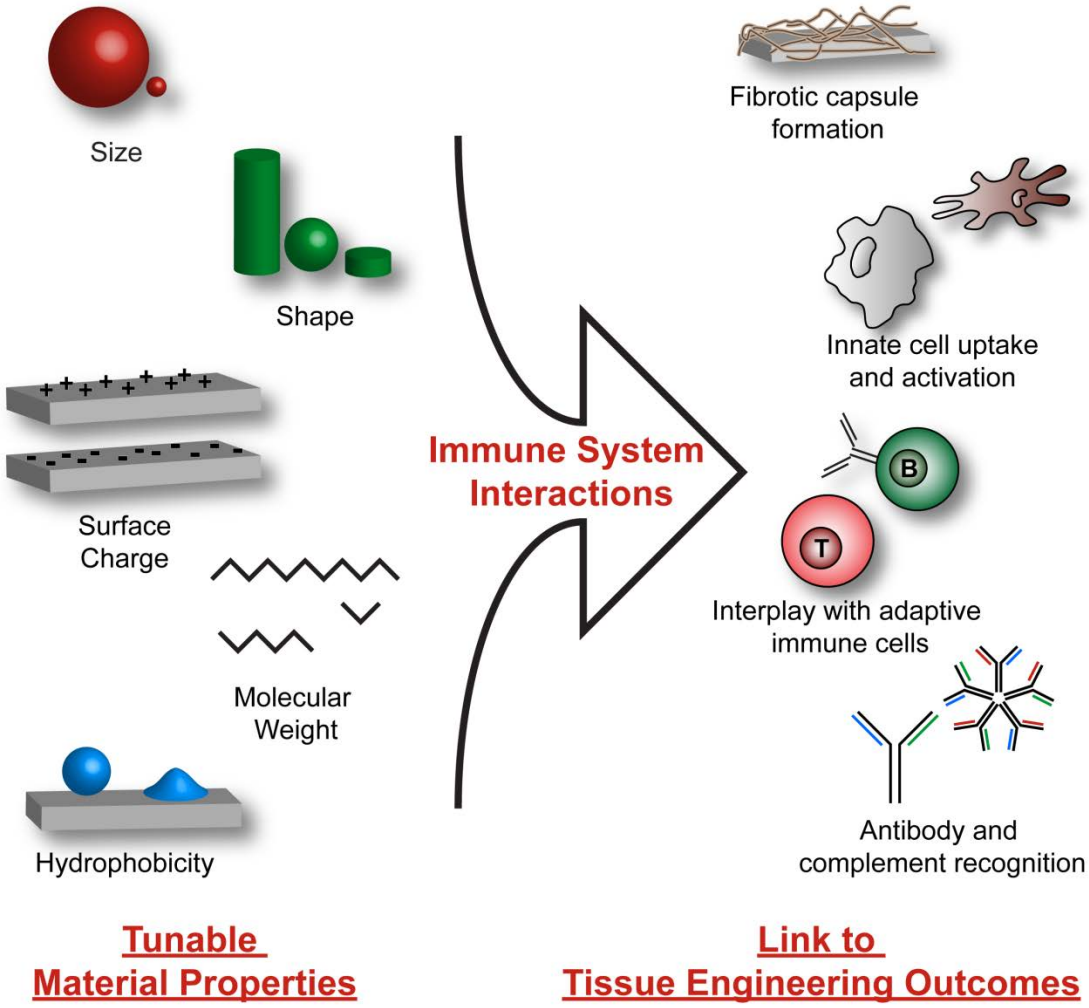

Figure 8.1: Intrinsic properties of materials influence immune responses.
Biomaterials commonly used in vaccine, immunotherapy, and tissue engineering exhibit features including size, shape, surface charge, hydrophobicity, and molecular weight that alter interactions with the immune system. Encountering components of the innate and adaptive immune system with these materials results in formation of fibrotic capsule to isolate the material, differential activation of dendritic cells and macrophages, recognition and removal by antibody and complement proteins, and even manipulating adaptive immune response.

8.2 The Immune Pathways Activated by Pathogens and Other Foreign Molecules also Respond to Biomaterials

Across vaccines, immunotherapies, and tissue engineering, the immune system represents both an opportunity for and barriers against successful outcomes. In order to protect the body from harmful pathogens, the immune system has evolved over time to quickly recognize pathogens or other non-self agents through general physicochemical features that are uncommon in the body. These include the particulate nature of bacteria and viruses, repetitive molecular patterns such as the polysaccharides that comprise bacterial cell walls, and structural motifs such as hydrophobic regions or double stranded RNA often found in molecules from viruses and bacteria.[156, 277] One component of the innate immune system – the segment that provides rapid, but less specific immune responses – are pattern-recognition receptors (PRRs. PRRs are present on antigen presenting cells (APCs), including dendritic cells (DCs) and macrophages, that scan the body for danger-associated molecular patterns (DAMPs) and pathogen-associated molecular patterns (PAMPs).[25, 26] PRRs, including toll-like receptors (TLRs) and the inflammasome, identify specific DAMPs and PAMPS and initiate different signaling pathways leading to the clearance of potentially harmful agents.[110, 278] The inflammasome is a cytoplasmic complex of proteins which activates caspases and the release of IL-1β, a key cytokine involved in initiating inflammatory processes.[110, 278] Interestingly, the inflammasome has been associated with immune cell activation in response to treatment with adjuvants, materials commonly added to vaccine formulations to increase immunogenicity or potency. One ubiquitous example is

alum, an FDA-approved adjuvant consisting of particulate aluminum salt formulations.[110, 278, 279] Since many existing vaccines use alum, and numerous technologies involving microparticles and nanoparticles are in development as vaccines and immunotherapies, continued research into how these materials activate the inflammasome is of great interest. The complement system is another mechanism of the immune system, consisting of serum proteins that assemble after encountering microbes or other extracellular pathogens. These proteins form complexes that tag, destroy, and eliminate the invading pathogens.[25, 280] Supporting these fast-acting innate immune responses is the adaptive immune system. In contrast to innate immunity, adaptive immunity arises more slowly, but is more specific and can lead to the generation of immunological memory. Broadly speaking, adaptive immunity includes cell-mediated and antibody-mediated responses against specific, foreign molecules, terms antigens.[25] Cell-mediated immunity involves activation of T lymphocytes that differentiation into cytotoxic T cells able to destroy self-cells infected with intracellular pathogens such as viruses. Antibody-mediated immunity arises from the activation of B lymphocytes that, upon differentiation, secrete antibodies that bind extracellular pathogens (e.g., bacteria) or toxins to neutralize and clear these targets.

The immune system, particularly innate immune cells, also plays a large role in the response to injury and after implantation of biomaterials.[25, 281-286] Initially, neutrophils and other innate immune cells infiltrate the site of injury to clear pathogens associated with the injury, and secrete cytokines and chemokines that

recruit other immune cells (e.g., macrophages).[25, 283, 284] The first macrophages to arrive at the injury site exhibit an inflammatory phenotype known as M1. These M1 macrophages phagocytose pathogens and damaged cells, and produce pro-inflammatory factors such as inducible nitric oxide synthase (iNOS), TNF-α, and IL-12. These factors promote inflammation and removal of pathogens, and recruit lymphocytes involved in generating adaptive immune repsonses.[284-290] M1 macrophages typically persist at the wound or implant site for 2-3 days after injury, at which time the function of these cells shifts towards the M2 macrophage phenotype; this phenotype is crucial for tissue repair and generating new blood vessels.[284-290] M2 macrophages are functionally different from M1 macrophages. This phenotype exhibits increased expression of key genes involved in wound-repair (e.g., arginase and Fizz1), secretes cytokines and growth factors to stimulate cell proliferation, and deposits extracellular matrix to support tissue regeneration.[25, 283-286] Macrophages also influence the response to implants by forming specialized foreign body cells. These cells create a fibrotic capsule around implanted materials that isolate the material from the surrounding environment of the body.[283] Since M1 and M2 macrophages have different functions, there is an opportunity to target these cells as immunomodulatory players to direct responses to tissue engineering constructs. Currently, it is understood that the phenotype and activation of macrophages is not always a binary process but rather a spectrum where cells upregulate or downregulate specific markers as they transition from one form (pro-inflammatory) to another (wound-healing).[286-290] Since implantation of

biomaterials involves these same mechanisms, there is a need to understand how the properties of materials alter immune interactions in the context of tissue engineering.

Many biomaterials exhibit structural features that trigger recognition as DAMPs and PAMPs. In particular, the immune system commonly responds to the repetitive patterns of polymer chains that can resemble bacterial polysaccharides, hydrophobic portions of materials, and the particulate nature of microparticles and nanoparticles that share characteristic dimensions of bacterial and viral pathogens.[123, 291, 292] Over the past decade, many studies have revealed that even the most common biomaterials can activate immune or inflammatory pathways in the absence of other immunostimulatory signals, and that the physicochemical material properties can alter the magnitude or features of this response. For example, DCs incubated on thin biomaterial-based films of naturally-derived polymers (e.g., alginate, agarose, chitosan, hyaluronic acid) or synthetic polymers (e.g., polylactic-co-glycolic acid (PLGA)) induce differential expression of surface activation markers. These signals include DC maturation markers (e.g., CD40), major histocompatibility class II (MHCII) complexes – proteins responsible for presenting antigens to naïve B and T cells, and co-stimulatory markers (e.g., CD80, CD86). These co-stimulatory signals act as a second signaling cue necessary for activation of B and T cells in response to antigen presented in MHC complexes.[25, 157] In other studies, particulate systems of PLGA, polystyrene, or silica were treated in conjunction with an inflammatory signal (e.g., TLR agonists) and the DC response to these treatments was evaluated.[9, 45, 293] As expected, the inflammatory signal activated DCs, but interestingly, when

treated along with particles, the particles synergistically increased the activation of DCs relative to the TLR agonist alone or the polymers alone. The pro-inflammatory responses were also associated with inflammasome signaling at levels comparable to those measured by alum, the strong human adjuvant discussed above.[9, 45, 293] These revelations have prompted a new area of study to understand which physicochemical properties influence intrinsic immune response and how these interactions occur. New studies are also now exploring such intrinsic immune features of materials to direct vaccine responses more specifically, to improve cancer therapies, and to promote immune tolerance in combating autoimmune diseases.[10, 104, 105, 294-301]

8.3 Understanding Intrinsic Immunogenicity of Biomaterial Delivery Systems Could Inform Tissue Engineering Applications

In the past few years the field has learned a great deal about how the properties of biomaterial vaccine and immunotherapy carriers trigger innate immune pathways. Many studies, recently reviewed[302-309], seek to overcome or evade immunological barriers by modulating these properties of biomaterials-based carriers. This is valuable insight that could be leveraged as the tissue engineering and regenerative medicine fields move forward. In this section, we will explore which properties of vaccine and immunotherapy carriers can be altered to modulate the immune response.

8.3.1 The Size of Biomaterial Carriers Alters Uptake and APC Activation

To drive immune responses, vaccines must reach lymph nodes, tissues that coordinate adaptive immunity through interactions between antigen-experienced APCs and naïve B and T cells. Many vaccines rely on particle size or drainage through the lymphatics to provide a pathway from peripheral injection sites to the lymph nodes.[21, 22, 49, 67, 310] Past studies have shown particles with diameters between 20-50nm can passively drain through lymphatics, and larger particles are more dependent on phagocytosis by APCs which carry the engulfed cargo to lymph nodes.[22, 67] The phenomena occur because particle trafficking is driven in part by the pressure gradient that exists between the blood and lymphatic vessels, causing convective forces that propel smaller particles into lymphatic vessels.[22, 67, 310] As particle size increases, particles flow at much lower rates due to steric hindrance in the interstitial space, or mechanical size limitation for micron-size particles. These larger particles are thus more reliant on internalization and trafficking by APCs to reach lymph nodes.[22, 67, 310] Thus, the size of particles used to deliver vaccines and immunotherapies plays a large role in the uptake, trafficking, and retention of the cargo and carrier in immune cells and tissues.[30, 167, 311]

While particle size impacts trafficking and can alter how much carrier, drug, or vaccine reaches lymph nodes, changes in particle size also play a major role in modulating immune response. For example, with the same antigens and adjuvants present in a material-based vaccine, the size of these particles biases the interaction with innate immune cells and skews the type of antibodies produced.[115, 117, 122]

In one recent study, gold nanoparticles with diameters of 3nm and 12nm were incubated with human-derived DCs. These sizes caused different levels of DC activation, as indicated by common surface maturation markers (e.g., CD80, CD83, CD86, MHCII) and inflammatory cytokine secretion.[312] While both sizes of particles activated DCs, 3nm particles caused higher activation levels and greater secretion of IL-12 and IFN-γ. These effects translated to increased pro-inflammatory T cell function during co-culture.[312] In contrast, treatments with the 12nm particles increased IL-4 production, skewing the resulting T cell-mediated immune responses towards a different function, wound healing.[312] In another study, macrophages treated with particles of varying sizes induced different effects on the levels of the anti-inflammatory cytokine IL-10 and the pro-inflammatory cytokine TNF-α.[108] While the largest particles did not induce cytokines, smaller particles with diameters ranging from 2-40μm induced size-dependent production of IL-10 and TNF-α; this activation was also shown to involve TLR-2 stimulation.[108] Many tissue engineering approaches involve implantation of macroscopic scaffolds or devices that degrade, release fragments, or experience wear effects.[283] Thus, particulates can be generated that also trigger the same size-dependent modulatory immune pathways.[283] Additionally, bulk wear or fracture of implantable devices or scaffolds is often a key design focus since this can lead to acute device failure. From an immunological perspective, however, the inflammatory profile of the nano- and micro-scale wear products or particles will take on an emerging roll in tailoring immune responses to improve device or implant performance.

8.3.2 Immune Activation is Influenced by Biomaterial Shape

While size is an important feature in determining trafficking, uptake, and intrinsic immunogenicity, the shape of materials also impacts these responses.[122, 313-316] For example, in one study, gold nanorods were internalized by macrophages at greater levels than nanospheres owing to preferential uptake of the former via micropinocytosis.[317] In a separate study, glass rods were used as a tool to assess shape dependence by incubating rods of varying lengths with macrophages.[318] Short rods were more rapidly taken up than longer rods, but interestingly, the longer rods, while not readily phagocytosed, induced greater levels of the inflammatory signals IL-1α and TNF-α.[318] This inflammatory response was attributed to "frustrated" phagocytic interactions, a phenomenon that occurs when cells are unable to phagocytose larger-scale objects. This failure results in the production of reactive oxygen species and inflammatory cytokines which ultimately could lead to chronic inflammation and fibrosis.[318] This shape effect might also be important in the context of scaffolds and implants since these constructs are commonly too large for engulfment and often shed long fibers or other geometries upon degradation or wear. Other work has studied shape effects using titanium dioxide to prepare particles with diameters of 7-10nm (anatase) or 15-20nm (rutile), or nanotubes with diameters of 10-15nm and lengths of 70-150nm.[319] These studies revealed shape dependence across cytokine secretion, production of reactive-oxygen species, and DC maturation.[319] In particular, the nanotubes generally caused the largest immunogenic effects,[319] further demonstrating that particle shape impacts immunogenicity. Later in this section, we will discuss some of the mechanistic

studies beginning to ascertain how the interactions of differently-shaped particles with immune cells cause these differential effects.

The extent to which the shape of particulate carriers impacts inflammasome activation is important because, while seminal work has shown particle-based carrier systems can act as adjuvants through inflammasome signaling, other work demonstrates these outcomes are not a feature of all particulate systems.[9, 45, 119, 279, 293, 320] In a study from Vaine *et al*., particles synthesized from block copolymers to either exhibit rough or smooth surfaces (**Figure 8.2A**) differentially activated the inflammasome in mice.[121] In this study, polystyrene-polyethylene oxide particles with a rough surface morphology increased neutrophil recruitment and IL-1β secretion compared with smooth polystyrene-polyethylene oxide particles.[121] This study also found that while the particles had comparable diameters, rough particles were preferentially taken up by macrophages, leading to increased inflammasome activity that was comparable to a positive control treatment with alum. Interestingly, this activation was absent when uptake was inhibited, suggesting that phagocytosis and endosomal destabilization were needed for the materials to activate the inflammasome.[121, 293] In another study, antigen-coated gold nanostructures formed as spheres, rods, or cubes (**Figure 8.2B**) triggered differential levels of cytokine secretion in DCs, leading to differences in antibody production in mice.[321] The rod-shaped particles induced an IL-1β (i.e., inflammasome-mediated) response, while spheres and cubes activated less specific (e.g., TNF-α) inflammatory responses.[321] These studies reveal that the inflammasome, an important pro-

inflammatory signaling cascade of the innate immune system, can be manipulated simply by altering particle shape. More work is needed to understand why these effects occur with some material shapes and not others. In particular, tissue engineering uses materials spanning biological building blocks to synthetic polymers, enabling a variety of shapes and topographies. Thus, understanding how these different parameters promote or diminish inflammasome activation could allow the design of more tunable constructs.

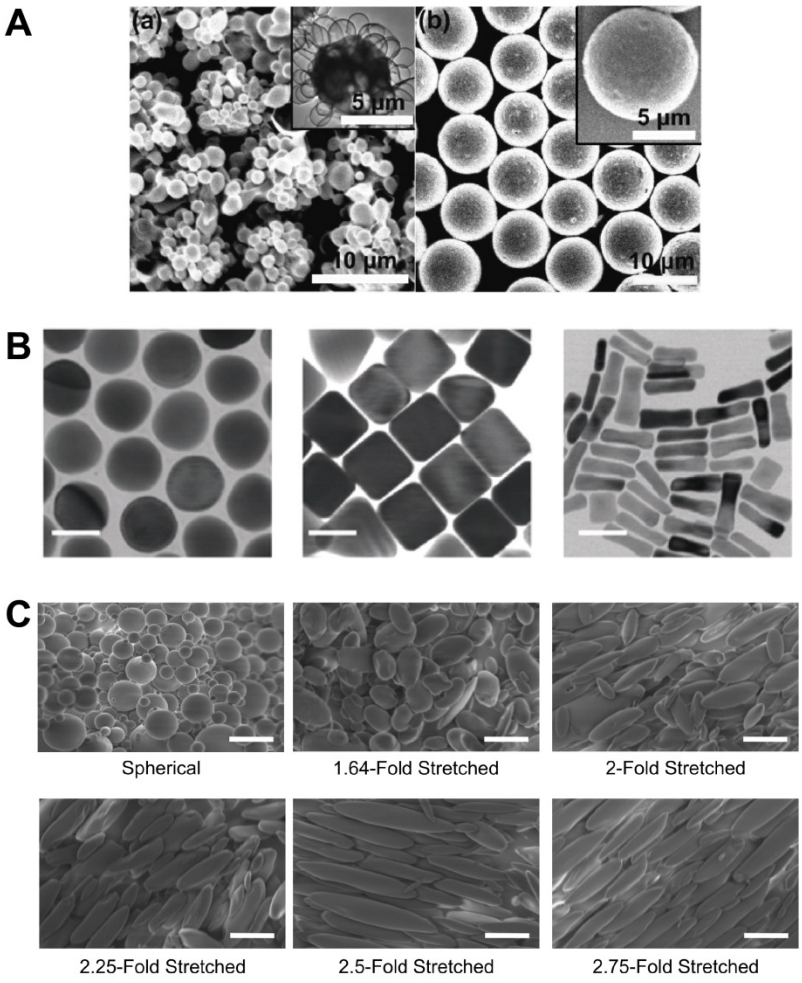

Figure 8.2: Particle shape dictates immune cell uptake and activation.
(A) Spherical polymeric particles fabricated from polystyrene-polyethylene oxide that exhibit rough surfaces (left) were preferentially taken up by macrophages and induced a pro-inflammatory response compared to smooth particles (right) (Scale bar, 10µm; inset scale bar, 5µm). (B) Electron micrographs of gold nanoconstructs with spherical (left), cube (center), or rod-like (right) shapes. When incubated with DCs, rod-like particles induced inflammatory IL-1β and activated the inflammasome, while sphere and cubes caused secretion of TNF-α (Scale bar, 40nm). (C) Spherical PLGA particles that are mechanically stretched to form ellipsoidal particles increase surface interactions with immune cells, leading to increased T cell proliferation. (Scale bar, 10µm). (A) reprinted with permission from ref [121]. (B) reprinted with permission from ref [321]. (C) reprinted from ref [41] with permission from Elsevier.

Research from the Green and Schneck groups has focused on using polymeric particles as artificial antigen presenting cells (aAPCs), mimicking the ability of APCs such as DCs to simultaneously present antigen fragments and costimulatory markers to T cells. [41, 322, 323] In this work, the authors studied the impact of aAPC shape

on T cell response.[41, 322, 323] Spherical PLGA nanoparticles were first synthesized, then mechanically stretched to form elongated, ellipsoidal particles with different aspect ratios (**Figure 8.2C**). To properly mimic the way natural APCs interact with T cells, both antigen and costimulatory molecules need to be presented in the correct contexts to promote T cell activation and proliferation. To accomplish this, antigen within MHC molecules along with a co-stimulatory antibody (anti-CD28) were coupled to the surface of either spherical or ellipsoidal particles to the form biomimetic aAPCs.[41, 322, 323] Since aAPCs need to interact with T cells, the parameters to ensure they remain extracellular were explored by incubating both spherical and ellipsoidal particles with macrophages and human umbilical cord vein endothelial cells. These studies revealed spherical aAPCs were phagocytosed quicker and at higher levels compared to ellipsoidal aAPCs.[322] As a result, ellipsoidal aAPCs injected intravenously in mice experienced increased circulation time and greater biodistribution compared to spherical formulations. Since ellipsoidal aAPCs with increased circulation time had more opportunity to interact with T cells, this shape ultimately led to increased T cell proliferation compared to spherical aAPCs.[322] Further analysis of aAPC properties revealed that the degree of stretching influenced the extent of T cell proliferation, with optimal stimulation occurring when aAPCs were stretched 2-2.5 fold, relative to the original diameter.[41, 322] One possible reason for this difference is that the ellipsoidal aAPCs allowed increased contact length with T cells, supporting increased numbers of surface-to-surface interactions.[41] Ultimately, treatment with ellipsoidal aAPCs displaying cancer antigens, in conjunction with a common cancer immunotherapy, reduced

tumor burden and increased survival.[323] The examples in this section demonstrate that micro- and nano-scale shape changes can significantly alter the interactions with immune cells, promoting either a pro-inflammatory or pro-regenerative niche. These phenomena need to be further explored with tissue engineering constructs which exhibiting complex conformations, commonly employed to recapitulate the natural tissue the implant is replacing while allowing for multiple contact points with the cellular environment.

8.3.3 Biomaterial Surface Features and Chemical Functionality Impact Immune Recognition

As alluded to in section above, upon injection or implantation, surface features (e.g., roughness) and specific chemical moieties or properties can impact both the extent of interactions with immune cells and the immunogenicity.[124-126, 128, 324] An important aspect along these lines is the role hydrophobicity plays in intrinsic immunogenicity.[120, 123] The immune system has evolved to recognize molecules with highly hydrophobic portions as foreign, potentially-dangerous materials (see **Chapter 8.2**). This property can thus trigger PRRs, leading to elimination.[123] In one study, gold nanoparticles functionalized with increasingly hydrophobic chemical groups (**Figure 8.3A**) were incubated with immune cells isolated from the spleens of mice.[120] Particles with greater hydrophobicity increased gene expression of pro-inflammatory cytokines (e.g., TNF-α, IFN-γ) and similar effects were observed after intravenous injection in mice (**Figure 8.3B**).[120] To combat the immunogenic effects of hydrophobic surfaces, hydrophilic molecules such as polyethylene oxide

(PEO) and polyethylene glycol (PEG) are often added to delivery vehicles and tissue engineering scaffolds to increase hydrophilicity and reduce surface protein absorption.[325-327] This increased hydrophilicity and resistance to protein absorption can also lead to decreased interactions with immune cells, which might reduce immunomodulatory responses.[325-327] While diminishing interactions with immune cells could be beneficial in combating undesirable, pro-inflammatory responses, future approaches could leverage changes in surface chemistry to bias immune response toward natural healing responses to injury.

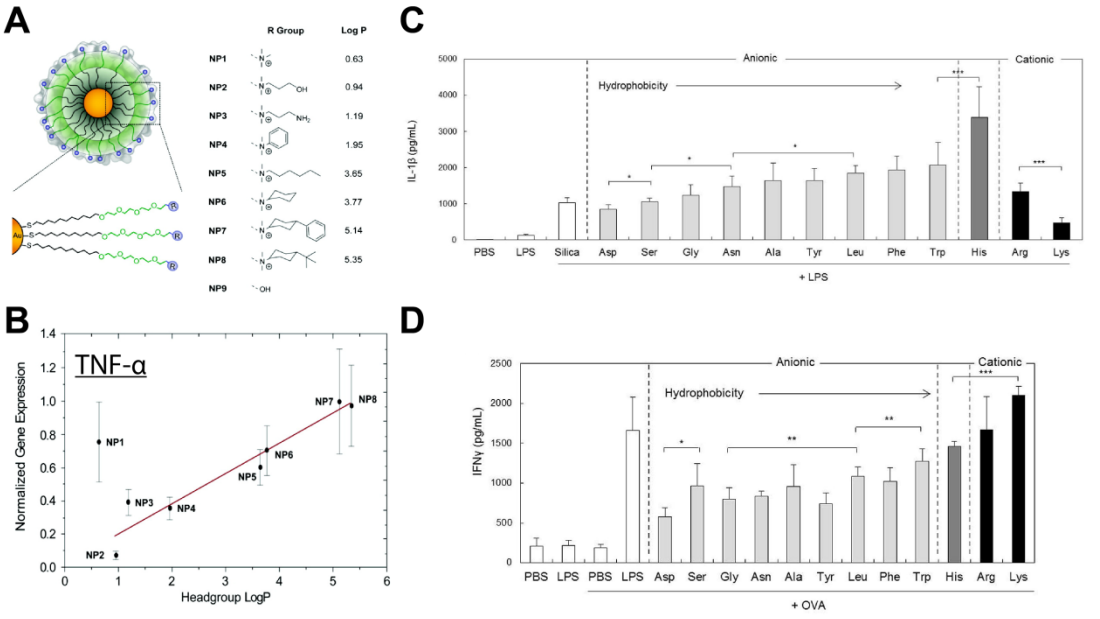

Figure 8.3: Surface chemistry of particulate systems impacts immunogenicity.
(A) Gold nanoparticles are functionalized with different chemical ('R') groups to exhibit varied hydrophobicity, denoted as 'Log P'. (B) Immune cells isolated from mouse spleens were treated with these particles and revealed a correlation between increased hydrophobicity and elevated gene expression of pro-inflammatory cytokines (TNF-α). (C) Silica particles functionalized with different polypeptides with defined charges and levels of hydrophobicity increase the IL-1β response to treatment with an immune stimulant (LPS). Increasingly hydrophobic surface chemistries promote increased IL-1β secretion. (D) When these silica particles were treated in conjunction with a model antigen (OVA), particle immunogenicity increased T cell production of pro-inflammatory IFN-γ, with cationic particles inducing the highest levels. (A-B) Adapted with permission from ref [120]. Copyright 2012 American Chemical Society. (C-D) Reprinted from ref [328] with permission from Elsevier.

The surface charge of a biomaterial also plays an important role in modulating immune function.[118, 119, 317, 329] For example, using the same gold nanorod platform discussed in above,[317] surface charge of the nanoconstructs was found to impact immunogenicity, in addition to size and shape. Nanorods altered the inflammatory profile of macrophages, as indicated by changes in gene expression and surface activation markers, depending on the exposed functional groups.[317] Amine-terminated nanorods exhibiting a positive surface charge shifted macrophages to an anti-inflammatory M2 phenotype, while carboxylic acid-terminated nanorods with a negative surface charge induced an inflammatory M1 phenotype.[317] Interestingly, other studies have revealed particles with positively charged surfaces lead to activation of the inflammasome at greater levels than negatively charged particles.[119] Further, other work has shown particles with a negative surface charge can actually block or inhibit immune function.[99, 329] In one such study, particles synthesized from carboxylated PLGA, polystyrene, or microdiamonds, all exhibiting negative surface charges, were able to suppress inflammatory macrophages.[99] These cells were the drivers of various mouse models of disease, including West Nile Virus brain infection, kidney injury, colitis, multiple sclerosis, and cardiac infarction. In each case, suppression was achieved following treatment with negatively charged particles by shifting macrophage accumulation from sites of disease to the spleen, where apoptosis of these cells occurred, leading to reduced inflammatory responses and promoting regulatory T cell phenotypes.[99] As discussed directly in the coming sections, the studies already presented reveal one of main challenges to understand

intrinsic immunogenicity, the difficulty in decoupling related properties such as hydrophobicity and chemical functionality.

Several studies have focused directly on the role of chemical functionality presented on surfaces to decipher how immune response is altered.[328, 330, 331] For instance, peptides synthesized with either an L or D stereochemistry have been linked to a model antigen (ovalbumin, OVA) and used to vaccinate mice.[330] The D stereochemistry, which is less susceptible to enzymatic degradation, led to stronger antibody responses and prolonged antigen presentation compared to the L stereotype.[330] Additionally, it was determined that when macrophages were treated with particles that contained either oxidized, reduced, or native protein antigens, the particles with native or reduced antigen were preferentially taken up *in vitro*, and promoted strong immune responses in mice.[331] The Fahmy Lab has used silica particles as a platform to understand how surface modification with polypeptides exhibiting different hydrophobicities and charges influence inflammasome signaling and DC activation *in vitro*.[328] As expected based on the discussion above, these studies determined inflammasome activation was size dependent.[328] Interestingly, however, investigation into how the surface chemistry of 300nm particles impacted IL-1β secretion revealed that particles functionalized with amino acids of increasing hydrophobicity drove increasing IL-1β secretion (**Figure 8.3C**).[328] Anionic particles caused the highest levels of activation, while cationic particles, shown above to activate pro-inflammatory responses, induced lower levels of IL-1β in this case. These differences were found to result from endocytic uptake and lysosomal rupture,

a result supported by a reduction in IL-1β secretion when uptake was chemically inhibited.[328] When cells were treated with these particles mixed with OVA, cationic particles caused increased IFN-γ production by T cells. Additionally, these elevated expression levels correlated to increasing particle hydrophobicity (**Figure 8.3D**).[328] Since the balance of M1 and M2 macrophages play a major role in many tissues engineering applications, the studies in this section highlight opportunities to modulate immune cell phenotypes by altering the hydrophobicity, charge, or surface chemical functional groups of materials used to fabricate tissue engineering constructs. Two common, naturally derived biomaterials, alginate and hyaluronic acid, are highly studied as scaffold materials and both exhibit negatively charged surfaces. The studies above have revealed that a negatively charged surface could either halt or promote immune responses. These differences highlight the need for more detailed studies to elucidate how hyaluronic acid, alginate, or other materials can be formulated to leverage surface charge in supporting regenerative outcomes.

8.3.4 Molecular Weight and Extent of Material Degradation Impact Immunogenicity

Many drug delivery and tissue engineering approaches employ biodegradable materials as vehicles or scaffold to deliver signals to target cells or tissues over time. However, most of the studies investigating the intrinsic immunogenicity of materials have focused on a single snapshot in time or at stage of degradation. Thus, there is a strong need to understand how the immunogenicity of materials change over time as degradation progresses, material properties change, and byproducts are formed.

Early research investigating how the degradation of biomaterials influenced immunogenicity centered on hyaluronic acid, an extracellular matrix glycosaminoglycan.[107, 111-113] In this work, hyaluronic acid was enzymatically degraded to form fragments of varying molecular weight, then incubated with DCs or in DC and T cell co-cultures. These experiments revealed low molecular weight hyaluronic acid (1500-5300 Da) increased DC activation, inflammatory cytokine secretion, and T cell proliferation by triggering TLR-2 and TLR-4 signaling.[107, 111-113] Subsequent research has studied how macrophage differentiation is impacted by hyaluronic acid fragments with different molecular weights.[114, 332] In these studies, macrophages were polarized to an M1 phenotype by low molecular weight hyaluronic acid, while high molecular weight hyaluronic acid induced a M2 phenotype, preferred for tissue repair and healing.[114, 332]

Our lab has investigated how the immunogenicity of synthetic polymers evolves as degradation progresses. Poly(beta amino esters) (PBAEs) provide an ideal system to address this question since these polymers are rapidly degradable and can be readily synthesized with different functionalities in a high-throughput manner.[129, 163, 333, 334] In one study investigating the effect of PBAE formulation and degradation on immunogenicity, PBAEs were formulated via Michael-addition reactions between a diamine and one of three diacrylate monomers differing in the number of carbons in the polymer backbone (e.g., 4, 6, 10 carbons) (**Figure 8.4A**). These reactions resulted in polymers with varied starting molecular weight but similar degradation profiles (**Figure 8.4B**).[334] These PBAEs (PBAE-4, PBAE-6, and PBAE-10) were degraded

for defined times to form distinct molecular weight ranges, then incubated with DCs in either a soluble or particulate form. In soluble form, none of the PBAE formulations activated DCs.[334] However, when condensed into a particulate form, PBAEs activated DCs in a molecular weight specific manner. PBAE-4 particles activated DCs at molecular weights corresponding to early stages of degradation (less degradation time). Meanwhile, PBAE-6 particles activated DCs after intermediate degradation times and PBAE-10 showed little to no immunomodulatory activity, with minimal activation occurring only after long degradation times.[334] Together, these results indicated that irrespective of degradation stage, the greatest activation levels were induced by particles formed from PBAEs fragments with molecular weights between 1500-3000Da (**Figure 8.4C**).[334] When DCs were treated with particles in the presence of an antigen, then co-cultured with T cells, both antigen presentation and T cell proliferation increased significantly.[163] Similarly, when injected into lymph nodes of mice using a new technique to control the dose and combination of signals,[13, 14, 163] immunogenic PBAE particles (‘Particle’) activated lymph node resident innate immune cells compared to a sham injection (‘Vehicle’), or an injection of soluble PBAEs (‘Free’) (**Figure 8.4D**).[163] These studies highlight the fact that materials may be non-immunogenic or pro-inflammatory at one time point, but as the material degrades, the physicochemical properties can change in ways that alter the immunogenicity. Analogous experiments are still necessary with other common polymers (e.g., PLGA) or extracellular matrix components (e.g., collagen, hyaluronic acid, fibronectin) that cause differential immune responses as the scaffold degrades or is reabsorbed after implantation. In the case of these bioresorbable scaffolds, it would

be advantageous to choose a material whose immunogenic profile promotes a natural wound healing response, with the implanted construct first promoting inflammation and immune cell recruitment then, as the material degrades, shifting towards a regenerative microenvironment.

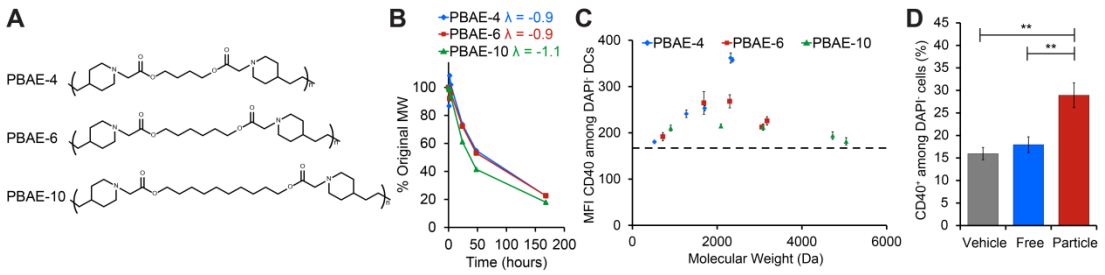

Figure 8.4: Polymer degradation and molecular weight influence DC activation in cell culture and mice.
(A) PBAEs formulated with 4 (PBAE-4, blue), 6 (PBAE-6, red), or 10 (PBAE-10, green) carbons in the diacrylate monomer backbone were synthesized with (B) different starting molecular weights, but similar degradation profiles. (C) PBAEs were degraded to distinct molecular weight ranges, formulated into particles, and used to treat DCs. Maximum activation, as indicated by CD40 expression on live ($DAPI^-$) DCs, correlated with a molecular weight range of 1500-3000Da. (D) After introduction into mice, immunogenic PBAE particles (red) induced statistically significant activation of lymph node resident immune cells compared to treatment with soluble (blue, 'Free') or buffer control (gray, 'Vehicle') treatments. (A-C) adapted with permission from ref [334]. (D) reprinted with permission from ref [163].

With the growing understanding of the intrinsic immunogenicity of materials, an important concept is the interconnected nature of these properties. For instance, changing the shape of a particle by stretching may also change the size.[41, 322] Similarly changing a functional group on the surface of a material may also change the surface charge and hydrophobicity; any of these variations might change the immune signatures of the materials.[328] Therefore, one goal of future research should be to understand the relative contributions of properties or sets of properties to modulate immune function. An alternate strategy to understanding these interactions, is to mimic the attractive features of synthetic materials, but eliminate carriers completely by self-assembling immune signals into nanostructures.[159-161, 335-

340] However, all of these strategies share the same goal, to design materials – whether natural or synthetic – that better control immune function.

8.4 Tissue Engineering Constructs Exhibit Intrinsic Immunogenicity

Classical tissue engineering approaches generally consist of scaffolds incorporating signals or cells that upon implantation, induce proliferation of the encapsulated cells, alter the phenotype of native cells infiltrating the implant, or promote changes in tissue growth and function. Mesenchymal stem cells are an immunomodulatory cell type that has been particularly important in this area to enhance responses to tissue engineering constructs.[341-346] These cells have the ability to differentiate into a number of cell lineages, making them attractive in tissue engineering and regenerative medicine approaches aimed at a range of tissue types.[341-344] Additionally, mesenchymal stem cells have the ability to interact with innate and adaptive immune cells, for instance, by secreting immune suppressive molecules such as prostaglandin E_2.[341-344] Integration of chemical signals, growth factors, and cytokines into scaffolds is another important component widely explored in the field.[25, 302, 305, 306] While these cells and signals incorporated in scaffolds and implants are being intensely studied, there is a gap in the understanding of how intrinsic immunogenicity of materials might be exploited to help tune and improve outcomes in tissue engineering. Building on the discussion above of what has been learned about inherent immunogenicity from the vaccine and immunotherapy area, this section will focus on how the physicochemical properties of common tissue engineering materials and extracellular matrix components can modulate immunological responses.

8.4.1 Macrophage Responses to Injury are Influenced by the Presence of Acellular Biomaterial Scaffolds

Most tissue engineering approaches involve implants made from metallic, ceramic, or composite materials, or scaffolds comprised of synthetic materials, decellularized constructs, or extracellular matrix components.[283] These structures must be able to overcome immunological rejection, a process resulting from recognition by innate and adaptive immune cells.[25, 292] As explained in **Chapter 8.2**, macrophages play a large role in tissue repair with a balance of M1 and M2 phenotypes needed to promote proper healing. Interestingly, new studies show that the activation state of macrophages at the time of encounter with a biomaterial impact the uptake of the biomaterial and subsequent macrophage activation.[347] For example, in the case of an injury where the wound is too large for conventional wound healing to occur, recovery would generally result in scar tissue formation. To test if addition of an acellular biomaterial scaffold could reduce adverse effects and promote proper healing, one recent report fabricated a scaffold by isolating extra cellular matrix components from a portion of the small intestine. This scaffold was then implanted at the injury site.[348] In this study, the macrophage response to an untreated injury resulted in a pro-inflammatory M1 phenotype, while implantation of the scaffold shifted this response to the M2 phenotype.[348] This example highlights how just the presence of a biomaterial at an injury site can shift the immune response to promote tissue repair, motivating research to tease out the mechanisms that modulate immune function to promote healing.

8.4.2 Scaffold Composition Alters Interactions with the Immune System

There are a variety of biomaterials that can be used as tissue engineering constructs. Early research from the Babensee Lab highlights how DCs incubated on thin films of naturally occurring or synthetic materials - including PLGA, chitosan, alginate, hyaluronic acid, and agarose - cause differences in DC activation, cytokine production, and T cell proliferation.[109, 125, 157] Based on these findings, recent studies have directly explored how materials commonly used in tissue engineering impact innate immune cells. In one study, extracellular matrix scaffolds were derived from diverse tissue sources including matrices from small intestine submucosa (SIS), urinary bladder (UBM), skeletal muscle (mECM), brain (bECM), esophagus (eECM), skin (dECM), liver (LECM), and colon (coECM) and enzymatically solubilized with pepsin.[349] These solubilized extracellular matrix scaffolds were then used to treat macrophages. The level of M1 and M2 phenotype were determined by assessing iNOS and Fizz1 expression as markers for the M1 and M2 phenotypes, respectively.[349] SIS, bECM, eECM, and coECM treatments induced an M2 phenotype at levels comparable to macrophages treated with a positive control signal (IL-4) used to promote M2 differentiation (**Figure 8.5A**).[349] In contrast, dECM treatment promoted a shift toward M1, with heightened iNOS expression on the macrophages stained with a classical macrophage marker, F480 (**Figure 8.5A**).[349] Further investigation of macrophage lysates following treatment revealed SIS, UBM, bECM, and coECM solubilized ECM scaffolds caused decreased iNOS expression, while SIS, UBM, eECM, coECM increased CD206 expression; CD206 is another marker for the M2 macrophage phenotype (**Figure 8.5B**). These results confirmed a

wound healing phenotype could be induced, and emphasizes that the selection of the tissue from which a scaffold is derived from can significantly bias immune function to improve scaffold performance.[349]

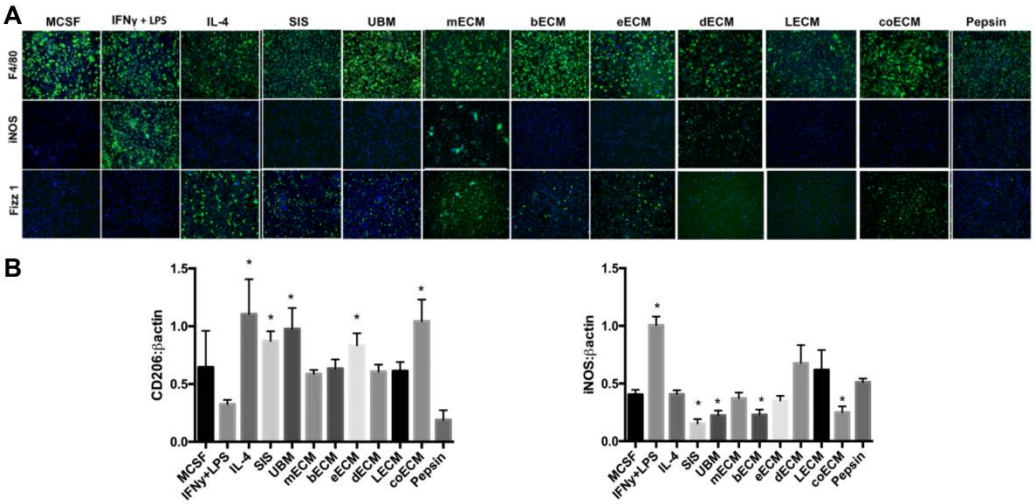

Figure 8.5: Scaffolds derived from extracellular matrix components of specific tissues polarize macrophage function.
(A) Macrophages (stained with F4/80) and treated for 18 hours with control cytokines (MCSF, IFN-γ + LPS, IL-4) or solubilized extracellular matrix scaffolds cause differential expression of markers for the pro-inflammatory M1 macrophage phenotype (iNOS) and the wound-healing M2 macrophage (Fizz1). Solubilized scaffolds were produced via pepsin incubation of small intestine submucosa (SIS), urinary bladder (UBM), skeletal muscle (mECM), brain (bECM), esophagus (eECM), skin (dECM), liver (LECM), or colon (coECM) extracellular matrix components. MCSF was used as a negative control for macrophages while pepsin was a control for ECM solubilization, IFN-γ + LPS was a positive control for M1 macrophages, and IL-4 was a positive control for M2 macrophages. (B) Treatment with matrices also induces varied levels of M2 associated (CD206) and M1 associated (iNOS) proteins in macrophage lysates. Adapted with permission from ref [349].

While the studies above used scaffold prepared directly from complex tissues, other recent studies are investigating constructs formed from specific biological molecules or synthetic materials.[350-354] One such molecule is collagen, a protein abundant in the extracellular matrix that has been widely explored as a scaffold component.[355] During recent studies in mice, a collagen scaffold with silica integrated between the collagen fibers activated monocytes. These cells have the ability to differentiate into macrophages. Compared to sham surgeries, the scaffolds with silica promoted new

bone and blood vessel formation.[350] The authors hypothesized this response resulted from increased IL-4 detected in serum one week after implantation; IL-4 has previously been shown to induce wound healing phenotypes.[350] Fibrin and fibrinogen have also been frequently used for tissues engineering applications; both of these proteins play a crucial role in the formation of blood clots during normal response to injury.[25, 283-285] One study investigating the effect of fibrin and fibrinogen found that thin films of fibrin promoted macrophage secretion of anti-inflammatory IL-10, and were able to reverse the secretion of inflammatory cytokines (e.g., IFN-γ) from macrophages stimulated with a TLR4 agonist.[351] In contrast, soluble fibrinogen increased the pro-inflammatory cytokine, TNF-α. Interestingly, when macrophages were co-treated with both fibrin films and soluble fibrinogen, fibrin played a dominate role, resulting in an anti-inflammatory response.[351] In a separate study, fibrinogen was prepared as a porous scaffold and the immunomodulatory effects on immune cells were investigated during a bone injury model. After implantation in mice, the fibrinogen scaffold outperformed sham implantations, promoting bone regrowth. These improvements were correlated with altered cytokine gene expression and changes in both the local and systemic immune cell responses.[352] Similarly, other studies have investigated synthetic ceramic materials. These studies have revealed that treatment with a clinical standard for ceramic implants (tricalcium phosphate–hydroxyapatite) promotes an M1 macrophage phenotype.[353] Alternatively, treatment with scaffolds formed from newer ceramic materials (e.g., baghdadite and strontium–hardystonite–gahnite) induced greater expression of markers indicative of M2 macrophage

phenotypes.[353] Lastly, synthetic polymers have also played a large role as scaffold materials. One recent example demonstrates that nondegradable polypropylene meshes induced M1 macrophages, while meshes coated with dermis or urinary bladder extracellular matrix components promote M2 macrophages.[354] After implantation in rats, the meshes coated with extracellular matrix components also decreased the number of foreign body cells, a signal that a fibrous capsule would not form around the implant.[354] These studies highlight how even with commonly used polymers or extracellular matrix components, dramatically different responses are possible because of differences in interactions with immune cells. However, further studies are needed to ascertain which properties of the scaffold are ultimately responsible for the immunogenic responses. With continued investigation into the chemical and biological differences between these ECM matrices and synthetic scaffolds, one could identify the key signals needed to shift the immune response towards a wound healing phenotype. After ascertaining which cues are important, future tissue engineering constructs could be designed with either synthetic materials supplemented with the pro-regenerative signals or from a subset of the tissue ECM scaffolds that only contains the desired signals. This approach would allow for the fine tuning of the immune system response to the implanted biomaterial and promote tissue regeneration and wound healing.

8.4.3 Physicochemical Properties of Tissue Engineering Constructs Also Alter Intrinsic Immunogenicity

As with particle based delivery systems, the physicochemical properties of materials used in scaffolds can dramatically impact the interactions with the immune system. While this vein of research has garnered interest for particulate systems (see **Chapter 8.3**), interest in the tissue engineering field is just arising over the past few years. New studies are investigating how shape, composition, and charge of tissue engineering constructs impact the immune response.[356-361] For example, polymeric scaffolds have been synthesized by electrospinning polycaprolactone, then the resulting fibers were modified to exhibit different shapes.[356] Scaffolds were then formed from either the random or aligned fibers. Afterward, these scaffolds were left unmodified or expanded to exhibit macro-scale thicknesses of 3mm or 10mm.[356] Following subcutaneous implantation into rats, macrophages were able to infiltrate into scaffolds formed from randomly aligned fibers with expanded thickness of 3mm or 10mm. However, scaffolds formed from aligned fibers that were expanded to 3mm supported greater macrophage penetration and the smallest number of giant cells, a trait the authors attributed to the gap distance between the aligned fibers.[356] In a similar study, scaffolds with varying pore sizes were formed from electrospun polydioxanone. These experiments revealed a correlation between increased pore size and a shift towards M2 function and away from M1 macrophages.[357] An ongoing question in the tissue engineering field centers on the balance between the porosity of scaffolds and the mechanical properties required for the implant. As shown above, with increased porosity and an expanded conformation,

tissue engineering constructs can promote pro-regenerative environments by altering macrophage function. However, this change in scaffold structure may negatively influence mechanical strength and, in the case of tissue-mimicking implants for structural components (e.g., bone), the mechanical strength of the scaffold needs to recapitulate that of the native tissue. Thus, while scaffold shape and porosity can be exploited to promote inflammation or repair by modulating macrophage phenotype and limiting fibrosis (i.e., reducing the number of foreign body cells), there is also a need to better understand the interplay between these immunological outcomes and material properties.[356, 357]

Another new avenue of research has focused on the chemical composition of scaffolds and how this influences the functions of DCs and macrophages. One study showed that calcium alginate gels promote inflammatory responses in cells and in mice by releasing calcium, a signal that increased DC activation and IL-1β secretion.[358] This work revealed the intrinsic immune function stemmed from the calcium, as gels formed with barium instead of calcium led to reduced scaffold immunogenicity.[358] Since alginate hydrogels are commonly used for tissue engineering constructs and generally use calcium as the divalent ion for crosslinking, this discovery provides evidence that even the choice of molecule for cross linking could impact the resulting immune response and thus inform which divalent molecules should be used for crosslinking hydrogels. Experiments with hyaluronic acid formed into films via electrostatic interactions with poly-L-lysine caused monocytes to secrete pro-inflammatory cytokines (e.g., IL-1β, TNF-α).[359]

Interestingly, after crosslinking the hyaluronic acid with aldehyde, there was a reduction in TNF-α and IL-1β secretion and slight increases in anti-inflammatory cytokines.[359] This result is in agreement with the studies discussed in above relating to molecular weight, revealing increased activation from low molecular weight hyaluronic acid fragments; these particles might be generated as non-crosslinked scaffolds begin to degrade. However, using crosslinking, the rate of degradation and the production of low molecular weight hyaluronic acid fragments generated via degradation could be slowed. This reduction decreased the overall level of pro-inflammatory molecules. Other work investigated how the charge of hydrogel scaffolds impacts immunogenicity by evading foreign-body reactions.[360] In this study, zwitterionic poly(carboxybetaine methacrylate) hydrogels prepared from a carboxybetaine monomer and a carboxybetaine cross-linker shifted macrophage phenotype to an anti-inflammatory state compared to samples treated with poly(2-hydroxyethyl methacrylate) hydrogels, a commonly used molecule similar to PEG that reduces protein absorption.[360] Thus, the hydrogels were able to diminished macrophage activation in mice by reducing the underlying protein adsorption to the scaffold after implantation.[360] This feature could be beneficial for future implanted biomaterial scaffolds designed to limit fibrotic buildup and implant rejection. Together, the results from this section suggest that the material with which a hydrogel is formed, the extent of crosslinking, and the molecule used for crosslinking can all impact the immunogenicity of the scaffold. Similar to the discussion above, there is an ongoing need to understand the interplay between these properties. For instance, if a hydrogel is formed from a material that is immunostimulatory as it degrades,

crosslinking of this scaffold with calcium may result in reduced immunogenicity by reducing the degradation but could also cause a local increase in pro-inflammatory cytokines. Therefore, it will be crucial for future tissue engineering approaches to understand which properties of hydrogels are the main drivers of this intrinsic immunogenicity.

In an elegant study by Christo *et al*., complex surface nanotopography and chemical composition commonly seen in tissue engineering constructs were mimicked to test the impact on the response of innate immune cells.[361] Glass cover slips were coated with gold nanoparticles exhibiting varying diameters. These materials were then modified by deposition of allylamine, (AA), octadiene (OD), or acrylic acid (AC) to create surfaces abundant in either amino, alkyl, or carboxylic acid groups, respectively (**Figure 8.6A**).[361] Because the surfaces were formed with nanoparticles of varying diameters, these constructs mimicked scaffolds with either smooth surfaces or exhibited tunable degrees of surface roughness (**Figure 8.6B**).[361] When neutrophils were incubated with the surfaces, rough and, in particular, acidic surfaces increased section of MMP-9, a protein involved in extracellular matrix degradation.[361] Additionally, when incubated with macrophages, these surfaces caused differential effects on the secretion of pro-inflammatory cytokines. The rough, acidic surfaces again shifted the environment away from inflammation by decreasing the secretion of pro-inflammatory cytokines TNF-α, IL-6, and IL-1β (**Figure 8.6C)**.[361] This type of experiment, where multiple parameters are systematically investigated, could inform the rational design of future

scaffolds fabricated with physicochemical properties that can modulate the immune response between inflammation and tissue repair.

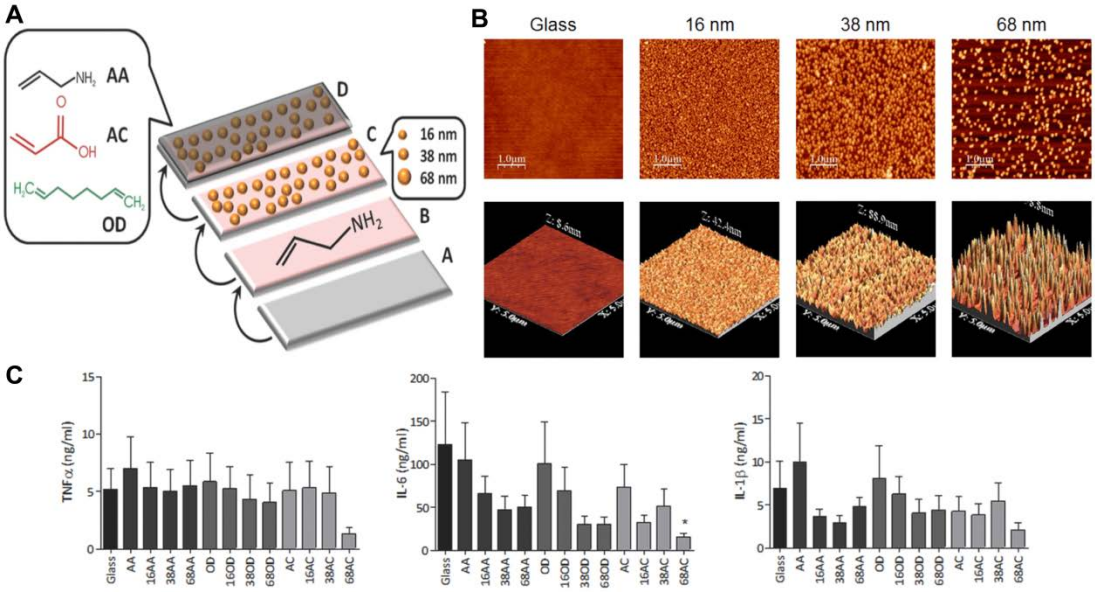

Figure 8.6: Implant surface morphology and chemical composition induces innate cell activation and cytokine secretion.
(A) Schematic depiction of glass cover slips coated with gold nanoparticles, then functionalized with allylamine (AA), octadiene (OD), or acrylic acid (AC) to form biomimetic surfaces abundant in amino, alkyl, or carboxylic acid groups, respectively. (B) Atomic force micrographs showing 2-D (top) and 3-D (bottom) surfaces with different roughness due to the different particles diameters. (Top scale bar, 1µm; lower scale 5µm x 5 µm). (C) Macrophages cultured on these surfaces exhibited different secretion levels of pro-inflammatory cytokines TNF-α (left), IL-6 (center), and IL-1β (right); cells cultures on the roughest surfaces (prepared with 68nm particles) reduced inflammatory cytokine secretion. Reprinted with permission from ref [361].

8.5 New Technologies and Analysis Methods will Exploit Intrinsic Immunogenicity to Advance Tissue Engineering Capabilities

Recent studies in tissue engineering investigating the impact of material properties on immune activation have yet to fully elucidate the mechanism through which this activation occurs. Future research endeavors will need to incorporate more experimental parameters and higher, more complex animal models to determine the biomaterial features that contribute the most to immunogenicity. In one such study

from the Langer and Anderson labs, mouse, rat, and non-human primate models were used to investigate how the size and shape of various biomaterial implants fabricated from ceramics, hydrogels, metals, and plastics activated innate cells and led to fibrosis.[116] First, alginate particles were prepared with sizes from 0.3mm to 1.9mm, then implanted in mice.[116] Following implant retrieval after two weeks, particles size was inversely correlated with expression of genes involved in fibrosis: α-SMA (**Figure 8.7A**, left), collagen 1a1(**Figure 8.7A**, center), and collagen 1a2 (**Figure 8.7A**, right).[116] After determining that size impacted the foreign body response to alginate, the authors compared the response to different biomaterials exhibiting similar sizes. Particles with a diameter of 0.5mm were formulated from alginate, stainless steel, glass, polycaprolactone, or polystyrene, then implanted intraperitoneally in mice. The implants were removed after 14 days, and all resulted in fibrotic growth (**Figure 8.7B**, top).[116] Interestingly, particles fabricated from the same materials but with larger diameters (1.5-2mm) reduced fibrotic tissue formation (**Figure 8.7B**, bottom), a phenomena attributed to reduced infiltration of macrophages and neutrophils at the implant site.[116] Further investigation with alginate particles of medium (0.5mm) and large (1.5mm) sizes implanted into non-human primates resulted in similar findings.[116] After implantation of both medium (0.5mm) and large (1.5mm) particles into mice, the number of neutrophils and macrophages on the excised particle as well as macrophage phenotype was determined at various times post-implantation (e.g., day 1, 4, 7).[116] Larger particles caused a shift towards immune regulatory and wound healing macrophage phenotypes, while medium particles biased responses toward inflammatory phenotypes.[116] In another study

from the Anderson lab, the mechanism through which fibrosis occurred after implantation of alginate spheres was determined.[362] This study incorporated both mouse and primate models to study the response to the implanted particles. While implantation of alginate spheres increased the macrophage, neutrophil, and B cell responses to the implants, macrophages and not neutrophils were determined to be the main cell type that drives fibrosis.[362] Using knock out mice for neutrophils, macrophages, and B cells, it was determined that macrophages were essential for the formation of fibrosis on the alginate spheres and lead to B cell recruit which further promoted fibrosis.[362] High throughput gene expression analysis revealed colony stimulating factor-1 receptor was ultimately the driving mechanism for fibrosis in response and direct inhibition of this receptor was able to control fibrosis without the complete depletion of macrophage function.[362] These studies highlight the utility of using multiple animal models and emerging technologies to determine how specific physicochemical properties influence immune responses to tissue engineering constructs. Such approaches could provide a generalizable framework for other materials and questions.

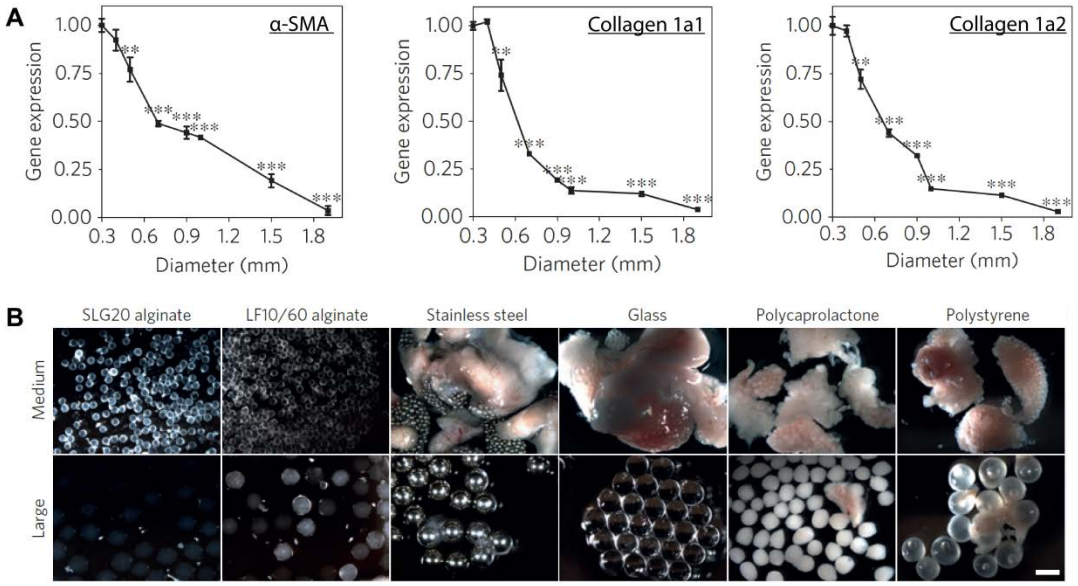

Figure 8.7: Implanted materials with distinct sizes and compositions alter fibrotic capsule formation.
(A) Following implantation of alginate spheres of different sizes the peritoneum of mice, gene expression profiles of the pro-fibrotic markers α-SMA (left), collagen 1a1 (center), and collagen 1a2 (right) revealed larger particles reduced fibrotic build-up. (B) Images revealing the level of fibrosis for particles with diameters of 0.5mm (medium) or 1.5-2mm (large) prepared from alginate, stainless steel, glass, polycaprolactone, or polystyrene. For all materials, large particles were associated with reduced fibrosis 14 days after implantation. (Scale bar, 2mm). Adapted with permission from Macmillan Publisher Ltd: *Nature Materials* from ref [116], copyright 2015.

Other recent research has focused not just on innate immunity, but on the role of implanted materials in modulating adaptive immunity. In a study by the Elisseeff and Pardoll labs, scaffolds were derived from bone (B-ECM) and cardiac muscle (C-ECM) extracellular matrix components, then used to treat critical muscle injuries in mice.[363] The response to these scaffolds was compared to collagen scaffolds and saline treatments to study the underlying immune mechanisms.[363] In a normal immune response to a pathogen, APCs such as macrophages and DCs present antigen to naïve, $CD3^+$ T cells which then proliferate and, depending on the signals also delivered to the T cell, differentiate into various T cell subsets.[25] These subsets consist of cytotoxic $CD8^+$ T cells that kill infected host cells and $CD4^+$ T cells that

include T helper 1 (T_H1) cells which assist in M1 macrophage activation, T helper 2 (T_H2) cells that promote M2 macrophage activation, and T_H17 T cells which cause inflammation through activation of neutrophils.[25] In wild type mice, treatment with collagen, B-ECM, and C-ECM scaffolds increased $CD4^+$ T cells and the expression of IL-4 genes, an important cytokine for T_H2 cell differentiation and tissue repair via M2 macrophages.[363] Supporting this finding, transcriptome analysis of genetic material from $CD3^+$ T cells one week after treatment with the biomaterial scaffolds revealed increased messenger RNA that drives development of T_H2 responses (**Figure 8.8A**).[363] When repeating these treatments in $Rag1^{-/-}$ mice, which are deficient in mature B and T cells, IL-4 gene expression was decreased to levels comparable to saline treatments, further supporting the hypothesis that T cells were responsible for IL-4 production.[363] Additional studies showed the increase in IL-4 expression was present in both the draining (e.g., inguinal) and distal lymph nodes (e.g., axillary, brachial) (**Figure 8.8B**), indicating local changes to immune function can lead to systemic responses.[363] When mice deficient in $CD4^+$ T cells were used, this response was diminished, though not as low as measured when both B and T cells were knocked out in $Rag1^{-/-}$ mice (**Figure 8.8B**).[363] These results suggest T_H2 cells play a critical role in wound healing and creating a regenerative microenvironment, while other adaptive immune cells (e.g., $CD8^+$ T cells, B cells) may play a supporting role in these processes.[363] While the majority of research in tissue engineering has focused on the innate immune cells (e.g., macrophages) that play a major role in both regeneration and in scaffold failure, this study reveals the need for more work elucidating the role that adaptive immune cells play in promoting or inhibiting tissue

repair. Through a better understanding of how T cells support tissue regeneration or how antibodies produced by B cells impact a host reaction to implanted materials, future constructs could be designed with materials that control these pathways.

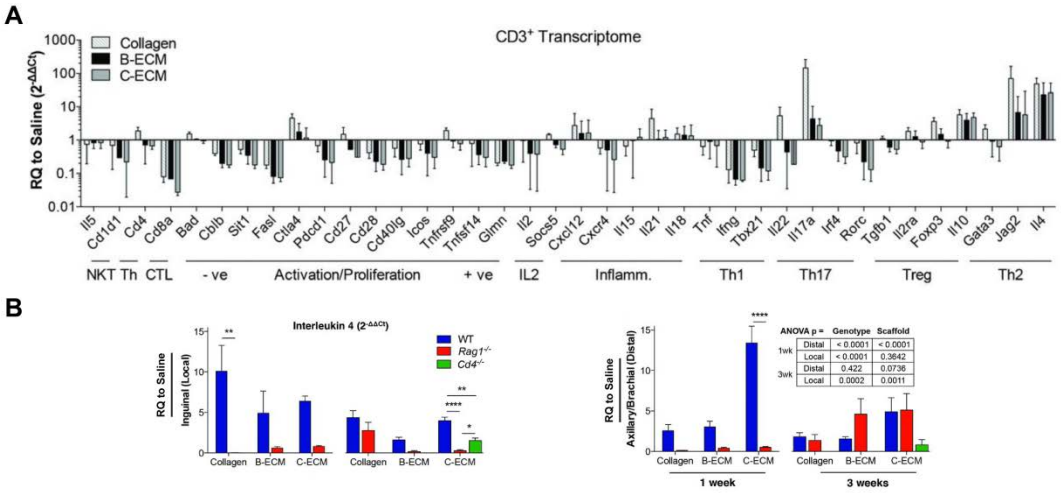

Figure 8.8: Adaptive immune cells play a role in the response to implanted scaffolds.
After inducing a critical muscle injury in mice, scaffolds derived from collagen, bone (B-ECM), or cardiac muscle extracellular matrix (C-ECM) were implanted. (A) $CD3^+$ T cell transcriptome analysis was used to evaluate the gene expression of markers for distinct immune cell populations and phenotypes compared to a sham saline surgery control, denoted as 'RQ to Saline'. Treatment with B-ECM and C-ECM scaffolds revealed an increase in T_H2-associated genes (e.g., Jag2, IL-4). (B) Treatment with scaffolds in wild-type mice (blue, 'WT') increased IL-4 gene expression in local (left) and distal lymph nodes (right) compared to saline treatments. When $CD4^+$ T cell-deficient mice (green, '$Cd4^{-/-}$'), or B and T cell-deficient mice (red, '$Rag1^{-/-}$') were treated with ECM scaffolds, IL-4 gene expression decreased. (A-B) from ref [363]. Reprinted with permission from AAAS.

As the field of tissue engineering and regenerative medicine progresses, novel biomaterials and scaffold preparation methods will motivate further studies to investigate the immunogenicity of these new materials. One exciting avenue of research is 3-D printing of tissue engineering constructs.[364-367] These new approaches allow for the synthesis of implants with precise shapes and architectures fabricated from a variety of materials. In a recent study from Kang *et al.*, biodegradable polymers and hydrogels encapsulating cells were printed together in human-scale and tissue shape-mimicking constructs.[368] This system allowed

mixing of polycaprolactone with hydrogels consisting of gelatin, fibrinogen, hyaluronic acid, and glycerol to create stable structures with various pore sizes.[368] Scaffolds prepared in this way supported high viability of implanted cells and promoted tissue reconstruction for a variety of tissues types, including bone, cartilage, and muscle.[368] While this research presents a new, flexible system to synthetically create biomaterial-based scaffolds, the researchers note that the host immune response to their new materials was not investigated.[368] This comment highlights some of the broader issues facing the field, in particular, that systematic studies will be important to fully understand the mechanisms through which the immune system is activated and interacts with these constructs during wound healing and regenerative processes.

8.6 Conclusion

The vaccine and immunotherapy fields have provided valuable insight into how materials properties impact immune responses. This work has already shown physicochemical features alter the immunogenicity of biomaterials and is helping to inform the design of better materials that actively drive immune response towards a desired outcome. The field of tissue engineering provides a rich avenue to explore some of these same concepts and opportunities. With new knowledge of how these physicochemical properties influence the response to implanted materials, greater flexibility will arise for controlling immune response by carefully designing or selecting the material properties of implants and scaffolds. To reach this goal, future studies should broaden *in vitro* research to understand how well-controlled, 3D

architecture might impact intrinsic immunogenicity, and utilize animal models where material constructs with systematically introduced property variations are studied. Conducting these studies in the absence, and in the presence, of other immunomodulatory factors will help reveal the interplay between material properties and the resulting local and systemic immune responses.

Chapter 9: Outlook and Future Directions

9.1 Outlook

The research conducted in this dissertation has revealed for the first time that poly(beta-amino esters) (PBAEs) exhibit intrinsic immunogenicity and that this phenomena is a function of polymer form (e.g., soluble versus particulate) and physicochemical properties (e.g. molecular weight, MW). Additionally, through the use of intra-lymph node (*i.LN.*) injection, this research revealed that the deposition of biomaterial carriers and immune cues into the lymph nodes (LNs) of mice alters the local microenvironment by increasing the number of innate immune cells, ultimately leading to increased local and systemic antigen-specific immunity and survival in melanoma cancer models. These developments also revealed a number of research avenues for future exploration. The key areas are outlined in the sections below.

9.2 Future studies exploring polymer intrinsic immunogenicity

As revealed in **Chapters 3-5**, PBAEs degraded to form low MW fragments and fabricated into particles exhibit properties that activate dendritic cells (DCs), promote antigen presentation, and cause T cell proliferation. These effects were also maintained in animals when introduced into mice via *i.LN.* injection. Since these *in vivo* studies were conducted with a single polymer formulation, at one extent of degradation, and activation was only measured at a single time point after injection,

future studies should explore PBAE immunogenicity in mice with more experimental groups and time points. For instance, each of the PBAEs synthesized in **Chapter 4** could be introduced into LNs of mice at various states of degradation (e.g., after 0, 1, 3, or 7 days of degradation), and the activation state of LN-resident DCs and macrophages could be quantified at multiple time points corresponding to initial cell uptake (e.g., 1, 2, or 4 hours after injection), innate cell activation (e.g., 8, 12, 24, or 48 hours after injection), or at the onset and height of the adaptive immune response (e.g., 3, 7, or 14 days after injection). These types of studies could elucidate how the immunogenicity of PBAEs shown in cell culture translates to mice and the persistence and phenotype of activation over time.

In the work conducted in **Chapters 3-5**, PBAEs were complexed with a model anion (poly(sodium 4-styrenesulfonate), SPS) via electrostatic condensation to mimic a common DNA vaccine delivery strategy. Ongoing research could be conducted with a control oligonucleotide or nucleic acids designed to be non-immunogenic. This choice would provide a better model for DNA delivery and could help to reduce any confounding, immunostimulatory effects from the SPS. Additionally, in a separate research arm, PBAEs could be complexed with known immunostimulatory nucleic acids such as TLRa (e.g., PolyIC, CpG, PolyU). In this type of study, PBAEs would act as both an additional immune stimulant and as a controlled release vehicle, providing an opportunity to tune the release of the other immunogenic cargos. These studies could be used to test complexes as potentially new adjuvants while also revealing any synergistic enhancements to treatments with the TLRas alone.

Supplementary studies to understand the intrinsic immunogenicity of polymers would benefit from the formulation of a library of polymers with varied degradation rates. This way, instead of just comparing chemical structure and starting MW, distinctly different degradation rates could be compared to determine the impact on immunogenicity. This could be accomplished by a variety of polymers (e.g., PBAEs, polycaprolactone, PLGA) or using the same polymer (e.g., PLGA) synthesized with varied monomer ratios. In a pilot study exploring this idea, the ability of PLGA and Poly1 particles to adjuvant the immune response to soluble antigen was explored. After confirming that the PLGA and Poly1 degraded at different rates (**Figure 9.1A**), microparticles were formed from each polymer using the double emulsion, solvent evaporation methods detailed above and treated with soluble antigen (OVA) via *i.LN.* injection. Next, the systemic response was quantified by measuring the frequency of antigen-specific T cells weekly and comparing the response to control treatments including untreated mice, mice treated with just the particles and no antigen, or treatment with antigen alone (**Figure 9.1B**). Interestingly, it can be seen that while soluble antigen elevates antigen specific cells seven days after treatment, treating with PLGA particles and OVA increases this response while treating with Poly1 particles does not. This response then further increases at Day 14 post treatment, possibly due to the immunogenicity of PLGA particles evolving as the materials begin to degrade. Continued research is needed to confirm these preliminary results, discern what polymer properties cause these differences, and reveal features maintained across different polymers that drive specific immunostimulatory effects.

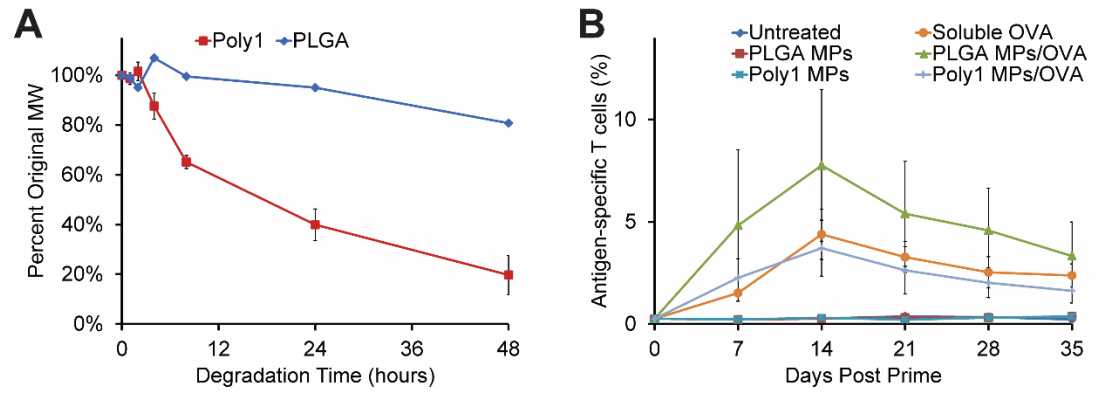

Figure 9.1: PLGA particles increase the antigen-specific response to soluble antigen treatment. (A) The degradation of Poly1 (red) and PLGA (blue) was quantified via gel permeation chromatography. (B) After treating mice via *i.LN.* injection, the antigen-specific T cell response in blood was quantified.

Additional future studies should also be conducted to understand the mechanism of action for DC activation in response to polymer treatment. These studies could use assays including TLR reporter cell lines that respond only to activation of particular TLRs or knockout mice that lack the machinery for specific signaling pathways (e.g., inflammasome or TLR). By fluorescently tagging polymers, degradation products could be tracked in cells and mice to also help determine the mechanism of activation and with which cells and organelles these polymer products are interacting with. For example, after systemic injections, it would be important to understand with which immune tissues the treatments are interacting. Additionally, on a cellular level, it would be important to ascertain whether the materials remain extracellular where certain immune receptors could be activated, or if vaccines are able to enter the intracellular space where other pathways could be engaged.

9.3 Continued research for engineering the local LN microenvironment

The work in **Chapters 5 and 6** provides clear evidence that deposition of biomaterials and immune cues in LNs results in potent, antigen-specific local and systemic immune responses. These responses were quantified over time to determine the longevity of the resulting immune responses while providing new knowledge about the interplay between local LN rearrangement and antigen-specific responses in untreated tissues and blood. Future mechanistic studies could analyze specific cell migration or transport mechanisms to elucidate the prominent cell types or signals that are needed to provoke a potent systemic response. These studies should investigate if the particles or immune signals (e.g., antigen and adjuvant) are trafficking to uninjected LNs after *i.LN.* administration or if activated cells (e.g., DCs and macrophages) traffic from the treated nodes to other tissues to subsequently activate naïve lymphocytes in these tissues. Each immune cargo could be fluorescently labeled and tracked using whole animal imaging to determine the biodistribution of signals following treatment. Additionally, through the use of transport inhibitors such as FTY720, lymphocyte egress from LNs could be blocked. In this type of study, mice treated via *i.LN.* injection with biomaterial vaccines would, based on previous data from this work, activate the local cells. However, by treating with first FTY720, these activated cells would be unable to move out of LNs via efferent lymphatics and thus be sequestered in the treated tissues. Therefore, if cells in other, untreated LNs were found to be activated, it could be reasoned that the immune signals were trafficking to those tissues, not the activated cells.

Building on the work from **Chapter 6**, pilot studies were conducted to determine if the localization of immune signals to one or more LN were necessary for cell activation (**Figure 9.2A**). Microparticles containing an adjuvant (PolyIC) were mixed with soluble whole protein antigen (ovalbumin, OVA) and injected via *i.LN.* injection. Seven days after injection, the local response to treatment was quantified and each week the systemic antigen-specific responses in blood were evaluated (**Figure 9.2B**). Seven days after treatment at the height of T cell expansion, treatment with PolyIC MPs and OVA lead to increased levels of T cells within the treated nodes that were specific to the antigen (**Figure 9.2C**). As expected, LNs that were treated with vaccines containing OVA had dose dependent responses, with the One LN and Split treatment having the highest levels of antigen-specific T cells, while the Two LN treatment, which received half the dose of vaccine per LN, had a diminished response. Interestingly, priming both LNs resulted in the highest levels of antigen-specific T cells, followed by treating One LN, and finally the Split LN treatment (**Figure 9.2D**). When evaluating the B cell-mediated antibody response, serum collected from treated mice seven days after treatment had slightly increased levels of OVA-specific IgG antibodies (**Figure 9.2E**). However, at day 28 after treatment, the difference between groups was even more pronounced, with all groups inducing a heightened antibody response (**Figure 9.2F**).

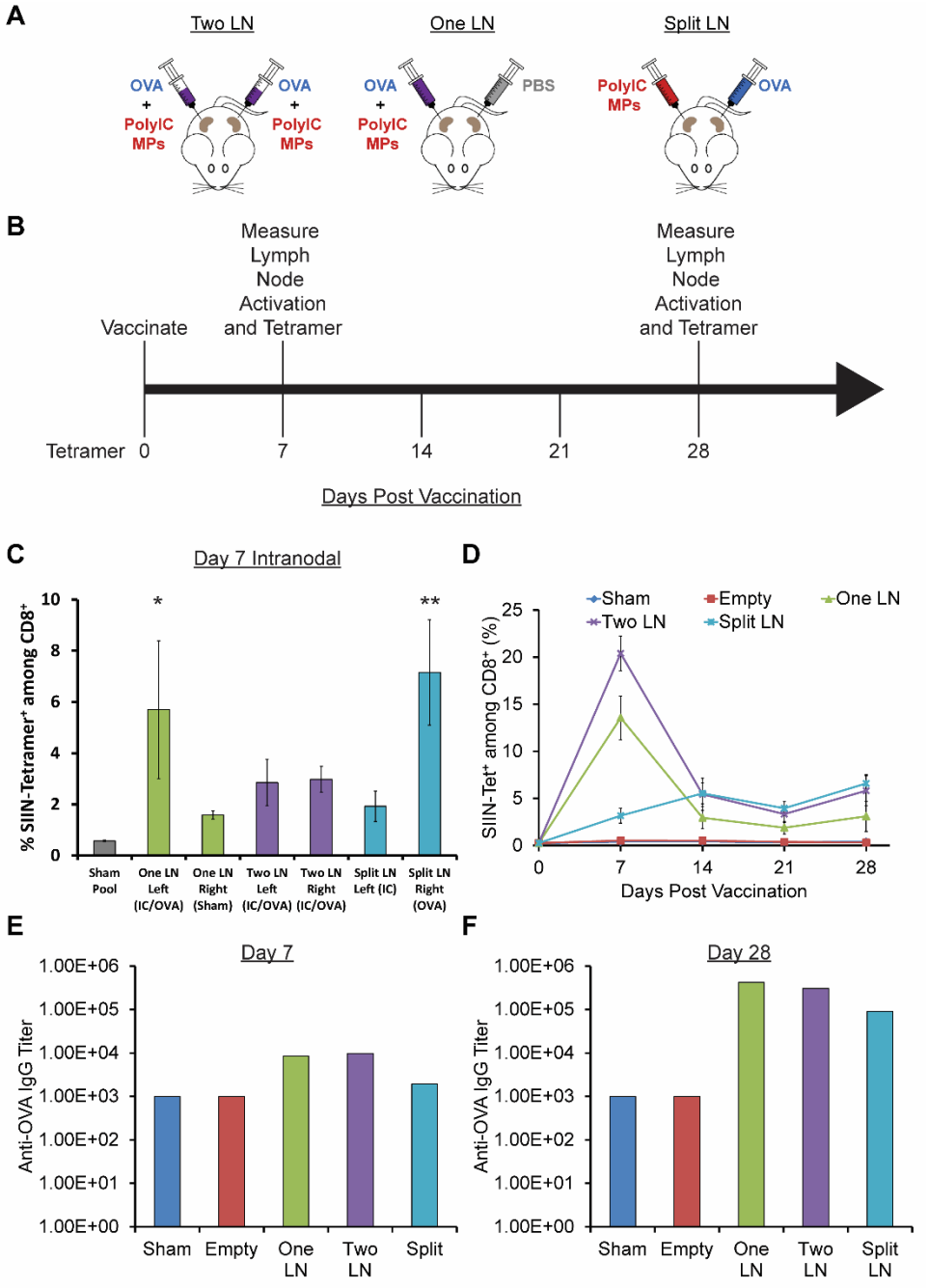

Figure 9.2: Localization of vaccines to numerous LNs results in heightened immune responses. (A) Schematic representation of vaccination strategy used to treat multiple LNs in mice via *i.LN.* injection. Using the treatment scheme in (B), local and systemic immune responses were determined. Antigen-specific tetramer levels both in the treated LNs (C) and blood (D) were quantified via flow cytometry. Antigen-specific IgG titers were evaluated 7 (E) and 28 (F) days after treatment.

While these initial studies will need to be repeated, the results reveal that both B and T cells are being primed against the antigen and motivate future studies to determine

the phenotype of these cells. To do this, germinal centers (GCs), the LN microdomains formed when activated B cells undergo proliferation, somatic mutation, and affinity maturation, can be quantified to determine whether the localization or the combination of specific immune signals impacts the GC numbers. Further experiments could also investigate the antibody isotypes that form after treatment to determine if treatment causes any antibody isotype class switching. Other mechanistic studies could exploit knockout mice that are genetically modified to be deficient in particular cells types. By using mice that lack important immune cell subsets (e.g., B cells, T cells, antigen presenting cells), the role that each of these cells play in response to *i.LN.* treatment could be evaluated and could motivate future studies that target the most prominent cell types with signals specifically selected to modulate the immune response towards a desired function.

Pilot studies were also conducted to build on the results presented in **Chapter 6** showing that *i.LN.* injection could cause protection in cancer models. In these studies, the same treatment scheme as in **Figure 9.2A** was used to determine if vaccine localization impacts survival. In these studies, treatments of one LN were injected into both the tumor draining LNs (tdLNs) and non-tumor draining LNs (non-tdLNs). Additionally, when splitting the vaccine components between LNs, groups had either PolyIC MPs in the tdLN or OVA in the tdLN. Seven days after vaccination, mice were 1,000,000 B16-0VA melanoma cells, cancer cells modified to overexpress OVA antigen. As expected, a sham treatment of PBS had no therapeutic effect and inoculated mice all succumbed quickly (**Figure 9.3A, Sham**). When treating two LNs

or one LN, regardless of whether this LN was tumor-draining or not, mice had decreased tumor incidence and increased survival, with all but one of the treated mice never establishing a tumor (**Figure 9.3B**). Interestingly, when splitting the treatments between LNs, having the PolyIC MP in the tdLN had a larger therapeutic effect than having OVA in the tdLN. When PolyIC was in the LN, only 1 mouse succumbed to their tumor while five of six mice established tumors in the other group.

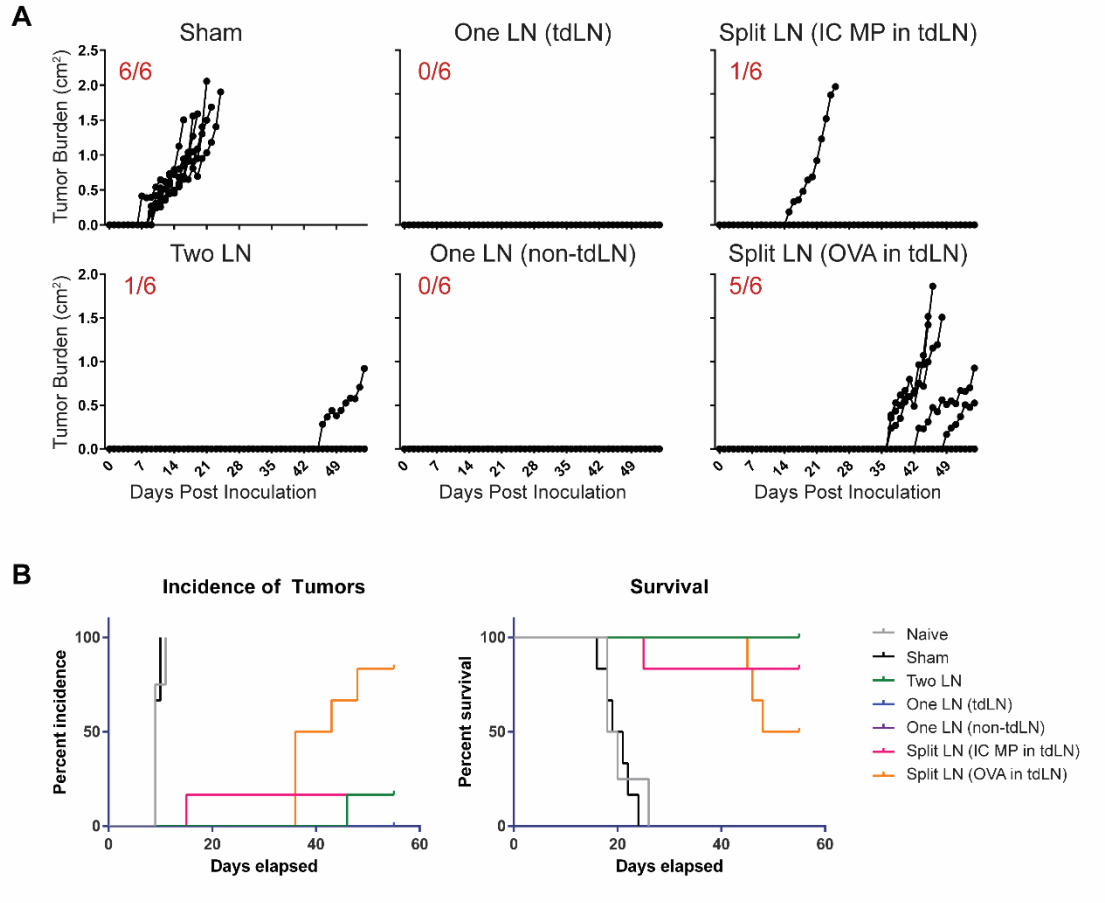

Figure 9.3: Vaccine localization impacts anti-cancer immunity.
(A) Individual tumor traces of mice treated with PBS (Sham), PolyIC MPs and soluble OVA in two LNs, one LN, or split between LNs in tdLNs and non-tdLNs. (B) Treatments lead to decreased tumor incidence and increased survival.

Future studies expanding on the cancer models presented in **Chapter 6** and the pilot study above could be conducted to determine the robustness of the immune response

and the longevity. First, mice that were primed via. *i.LN.* injection with a vaccine, then inoculated with cancer cells who do not form a primary tumor could be re-challenged with a second inoculation of cells. In these studies, mice that have immunological memory would have lymphocytes that are antigen-specific and could thus clear the tumor when re-encountering the cells. This study could help differentiate the treatments that are only able to clear initial tumors and those treatment regimens that result in a potent response that produces memory cells. Another way to test the robustness of vaccination would be to isolate T cells from mice following *i.LN.* treatment and then adoptively transfer these cells to naïve mice. The recipient mice could then undergo a cancer challenge and the ability to confer immunity to the recipient mice can be quantified. Similarly, T cells could be removed from treated mice and *ex vivo* assays to quantify CD8-specific killing of cells could determine the optimal treatment scheme. Finally, while this work has shown efficacy in melanoma models, in order to convey the robustness of the *i.LN.* platform, other models could be used with different, clinically-relevant antigens and other cancers types to explore the variety of diseases that could benefit from this technique.

Chapter 10: Contributions

My research has resulted in 15 manuscripts published: 7 first author publications and 8 manuscripts where I was a supporting author. 2 of my first author papers were based on PBAEs and their intrinsic immunogenicity, 2 focused on intra-lymph node injection and how to use this technique to understand changes in lymph nodes, 1 paper centered on immobilizing cells while maintaining their free-floating dynamics, and 2 were review papers that discussed how biomaterials can be used to engineering the lymph node microenvironment and how the intrinsic immunogenicity of materials could inform tissue engineering approaches. I also have another first author publication in preparation based on the work in **Chapter 7**. For the 8 additional papers where I was a supporting author (See **Appendix A**), my contributions included isolation, fluorescent staining, and imaging of treated lymph nodes, providing insight and assistance with forming electrostatic complexes, and aiding experimentally in various cell and animal studies. A portion of this research has also resulted in 1 issued US patent, 1 US utility patent application, and 1 international patent application (See **Appendix B**). The issued patent centers on intra-lymph node injection and was voted as a finalist for the 2014 University of Maryland Invention of the Year. The utility patent and international patent applications both focus on the immobilization of cells and a licensing agreement has been reached for this work. I have also presented my research 18 times at a number of conferences including those for the Biomedical Engineering Society, American Chemical Society, Society for Biomaterials, World Biomaterials Congress, American Association of Pharmaceutical Scientists, and a

Keystone Symposia on Vaccines. To support these presentations, I have received 7 travel awards. My research has been funded by 3 fellowships including the University of Maryland Graduate Dean's Dissertation Fellowship, the American Association of Pharmaceutical Scientists Foundation Graduate Fellowship, and a National Institutes of Health T32 Host-Pathogen Interaction Fellowship. I have also been awarded a Keystone Symposia Future of Science Fund Scholarship, named as the recipient of the 2016 Bioengineering Outstanding Graduate Student Research Award, was chosen as a University of Maryland Clark School Future Faculty Program Fellow, and received the 2017 University of Maryland Graduate School Michael J. Pelczar Award for Excellence in Graduate Study. My work with PBAEs is the first to systematically investigate how the intrinsic immunogenicity of materials is altered during degradation. Our work is unique in the use of intra-lymph node injection to specifically study the role that vaccine carriers and immune cues play in altering the local and systemic immune responses without relying on passive drainage following a systemic injection. Investigations using this technique have identified that altering the local tissue microenvironment can lead to antigen-specific, systemic changes to the immune response.

Appendix A: List of Co-author Publications

1. K.L. Hess, E. Oh, L.H. Tostanoski, **J.I. Andorko**, K. Susumu, J.R. Deschamps, I.L. Medintz, and C.M. Jewell. "Engineering immunological tolerance using quantum dots to tune the density of self-antigen display." *Advanced Functional Materials*. **2017**. *In press.* (cover article)

2. K.L. Hess, **J.I. Andorko**, L.H. Tostanoski, and C.M. Jewell. "Polyplexes assembled from self-peptides and regulatory nucleic acids blunt toll-like receptor signaling and induce immunological tolerance." *Biomaterials.* **2017** 118, 51-62.

3. L.H. Tostanoski, Y.C. Chiu, J.M. Gammon, T. Simon, **J.I. Andorko**, J.S. Bromberg, and C.M. Jewell. "Reprogramming the local lymph node microenvironment during autoimmunity promotes antigen-specific systemic tolerance." *Cell Reports.* **2016**, 16, 2940-2952.
"Featured on *Cell* Press Blog"
"Featured in American Chemical Society Press Conference"

4. Y.C. Chiu, J.M. Gammon, **J.I. Andorko**, L.H. Tostanoski, and C.M. Jewell. "Assembly and immunological processing of polyelectrolyte multilayers composed of antigens and adjuvants." *ACS Appl. Mater. Interfaces.* **2016**, 8, 18722-18731. doi: 10.1021/acsami.6b06275.

5. P. Zhang, **J.I. Andorko**, and C.M. Jewell. "Impact of dose, route, and composition on the immunogenicity of immune polyelectrolyte multilayers delivered on gold templates." *Biotechnol. Bioeng.* **2016**, 8, 18722-18731.
"Featured as monthly Spotlight Article in *Biotechnology and Bioengineering*"

6. L.H. Tostanoski, Y.C. Chiu, **J.I. Andorko**, M. Guo, X. Zeng, P. Zeng, W. Royal, and C.M. Jewell. "Design of polyelectrolyte multilayers to promote immune tolerance." *ACS Nano.* **2016**. 10, 9334-9345.
"Featured in American Chemical Society's C&E News online and in print"
"Featured in Controlled Release Society Newsletter"

7. Y.C. Chiu, J.M. Gammon, **J.I. Andorko**, L.H. Tostanoski, and C.M. Jewell. "Modular vaccine design using carrier-free capsules assembled from polyionic immune signals." *ACS Biomater Sci Eng.* **2015**, 1, 1200-1205**.** doi:10.1021/acsbiomaterials.5b00375. (cover article)

8. E. Ory, D.Chen, K. Chakrabarti, P. Zhang, **J.I. Andorko**, C.M. Jewell, W. Losert, and S.S. Martin "Extracting microtentacle dynamics in non-adherent tumor cells." **2017**. *In review*.

Appendix B: List of Patents and Intellectual Property Filings

1. C. M. Jewell, **J. I. Andorko**, L. H. Tostanoski. “Local Engineering of the Lymph Node Environment to Promote Immune Tolerance.” U.S. Patent No. 9,610,349. Issued April 4, **2017**.

2. S.S. Martin, C.M. Jewell, **J.I. Andorko**, E.L. Sooklal, R.A. Whipple, K. Chakrabarti; “Materials and Methods for Assaying Living Cells.” U.S. Patent Application No. 62/068034. Filed October 7, **2015**.

3. S.S. Martin, C.M. Jewell, **J.I. Andorko**, E.L. Sooklal, R.A. Whipple, K. Chakrabarti. “Materials and Methods for Assaying Living Cells.” PCT application number US2015/054571. Filed October 7, **2015**.

References

[1] S. W. Roush and T. V. Murphy, "Historical comparisons of morbidity and mortality for vaccine-preventable diseases in the United States," *JAMA,* vol. 298, pp. 2155-63, 2007.

[2] L. A. Brito and D. T. O'Hagan, "Designing and building the next generation of improved vaccine adjuvants," *J Control Release,* vol. 190, pp. 563-79, 2014.

[3] D. T. O'Hagan and C. B. Fox, "New generation adjuvants – From empiricism to rational design," *Vaccine,* vol. 33, Supplement 2, pp. B14-B20, 2015.

[4] C. Therapeutics. Phase III Study of Rindopepimut/GM-CSF in Patients With Newly Diagnosed Glioblastoma (ACT IV). *ClinicalTrials.gov [Internet]. Bethesda (MD): National Library of Medicine (US)* **2017 (Accessed 04/24/2017),** Available using NLM Identifier NCT01480479.

[5] D. N. Thomas. A Study to Evaluate the Efficacy of an RSV F Vaccine in Older Adults. *ClinicalTrials.gov [Internet]. Bethesda (MD): National Library of Medicine (US)* **2017 (Accessed 04/24/2017),** Available using NLM Identifier NCT02608502.

[6] N. N. Vahanian. Immunotherapy Study for Surgically Resected Pancreatic Cancer. *ClinicalTrials.gov [Internet]. Bethesda (MD): National Library of Medicine (US)* **2016 (Accessed 04/24/2017),** Available using NLM Identifier NCT01072981.

[7] H. Adewoye. A Randomized, Double-Blind and Placebo-Controlled Study of Idelalisib in Combination With Bendamustine and Rituximab for Previously Treated Chronic Lymphocytic Leukemia (CLL). *ClinicalTrials.gov [Internet]. Bethesda (MD): National Library of Medicine (US)* **2016 (Accessed 04/24/2017),** Available using NLM Identifier NCT01569295.

[8] S. Mitra. Efficacy and Safety of Idelalisib (GS-1101) in Combination With Rituximab for Previously Treated Indolent Non-Hodgkin Lymphomas (Yosemite). *ClinicalTrials.gov [Internet]. Bethesda (MD): National Library of Medicine (US)* **2016 (Accessed 04/24/2017),** Available using NLM Identifier NCT01732913.

[9] F. A. Sharp, D. Ruane, B. Claass, E. Creagh, J. Harris, P. Malyala, M. Singh, D. T. O'Hagan, V. Pétrilli, J. Tschopp, L. A. J. O'Neill, and E. C. Lavelle, "Uptake of particulate vaccine adjuvants by dendritic cells activates the NALP3 inflammasome," *Proc. Natl. Acad. Sci. U.S.A.,* vol. 106, pp. 870-875, 2009.

[10] J. I. Andorko, K. L. Hess, and C. M. Jewell, "Harnessing Biomaterials to Engineer the Lymph Node Microenvironment for Immunity or Tolerance," *The AAPS Journal,* vol. 17, pp. 323-338, 2015.

[11] T. Katakai, T. Hara, M. Sugai, H. Gonda, and A. Shimizu, "Lymph Node Fibroblastic Reticular Cells Construct the Stromal Reticulum via Contact with Lymphocytes," *The Journal of Experimental Medicine,* vol. 200, pp. 783-795, 2004.

[12] K. J. Warren, D. Iwami, D. G. Harris, J. S. Bromberg, and B. E. Burrell, "Laminins affect T cell trafficking and allograft fate," *Journal of Clinical Investigation,* vol. 124, pp. 2204-2218, 2014.

[13] C. M. Jewell, S. C. B. Lopez, and D. J. Irvine, "In situ engineering of the lymph node microenvironment via intranodal injection of adjuvant-releasing polymer particles," *Proc. Natl. Acad. Sci. U.S.A.*, vol. 108, pp. 15745-15750, 2011.

[14] J. I. Andorko, L. H. Tostanoski, E. Solano, M. Mukhamedova, and C. M. Jewell, "Intra-lymph Node Injection of Biodegradable Polymer Particles," *J. Vis. Exp.*, p. e50984, 2014.

[15] D. J. Irvine, M. A. Swartz, and G. L. Szeto, "Engineering synthetic vaccines using cues from natural immunity," *Nature Materials,* vol. 12, pp. 978-990, 2013.

[16] D. J. Irvine and C. M. Jewell, "Vaccine and Immunotherapy Delivery," in *Comprehensive Biomaterials*, P. Ducheyne, Ed., ed New York, NY: Elsevier Press, 2012.

[17] M. A. Swartz, S. Hirosue, and J. A. Hubbell, "Engineering Approaches to Immunotherapy," *Science Translational Medicine,* vol. 4, 2012.

[18] S. N. Mueller and R. N. Germain, "Stromal cell contributions to the homeostasis and functionality of the immune system," *Nature Reviews Immunology*, vol. 9, pp. 618-629, 2009.

[19] N. H. Ruddle and E. M. Akirav, "Secondary Lymphoid Organs: Responding to Genetic and Environmental Cues in Ontogeny and the Immune Response," *Journal of Immunology,* vol. 183, pp. 2205-2212, 2009.

[20] J. P. Girard, C. Moussion, and R. Forster, "HEVs, lymphatics and homeostatic immune cell trafficking in lymph nodes," *Nature Reviews Immunology,* vol. 12, pp. 762-773, 2012.

[21] C. M. Card, S. S. Yu, and M. A. Swartz, "Emerging roles of lymphatic endothelium in regulating adaptive immunity," *Journal of Clinical Investigation,* vol. 124, pp. 943-952, 2014.

[22] S. T. Reddy, A. J. van der Vlies, E. Simeoni, V. Angeli, G. J. Randolph, C. P. O'Neil, L. K. Lee, M. A. Swartz, and J. A. Hubbell, "Exploiting lymphatic transport and complement activation in nanoparticle vaccines," *Nat Biotech,* vol. 25, pp. 1159-1164, 2007.

[23] D. L. Drayton, S. Liao, R. H. Mounzer, and N. H. Ruddle, "Lymphoid organ development: from ontogeny to neogenesis," *Nature Immunology,* vol. 7, pp. 344-353, 2006.

[24] S. J. Turley, A. L. Fletcher, and K. G. Elpek, "The stromal and haematopoietic antigen-presenting cells that reside in secondary lymphoid organs," *Nature Reviews Immunology,* vol. 10, pp. 813-825, 2010.

[25] A. K. Abbas, A. H. Lichtman, and S. Pillai, *Cellular and molecular immunology*. Philadelphia: Elsevier/Saunders, 2012.

[26] K. Murphy, P. Travers, M. Walport, and C. Janeway, *Janeway's immunobiology*. New York: Garland Science, 2012.

[27] S. L. Nutt and D. M. Tarlinton, "Germinal center B and follicular helper T cells: siblings, cousins or just good friends?," *Nature Immunology,* vol. 12, pp. 472-477, 2011.

[28] C. G. Vinuesa, M. A. Linterman, C. C. Goodnow, and K. L. Randall, "T cells and follicular dendritic cells in germinal center B-cell formation and selection," *Immunological Reviews,* vol. 237, pp. 72-89, 2010.

[29] T. Katakai, T. Hara, M. Sugai, H. Gonda, and A. Shimizu, "Lymph node fibroblastic reticular cells construct the stromal reticulum via contact with lymphocytes," *J Exp Med,* vol. 200, pp. 783-95, 2004.

[30] M. F. Bachmann and G. T. Jennings, "Vaccine delivery: a matter of size, geometry, kinetics and molecular patterns," *Nat Rev Immunol,* vol. 10, pp. 787-796, 2010.

[31] C. Foged, B. Brodin, S. Frokjaer, and A. Sundblad, "Particle size and surface charge affect particle uptake by human dendritic cells in an in vitro model," *International Journal of Pharmaceutics,* vol. 298, pp. 315-322, 2005.

[32] R. Kaur, V. W. Bramwell, D. J. Kirby, and Y. Perrie, "Manipulation of the surface pegylation in combination with reduced vesicle size of cationic liposomal adjuvants modifies their clearance kinetics from the injection site,

and the rate and type of T cell response," *Journal of Controlled Release,* vol. 164, pp. 331-337, 2012.

[33] K. A. Scheibner, M. A. Lutz, S. Boodoo, M. J. Fenton, J. D. Powell, and M. R. Horton, "Hyaluronan Fragments Act as an Endogenous Danger Signal by Engaging TLR2," *The Journal of Immunology,* vol. 177, pp. 1272-1281, 2006.

[34] C. Termeer, F. Benedix, J. Sleeman, C. Fieber, U. Voith, T. Ahrens, K. Miyake, M. Freudenberg, C. Galanos, and J. C. Simon, "Oligosaccharides of Hyaluronan Activate Dendritic Cells via Toll-like Receptor 4," *The Journal of Experimental Medicine,* vol. 195, pp. 99-111, 2002.

[35] C. C. Termeer, J. Hennies, U. Voith, T. Ahrens, J. M. Weiss, P. Prehm, and J. C. Simon, "Oligosaccharides of Hyaluronan Are Potent Activators of Dendritic Cells," *The Journal of Immunology,* vol. 165, pp. 1863-1870, 2000.

[36] C. A. Da Silva, C. Chalouni, A. Williams, D. Hartl, C. G. Lee, and J. A. Elias, "Chitin is a size-dependent regulator of macrophage TNF and IL-10 production," *J Immunol,* vol. 182, pp. 3573-82, 2009.

[37] S. Y. Seong and P. Matzinger, "Hydrophobicity: an ancient damage-associated molecular pattern that initiates innate immune responses," *Nat Rev Immunol,* vol. 4, pp. 469-78, 2004.

[38] D. F. Moyano, M. Goldsmith, D. J. Solfiell, D. Landesman-Milo, O. R. Miranda, D. Peer, and V. M. Rotello, "Nanoparticle Hydrophobicity Dictates Immune Response," *Journal of the American Chemical Society,* vol. 134, pp. 3965-3967, 2012.

[39] S. Gallorini, F. Berti, P. Parente, R. Baronio, S. Aprea, U. D'Oro, M. Pizza, J. L. Telford, and A. Wack, "Introduction of zwitterionic motifs into bacterial polysaccharides generates TLR2 agonists able to activate APCs," *J Immunol,* vol. 179, pp. 8208-15, 2007.

[40] H. Liu, K. D. Moynihan, Y. Zheng, G. L. Szeto, A. V. Li, B. Huang, D. S. Van Egeren, C. Park, and D. J. Irvine, "Structure-based programming of lymph-node targeting in molecular vaccines," *Nature,* vol. 507, pp. 519-522, 2014.

[41] J. C. Sunshine, K. Perica, J. P. Schneck, and J. J. Green, "Particle shape dependence of CD8+ T cell activation by artificial antigen presenting cells," *Biomaterials,* vol. 35, pp. 269-277, 2014.

[42] P. M. Kou, Z. Schwartz, B. D. Boyan, and J. E. Babensee, "Dendritic cell responses to surface properties of clinical titanium surfaces," *Acta Biomaterialia,* vol. 7, pp. 1354-1363, 2011.

[43] P. M. Kou, N. Pallassana, R. Bowden, B. Cunningham, A. Joy, J. Kohn, and J. E. Babensee, "Predicting biomaterial property-dendritic cell phenotype relationships from the multivariate analysis of responses to polymethacrylates," *Biomaterials,* vol. 33, pp. 1699-1713, 2012.

[44] F. A. Sharp, D. Ruane, B. Claass, E. Creagh, J. Harris, P. Malyala, M. Singh, D. T. O'Hagan, V. Pétrilli, J. Tschopp, L. A. J. O'Neill, and E. C. Lavelle, "Uptake of particulate vaccine adjuvants by dendritic cells activates the NALP3 inflammasome," *Proceedings of the National Academy of Sciences,* vol. 106, pp. 870-875, 2009.

[45] S. L. Demento, S. C. Eisenbarth, H. G. Foellmer, C. Platt, M. J. Caplan, W. Mark Saltzman, I. Mellman, M. Ledizet, E. Fikrig, R. A. Flavell, and T. M. Fahmy, "Inflammasome-activating nanoparticles as modular systems for optimizing vaccine efficacy," *Vaccine,* vol. 27, pp. 3013-3021, 2009.

[46] W. Zhang, L. Wang, Y. Liu, X. Chen, J. Li, T. Yang, W. An, X. Ma, R. Pan, and G. Ma, "Comparison of PLA Microparticles and Alum as Adjuvants for H5N1 Influenza Split Vaccine: Adjuvanticity Evaluation and Preliminary Action Mode Analysis," *Pharmaceutical Research,* vol. 31, pp. 1015-1031, 2014.

[47] A. L. St. John, C. Y. Chan, H. F. Staats, K. W. Leong, and S. N. Abraham, "Synthetic mast-cell granules as adjuvants to promote and polarize immunity in lymph nodes," *Nat Mater,* vol. 11, pp. 250-257, 2012.

[48] L. Jeanbart, M. Ballester, A. de Titta, P. Corthesy, P. Romero, J. A. Hubbell, and M. A. Swartz, "Enhancing efficacy of anti-cancer vaccines by targeted delivery to tumor-draining lymph nodes," *Cancer Immunology Research,* 2014.

[49] S. N. Thomas, E. Vokali, A. W. Lund, J. A. Hubbell, and M. A. Swartz, "Targeting the tumor-draining lymph node with adjuvanted nanoparticles reshapes the anti-tumor immune response," *Biomaterials,* vol. 35, pp. 814-824, 2014.

[50] J. J. Moon, H. Suh, A. V. Li, C. F. Ockenhouse, A. Yadava, and D. J. Irvine, "Enhancing humoral responses to a malaria antigen with nanoparticle vaccines that expand Tfh cells and promote germinal center induction," *Proceedings of the National Academy of Sciences,* vol. 109, pp. 1080-1085, 2012.

[51] A. V. Li, J. J. Moon, W. Abraham, H. Suh, J. Elkhader, M. A. Seidman, M. Yen, E.-J. Im, M. H. Foley, D. H. Barouch, and D. J. Irvine, "Generation of Effector Memory T Cell–Based Mucosal and Systemic Immunity with

Pulmonary Nanoparticle Vaccination," *Science Translational Medicine,* vol. 5, p. 204ra130, 2013.

[52] J. J. Moon, H. Suh, A. Bershteyn, M. T. Stephan, H. Liu, B. Huang, M. Sohail, S. Luo, S. Ho Um, H. Khant, J. T. Goodwin, J. Ramos, W. Chiu, and D. J. Irvine, "Interbilayer-crosslinked multilamellar vesicles as synthetic vaccines for potent humoral and cellular immune responses," *Nat Mater,* vol. 10, pp. 243-251, 2011.

[53] S. P. Kasturi, I. Skountzou, R. A. Albrecht, D. Koutsonanos, T. Hua, H. I. Nakaya, R. Ravindran, S. Stewart, M. Alam, M. Kwissa, F. Villinger, N. Murthy, J. Steel, J. Jacob, R. J. Hogan, A. Garcia-Sastre, R. Compans, and B. Pulendran, "Programming the magnitude and persistence of antibody responses with innate immunity," *Nature,* vol. 470, pp. 543-547, 2011.

[54] C. M. Jewell, S. C. B. Lopez, and D. J. Irvine, "In situ engineering of the lymph node microenvironment via intranodal injection of adjuvant-releasing polymer particles," *Proceedings of the National Academy of Sciences of the United States of America,* vol. 108, pp. 15745-15750, 2011.

[55] J. I. Andorko, L. H. Tostanoski, E. Solano, M. Mukhamedova, and C. M. Jewell, "Intra-lymph Node Injection of Biodegradable Polymer Particles," *Journal of Visualized Experiments,* p. e50984, 2014.

[56] C. Keijzer, R. Spiering, A. L. Silva, W. van Eden, W. Jiskoot, L. Vervelde, and F. Broere, "PLGA nanoparticles enhance the expression of retinaldehyde dehydrogenase enzymes in dendritic cells and induce FoxP3(+) T-cells in vitro," *J Control Release,* vol. 168, pp. 35-40, 2013.

[57] A. C. Shirali, M. Look, W. Du, E. Kassis, H. W. Stout-Delgado, T. M. Fahmy, and D. R. Goldstein, "Nanoparticle Delivery of Mycophenolic Acid Upregulates PD-L1 on Dendritic Cells to Prolong Murine Allograft Survival," *American Journal of Transplantation,* vol. 11, pp. 2582-2592, 2011.

[58] P. Johansen, T. Storni, L. Rettig, Z. Qiu, A. Der-Sarkissian, K. A. Smith, V. Manolova, K. S. Lang, G. Senti, B. Müllhaupt, T. Gerlach, R. F. Speck, A. Bot, and T. M. Kündig, "Antigen kinetics determines immune reactivity," *Proceedings of the National Academy of Sciences,* vol. 105, pp. 5189-5194, 2008.

[59] C. Keijzer, B. Slutter, R. van der Zee, W. Jiskoot, W. van Eden, and F. Broere, "PLGA, PLGA-TMC and TMC-TPP nanoparticles differentially modulate the outcome of nasal vaccination by inducing tolerance or enhancing humoral immunity," *PLoS One,* vol. 6, p. e26684, 2011.

[60] J. Park, W. Gao, R. Whiston, T. B. Strom, S. Metcalfe, and T. M. Fahmy, "Modulation of CD4+ T lymphocyte lineage outcomes with targeted, nanoparticle-mediated cytokine delivery," *Mol Pharm,* vol. 8, pp. 143-52, 2011.

[61] C. Capini, M. Jaturanpinyo, H. I. Chang, S. Mutalik, A. McNally, S. Street, R. Steptoe, B. O'Sullivan, N. Davies, and R. Thomas, "Antigen-Specific Suppression of Inflammatory Arthritis Using Liposomes," *Journal of Immunology*, vol. 182, pp. 3556-3565, 2009.

[62] S. E. Tsai, A. Shameli, J. Yamanouchi, X. Clemente-Casares, J. G. Wang, P. Serra, Y. Yang, Z. Medarova, A. Moore, and P. Santamaria, "Reversal of Autoimmunity by Boosting Memory-like Autoregulatory T Cells," *Immunity,* vol. 32, pp. 568-580, 2010.

[63] D. R. Getts, A. J. Martin, D. P. McCarthy, R. L. Terry, Z. N. Hunter, W. T. Yap, M. T. Getts, M. Pleiss, X. Luo, N. J. King, L. D. Shea, and S. D. Miller, "Microparticles bearing encephalitogenic peptides induce T-cell tolerance and ameliorate experimental autoimmune encephalomyelitis," *Nat Biotechnol,* vol. 30, pp. 1217-24, 2012.

[64] L. Huang, H. P. Lemos, L. Li, M. Li, P. R. Chandler, B. Baban, T. L. McGaha, B. Ravishankar, J. R. Lee, D. H. Munn, and A. L. Mellor, "Engineering DNA nanoparticles as immunomodulatory reagents that activate regulatory T cells," *J Immunol,* vol. 188, pp. 4913-20, 2012.

[65] J. Azzi, L. Tang, R. Moore, R. Tong, N. El Haddad, T. Akiyoshi, B. Mfarrej, S. Yang, M. Jurewicz, T. Ichimura, N. Lindeman, J. Cheng, and R. Abdi, "Polylactide-cyclosporin A nanoparticles for targeted immunosuppression," *FASEB J,* vol. 24, pp. 3927-38, 2010.

[66] L. Tang, J. Azzi, M. Kwon, M. Mounayar, R. Tong, Q. Yin, R. Moore, N. Skartsis, T. M. Fan, R. Abdi, and J. Cheng, "Immunosuppressive Activity of Size-Controlled PEG-PLGA Nanoparticles Containing Encapsulated Cyclosporine A," *J Transplant,* vol. 2012, p. 896141, 2012.

[67] S. T. Reddy, A. Rehor, H. G. Schmoekel, J. A. Hubbell, and M. A. Swartz, "In vivo targeting of dendritic cells in lymph nodes with poly(propylene sulfide) nanoparticles," *Journal of Controlled Release,* vol. 112, pp. 26-34, 2006.

[68] R. Cubas, S. Zhang, S. Kwon, E. M. Sevick-Muraca, M. Li, C. Chen, and Q. Yao, "Virus-like particle (VLP) lymphatic trafficking and immune response generation after immunization by different routes," *J Immunother,* vol. 32, pp. 118-28, 2009.

[69] Y. J. Kwon, E. James, N. Shastri, and J. M. J. Fréchet, "In vivo targeting of dendritic cells for activation of cellular immunity using vaccine carriers based on pH-responsive microparticles," *Proceedings of the National Academy of Sciences of the United States of America,* vol. 102, pp. 18264-18268, 2005.

[70] C. L. van Broekhoven, C. R. Parish, C. Demangel, W. J. Britton, and J. G. Altin, "Targeting dendritic cells with antigen-containing liposomes: a highly effective procedure for induction of antitumor immunity and for tumor immunotherapy," *Cancer Res,* vol. 64, pp. 4357-65, 2004.

[71] W. Zou, "Immunosuppressive networks in the tumour environment and their therapeutic relevance," *Nat Rev Cancer,* vol. 5, pp. 263-274, 2005.

[72] B. Kwong, H. Liu, and D. J. Irvine, "Induction of potent anti-tumor responses while eliminating systemic side effects via liposome-anchored combinatorial immunotherapy," *Biomaterials,* vol. 32, pp. 5134-5147, 2011.

[73] M. T. Stephan, J. J. Moon, S. H. Um, A. Bershteyn, and D. J. Irvine, "Therapeutic cell engineering with surface-conjugated synthetic nanoparticles," *Nat Med,* vol. 16, pp. 1035-41, 2010.

[74] I. J. de Vries, W. J. Lesterhuis, J. O. Barentsz, P. Verdijk, J. H. van Krieken, O. C. Boerman, W. J. Oyen, J. J. Bonenkamp, J. B. Boezeman, G. J. Adema, J. W. Bulte, T. W. Scheenen, C. J. Punt, A. Heerschap, and C. G. Figdor, "Magnetic resonance tracking of dendritic cells in melanoma patients for monitoring of cellular therapy," *Nat Biotechnol,* vol. 23, pp. 1407-13, 2005.

[75] G. Senti, B. M. Prinz Vavricka, I. Erdmann, M. I. Diaz, R. Markus, S. J. McCormack, J. J. Simard, B. Wüthrich, R. Crameri, N. Graf, P. Johansen, and T. M. Kündig, "Intralymphatic allergen administration renders specific immunotherapy faster and safer: A randomized controlled trial," *Proceedings of the National Academy of Sciences,* vol. 105, pp. 17908-17912, 2008.

[76] G. Senti, R. Crameri, D. Kuster, P. Johansen, J. M. Martinez-Gomez, N. Graf, M. Steiner, L. A. Hothorn, H. Grönlund, C. Tivig, A. Zaleska, O. Soyer, M. van Hage, C. A. Akdis, M. Akdis, H. Rose, and T. M. Kündig, "Intralymphatic immunotherapy for cat allergy induces tolerance after only 3 injections," *Journal of Allergy and Clinical Immunology,* vol. 129, pp. 1290-1296, 2012.

[77] G. Senti, P. Johansen, and T. M. Kundig, "Intralymphatic immunotherapy," *Curr Opin Allergy Clin Immunol,* vol. 9, pp. 537-43, 2009.

[78] M. Witten, H. J. Malling, L. Blom, B. C. Poulsen, and L. K. Poulsen, "Is intralymphatic immunotherapy ready for clinical use in patients with grass

pollen allergy?," *Journal of Allergy and Clinical Immunology*, vol. 132, pp. 1248-1252, 2013.

[79] C. A. Akdis, "Therapies for allergic inflammation: refining strategies to induce tolerance," *Nature Medicine,* vol. 18, pp. 736-749, 2012.

[80] P. Johansen, A. C. Haffner, F. Koch, K. Zepter, I. Erdmann, K. Maloy, J. J. Simard, T. Storni, G. Senti, A. Bot, B. Wuthrich, and T. M. Kundig, "Direct intralymphatic injection of peptide vaccines enhances immunogenicity," *Eur J Immunol,* vol. 35, pp. 568-74, 2005.

[81] K. A. Smith, B. L. Meisenburg, V. L. Tam, R. R. Pagarigan, R. Wong, D. K. Joea, L. Lantzy, M. A. Carrillo, T. M. Gross, U. M. Malyankar, C.-S. Chiang, D. M. Da Silva, T. M. Kündig, W. M. Kast, Z. Qiu, and A. Bot, "Lymph Node–Targeted Immunotherapy Mediates Potent Immunity Resulting in Regression of Isolated or Metastatic Human Papillomavirus–Transformed Tumors," *Clinical Cancer Research,* vol. 15, pp. 6167-6176, 2009.

[82] K. A. Smith, V. L. Tam, R. M. Wong, R. R. Pagarigan, B. L. Meisenburg, D. K. Joea, X. Liu, C. Sanders, D. Diamond, T. M. Kundig, Z. Qiu, and A. Bot, "Enhancing DNA vaccination by sequential injection of lymph nodes with plasmid vectors and peptides," *Vaccine,* vol. 27, pp. 2603-15, 2009.

[83] M. Adamina, R. Rosenthal, W. P. Weber, D. M. Frey, C. T. Viehl, M. Bolli, R. W. Huegli, A. L. Jacob, M. Heberer, D. Oertli, W. Marti, G. C. Spagnoli, and P. Zajac, "Intranodal immunization with a vaccinia virus encoding multiple antigenic epitopes and costimulatory molecules in metastatic melanoma," *Mol Ther,* vol. 18, pp. 651-9, 2010.

[84] A. Ribas, J. S. Weber, B. Chmielowski, B. Comin-Anduix, D. Lu, M. Douek, N. Ragavendra, S. Raman, E. Seja, D. Rosario, S. Miles, D. C. Diamond, Z. Y. Qiu, M. Obrocea, and A. Bot, "Intra-Lymph Node Prime-Boost Vaccination against Melan A and Tyrosinase for the Treatment of Metastatic Melanoma: Results of a Phase 1 Clinical Trial," *Clinical Cancer Research,* vol. 17, pp. 2987-2996, 2011.

[85] Y. Waeckerle-Men, N. Bruffaerts, Y. Liang, F. Jurion, P. Sander, T. M. Kündig, K. Huygen, and P. Johansen, "Lymph node targeting of BCG vaccines amplifies CD4 and CD8 T-cell responses and protection against Mycobacterium tuberculosis," *Vaccine,* vol. 31, pp. 1057-1064, 2013.

[86] D. Mohanan, B. Slütter, M. Henriksen-Lacey, W. Jiskoot, J. A. Bouwstra, Y. Perrie, T. M. Kündig, B. Gander, and P. Johansen, "Administration routes affect the quality of immune responses: A cross-sectional evaluation of particulate antigen-delivery systems," *Journal of Controlled Release,* vol. 147, pp. 342-349, 2010.

[87] M. Comabella and S. J. Khoury, "Immunopathogenesis of multiple sclerosis," *Clin Immunol,* vol. 142, pp. 2-8, 2012.

[88] A. Nylander and D. A. Hafler, "Multiple sclerosis," *J Clin Invest,* vol. 122, pp. 1180-8, 2012.

[89] A. Lutterotti and R. Martin, "Antigen-specific tolerization approaches in multiple sclerosis," *Expert Opin Investig Drugs,* vol. 23, pp. 9-20, 2014.

[90] X. Clemente-Casares and P. Santamaria, "Nanomedicine in autoimmunity," *Immunology Letters,* vol. 158, pp. 167-174, 2014.

[91] A. Yeste, M. Nadeau, E. J. Burns, H. L. Weiner, and F. J. Quintana, "Nanoparticle-mediated codelivery of myelin antigen and a tolerogenic small molecule suppresses experimental autoimmune encephalomyelitis," *Proceedings of the National Academy of Sciences of the United States of America,* vol. 109, pp. 11270-11275, 2012.

[92] M. Look, E. Stern, Q. A. Wang, L. D. DiPlacido, M. Kashgarian, J. Craft, and T. M. Fahmy, "Nanogel-based delivery of mycophenolic acid ameliorates systemic lupus erythematosus in mice," *Journal of Clinical Investigation,* vol. 123, pp. 1741-1749, 2013.

[93] K. J. Peine, M. Guerau-de-Arellano, P. Lee, N. Kanthamneni, M. Severin, G. D. Probst, H. Y. Peng, Y. H. Yang, Z. Vangundy, T. L. Papenfuss, A. E. Lovett-Racke, E. M. Bachelder, and K. M. Ainslie, "Treatment of Experimental Autoimmune Encephalomyelitis by Codelivery of Disease Associated Peptide and Dexamethasone in Acetalated Dextran Microparticles," *Molecular Pharmaceutics,* vol. 11, pp. 828-835, 2014.

[94] J. S. Lewis, C. Roche, Y. Zhang, T. M. Brusko, C. H. Wasserfall, M. Atkinson, M. J. Clare-Salzler, and B. G. Keselowsky, "Combinatorial delivery of immunosuppressive factors to dendritic cells using dual-sized microspheres," *J Mater Chem B Mater Biol Med,* vol. 2, pp. 2562-2574, 2014.

[95] S. Jhunjhunwala, G. Raimondi, A. J. Glowacki, S. J. Hall, D. Maskarinec, S. H. Thorne, A. W. Thomson, and S. R. Little, "Bioinspired controlled release of CCL22 recruits regulatory T cells in vivo," *Adv Mater,* vol. 24, pp. 4735-8, 2012.

[96] S. Jhunjhunwala, S. C. Balmert, G. Raimondi, E. Dons, E. E. Nichols, A. W. Thomson, and S. R. Little, "Controlled release formulations of IL-2, TGF-beta1 and rapamycin for the induction of regulatory T cells," *J Control Release,* vol. 159, pp. 78-84, 2012.

[97] B. Buyuktimkin, Q. Wang, P. Kiptoo, J. M. Stewart, C. Berkland, and T. J. Siahaan, "Vaccine-like controlled-release delivery of an immunomodulating peptide to treat experimental autoimmune encephalomyelitis," *Mol Pharm,* vol. 9, pp. 979-85, 2012.

[98] Z. Hunter, D. P. McCarthy, W. T. Yap, C. T. Harp, D. R. Getts, L. D. Shea, and S. D. Miller, "A biodegradable nanoparticle platform for the induction of antigen-specific immune tolerance for treatment of autoimmune disease," *ACS Nano,* vol. 8, pp. 2148-60, 2014.

[99] D. R. Getts, R. L. Terry, M. T. Getts, C. Deffrasnes, M. Muller, C. van Vreden, T. M. Ashhurst, B. Chami, D. McCarthy, H. Wu, J. Ma, A. Martin, L. D. Shae, P. Witting, G. S. Kansas, J. Kuhn, W. Hafezi, I. L. Campbell, D. Reilly, J. Say, L. Brown, M. Y. White, S. J. Cordwell, S. J. Chadban, E. B. Thorp, S. Bao, S. D. Miller, and N. J. King, "Therapeutic inflammatory monocyte modulation using immune-modifying microparticles," *Sci Transl Med,* vol. 6, p. 219ra7, 2014.

[100] J. Bryant, K. A. Hlavaty, X. Zhang, W. T. Yap, L. Zhang, L. D. Shea, and X. Luo, "Nanoparticle delivery of donor antigens for transplant tolerance in allogeneic islet transplantation," *Biomaterials,* vol. 35, pp. 8887-94, 2014.

[101] C. P. Berg, I. H. Engels, A. Rothbart, K. Lauber, A. Renz, S. F. Schlosser, K. Schulze-Osthoff, and S. Wesselborg, "Human mature red blood cells express caspase-3 and caspase-8, but are devoid of mitochondrial regulators of apoptosis," *Cell Death Differ,* vol. 8, pp. 1197-206, 2001.

[102] S. Kontos, I. C. Kourtis, K. Y. Dane, and J. A. Hubbell, "Engineering antigens for in situ erythrocyte binding induces T-cell deletion," *Proceedings of the National Academy of Sciences,* vol. 110, pp. E60-8, 2013.

[103] J. I. Andorko, K. L. Hess, and C. M. Jewell, "Harnessing Biomaterials to Engineer the Lymph Node Microenvironment for Immunity or Tolerance," *AAPS J,* pp. 1-16, 2014.

[104] M. A. Swartz, S. Hirosue, and J. A. Hubbell, "Engineering Approaches to Immunotherapy," *Sci. Transl. Med.,* vol. 4, p. 148rv9, 2012.

[105] D. J. Irvine, M. A. Swartz, and G. L. Szeto, "Engineering synthetic vaccines using cues from natural immunity," *Nat. Mater.,* vol. 12, pp. 978-990, 2013.

[106] J. E. Babensee and A. Paranjpe, "Differential levels of dendritic cell maturation on different biomaterials used in combination products," *J. Biomed. Mater. Res. A,* vol. 74, pp. 503-10, 2005.

[107] B. M. Tesar, D. Jiang, J. Liang, S. M. Palmer, P. W. Noble, and D. R. Goldstein, "The role of hyaluronan degradation products as innate alloimmune agonists," *Am. J. Transplant.,* vol. 6, pp. 2622-35, 2006.

[108] C. A. Da Silva, C. Chalouni, A. Williams, D. Hartl, C. G. Lee, and J. A. Elias, "Chitin is a size-dependent regulator of macrophage TNF and IL-10 production," *J. Immunol.,* vol. 182, pp. 3573-82, 2009.

[109] J. Park and J. E. Babensee, "Differential functional effects of biomaterials on dendritic cell maturation," *Acta Biomater.,* vol. 8, pp. 3606-3617, 2012.

[110] F. Martinon, A. Mayor, and J. Tschopp, "The Inflammasomes: Guardians of the Body," *Annu. Rev. Immunol.,* vol. 27, pp. 229-265, 2009.

[111] C. C. Termeer, J. Hennies, U. Voith, T. Ahrens, J. M. Weiss, P. Prehm, and J. C. Simon, "Oligosaccharides of Hyaluronan Are Potent Activators of Dendritic Cells," *J. Immunol.,* vol. 165, pp. 1863-1870, 2000.

[112] C. Termeer, F. Benedix, J. Sleeman, C. Fieber, U. Voith, T. Ahrens, K. Miyake, M. Freudenberg, C. Galanos, and J. C. Simon, "Oligosaccharides of Hyaluronan Activate Dendritic Cells via Toll-like Receptor 4," *J. Exp. Med.,* vol. 195, pp. 99-111, 2002.

[113] K. A. Scheibner, M. A. Lutz, S. Boodoo, M. J. Fenton, J. D. Powell, and M. R. Horton, "Hyaluronan Fragments Act as an Endogenous Danger Signal by Engaging TLR2," *J. Immunol.,* vol. 177, pp. 1272-1281, 2006.

[114] J. E. Rayahin, J. S. Buhrman, Y. Zhang, T. J. Koh, and R. A. Gemeinhart, "High and Low Molecular Weight Hyaluronic Acid Differentially Influence Macrophage Activation," *ACS Biomaterials Science & Engineering,* vol. 1, pp. 481-493, 2015.

[115] N. Benne, J. van Duijn, J. Kuiper, W. Jiskoot, and B. Slütter, "Orchestrating immune responses: How size, shape and rigidity affect the immunogenicity of particulate vaccines," *Journal of Controlled Release,* vol. 234, pp. 124-134, 2016.

[116] O. Veiseh, J. C. Doloff, M. Ma, A. J. Vegas, H. H. Tam, A. R. Bader, J. Li, E. Langan, J. Wyckoff, W. S. Loo, S. Jhunjhunwala, A. Chiu, S. Siebert, K. Tang, J. Hollister-Lock, S. Aresta-Dasilva, M. Bochenek, J. Mendoza-Elias, Y. Wang, M. Qi, D. M. Lavin, M. Chen, N. Dholakia, R. Thakrar, I. Lacik, G. C. Weir, J. Oberholzer, D. L. Greiner, R. Langer, and D. G. Anderson, "Size- and shape-dependent foreign body immune response to materials implanted in rodents and non-human primates," *Nat Mater,* vol. 14, pp. 643-651, 2015.

[117] V. B. Joshi, A. Adamcakova-Dodd, X. Jing, A. Wongrakpanich, K. N. Gibson-Corley, P. S. Thorne, and A. K. Salem, "Development of a Poly (lactic-co-glycolic acid) Particle Vaccine to Protect Against House Dust Mite Induced Allergy," *The AAPS Journal,* vol. 16, pp. 975-985, 2014.

[118] S. Gallorini, F. Berti, P. Parente, R. Baronio, S. Aprea, U. D'Oro, M. Pizza, J. L. Telford, and A. Wack, "Introduction of zwitterionic motifs into bacterial polysaccharides generates TLR2 agonists able to activate APCs," *J. Immunol.,* vol. 179, pp. 8208-15, 2007.

[119] S. Neumann, K. Burkert, R. Kemp, T. Rades, P. Rod Dunbar, and S. Hook, "Activation of the NLRP3 inflammasome is not a feature of all particulate vaccine adjuvants," *Immunol Cell Biol,* vol. 92, pp. 535-42, 2014.

[120] D. F. Moyano, M. Goldsmith, D. J. Solfiell, D. Landesman-Milo, O. R. Miranda, D. Peer, and V. M. Rotello, "Nanoparticle Hydrophobicity Dictates Immune Response," *J. Am. Chem. Soc.,* vol. 134, pp. 3965-3967, 2012.

[121] C. A. Vaine, M. K. Patel, J. Zhu, E. Lee, R. W. Finberg, R. C. Hayward, and E. A. Kurt-Jones, "Tuning innate immune activation by surface texturing of polymer microparticles: the role of shape in inflammasome activation," *J Immunol,* vol. 190, pp. 3525-32, 2013.

[122] S. Kumar, A. C. Anselmo, A. Banerjee, M. Zakrewsky, and S. Mitragotri, "Shape and size-dependent immune response to antigen-carrying nanoparticles," *J Control Release,* vol. 220, pp. 141-8, 2015.

[123] S.-Y. Seong and P. Matzinger, "Hydrophobicity: an ancient damage-associated molecular pattern that initiates innate immune responses," *Nat. Rev. Immunol.,* vol. 4, pp. 469-478, 2004.

[124] R. Maitra, C. C. Clement, G. M. Crisi, N. Cobelli, and L. Santambrogio, "Immunogenecity of Modified Alkane Polymers Is Mediated through TLR1/2 Activation," *PLoS ONE,* vol. 3, p. e2438, 2008.

[125] J. E. Babensee, "Interaction of dendritic cells with biomaterials," *Sem. Immunol.,* vol. 20, pp. 101-108, 2008.

[126] J. C. Sunshine, D. Y. Peng, and J. J. Green, "Uptake and Transfection with Polymeric Nanoparticles Are Dependent on Polymer End-Group Structure, but Largely Independent of Nanoparticle Physical and Chemical Properties," *Mol. Pharm.,* vol. 9, pp. 3375-3383, 2012.

[127] G. M. Lynn, R. Laga, P. A. Darrah, A. S. Ishizuka, A. J. Balaci, A. E. Dulcey, M. Pechar, R. Pola, M. Y. Gerner, A. Yamamoto, C. R. Buechler, K. M. Quinn, M. G. Smelkinson, O. Vanek, R. Cawood, T. Hills, O. Vasalatiy, K.

Kastenmuller, J. R. Francica, L. Stutts, J. K. Tom, K. A. Ryu, A. P. Esser-Kahn, T. Etrych, K. D. Fisher, L. W. Seymour, and R. A. Seder, "In vivo characterization of the physicochemical properties of polymer-linked TLR agonists that enhance vaccine immunogenicity," *Nat Biotech*, vol. 33, pp. 1201-1210, 2015.

[128] W. A. Li, B. Y. Lu, L. Gu, Y. Choi, J. Kim, and D. J. Mooney, "The effect of surface modification of mesoporous silica micro-rod scaffold on immune cell activation and infiltration," *Biomaterials*, vol. 83, pp. 249-256, 2016.

[129] D. M. Lynn and R. Langer, "Degradable Poly(β-amino esters): Synthesis, Characterization, and Self-Assembly with Plasmid DNA," *J. Am. Chem. Soc.*, vol. 122, pp. 10761-10768, 2000.

[130] D. M. Lynn, M. M. Amiji, and R. Langer, "pH-Responsive Polymer Microspheres: Rapid Release of Encapsulated Material within the Range of Intracellular pH," *Angew. Chem. Int. Ed.*, vol. 40, pp. 1707-1710, 2001.

[131] A. Akinc, D. M. Lynn, D. G. Anderson, and R. Langer, "Parallel Synthesis and Biophysical Characterization of a Degradable Polymer Library for Gene Delivery," *J. Am. Chem. Soc.*, vol. 125, pp. 5316-5323, 2003.

[132] C. M. Jewell, J. Zhang, N. J. Fredin, and D. M. Lynn, "Multilayered polyelectrolyte films promote the direct and localized delivery of DNA to cells," *J. Control. Release*, vol. 106, pp. 214-223, 2005.

[133] J. Zhang, S. I. Montañez, C. M. Jewell, and D. M. Lynn, "Multilayered Films Fabricated from Plasmid DNA and a Side-Chain Functionalized Poly(β-amino Ester): Surface-Type Erosion and Sequential Release of Multiple Plasmid Constructs from Surfaces," *Langmuir*, vol. 23, pp. 11139-11146, 2007.

[134] C. M. Jewell and D. M. Lynn, "Multilayered polyelectrolyte assemblies as platforms for the delivery of DNA and other nucleic acid-based therapeutics," *Adv. Drug Deliv. Rev.*, vol. 60, pp. 979-999, 2008.

[135] J. J. Green, R. Langer, and D. G. Anderson, "A Combinatorial Polymer Library Approach Yields Insight into Nonviral Gene Delivery," *Acc. Chem. Res.*, vol. 41, pp. 749-759, 2008.

[136] S. Ganta, H. Devalapally, A. Shahiwala, and M. Amiji, "A review of stimuli-responsive nanocarriers for drug and gene delivery," *J. Control. Release*, vol. 126, pp. 187-204, 2008.

[137] D. N. Nguyen, J. J. Green, J. M. Chan, R. Langer, and D. G. Anderson, "Polymeric Materials for Gene Delivery and DNA Vaccination," *Adv. Mater.*, vol. 21, pp. 847-867, 2009.

[138] S. L. Bechler and D. M. Lynn, "Design and synthesis of a fluorescently end-labeled poly(β-amino ester): Application to the characterization of degradable polyelectrolyte multilayers," *J. Polym. Sci. A Polym. Chem.*, vol. 49, pp. 1572-1581, 2011.

[139] S. L. Bechler and D. M. Lynn, "Reactive Polymer Multilayers Fabricated by Covalent Layer-by-Layer Assembly: 1,4-Conjugate Addition-Based Approaches to the Design of Functional Biointerfaces," *Biomacromolecules*, vol. 13, pp. 1523-1532, 2012.

[140] S. L. Bechler and D. M. Lynn, "Characterization of Degradable Polyelectrolyte Multilayers Fabricated Using DNA and a Fluorescently-Labeled Poly(β-amino ester): Shedding Light on the Role of the Cationic Polymer in Promoting Surface-Mediated Gene Delivery," *Biomacromolecules*, vol. 13, pp. 542-552, 2012.

[141] M. Keeney, S.-G. Ong, A. Padilla, Z. Yao, S. Goodman, J. C. Wu, and F. Yang, "Development of Poly(β-amino ester)-Based Biodegradable Nanoparticles for Nonviral Delivery of Minicircle DNA," *ACS Nano*, vol. 7, pp. 7241-7250, 2013.

[142] S. R. Little, D. M. Lynn, Q. Ge, D. G. Anderson, S. V. Puram, J. Chen, H. N. Eisen, and R. Langer, "Poly-β amino ester-containing microparticles enhance the activity of nonviral genetic vaccines," *Proc. Natl. Acad. Sci. U.S.A.*, vol. 101, pp. 9534-9539, 2004.

[143] S. R. Little, D. M. Lynn, S. V. Puram, and R. Langer, "Formulation and characterization of poly (β amino ester) microparticles for genetic vaccine delivery," *J. Control. Release*, vol. 107, pp. 449-462, 2005.

[144] X. F. Su, J. Fricke, D. G. Kavanagh, and D. J. Irvine, "In Vitro and in Vivo mRNA Delivery Using Lipid-Enveloped pH-Responsive Polymer Nanoparticles," *Mol. Pharm.*, vol. 8, pp. 774-787, 2011.

[145] P. C. DeMuth, J. J. Moon, H. Suh, P. T. Hammond, and D. J. Irvine, "Releasable Layer-by-Layer Assembly of Stabilized Lipid Nanocapsules on Microneedles for Enhanced Transcutaneous Vaccine Delivery," *ACS Nano*, vol. 6, pp. 8041-8051, 2012.

[146] H. Guerrero-Cázares, S. Y. Tzeng, N. P. Young, A. O. Abutaleb, A. Quiñones-Hinojosa, and J. J. Green, "Biodegradable Polymeric Nanoparticles Show High Efficacy and Specificity at DNA Delivery to Human Glioblastoma in Vitro and in Vivo," *ACS Nano*, vol. 8, pp. 5141-5153, 2014.

[147] K. L. Kozielski, S. Y. Tzeng, B. A. Hurtado De Mendoza, and J. J. Green, "Bioreducible Cationic Polymer-Based Nanoparticles for Efficient and Environmentally Triggered Cytoplasmic siRNA Delivery to Primary Human Brain Cancer Cells," *ACS Nano,* vol. 8, pp. 3232-3241, 2014.

[148] C. H. Jones, M. Chen, A. Ravikrishnan, R. Reddinger, G. Zhang, A. P. Hakansson, and B. A. Pfeifer, "Mannosylated poly(beta-amino esters) for targeted antigen presenting cell immune modulation," *Biomaterials,* vol. 37, pp. 333-344, 2015.

[149] I. S. Grewal and R. A. Flavell, "CD40 and CD154 in Cell-mediated Immunity," *Annual Review of Immunology,* vol. 16, pp. 111-135, 1998.

[150] J. a. Charles A. Janeway and R. Medzhitov, "INNATE IMMUNE RECOGNITION," *Annual Review of Immunology,* vol. 20, pp. 197-216, 2002.

[151] S. W. Van Gool, P. Vandenberghe, M. d. Boer, and J. L. Ceuppens, "CD80, CD86 and CD40 Provide Accessory Signals in a Multiple-Step T-Cell Activation Model," *Immunological Reviews,* vol. 153, pp. 47-83, 1996.

[152] I. S. Grewal and R. A. Flavell, "The Role of CD40 Ligand in Costimulation and T-Cell Activation," *Immunological Reviews,* vol. 153, pp. 85-106, 1996.

[153] J. Banchereau, F. Briere, C. Caux, J. Davoust, S. Lebecque, Y.-J. Liu, B. Pulendran, and K. Palucka, "Immunobiology of Dendritic Cells," *Annu. Rev. Immunol.,* vol. 18, pp. 767-811, 2000.

[154] A. E. Nel, L. Mädler, D. Velegol, T. Xia, E. M. V. Hoek, P. Somasundaran, F. Klaessig, V. Castranova, and M. Thompson, "Understanding biophysicochemical interactions at the nano–bio interface," *Nat. Mater.,* vol. 8, pp. 543-557, 2009.

[155] C. J. Bishop, T.-M. Ketola, S. Y. Tzeng, J. C. Sunshine, A. Urtti, H. Lemmetyinen, E. Vuorimaa-Laukkanen, M. Yliperttula, and J. J. Green, "The Effect and Role of Carbon Atoms in Poly(β-amino ester)s for DNA Binding and Gene Delivery," *J. Am. Chem. Soc.,* vol. 135, pp. 6951-6957, 2013.

[156] P. Matzinger, "The Danger Model: A Renewed Sense of Self," *Science,* vol. 296, pp. 301-305, 2002.

[157] J. E. Babensee and A. Paranjpe, "Differential levels of dendritic cell maturation on different biomaterials used in combination products," *J Biomed Mater Res A,* vol. 74, pp. 503-10, 2005.

[158] Y. C. Chiu, J. M. Gammon, J. I. Andorko, L. H. Tostanoski, and C. M. Jewell, "Modular Vaccine Design Using Carrier-Free Capsules Assembled from

Polyionic Immune Signals," *ACS Biomater Sci Eng,* vol. 1, pp. 1200-1205, 2015.

[159] P. Zhang, Y. C. Chiu, L. H. Tostanoski, and C. M. Jewell, "Polyelectrolyte Multilayers Assembled Entirely from Immune Signals on Gold Nanoparticle Templates Promote Antigen-Specific T Cell Response," *ACS Nano,* vol. 9, pp. 6465-77, 2015.

[160] L. H. Tostanoski, Y. C. Chiu, J. I. Andorko, M. Guo, X. Zeng, P. Zhang, W. Royal, 3rd, and C. M. Jewell, "Design of Polyelectrolyte Multilayers to Promote Immunological Tolerance," *ACS Nano,* 2016.

[161] Y. C. Chiu, J. M. Gammon, J. I. Andorko, L. H. Tostanoski, and C. M. Jewell, "Assembly and Immunological Processing of Polyelectrolyte Multilayers Composed of Antigens and Adjuvants," *ACS Appl Mater Interfaces,* vol. 8, pp. 18722-31, 2016.

[162] P. Zhang, J. I. Andorko, and C. M. Jewell, "Impact of dose, route, and composition on the immunogenicity of immune polyelectrolyte multilayers delivered on gold templates," *Biotechnol Bioeng,* 2016.

[163] J. I. Andorko, K. L. Hess, K. G. Pineault, and C. M. Jewell, "Intrinsic immunogenicity of rapidly-degradable polymers evolves during degradation," *Acta Biomaterialia,* vol. 32, pp. 24-34, 2016.

[164] X. Cai, M. Liu, C. Zhang, D. Sun, and G. Zhai, "pH-responsive copolymers based on pluronic P123-poly(β-amino ester): Synthesis, characterization and application of copolymer micelles," *Colloids and Surfaces B: Biointerfaces,* vol. 142, pp. 114-122, 2016.

[165] D. Zhou, L. Cutlar, Y. Gao, W. Wang, J. O'Keeffe-Ahern, S. McMahon, B. Duarte, F. Larcher, B. J. Rodriguez, U. Greiser, and W. Wang, "The transition from linear to highly branched poly(β-amino ester)s: Branching matters for gene delivery," *Science Advances,* vol. 2, 2016.

[166] A. C. Anselmo, C. L. Modery-Pawlowski, S. Menegatti, S. Kumar, D. R. Vogus, L. L. Tian, M. Chen, T. M. Squires, A. Sen Gupta, and S. Mitragotri, "Platelet-like Nanoparticles: Mimicking Shape, Flexibility, and Surface Biology of Platelets To Target Vascular Injuries," *ACS Nano,* vol. 8, pp. 11243-11253, 2014.

[167] A. Banerjee, J. Qi, R. Gogoi, J. Wong, and S. Mitragotri, "Role of nanoparticle size, shape and surface chemistry in oral drug delivery," *Journal of Controlled Release,* vol. 238, pp. 176-185, 2016.

[168] M. Rescigno, M. Martino, C. L. Sutherland, M. R. Gold, and P. Ricciardi-Castagnoli, "Dendritic Cell Survival and Maturation Are Regulated by Different Signaling Pathways," *The Journal of Experimental Medicine,* vol. 188, pp. 2175-2180, 1998.

[169] G. Senti, B. M. Prinz Vavricka, I. Erdmann, M. I. Diaz, R. Markus, S. J. McCormack, J. J. Simard, B. Wuthrich, R. Crameri, N. Graf, P. Johansen, and T. M. Kundig, "Intralymphatic allergen administration renders specific immunotherapy faster and safer: a randomized controlled trial," *Proc Natl Acad Sci U S A,* vol. 105, pp. 17908-12, 2008.

[170] P. Johansen, T. Storni, L. Rettig, Z. Qiu, A. Der-Sarkissian, K. A. Smith, V. Manolova, K. S. Lang, G. Senti, B. Mullhaupt, T. Gerlach, R. F. Speck, A. Bot, and T. M. Kundig, "Antigen kinetics determines immune reactivity," *Proceedings of the National Academy of Sciences of the United States of America,* vol. 105, pp. 5189-94, 2008.

[171] G. J. Randolph, V. Angeli, and M. A. Swartz, "Dendritic-cell trafficking to lymph nodes through lymphatic vessels," *Nat Rev Immunol,* vol. 5, pp. 617-28, 2005.

[172] D. J. Irvine and C. M. Jewell, "Vaccine and Immunotherapy Delivery," in *Comprehensive Biomaterials*, P. Ducheyne, K. Healy, D. E. Hutmacher, D. W. Garinger, and C. J. Kirkpatrick, Eds., ed, 2011.

[173] J. J. Moon, B. Huang, and D. J. Irvine, "Engineering Nano- and Microparticles to Tune Immunity," *Advanced Materials,* vol. 24, pp. 3724-3746, 2012.

[174] S. T. Reddy, A. J. van der Vlies, E. Simeoni, C. P. O'Neil, M. A. Swartz, and J. A. Hubbell, "Exploiting lymphatic transport and complement activation in nanoparticle vaccines," *Tissue Engineering Part A,* vol. 14, pp. 734-735, 2008.

[175] P. Johansen, A. C. Haffner, E. Koch, K. Zepter, L. Erdmann, K. Maloy, J. J. Simard, T. Storni, G. Senti, A. Bot, B. Wuthrich, and T. M. Kundig, "Direct intralymphatic injection of peptide vaccines enhances immunogenicity," *European Journal of Immunology,* vol. 35, pp. 568-574, 2005.

[176] D. Mohanan, B. Slutter, M. Henriksen-Lacey, W. Jiskoot, J. A. Bouwstra, Y. Perrie, T. M. Kundig, B. Gander, and P. Johansen, "Administration routes affect the quality of immune responses: A cross-sectional evaluation of particulate antigen-delivery systems," *J Control Release,* vol. 147, pp. 342-9, 2010.

[177] A. Bershteyn, J. Chaparro, R. Yau, M. Kim, E. Reinherz, L. Ferreira-Moita, and D. J. Irvine, "Polymer-supported lipid shells, onions, and flowers," *Soft Matter,* vol. 4, pp. 1787-1791, 2008.

[178] M. I. Harrell, B. M. Iritani, and A. Ruddell, "Lymph node mapping in the mouse," *J Immunol Methods,* vol. 332, pp. 170-4, 2008.

[179] J. I. Andorko, K. G. Pineault, and C. M. Jewell, "Impact of molecular weight on the intrinsic immunogenic activity of poly(beta amino esters)," *Journal of Biomedical Materials Research Part A,* vol. 105, pp. 1219-1229, 2017.

[180] J. M. Anderson and M. S. Shive, "Biodegradation and biocompatibility of PLA and PLGA microspheres," *Advanced Drug Delivery Reviews,* vol. 28, pp. 5-24, 1997.

[181] F. Danhier, E. Ansorena, J. M. Silva, R. Coco, A. Le Breton, and V. Preat, "PLGA-based nanoparticles: an overview of biomedical applications," *J Control Release,* vol. 161, pp. 505-22, 2012.

[182] M. S. Shive and J. M. Anderson, "Biodegradation and biocompatibility of PLA and PLGA microspheres," *Adv Drug Deliv Rev,* vol. 28, pp. 5-24, 1997.

[183] J. G. Crompton, M. Sukumar, and N. P. Restifo, "Uncoupling T-cell expansion from effector differentiation in cell-based immunotherapy," *Immunological Reviews,* vol. 257, pp. 264-276, 2014.

[184] G. T. Motz and G. Coukos, "Deciphering and Reversing Tumor Immune Suppression," *Immunity,* vol. 39, pp. 61-73, 2013.

[185] M. I. Barria, J. L. Garrido, C. Stein, E. Scher, Y. C. Ge, S. M. Engel, T. A. Kraus, D. Banach, and T. M. Moran, "Localized Mucosal Response to Intranasal Live Attenuated Influenza Vaccine in Adults," *Journal of Infectious Diseases,* vol. 207, pp. 115-124, 2013.

[186] A. Bagchi, E. A. Herrup, H. S. Warren, J. Trigilio, H. S. Shin, C. Valentine, and J. Hellman, "MyD88-dependent and MyD88-independent pathways in synergy, priming, and tolerance between TLR agonists," *Journal of Immunology,* vol. 178, pp. 1164-1171, 2007.

[187] S. P. Kasturi, I. Skountzou, R. A. Albrecht, D. Koutsonanos, T. Hua, H. I. Nakaya, R. Ravindran, S. Stewart, M. Alam, M. Kwissa, F. Villinger, N. Murthy, J. Steel, J. Jacob, R. J. Hogan, A. Garcia-Sastre, R. Compans, and B. Pulendran, "Programming the magnitude and persistence of antibody responses with innate immunity," *Nature,* vol. 470, pp. 543-U136, 2011.

[188] K. Timmermans, T. S. Plantinga, M. Kox, M. Vaneker, G. J. Scheffer, G. J. Adema, L. A. B. Joosten, and M. G. Netea, "Blueprints of Signaling Interactions between Pattern Recognition Receptors: Implications for the Design of Vaccine Adjuvants," *Clinical and Vaccine Immunology,* vol. 20, pp. 427-432, 2013.

[189] J. K. Tom, R. J. Mancini, and A. P. Esser-Kahn, "Covalent modification of cell surfaces with TLR agonists improves & directs immune stimulation," *Chemical Communications,* vol. 49, pp. 9618-9620, 2013.

[190] Q. Zhu, C. Egelston, S. Gagnon, Y. J. Sui, I. M. Belyakov, D. M. Klinman, and J. A. Berzofsky, "Using 3 TLR ligands as a combination adjuvant induces qualitative changes in T cell responses needed for antiviral protection in mice," *Journal of Clinical Investigation,* vol. 120, pp. 607-616, 2010.

[191] H. P. Liu, K. D. Moynihan, Y. R. Zheng, G. L. Szeto, A. V. Li, B. Huang, D. S. Van Egeren, C. Park, and D. J. Irvine, "Structure-based programming of lymph-node targeting in molecular vaccines," *Nature,* vol. 507, pp. 519-+, 2014.

[192] V. B. Joshi, S. M. Geary, B. R. Carrillo-Conde, B. Narasimhan, and A. K. Salem, "Characterizing the antitumor response in mice treated with antigen-loaded polyanhydride microparticles," *Acta Biomaterialia,* vol. 9, pp. 5583-5589, 2013.

[193] J. J. Moon, H. Suh, A. Bershteyn, M. T. Stephan, H. P. Liu, B. Huang, M. Sohail, S. Luo, S. H. Um, H. Khant, J. T. Goodwin, J. Ramos, W. Chiu, and D. J. Irvine, "Interbilayer-crosslinked multilamellar vesicles as synthetic vaccines for potent humoral and cellular immune responses," *Nature Materials,* vol. 10, pp. 243-251, 2011.

[194] M. C. Hanson, M. P. Crespo, W. Abraham, K. D. Moynihan, G. L. Szeto, S. H. Chen, M. B. Melo, S. Mueller, and D. J. Irvine, "Nanoparticulate STING agonists are potent lymph node-targeted vaccine adjuvants," *J Clin Invest,* vol. 125, pp. 2532-46, 2015.

[195] B. Slutter, S. M. Bal, Z. Ding, W. Jiskoot, and J. A. Bouwstra, "Adjuvant effect of cationic liposomes and CpG depends on administration route," *Journal of Controlled Release,* vol. 154, pp. 123-130, 2011.

[196] V. Jerome, A. Graser, R. Muller, R. E. Kontermann, and A. Konur, "Cytotoxic T lymphocytes responding to low dose TRP2 antigen are induced against B16 melanoma by liposome-encapsulated TRP2 peptide and CpG DNA adjuvant," *Journal of Immunotherapy,* vol. 29, pp. 294-305, 2006.

[197] S. T. Reddy, A. J. van der Vlies, E. Simeoni, V. Angeli, G. J. Randolph, C. P. O'Neill, L. K. Lee, M. A. Swartz, and J. A. Hubbell, "Exploiting lymphatic transport and complement activation in nanoparticle vaccines," *Nature Biotechnology,* vol. 25, pp. 1159-1164, 2007.

[198] J. I. Andorko, K. L. Hess, K. G. Pineault, and C. M. Jewell, "Intrinsic immunogenicity of rapidly-degradable polymers evolves during degradation," *Acta Biomater,* vol. 32, pp. 24-34, 2016.

[199] J. Park and J. E. Babensee, "Differential functional effects of biomaterials on dendritic cell maturation," *Acta Biomaterialia,* vol. 8, pp. 3606-3617, 2012.

[200] F. A. Sharp, D. Ruane, B. Claass, E. Creagh, J. Harris, P. Malyala, M. Singh, D. T. O'Hagan, V. Petrilli, J. Tschopp, L. A. J. O'Neill, and E. C. Lavelle, "Uptake of particulate vaccine adjuvants by dendritic cells activates the NALP3 inflammasome," *Proceedings of the National Academy of Sciences of the United States of America,* vol. 106, pp. 870-875, 2009.

[201] M. R. Parkhurst, E. B. Fitzgerald, S. Southwood, A. Sette, S. A. Rosenberg, and Y. Kawakami, "Identification of a shared HLA-A*0201-restricted T-cell epitope from the melanoma antigen tyrosinase-related protein 2 (TRP2)," *Cancer Res,* vol. 58, pp. 4895-901, 1998.

[202] A. de Titta, M. Ballester, Z. Julier, C. Nembrini, L. Jeanbart, A. J. van der Vlies, M. A. Swartz, and J. A. Hubbell, "Nanoparticle conjugation of CpG enhances adjuvancy for cellular immunity and memory recall at low dose," *Proceedings of the National Academy of Sciences of the United States of America,* vol. 110, pp. 19902-19907, 2013.

[203] W. W. Overwijk, M. R. Theoret, S. E. Finkelstein, D. R. Surman, L. A. de Jong, F. A. Vyth-Dreese, T. A. Dellemijn, P. A. Antony, P. J. Spiess, D. C. Palmer, D. M. Heimann, C. A. Klebanoff, Z. Y. Yu, L. N. Hwang, L. Feigenbaum, A. M. Kruisbeek, S. A. Rosenberg, and N. P. Restifo, "Tumor regression and autoimmunity after reversal of a functionally tolerant state of self-reactive CD8+ T cells," *Journal of Experimental Medicine,* vol. 198, pp. 569-580, 2003.

[204] C. A. Klebanoff, L. Gattinoni, D. C. Palmer, P. Muranski, Y. Ji, C. S. Hinrichs, Z. A. Borman, S. P. Kerkar, C. D. Scott, S. E. Finkelstein, S. A. Rosenberg, and N. P. Restifo, "Determinants of Successful CD8(+) T-Cell Adoptive Immunotherapy for Large Established Tumors in Mice," *Clinical Cancer Research,* vol. 17, pp. 5343-5352, 2011.

[205] G. G. Kenter, M. J. Welters, A. R. Valentijn, M. J. Lowik, D. M. Berends-van der Meer, A. P. Vloon, F. Essahsah, L. M. Fathers, R. Offringa, J. W. Drijfhout, A. R. Wafelman, J. Oostendorp, G. J. Fleuren, S. H. van der Burg,

and C. J. Melief, "Vaccination against HPV-16 oncoproteins for vulvar intraepithelial neoplasia," *N Engl J Med,* vol. 361, pp. 1838-47, 2009.

[206] T. Y. H. Wu, M. Singh, A. T. Miller, E. De Gregorio, F. Doro, U. D'Oro, D. A. G. Skibinski, M. L. Mbow, S. Bufali, A. E. Herman, A. Cortez, Y. Li, B. P. Nayak, E. Tritto, C. M. Filippi, G. R. Otten, L. A. Brito, E. Monaci, C. Li, S. Aprea, S. Valentini, S. Calabro, D. Laera, B. Brunelli, E. Caproni, P. Malyala, R. G. Panchal, T. K. Warren, S. Bavari, D. T. O'Hagan, M. P. Cooke, and N. M. Valiante, "Rational design of small molecules as vaccine adjuvants," *Science Translational Medicine,* vol. 6, 2014.

[207] G. J. Randolph, V. Angeli, and M. A. Swartz, "Dendritic-cell trafficking to lymph nodes through lymphatic vessels," *Nature Reviews. Immunology,* vol. 5, pp. 617-28, 2005.

[208] R. Noubade, K. Wong, N. Ota, S. Rutz, C. Eidenschenk, P. A. Valdez, J. Ding, I. Peng, A. Sebrell, P. Caplazi, J. DeVoss, R. H. Soriano, T. Sai, R. Lu, Z. Modrusan, J. Hackney, and W. Ouyang, "NRROS negatively regulates reactive oxygen species during host defence and autoimmunity," *Nature,* vol. 509, pp. 235-239, 2014.

[209] R. M. Zinkernagel, S. Ehl, P. Aichele, S. Oehen, T. Kündig, and H. Hengartner, "Antigen localisation regulates immune responses in a dose- and time-dependent fashion: a geographical view of immune reactivity," *Immunological Reviews,* vol. 156, pp. 199-209, 1997.

[210] B. Pulendran and R. Ahmed, "Immunological mechanisms of vaccination," *Nature Immunology,* vol. 12, pp. 509-517, 2011.

[211] P. Johansen, T. Storni, L. Rettig, Z. Qiu, A. Der-Sarkissian, K. A. Smith, V. Manolova, K. S. Lang, G. Senti, B. Mullhaupt, T. Gerlach, R. F. Speck, A. Bot, and T. M. Kundig, "Antigen kinetics determines immune reactivity," *Proc Natl Acad Sci U S A,* vol. 105, pp. 5189-94, 2008.

[212] B. Dankbar, K. Neugebauer, C. Wunrau, C. O. Tibesku, A. Skwara, T. Pap, and S. Fuchs-Winkelmann, "Hepatocyte growth factor induction of macrophage chemoattractant protein-1 and osteophyte-inducing factors in osteoarthritis," *Journal of Orthopaedic Research,* vol. 25, pp. 569-577, 2007.

[213] I. Miconnet, S. Koenig, D. Speiser, A. Krieg, P. Guillaume, J. C. Cerottini, and P. Romero, "CpG are efficient Adjuvants for specific CTL induction against tumor antigen-derived peptide," *Journal of Immunology,* vol. 168, pp. 1212-1218, 2002.

[214] R. D. Schreiber, L. J. Old, and M. J. Smyth, "Cancer Immunoediting: Integrating Immunity's Roles in Cancer Suppression and Promotion," *Science,* vol. 331, pp. 1565-1570, 2011.

[215] S. Hirosue, I. C. Kourtis, A. J. van der Vlies, J. A. Hubbell, and M. A. Swartz, "Antigen delivery to dendritic cells by poly(propylene sulfide) nanoparticles with disulfide conjugated peptides: Cross-presentation and T cell activation," *Vaccine,* vol. 28, pp. 7897-7906, 2010.

[216] M. Kovacsovicsbankowski and K. L. Rock, "A Phagosome-to-Cytosol Pathway for Exogenous Antigens Presented on Mhc Class-I Molecules," *Science,* vol. 267, pp. 243-246, 1995.

[217] Y. A. Alpizar, B. Chain, M. K. Collins, J. Greenwood, D. Katz, H. J. Stauss, and N. A. Mitchison, "Ten years of progress in vaccination against cancer: the need to counteract cancer evasion by dual targeting in future therapies," *Cancer Immunol Immunother,* vol. 60, pp. 1127-35, 2011.

[218] L. Delamarre, I. Mellman, and M. Yadav, "Cancer immunotherapy. Neo approaches to cancer vaccines," *Science,* vol. 348, pp. 760-1, 2015.

[219] E. Vacchelli, A. Eggermont, C. Sautes-Fridman, J. Galon, L. Zitvogel, G. Kroemer, and L. Galluzzi, "Trial Watch: Toll-like receptor agonists for cancer therapy," *Oncoimmunology,* vol. 2, p. e25238, 2013.

[220] F. Aranda, E. Vacchelli, F. Obrist, A. Eggermont, J. Galon, C. Sautes-Fridman, I. Cremer, J. Henrik Ter Meulen, L. Zitvogel, G. Kroemer, and L. Galluzzi, "Trial Watch: Toll-like receptor agonists in oncological indications," *Oncoimmunology,* vol. 3, p. e29179, 2014.

[221] A. Ribas, J. S. Weber, B. Chmielowski, B. Comin-Anduix, D. Lu, M. Douek, N. Ragavendra, S. Raman, E. Seja, D. Rosario, S. Miles, D. C. Diamond, Z. Qiu, M. Obrocea, and A. Bot, "Intra-lymph node prime-boost vaccination against Melan A and tyrosinase for the treatment of metastatic melanoma: results of a phase 1 clinical trial," *Clin Cancer Res,* vol. 17, pp. 2987-96, 2011.

[222] J. G. Crompton, D. Clever, R. Vizcardo, M. Rao, and N. P. Restifo, "Reprogramming antitumor immunity," *Trends Immunol,* vol. 35, pp. 178-85, 2014.

[223] T. Hiura, H. Kagamu, S. Miura, A. Ishida, H. Tanaka, J. Tanaka, F. Gejyo, and H. Yoshizawa, "Both regulatory T cells and antitumor effector T cells are primed in the same draining lymph nodes during tumor progression," *Journal of Immunology,* vol. 175, pp. 5058-5066, 2005.

[224] M. P. Colombo and S. Piconese, "Regulatory T-cell inhibition versus depletion: the right choice in cancer immunotherapy," *Nature Reviews Cancer,* vol. 7, pp. 880-887, 2007.

[225] D. M. Pardoll, "The blockade of immune checkpoints in cancer immunotherapy," *Nature Reviews Cancer,* vol. 12, pp. 252-264, 2012.

[226] P. Sharma and J. P. Allison, "Immune Checkpoint Targeting in Cancer Therapy: Toward Combination Strategies with Curative Potential," *Cell,* vol. 161, pp. 205-214, 2015.

[227] S. A. Joosse, T. M. Gorges, and K. Pantel, "Biology, detection, and clinical implications of circulating tumor cells," *EMBO Mol Med,* vol. 7, pp. 1-11, 2015.

[228] M. Cristofanilli, G. T. Budd, M. J. Ellis, A. Stopeck, J. Matera, M. C. Miller, J. M. Reuben, G. V. Doyle, W. J. Allard, L. W. Terstappen, and D. F. Hayes, "Circulating tumor cells, disease progression, and survival in metastatic breast cancer," *N Engl J Med,* vol. 351, pp. 781-91, 2004.

[229] M. G. Krebs, R. Sloane, L. Priest, L. Lancashire, J. M. Hou, A. Greystoke, T. H. Ward, R. Ferraldeschi, A. Hughes, G. Clack, M. Ranson, C. Dive, and F. H. Blackhall, "Evaluation and prognostic significance of circulating tumor cells in patients with non-small-cell lung cancer," *J Clin Oncol,* vol. 29, pp. 1556-63, 2011.

[230] M. Yu, S. Stott, M. Toner, S. Maheswaran, and D. A. Haber, "Circulating tumor cells: approaches to isolation and characterization," *J Cell Biol,* vol. 192, pp. 373-82, 2011.

[231] S. L. Stott, C. H. Hsu, D. I. Tsukrov, M. Yu, D. T. Miyamoto, B. A. Waltman, S. M. Rothenberg, A. M. Shah, M. E. Smas, G. K. Korir, F. P. Floyd, Jr., A. J. Gilman, J. B. Lord, D. Winokur, S. Springer, D. Irimia, S. Nagrath, L. V. Sequist, R. J. Lee, K. J. Isselbacher, S. Maheswaran, D. A. Haber, and M. Toner, "Isolation of circulating tumor cells using a microvortex-generating herringbone-chip," *Proc Natl Acad Sci U S A,* vol. 107, pp. 18392-7, 2010.

[232] M. Yu, A. Bardia, N. Aceto, F. Bersani, M. W. Madden, M. C. Donaldson, R. Desai, H. Zhu, V. Comaills, Z. Zheng, B. S. Wittner, P. Stojanov, E. Brachtel, D. Sgroi, R. Kapur, T. Shioda, D. T. Ting, S. Ramaswamy, G. Getz, A. J. Iafrate, C. Benes, M. Toner, S. Maheswaran, and D. A. Haber, "Cancer therapy. Ex vivo culture of circulating breast tumor cells for individualized testing of drug susceptibility," *Science,* vol. 345, pp. 216-20, 2014.

[233] M. Yu, A. Bardia, B. S. Wittner, S. L. Stott, M. E. Smas, D. T. Ting, S. J. Isakoff, J. C. Ciciliano, M. N. Wells, A. M. Shah, K. F. Concannon, M. C.

Donaldson, L. V. Sequist, E. Brachtel, D. Sgroi, J. Baselga, S. Ramaswamy, M. Toner, D. A. Haber, and S. Maheswaran, "Circulating breast tumor cells exhibit dynamic changes in epithelial and mesenchymal composition," *Science,* vol. 339, pp. 580-4, 2013.

[234] Y. N. Kim, K. H. Koo, J. Y. Sung, U. J. Yun, and H. Kim, "Anoikis resistance: an essential prerequisite for tumor metastasis," *Int J Cell Biol,* vol. 2012, p. 306879, 2012.

[235] A. R. Grassian, J. L. Coloff, and J. S. Brugge, "Extracellular matrix regulation of metabolism and implications for tumorigenesis," *Cold Spring Harb Symp Quant Biol,* vol. 76, pp. 313-24, 2011.

[236] C. Fung, R. Lock, S. Gao, E. Salas, and J. Debnath, "Induction of autophagy during extracellular matrix detachment promotes cell survival," *Mol Biol Cell,* vol. 19, pp. 797-806, 2008.

[237] M. Charpentier and S. Martin, "Interplay of Stem Cell Characteristics, EMT, and Microtentacles in Circulating Breast Tumor Cells," *Cancers (Basel),* vol. 5, pp. 1545-65, 2013.

[238] R. A. Whipple, A. M. Cheung, and S. S. Martin, "Detyrosinated microtubule protrusions in suspended mammary epithelial cells promote reattachment," *Exp Cell Res,* vol. 313, pp. 1326-36, 2007.

[239] J. R. Yoon, R. A. Whipple, E. M. Balzer, E. H. Cho, M. A. Matrone, M. Peckham, and S. S. Martin, "Local anesthetics inhibit kinesin motility and microtentacle protrusions in human epithelial and breast tumor cells," *Breast Cancer Res Treat,* vol. 129, pp. 691-701, 2011.

[240] R. A. Whipple, M. A. Matrone, E. H. Cho, E. M. Balzer, M. I. Vitolo, J. R. Yoon, O. B. Ioffe, K. C. Tuttle, J. Yang, and S. S. Martin, "Epithelial-to-mesenchymal transition promotes tubulin detyrosination and microtentacles that enhance endothelial engagement," *Cancer Res,* vol. 70, pp. 8127-37, 2010.

[241] M. A. Matrone, R. A. Whipple, E. M. Balzer, and S. S. Martin, "Microtentacles tip the balance of cytoskeletal forces in circulating tumor cells," *Cancer Res,* vol. 70, pp. 7737-41, 2010.

[242] E. M. Balzer, R. A. Whipple, K. Thompson, A. E. Boggs, J. Slovic, E. H. Cho, M. A. Matrone, T. Yoneda, S. C. Mueller, and S. S. Martin, "c-Src differentially regulates the functions of microtentacles and invadopodia," *Oncogene,* vol. 29, pp. 6402-8, 2010.

[243] M. A. Matrone, R. A. Whipple, K. Thompson, E. H. Cho, M. I. Vitolo, E. M. Balzer, J. R. Yoon, O. B. Ioffe, K. C. Tuttle, M. Tan, and S. S. Martin, "Metastatic breast tumors express increased tau, which promotes microtentacle formation and the reattachment of detached breast tumor cells," *Oncogene,* vol. 29, pp. 3217-27, 2010.

[244] E. M. Balzer, R. A. Whipple, E. H. Cho, M. A. Matrone, and S. S. Martin, "Antimitotic chemotherapeutics promote adhesive responses in detached and circulating tumor cells," *Breast Cancer Res Treat,* vol. 121, pp. 65-78, 2010.

[245] G.-S. Park, H. Kwon, D. W. Kwak, S. Y. Park, M. Kim, J.-H. Lee, H. Han, S. Heo, X. S. Li, J. H. Lee, Y. H. Kim, J.-G. Lee, W. Yang, H. Y. Cho, S. K. Kim, and K. Kim, "Full Surface Embedding of Gold Clusters on Silicon Nanowires for Efficient Capture and Photothermal Therapy of Circulating Tumor Cells," *Nano Letters,* vol. 12, pp. 1638-1642, 2012.

[246] T. L. Halo, K. M. McMahon, N. L. Angeloni, Y. Xu, W. Wang, A. B. Chinen, D. Malin, E. Strekalova, V. L. Cryns, C. Cheng, C. A. Mirkin, and C. S. Thaxton, "NanoFlares for the detection, isolation, and culture of live tumor cells from human blood," *Proceedings of the National Academy of Sciences,* vol. 111, pp. 17104-17109, 2014.

[247] M. J. Mitchell, C. A. Castellanos, and M. R. King, "Surfactant functionalization induces robust, differential adhesion of tumor cells and blood cells to charged nanotube-coated biomaterials under flow," *Biomaterials,* vol. 56, pp. 179-186, 2015.

[248] A. A. Adams, P. I. Okagbare, J. Feng, M. L. Hupert, D. Patterson, J. Göttert, R. L. McCarley, D. Nikitopoulos, M. C. Murphy, and S. A. Soper, "Highly Efficient Circulating Tumor Cell Isolation from Whole Blood and Label-Free Enumeration Using Polymer-Based Microfluidics with an Integrated Conductivity Sensor," *Journal of the American Chemical Society,* vol. 130, pp. 8633-8641, 2008.

[249] S. L. Stott, C.-H. Hsu, D. I. Tsukrov, M. Yu, D. T. Miyamoto, B. A. Waltman, S. M. Rothenberg, A. M. Shah, M. E. Smas, G. K. Korir, F. P. Floyd, A. J. Gilman, J. B. Lord, D. Winokur, S. Springer, D. Irimia, S. Nagrath, L. V. Sequist, R. J. Lee, K. J. Isselbacher, S. Maheswaran, D. A. Haber, and M. Toner, "Isolation of circulating tumor cells using a microvortex-generating herringbone-chip," *Proceedings of the National Academy of Sciences,* vol. 107, pp. 18392-18397, 2010.

[250] A. F. Sarioglu, N. Aceto, N. Kojic, M. C. Donaldson, M. Zeinali, B. Hamza, A. Engstrom, H. Zhu, T. K. Sundaresan, D. T. Miyamoto, X. Luo, A. Bardia, B. S. Wittner, S. Ramaswamy, T. Shioda, D. T. Ting, S. L. Stott, R. Kapur, S. Maheswaran, D. A. Haber, and M. Toner, "A microfluidic device for label-

free, physical capture of circulating tumor cell clusters," *Nat Meth*, vol. 12, pp. 685-691, 2015.

[251] P. Li, Z. Mao, Z. Peng, L. Zhou, Y. Chen, P.-H. Huang, C. I. Truica, J. J. Drabick, W. S. El-Deiry, M. Dao, S. Suresh, and T. J. Huang, "Acoustic separation of circulating tumor cells," *Proceedings of the National Academy of Sciences*, vol. 112, pp. 4970-4975, 2015.

[252] H. Lee, Y. Jang, J. Seo, J.-M. Nam, and K. Char, "Nanoparticle-Functionalized Polymer Platform for Controlling Metastatic Cancer Cell Adhesion, Shape, and Motility," *ACS Nano*, vol. 5, pp. 5444-5456, 2011.

[253] J. P. Best, S. Javed, J. J. Richardson, K. L. Cho, M. M. J. Kamphuis, and F. Caruso, "Stiffness-mediated adhesion of cervical cancer cells to soft hydrogel films," *Soft Matter*, vol. 9, pp. 4580-4584, 2013.

[254] E. Reategui, N. Aceto, E. J. Lim, J. P. Sullivan, A. E. Jensen, M. Zeinali, J. M. Martel, A. J. Aranyosi, W. Li, S. Castleberry, A. Bardia, L. V. Sequist, D. A. Haber, S. Maheswaran, P. T. Hammond, M. Toner, and S. L. Stott, "Tunable nanostructured coating for the capture and selective release of viable circulating tumor cells," *Adv Mater*, vol. 27, pp. 1593-9, 2015.

[255] J. D. Mendelsohn, S. Y. Yang, J. Hiller, A. I. Hochbaum, and M. F. Rubner, "Rational design of cytophilic and cytophobic polyelectrolyte multilayer thin films," *Biomacromolecules*, vol. 4, pp. 96-106, 2003.

[256] L. Richert, F. Boulmedais, P. Lavalle, J. Mutterer, E. Ferreux, G. Decher, P. Schaaf, J.-C. Voegel, and C. Picart, "Improvement of Stability and Cell Adhesion Properties of Polyelectrolyte Multilayer Films by Chemical Cross-Linking," *Biomacromolecules*, vol. 5, pp. 284-294, 2004.

[257] J. Chen, R. Kohler, T. Gutberlet, H. Mohwald, and R. Krastev, "Asymmetric lipid bilayer sandwiched in polyelectrolyte multilayer films through layer-by-layer assembly," *Soft Matter*, vol. 5, pp. 228-233, 2009.

[258] S. Yamaguchi, S. Yamahira, K. Kikuchi, K. Sumaru, T. Kanamori, and T. Nagamune, "Photocontrollable dynamic micropatterning of non-adherent mammalian cells using a photocleavable poly(ethylene glycol) lipid," *Angew Chem Int Ed Engl*, vol. 51, pp. 128-31, 2012.

[259] Y. Zhang, L. Wang, X. Wang, G. Qi, and X. Han, "Forming lipid bilayer membrane arrays on micropatterned polyelectrolyte film surfaces," *Chemistry*, vol. 19, pp. 9059-63, 2013.

[260] S. Yamahira, S. Yamaguchi, M. Kawahara, and T. Nagamune, "Collagen surfaces modified with photo-cleavable polyethylene glycol-lipid support

versatile single-cell arrays of both non-adherent and adherent cells," *Macromol Biosci,* vol. 14, pp. 1670-6, 2014.

[261] S. Y. Yang and J.-Y. Seo, "Cellular interactions on nano-structured polyelectrolyte multilayers," *Colloids and Surfaces A: Physicochemical and Engineering Aspects,* vol. 313–314, pp. 526-529, 2008.

[262] S. M. Frisch, M. Schaller, and B. Cieply, "Mechanisms that link the oncogenic epithelial-mesenchymal transition to suppression of anoikis," *J Cell Sci,* vol. 126, pp. 21-9, 2013.

[263] L. B. Weiswald, D. Bellet, and V. Dangles-Marie, "Spherical cancer models in tumor biology," *Neoplasia,* vol. 17, pp. 1-15, 2015.

[264] S. Y. Yang, J. D. Mendelsohn, and M. F. Rubner, "New class of ultrathin, highly cell-adhesion-resistant polyelectrolyte multilayers with micropatterning capabilities," *Biomacromolecules,* vol. 4, pp. 987-94, 2003.

[265] R. A. Whipple, E. M. Balzer, E. H. Cho, M. A. Matrone, J. R. Yoon, and S. S. Martin, "Vimentin filaments support extension of tubulin-based microtentacles in detached breast tumor cells," *Cancer Res,* vol. 68, pp. 5678-88, 2008.

[266] C. L. Chaffer and R. A. Weinberg, "A perspective on cancer cell metastasis," *Science,* vol. 331, pp. 1559-64, 2011.

[267] M. Cristofanilli and J. Mendelsohn, "Circulating tumor cells in breast cancer: Advanced tools for "tailored" therapy?," *Proc Natl Acad Sci U S A,* vol. 103, pp. 17073-4, 2006.

[268] M. Halter, Y. Nogata, O. Dannenberger, T. Sasaki, and V. Vogel, "Engineered lipids that cross-link the inner and outer leaflets of lipid bilayers," *Langmuir,* vol. 20, pp. 2416-23, 2004.

[269] S. Y. Yang and M. F. Rubner, "Micropatterning of polymer thin films with pH-sensitive and cross-linkable hydrogen-bonded polyelectrolyte multilayers," *J Am Chem Soc,* vol. 124, pp. 2100-1, 2002.

[270] Y. S. Ziegler, J. J. Moresco, P. G. Tu, J. R. Yates, 3rd, and A. M. Nardulli, "Plasma membrane proteomics of human breast cancer cell lines identifies potential targets for breast cancer diagnosis and treatment," *PLoS One,* vol. 9, p. e102341, 2014.

[271] V. Plaks, C. D. Koopman, and Z. Werb, "Cancer. Circulating tumor cells," *Science,* vol. 341, pp. 1186-8, 2013.

[272] T. A. Yap, D. Lorente, A. Omlin, D. Olmos, and J. S. de Bono, "Circulating tumor cells: a multifunctional biomarker," *Clin Cancer Res,* vol. 20, pp. 2553-68, 2014.

[273] S. Maheswaran, L. V. Sequist, S. Nagrath, L. Ulkus, B. Brannigan, C. V. Collura, E. Inserra, S. Diederichs, A. J. Iafrate, D. W. Bell, S. Digumarthy, A. Muzikansky, D. Irimia, J. Settleman, R. G. Tompkins, T. J. Lynch, M. Toner, and D. A. Haber, "Detection of mutations in EGFR in circulating lung-cancer cells," *N Engl J Med,* vol. 359, pp. 366-77, 2008.

[274] N. Aceto, A. Bardia, D. T. Miyamoto, M. C. Donaldson, B. S. Wittner, J. A. Spencer, M. Yu, A. Pely, A. Engstrom, H. Zhu, B. W. Brannigan, R. Kapur, S. L. Stott, T. Shioda, S. Ramaswamy, D. T. Ting, C. P. Lin, M. Toner, D. A. Haber, and S. Maheswaran, "Circulating tumor cell clusters are oligoclonal precursors of breast cancer metastasis," *Cell,* vol. 158, pp. 1110-22, 2014.

[275] M. C. Koetting, J. T. Peters, S. D. Steichen, and N. A. Peppas, "Stimulus-responsive hydrogels: Theory, modern advances, and applications," *Materials Science and Engineering: R: Reports,* vol. 93, pp. 1-49, 2015.

[276] M. J. Webber, E. A. Appel, E. W. Meijer, and R. Langer, "Supramolecular biomaterials," *Nat Mater,* vol. 15, pp. 13-26, 2016.

[277] C. A. Janeway, Jr. and R. Medzhitov, "Innate immune recognition," *Annual Review of Immunology,* vol. 20, pp. 197-216, 2002.

[278] K. Schroder and J. Tschopp, "The Inflammasomes," *Cell,* vol. 140, pp. 821-832, 2010.

[279] S. C. Eisenbarth, O. R. Colegio, W. O'Connor, F. S. Sutterwala, and R. A. Flavell, "Crucial role for the Nalp3 inflammasome in the immunostimulatory properties of aluminium adjuvants," *Nature,* vol. 453, pp. 1122-6, 2008.

[280] J. Sarma and P. Ward, "The complement system," *Cell and Tissue Research,* vol. 343, pp. 227-235, 2011.

[281] J. G. Tidball and S. A. Villalta, "Regulatory interactions between muscle and the immune system during muscle regeneration," *Am J Physiol Regul Integr Comp Physiol,* vol. 298, pp. R1173-87, 2010.

[282] J. G. Tidball and M. Wehling-Henricks, "Macrophages promote muscle membrane repair and muscle fibre growth and regeneration during modified muscle loading in mice in vivo," *J Physiol,* vol. 578, pp. 327-36, 2007.

[283] J. M. Anderson, "Biological responses to materials," *Annual Review of Materials Research,* vol. 31, p. 81, 2001.

[284] A. J. Singer and R. A. F. Clark, "Cutaneous wound healing," *The New England Journal of Medicine,* vol. 341, pp. 738-746, 1999.

[285] P. Martin, "Wound Healing--Aiming for Perfect Skin Regeneration," *Science,* vol. 276, pp. 75-81, 1997.

[286] D. M. Mosser and J. P. Edwards, "Exploring the full spectrum of macrophage activation," *Nat Rev Immunol,* vol. 8, pp. 958-969, 2008.

[287] K. L. Spiller, R. R. Anfang, K. J. Spiller, J. Ng, K. R. Nakazawa, J. W. Daulton, and G. Vunjak-Novakovic, "The role of macrophage phenotype in vascularization of tissue engineering scaffolds," *Biomaterials,* vol. 35, pp. 4477-4488, 2014.

[288] K. L. Spiller, S. Nassiri, C. E. Witherel, R. R. Anfang, J. Ng, K. R. Nakazawa, T. Yu, and G. Vunjak-Novakovic, "Sequential delivery of immunomodulatory cytokines to facilitate the M1-to-M2 transition of macrophages and enhance vascularization of bone scaffolds," *Biomaterials,* vol. 37, pp. 194-207, 2015.

[289] F. O. Martinez, L. Helming, and S. Gordon, "Alternative activation of macrophages: an immunologic functional perspective," *Annu Rev Immunol,* vol. 27, pp. 451-83, 2009.

[290] A. Sica and A. Mantovani, "Macrophage plasticity and polarization: in vivo veritas," *The Journal of Clinical Investigation,* vol. 122, pp. 787-795, 2012.

[291] A. Shizuo and K. Takeda, "Toll-like receptor signalling," *Nature Reviews. Immunology,* vol. 4, pp. 499-511, 2004.

[292] J. L. Zakrzewski, M. R. M. van den Brink, and J. A. Hubbell, "Overcoming immunological barriers in regenerative medicine," *Nat Biotech,* vol. 32, pp. 786-794, 2014.

[293] V. Hornung, F. Bauernfeind, A. Halle, E. O. Samstad, H. Kono, K. L. Rock, K. A. Fitzgerald, and E. Latz, "Silica crystals and aluminum salts activate the NALP3 inflammasome through phagosomal destabilization," *Nat Immunol,* vol. 9, pp. 847-56, 2008.

[294] J. M. Gammon, L. H. Tostanoski, A. R. Adapa, Y. C. Chiu, and C. M. Jewell, "Controlled delivery of a metabolic modulator promotes regulatory T cells and restrains autoimmunity," *J Control Release,* vol. 210, pp. 169-78, 2015.

[295] J. I. Andorko, J. M. Gammon, L. H. Tostanoski, Q. Zeng, and C. M. Jewell, "Targeted Programming of the Lymph Node Environment Causes Evolution

of Local and Systemic Immunity," *Cell Mol Bioeng,* vol. 9, pp. 418-432, 2016.

[296] L. H. Tostanoski, Y. C. Chiu, J. M. Gammon, T. Simon, J. I. Andorko, J. S. Bromberg, and C. M. Jewell, "Reprogramming the Local Lymph Node Microenvironment Promotes Tolerance that Is Systemic and Antigen Specific," *Cell Rep,* vol. 16, pp. 2940-52, 2016.

[297] L. H. Tostanoski, E. A. Gosselin, and C. M. Jewell, "Engineering tolerance using biomaterials to target and control antigen presenting cells," *Discov Med,* vol. 21, pp. 403-10, 2016.

[298] J. M. Gammon, N. M. Dold, and C. M. Jewell, "Improving the clinical impact of biomaterials in cancer immunotherapy," *Oncotarget,* vol. 7, pp. 15421-43, 2016.

[299] L. Jeanbart and M. A. Swartz, "Engineering opportunities in cancer immunotherapy," *Proceedings of the National Academy of Sciences,* vol. 112, pp. 14467-14472, 2015.

[300] J. J. Green and J. H. Elisseeff, "Mimicking biological functionality with polymers for biomedical applications," *Nature,* vol. 540, pp. 386-394, 2016.

[301] K. L. Hess, E. Oh, L. H. Tostanoski, J. I. Andorko, K. Susumu, J. R. Deschamps, I. L. Medintz, and C. M. Jewell, "Engineering Immunological Tolerance Using Quantum Dots to Tune the Density of Self-Antigen Display," *Advanced Functional Materials,* pp. 1700290-n/a, 2017.

[302] N. A. Hotaling, L. Tang, D. J. Irvine, and J. E. Babensee, "Biomaterial Strategies for Immunomodulation," *Annu Rev Biomed Eng,* vol. 17, pp. 317-49, 2015.

[303] Z. Julier, A. J. Park, P. S. Briquez, and M. M. Martino, "Promoting tissue regeneration by modulating the immune system," *Acta Biomaterialia,* 2017.

[304] H. Knopf-Marques, M. Pravda, L. Wolfova, V. Velebny, P. Schaaf, N. E. Vrana, and P. Lavalle, "Hyaluronic Acid and Its Derivatives in Coating and Delivery Systems: Applications in Tissue Engineering, Regenerative Medicine and Immunomodulation," *Advanced Healthcare Materials,* vol. 5, pp. 2841-2855, 2016.

[305] Y. Yu, R.-X. Wu, Y. Yin, and F.-M. Chen, "Directing immunomodulation using biomaterials for endogenous regeneration," *Journal of Materials Chemistry B,* vol. 4, pp. 569-584, 2016.

[306] A. Vishwakarma, N. S. Bhise, M. B. Evangelista, J. Rouwkema, M. R. Dokmeci, A. M. Ghaemmaghami, N. E. Vrana, and A. Khademhosseini, "Engineering Immunomodulatory Biomaterials To Tune the Inflammatory Response," *Trends in Biotechnology,* vol. 34, pp. 470-482, 2016.

[307] R. Toy and K. Roy, "Engineering nanoparticles to overcome barriers to immunotherapy," *Bioengineering & Translational Medicine,* vol. 1, pp. 47-62, 2016.

[308] A. C. Anselmo and S. Mitragotri, "Nanoparticles in the clinic," *Bioengineering & Translational Medicine,* vol. 1, pp. 10-29, 2016.

[309] K. T. Gause, A. K. Wheatley, J. Cui, Y. Yan, S. J. Kent, and F. Caruso, "Immunological Principles Guiding the Rational Design of Particles for Vaccine Delivery," *ACS Nano,* 2017.

[310] L. Tang, T. M. Fan, L. B. Borst, and J. Cheng, "Synthesis and biological response of size-specific, monodisperse drug-silica nanoconjugates," *ACS Nano,* vol. 6, pp. 3954-66, 2012.

[311] E. Bracho-Sanchez, C. Q. Xia, M. J. Clare-Salzler, and B. G. Keselowsky, "Micro and Nano Material Carriers for Immunomodulation," *American Journal of Transplantation,* vol. 16, pp. 3362-3370, 2016.

[312] T. D. Fernández, J. R. Pearson, M. P. Leal, M. J. Torres, M. Blanca, C. Mayorga, and X. Le Guével, "Intracellular accumulation and immunological properties of fluorescent gold nanoclusters in human dendritic cells," *Biomaterials,* vol. 43, pp. 1-12, 2015.

[313] J. A. Champion, Y. K. Katare, and S. Mitragotri, "Particle shape: a new design parameter for micro- and nanoscale drug delivery carriers," *J Control Release,* vol. 121, pp. 3-9, 2007.

[314] K. M. Ainslie, S. L. Tao, K. C. Popat, and T. A. Desai, "In vitro Immunogenicity of Silicon-Based Micro- and Nanostructured Surfaces," *ACS Nano,* vol. 2, pp. 1076-1084, 2008.

[315] S. Muro, C. Garnacho, J. A. Champion, J. Leferovich, C. Gajewski, E. H. Schuchman, S. Mitragotri, and V. R. Muzykantov, "Control of endothelial targeting and intracellular delivery of therapeutic enzymes by modulating the size and shape of ICAM-1-targeted carriers," *Mol Ther,* vol. 16, pp. 1450-8, 2008.

[316] J. A. Champion and S. Mitragotri, "Shape induced inhibition of phagocytosis of polymer particles," *Pharm Res,* vol. 26, pp. 244-9, 2009.

[317] M. Bartneck, H. A. Keul, S. Singh, K. Czaja, J. Bornemann, M. Bockstaller, M. Moeller, G. Zwadlo-Klarwasser, and J. Groll, "Rapid Uptake of Gold Nanorods by Primary Human Blood Phagocytes and Immunomodulatory Effects of Surface Chemistry," *ACS Nano,* vol. 4, pp. 3073-3086, 2010.

[318] T. Padmore, C. Stark, L. A. Turkevich, and J. A. Champion, "Quantitative analysis of the role of fiber length on phagocytosis and inflammatory response by alveolar macrophages," *Biochim Biophys Acta,* vol. 1861, pp. 58-67, 2017.

[319] B. C. Schanen, A. S. Karakoti, S. Seal, D. R. Drake Iii, W. L. Warren, and W. T. Self, "Exposure to Titanium Dioxide Nanomaterials Provokes Inflammation of an in Vitro Human Immune Construct," *ACS Nano,* vol. 3, pp. 2523-2532, 2009.

[320] B. Sun, X. Wang, Z. Ji, R. Li, and T. Xia, "NLRP3 inflammasome activation induced by engineered nanomaterials," *Small,* vol. 9, pp. 1595-607, 2013.

[321] K. Niikura, T. Matsunaga, T. Suzuki, S. Kobayashi, H. Yamaguchi, Y. Orba, A. Kawaguchi, H. Hasegawa, K. Kajino, T. Ninomiya, K. Ijiro, and H. Sawa, "Gold Nanoparticles as a Vaccine Platform: Influence of Size and Shape on Immunological Responses in Vitro and in Vivo," *ACS Nano,* vol. 7, pp. 3926-3938, 2013.

[322] R. A. Meyer, J. C. Sunshine, K. Perica, A. K. Kosmides, K. Aje, J. P. Schneck, and J. J. Green, "Biodegradable nanoellipsoidal artificial antigen presenting cells for antigen specific T-cell activation," *Small,* vol. 11, pp. 1519-25, 2015.

[323] A. K. Kosmides, R. A. Meyer, J. W. Hickey, K. Aje, K. N. Cheung, J. J. Green, and J. P. Schneck, "Biomimetic biodegradable artificial antigen presenting cells synergize with PD-1 blockade to treat melanoma," *Biomaterials,* vol. 118, pp. 16-26, 2017.

[324] R. Dvash, A. Khatchatouriants, L. J. Solmesky, P. P. Wibroe, M. Weil, S. M. Moghimi, and D. Peer, "Structural profiling and biological performance of phospholipid–hyaluronan functionalized single-walled carbon nanotubes," *Journal of Controlled Release,* vol. 170, pp. 295-305, 2013.

[325] J. C. Tiller, G. Bonner, L.-C. Pan, and A. M. Klibanov, "Improving biomaterial properties of collagen films by chemical modification," *Biotechnology and Bioengineering,* vol. 73, pp. 246-252, 2001.

[326] J. L. Drury and D. J. Mooney, "Hydrogels for tissue engineering: scaffold design variables and applications," *Biomaterials,* vol. 24, pp. 4337-4351, 2003.

[327] N. A. Peppas, J. Z. Hilt, A. Khademhosseini, and R. Langer, "Hydrogels in Biology and Medicine: From Molecular Principles to Bionanotechnology," *Advanced Materials,* vol. 18, pp. 1345-1360, 2006.

[328] Y. Kakizawa, J. Seok Lee, B. Bell, and T. M. Fahmy, "Precise manipulation of biophysical particle parameters enables control of proinflammatory cytokine production in presence of TLR 3 and 4 ligands," *Acta Biomaterialia,* 2017, *in press*.

[329] Y. Wen, A. Waltman, H. Han, and J. H. Collier, "Switching the Immunogenicity of Peptide Assemblies Using Surface Properties," *ACS Nano,* vol. 10, pp. 9274-9286, 2016.

[330] R. Appavu, C. B. Chesson, A. Y. Koyfman, J. D. Snook, F. J. Kohlhapp, A. Zloza, and J. S. Rudra, "Enhancing the Magnitude of Antibody Responses through Biomaterial Stereochemistry," *ACS Biomaterials Science & Engineering,* vol. 1, pp. 601-609, 2015.

[331] K. T. Gause, Y. Yan, J. Cui, N. M. O'Brien-Simpson, J. C. Lenzo, E. C. Reynolds, and F. Caruso, "Physicochemical and Immunological Assessment of Engineered Pure Protein Particles with Different Redox States," *ACS Nano,* vol. 9, pp. 2433-2444, 2015.

[332] M. Sokolowska, L.-Y. Chen, M. Eberlein, A. Martinez-Anton, Y. Liu, S. Alsaaty, H.-Y. Qi, C. Logun, M. Horton, and J. H. Shelhamer, "Low Molecular Weight Hyaluronan Activates Cytosolic Phospholipase A2α and Eicosanoid Production in Monocytes and Macrophages," *Journal of Biological Chemistry,* vol. 289, pp. 4470-4488, 2014.

[333] J. J. Green, R. Langer, and D. G. Anderson, "A Combinatorial Polymer Library Approach Yields Insight into Nonviral Gene Delivery," *Accounts of Chemical Research,* vol. 41, pp. 749-759, 2008.

[334] J. I. Andorko, K. G. Pineault, and C. M. Jewell, "Impact of molecular weight on the intrinsic immunogenic activity of poly(beta amino esters)," *J Biomed Mater Res A,* vol. 105, pp. 1219-1229, 2017.

[335] K. L. Hess, J. I. Andorko, L. H. Tostanoski, and C. M. Jewell, "Polyplexes assembled from self-peptides and regulatory nucleic acids blunt toll-like receptor signaling to combat autoimmunity," *Biomaterials,* vol. 118, pp. 51-62, 2017.

[336] Y.-C. Chiu, J. M. Gammon, J. I. Andorko, L. H. Tostanoski, and C. M. Jewell, "Modular Vaccine Design Using Carrier-Free Capsules Assembled from Polyionic Immune Signals," *ACS Biomaterials Science & Engineering,* 2015.

[337] P. Zhang, J. I. Andorko, and C. M. Jewell, "Impact of dose, route, and composition on the immunogenicity of immune polyelectrolyte multilayers delivered on gold templates," *Biotechnol Bioeng*, vol. 114, pp. 423-431, 2017.

[338] N. M. Molino, A. K. L. Anderson, E. L. Nelson, and S.-W. Wang, "Biomimetic Protein Nanoparticles Facilitate Enhanced Dendritic Cell Activation and Cross-Presentation," *ACS Nano*, vol. 7, pp. 9743-9752, 2013.

[339] J. S. Rudra, T. Sun, K. C. Bird, M. D. Daniels, J. Z. Gasiorowski, A. S. Chong, and J. H. Collier, "Modulating Adaptive Immune Responses to Peptide Self-Assemblies," *ACS Nano*, vol. 6, pp. 1557-1564, 2012.

[340] L. H. Tostanoski and C. M. Jewell, "Engineering self-assembled materials to study and direct immune function," *Advanced Drug Delivery Reviews*, 2017, *in press*.

[341] A. Uccelli, L. Moretta, and V. Pistoia, "Mesenchymal stem cells in health and disease," *Nat Rev Immunol*, vol. 8, pp. 726-736, 2008.

[342] K. L. Blanc and O. Ringdén, "Immunomodulation by mesenchymal stem cells and clinical experience," *Journal of Internal Medicine*, vol. 262, pp. 509-525, 2007.

[343] K. Le Blanc and O. Ringdén, "Mesenchymal stem cells: properties and role in clinical bone marrow transplantation," *Current Opinion in Immunology*, vol. 18, pp. 586-591, 2006.

[344] G. Chamberlain, J. Fox, B. Ashton, and J. Middleton, "Concise Review: Mesenchymal Stem Cells: Their Phenotype, Differentiation Capacity, Immunological Features, and Potential for Homing," *STEM CELLS*, vol. 25, pp. 2739-2749, 2007.

[345] A. Papalamprou, C. W. Chang, N. Vapniarsky, A. Clark, N. Walker, and L. G. Griffiths, "Xenogeneic cardiac extracellular matrix scaffolds with or without seeded mesenchymal stem cells exhibit distinct in vivo immunosuppressive and regenerative properties," *Acta Biomaterialia*, vol. 45, pp. 155-168, 2016.

[346] E. R. Molina, B. T. Smith, S. R. Shah, H. Shin, and A. G. Mikos, "Immunomodulatory properties of stem cells and bioactive molecules for tissue engineering," *Journal of Controlled Release*, vol. 219, pp. 107-118, 2015.

[347] A. Gallud, O. Bondarenko, N. Feliu, N. Kupferschmidt, R. Atluri, A. Garcia-Bennett, and B. Fadeel, "Macrophage activation status determines the internalization of mesoporous silica particles of different sizes: Exploring the

role of different pattern recognition receptors," *Biomaterials,* vol. 121, pp. 28-40, 2017.

[348] J. L. Dziki, B. M. Sicari, M. T. Wolf, M. C. Cramer, and S. F. Badylak, "Immunomodulation and Mobilization of Progenitor Cells by Extracellular Matrix Bioscaffolds for Volumetric Muscle Loss Treatment," *Tissue Engineering Part A,* vol. 22, pp. 1129-1139, 2016.

[349] J. L. Dziki, D. S. Wang, C. Pineda, B. M. Sicari, T. Rausch, and S. F. Badylak, "Solubilized extracellular matrix bioscaffolds derived from diverse source tissues differentially influence macrophage phenotype," *Journal of Biomedical Materials Research Part A,* vol. 105, pp. 138-147, 2017.

[350] J.-l. Sun, K. Jiao, L.-n. Niu, Y. Jiao, Q. Song, L.-j. Shen, F. R. Tay, and J.-h. Chen, "Intrafibrillar silicified collagen scaffold modulates monocyte to promote cell homing, angiogenesis and bone regeneration," *Biomaterials,* vol. 113, pp. 203-216, 2017.

[351] J. Y. Hsieh, T. D. Smith, V. S. Meli, T. N. Tran, E. L. Botvinick, and W. F. Liu, "Differential regulation of macrophage inflammatory activation by fibrin and fibrinogen," *Acta Biomaterialia,* vol. 47, pp. 14-24, 2017.

[352] D. M. Vasconcelos, R. M. Gonçalves, C. R. Almeida, I. O. Pereira, M. I. Oliveira, N. Neves, A. M. Silva, A. C. Ribeiro, C. Cunha, A. R. Almeida, C. C. Ribeiro, A. M. Gil, E. Seebach, K. L. Kynast, W. Richter, M. Lamghari, S. G. Santos, and M. A. Barbosa, "Fibrinogen scaffolds with immunomodulatory properties promote in vivo bone regeneration," *Biomaterials,* vol. 111, pp. 163-178, 2016.

[353] P. L. Graney, S. I. Roohani-Esfahani, H. Zreiqat, and K. L. Spiller, "In vitro response of macrophages to ceramic scaffolds used for bone regeneration," *J R Soc Interface,* vol. 13, 2016.

[354] M. T. Wolf, C. L. Dearth, C. A. Ranallo, S. T. LoPresti, L. E. Carey, K. A. Daly, B. N. Brown, and S. F. Badylak, "Macrophage polarization in response to ECM coated polypropylene mesh," *Biomaterials,* vol. 35, pp. 6838-6849, 2014.

[355] A. M. Ferreira, P. Gentile, V. Chiono, and G. Ciardelli, "Collagen for bone tissue regeneration," *Acta Biomaterialia,* vol. 8, pp. 3191-3200, 2012.

[356] J. Jiang, Z. Li, H. Wang, Y. Wang, M. A. Carlson, M. J. Teusink, M. R. MacEwan, L. Gu, and J. Xie, "Expanded 3D Nanofiber Scaffolds: Cell Penetration, Neovascularization, and Host Response," *Advanced Healthcare Materials,* vol. 5, pp. 2993-3003, 2016.

[357] K. Garg, N. A. Pullen, C. A. Oskeritzian, J. J. Ryan, and G. L. Bowlin, "Macrophage functional polarization (M1/M2) in response to varying fiber and pore dimensions of electrospun scaffolds," *Biomaterials,* vol. 34, pp. 4439-4451, 2013.

[358] G. Chan and D. J. Mooney, "Ca2+ released from calcium alginate gels can promote inflammatory responses in vitro and in vivo," *Acta Biomaterialia,* vol. 9, pp. 9281-9291, 2013.

[359] H. Knopf-Marques, S. Singh, S. S. Htwe, L. Wolfova, R. Buffa, J. Bacharouche, G. Francius, J.-C. Voegel, P. Schaaf, A. M. Ghaemmaghami, N. E. Vrana, and P. Lavalle, "Immunomodulation with Self-Crosslinked Polyelectrolyte Multilayer-Based Coatings," *Biomacromolecules,* vol. 17, pp. 2189-2198, 2016.

[360] L. Zhang, Z. Cao, T. Bai, L. Carr, J.-R. Ella-Menye, C. Irvin, B. D. Ratner, and S. Jiang, "Zwitterionic hydrogels implanted in mice resist the foreign-body reaction," *Nat Biotech,* vol. 31, pp. 553-556, 2013.

[361] S. N. Christo, A. Bachhuka, K. R. Diener, A. Mierczynska, J. D. Hayball, and K. Vasilev, "The Role of Surface Nanotopography and Chemistry on Primary Neutrophil and Macrophage Cellular Responses," *Advanced Healthcare Materials,* vol. 5, pp. 956-965, 2016.

[362] J. C. Doloff, O. Veiseh, A. J. Vegas, H. H. Tam, S. Farah, M. Ma, J. Li, A. Bader, A. Chiu, A. Sadraei, S. Aresta-Dasilva, M. Griffin, S. Jhunjhunwala, M. Webber, S. Siebert, K. Tang, M. Chen, E. Langan, N. Dholokia, R. Thakrar, M. Qi, J. Oberholzer, D. L. Greiner, R. Langer, and D. G. Anderson, "Colony stimulating factor-1 receptor is a central component of the foreign body response to biomaterial implants in rodents and non-human primates," *Nat Mater,* 2017, *in press*.

[363] K. Sadtler, K. Estrellas, B. W. Allen, M. T. Wolf, H. Fan, A. J. Tam, C. H. Patel, B. S. Luber, H. Wang, K. R. Wagner, J. D. Powell, F. Housseau, D. M. Pardoll, and J. H. Elisseeff, "Developing a pro-regenerative biomaterial scaffold microenvironment requires T helper 2 cells," *Science,* vol. 352, pp. 366-370, 2016.

[364] S. V. Murphy and A. Atala, "3D bioprinting of tissues and organs," *Nat Biotech,* vol. 32, pp. 773-785, 2014.

[365] C. Norotte, F. S. Marga, L. E. Niklason, and G. Forgacs, "Scaffold-free vascular tissue engineering using bioprinting," *Biomaterials,* vol. 30, pp. 5910-5917, 2009.

[366] B. Derby, "Printing and Prototyping of Tissues and Scaffolds," *Science,* vol. 338, pp. 921-926, 2012.

[367] H. Cui, M. Nowicki, J. P. Fisher, and L. G. Zhang, "3D Bioprinting for Organ Regeneration," *Advanced Healthcare Materials,* vol. 6, 2017.

[368] H.-W. Kang, S. J. Lee, I. K. Ko, C. Kengla, J. J. Yoo, and A. Atala, "A 3D bioprinting system to produce human-scale tissue constructs with structural integrity," *Nat Biotech,* vol. 34, pp. 312-319, 2016.